Damage Accumulation in Hybrid Woven Fabric Composites

Mohammed Asaad

Thesis submitted in partial fulfilment of the requirement of Bournemouth University for award of the degree of Doctor of Philosophy

Bournemouth University

December 2002

ABSTRACT

Damage accumulation in glass fibre woven reinforced epoxy laminates manufactured from two different fabrics have been investigated under three different loading conditions. One of the woven fabrics was non-hybrid glass using E-glass fibre yarns in both warp and weft (fill) directions, the second fabric was a hybrid woven fabric using E-glass fibre yarns in the warp direction and R-glass fibre yarns in the weft direction.

Destructive tests such as interlaminar shear, flexural and uniaxial tension tests were carried out on two different categories. In the first category four different fibre volume fractions of non-hybrid E-glass woven fabric reinforced epoxy resin laminates have been investigated. In the second category hybrid and non-hybrid woven fabric reinforced epoxy resin laminates for similar fibre volume fractions have been investigated.

Acoustic Emission (AE) and Scanning Electron Microscopy (SEM) were employed as non-destructive tools to predict and characterise the damage events in the composites. All laminates were fabricated using the wet hand lay-up process to laminate the fabric layers prior to curing. Epoxy resin (L20-SL set) was the sole matrix used for all composites.

Test results showed higher mechanical performance for the hybrid composites and improvements in mechanical properties for higher fibre volume fraction in the non-hybrid composites. DMTA tests were carried out on the laminates of the categories mentioned above, the test results indicated the effect of fibre surface treatment concentration on the performance of mechanical properties of woven composites. DMTA data has been used to correlate the results of ILSS, flexural and tensile tests.

A model was developed in this study based on the damage event sequential process of glass woven fabric reinforced epoxy resin composites. The model is an experimental analysis model, supported by DMTA, AE, SEM and visual examination of specimen fracture surface.

TABLE OF CONTENTS

Title page.....i

Abstract ii

Table of contents.....iii

List of tables vii

List of figures viii

Acknowledgements.....x

Nomenclature xi

Chapter One

1 –1 Introduction 2

1 – 2 Objectives and scope of the research 5

Chapter Two –Hybrid Glass Reinforcement

2 – 1 Characteristics of Glass Fibre 7
2 – 1 – 1 Glass fibre manufacturing 8

2 – 2 Fabric Structure 8

2 – 3 Glass Woven Fabrics 9

2 – 4 Weave Pattern 10
2 – 4 – 1 Plain weave 10
2 – 4 – 2 Basket weave 10
2 – 4 – 3 Twill weave 10
2 – 4 – 4 Satin weaves 11
2 – 4 – 5 Hybrid fabrics 12

2 – 5 Types of Hybrid Laminates 12
2 – 5 – 1 Intraply 13
2 – 5 – 2 Interply 13
2 – 5 – 3 Interwoven 13
2 – 5 – 4 Hybrid interface 13

2 – 6 Fibre Surface Treatments 13

2 – 7 Interface 15

2 – 8 Interphase 16

2 – 9 Epoxy Resins 17

2 – 10 Acoustic Emission (AE) 18
2 – 10 – 1 Acoustic Emission in glass and glass fibre 19
2 – 10 – 2 Acoustic Emission in Composites 19
Tables and figures 22-25

Chapter Three Mechanical Characterisation

3–1 Elastic Properties of Woven Composites 27
3 –1–1 Classical Laminate Theory (CLT) 27
3 –1–2 Software packages 28
3 –1–3 The simple rule of mixtures 29

3 –2 Woven Fabric Models 31
3 –2 –1 Mosaic model 31
3 –2 –2 Fibre undulation model 32
3 –2 –3 Bridging model 33

3 –3 Mechanical Testing Characterisation 34
3 –3 –1 Interlaminar Shear Strength (ILSS) 34
3 –3 –2 Flexural properties 36
3 –3 –3 Viscoelastic properties 36
3 –3 –4 Tensile properties 38
Figures 41 – 43

Chapter Four Experimental Details

4 – 1 Material Characteristics 45
4 – 1 –1 Yarn nomenclature 45
4 – 1 –2 Finishing 46

4 – 2 The Matrix Resin System 47

4 – 3 Test and Equipment 48
4 – 3 – 1 Tensile test method 48
4 – 3 – 2 Flexural test method – three-point bending 49
4 – 3 – 3 ILSS – short-beam method 50
4 – 3 – 4 Acoustic Emission analyser 50
4 – 3 – 5 AE system calibration 51

4 – 3 – 6 Scanning Electron Microscope (SEM) 51
4 – 3 – 7 Dynamic Mechanical and Thermal Analysis (DMTA) 52
4 – 3 – 8 The DMTA system calibration 54

4 – 4 Porosity and Determination of Fibre Volume Fraction 55
4 – 4 – 1 Porosity 55
4 – 4 – 2 Determination of fibre volume fraction 56

4 – 5 Laminate Manufacture 57
4 – 5 – 1 Investigating the effect of hybridisation 58
4 – 5 – 2 Investigating the effect of V_f in the composites 59
4 – 6 Quality and Reliability Factor 59
Tables and figures 61 – 65

Chapter Five Results and Discussion 67

5 – 1 Section One - Interlaminar Shear Strength (ILSS) 67

5 – 1 – 1 Results 67
5 – 1 – 2 Discussion of the effect of V_f on ILSS 68
5 – 1 – 3 Discussion of the effect of fibre hybridisation on ILSS 71
Tables and figures 75 – 84

5 – 2 Section Two - Flexural Properties 85

5 – 2 – 1 Results 85
5 – 2 – 2 Discussion of the effect of V_f on flexural properties 85
5 – 2 – 3 Discussion of the of fibre hybridisation effect on flexural properties 87
Tables and figures 92 – 101

5 – 3 Section Three - Dynamic Mechanical and Thermal Analysis (DMTA) 102

5 – 3 – 1 Results 102
5 – 3 – 2 Discussion of the effect of V_f on viscoelastic properties 102
5 – 3 – 3 Discussion of the fibre hybridisation on viscoelastic properties 105
Tables and figures 109 – 117

5 – 4 Section Four - Tensile Properties 118

5 – 4 – 1 Results 118
5 – 4 – 2 Discussion of the effect of V_f on tensile properties 118
5 – 4 – 3 Discussion of fibre hybridisation effect on tensile properties 123
Tables and figures 128 – 143

5 – 5 Section Five – Damage Events Process Model 144

5 – 5 – 1 Damage event sequence modelling 144
5 – 5 – 2 The bridging validation modelling 147
Figures 155-158

Section Six – Evaluation of the Results 159

5 – 6 – 1 The correlation of experimental results with DMTA 159
5 – 6 – 2 t-test 160
Tables and figures 162 – 165

5 – 7 Section Seven – Microlam Software 166

5 – 7 – 1 Microlam software input 166
5 – 7 – 2 Microlam software output 169

Chapter Six 172

6 – 1 Summary 173
6 – 2 Conclusion and Originality of the Research 176
6 – 3 Further Work and Development 179

References 181
Appendices 197
A – Classical Laminate Theory (CLT) 197
B – Ring Down Counting (RDC) 201
C – t-Test 204

LIST OF TABLES

No. Table Content

2 – 1 Glass compositions of some fibreglass
2 – 2 Glass physical properties of some fibreglass
2 – 3 Glass thermal properties of some fibreglass
2 – 4 Mechanical properties of some glass fibre

4 – 1 Specification of the epoxy resin (L20-SL) system.

5 – 1 ILSS results of non-hybrid composites includes four different V_f.
5 – 2 AE activity during ILSS tests of non-hybrid composites includes four different V_f.
5 – 3 ILSS test results of hybrid and non-hybrid woven composites.
5 – 4 AE activity during ILSS tests for non-hybrid and hybrid glass woven composites.

5 – 5 Flexural test results of non-hybrid woven composites including four different V_f.
5 – 6 AE activities during flexural tests of non-hybrid composite including four different V_f.
5 – 7 Flexural test results of hybrid and non-hybrid woven composites.
5 – 8 AE activities during flexural tests of hybrid and non-hybrid glass woven composites.

5 – 9 DMTA results of non-hybrid woven composites including four different V_f.
5 – 10 DMTA results of hybrid and non-hybrid glass woven composites (weft direction).
5 – 11 DMTA results of hybrid and non-hybrid glass woven composites (warp direction).

5 – 12 Tensile test results of non-hybrid glass woven composites including four different V_f.
5 – 13 AE activities during tensile tests of non-hybrid composites including four different V_f.
5 – 14 Tensile test results for hybrid and non-hybrid glass woven composites.
5 – 15 AE activities during tensile tests of hybrid and non-hybrid glass woven composites.

5 – 16 DMTA results correlated with experimental results (effect of V_f).
5 – 17 DMTA results correlated with experimental results (effect of hybrid).
5 – 18 t-test.
5 – 19 Percentage points of t-distribution.
5 – 20 Microlam software output values.

LIST OF FIGURES

2 – 1 Three different weave patterns of fibre woven fabrics.
2 – 2 The difference in drapability between various weave patterns.
2 – 3 Hybrid weave patterns.
2 – 4 Three types of hybrid composites.

3 – 1 Mosaic model for a unit cell of 8-harness satin.
3 – 2 8-harness satin woven fabric.
3 – 3 Fibre crimp model.
3 – 4 Fibre crimp model in hybrid woven fabric
3 – 5 Bridging model
3 – 6 3D view of bridging model for 8-harness hybrid woven fabric.

4 – 1 SEM micrograph of 8-harness glass woven fabric
4 – 2 The presence of porosity in the glass woven composite
4 – 3 Zwick Z050 Tensile testing machine.
4 – 4 Tensile specimen and AE sensor
4 – 5 Flexural test configuration
4 – 6 ILSS test configuration
4 – 7 DMTA test configuration

5 – 1 ILSS plot of Load-Displacement and its RDC curves of four V_f composites
5 – 2 ILSS plot of L-D and its RDC curves of hybrid and non-hybrid composite weft dir.
5 – 3 ILSS plot of L-D and its RDC.
5 – 4 ILSS plot of L-D and its AE rate
5 – 5 SEM micrographs of ILSS fracture of non-hybrid composite at 38% V_f.
5 – 6 SEM micrographs of ILSS fracture of non-hybrid composite at 48% V_f.
5 – 7 SEM micrographs of ILSS fracture of non-hybrid composite at 64% V_f.
5 – 8 SEM micrographs of ILSS fracture of hybrid composite.

5 – 9 Flexural stress-strain and its RDC plot of four V_f composites.
5 – 10 Flexural stress-strain and its RDC plot of hybrid and non-hybrid composite weft dir.
5 –11 Flexural stress-strain and its RDC plot of hybrid and non-hybrid composite warp dir.
5 – 14 SEM micrograph of flexural fracture non-hybrid composite at 48% V_f.
5 – 15 SEM micrograph of flexural fracture non-hybrid composite at 64% V_f.
5 – 16 SEM micrograph of flexural fracture hybrid composite.

5 - 17 DMTA of non-hybrid composites. Plot of loss moduli of four different V_f.
5 - 18 DMTA of non-hybrid composites. Plot of storage moduli including four different V_f.
5 – 19 DMTA of non-hybrid composites. Plot of tan delta including three different V_f.
5 – 20 DMTA of hybrid and non-hybrid composites (weft direction). Plot of E` & E``.
5 – 21 DMTA of hybrid and non-hybrid (weft direction). Plot of tan (δ) and log (E`).
5 – 22 Visualisation of three-dimensional interphase.

5 – 23 Tensile S-S & RDC curves of non-hybrid composites, at four V_f.
5 – 24 Tensile S-S & AE rate curves of non-hybrid composites, at four V_f.
5 – 25 Tensile S-S & RDC curves of hybrid and non-hybrid composites (weft dir.)
5 – 26 Tensile S-S & AE rate curves of hybrid and non-hybrid composites (weft dir.)
5 – 27 Tensile S-S & AE RDC curves of hybrid and non-hybrid composites (warp dir.)
5 – 28 Tensile S-S & AE curves of glass woven composites (zone classification).
5 – 29 Tensile test specimens after test failure modes 1 & 2.
5 – 30 Tensile test specimens after test failure modes 3 & 4.
5 – 31 Tensile test specimens after test hybrid failure
5 – 32 SEM micrograph of fracture surface of non-hybrid composite at 38% V_f.
5 – 33 SEM micrograph of fracture surface of non-hybrid composite at 48% V_f.
5 – 34 SEM micrograph of fracture surface of non-hybrid composite at 56% V_f.
5 – 35 SEM micrograph of fracture surface of non-hybrid composite at 64% V_f.
5 – 36 SEM micrograph of fracture surface of hybrid composite at 48% V_f.

5 – 37 Flowchart of damage sequence modelling.
5 – 38 Flowchart of damage events identification.
5 – 39 Flowchart of quality control for glass woven composite

5 – 40 The relation between the glass transition temperature (T_g) and ILSS.
5 – 41 The relation between the glass transition temperature (T_g) and flexural strength.
5 – 42 Rule of mixtures application on tensile strength and Moduli.

ACKNOWLEDGEMENTS

I am highly obliged and owe a great debt of gratitude to my supervisor Prof. Terry Sheppard. This work would not have been possible without his consistent encouragement and guidance. His patience and continued guidance, and the technical and theoretical advice, which was generated from the scientific background, made this project an interesting task.

I would like to take this opportunity to thank a number of individuals and institutions for their important contributions towards this thesis.

First and foremost I would like to thank from the School of Design, Engineering and Computing Dr. Kamran Tabeshfar, Head of the Design Group, for his support and advice to this project. I would also like to thank Prof. Peter Hogarth, the deputy head of the school, for his patience and assistance. I express my deep appreciation to Dr. Hossein Saidpour of East London University for his previous supervision and Dr. Mehran Koohiglani for his assistance.

Special thanks are due to Interglas-Technologies – Sherborne UK, and in particular Mr Roger Price for all the material and emphatic and technical discussions and John James for his technical assistance. I would also like to thank Vetrotex and Bakelite for their technical assistance.

I would like to acknowledge my profound gratitude to Brian Wright and Peter Jones of the School of Design, Engineering and Computing and Rob Haslam from the School of Conservation Science for their technical assistance. I would like to acknowledge my profound gratitude to Heather Porter from the British Library, June Stagg and Lynne Rutter from Bournemouth University Library for their search assistance.

I wish to specially thank my mother for her faithful prayers, my brothers and sisters for their moral support and my wife Yasmine for her encouragement, immense help and her endless moral support. My daughter and my two sons have been also a source of inspiration toward completing my research in a congenial atmosphere. Finally, I would like to dedicate this thesis to the memory of my late father.

NOMENCLATURE

AE	Acoustic Emission
BS	British Standard
CLT	Classical Laminate Theory
DMTA	Dynamic Mechanical and Thermal Analysis
FRC	Fibre Reinforcement Composites
FRP	Fibre Reinforced Plastics
GRP	Glass Reinforced Plastics
ILSS	Interlaminar Shear Strength
L-D	Load-Displacement
RDC	Ring down count
SEM	Scanning Electronic Microscopy
S-S	Stress-Strain
UFS	Ultimate Flexural Strength
UTS	Ultimate Tensile Strength
VSE	Visual Specimen Examination
WF	Woven Fabric
WFD	Weft Direction
WPD	Warp Direction

SUBSCRIPTS

1	x-direction (or x is weft)
2	y-direction (or y is warp)
3	z-direction
E_l	Composite longitudinal modulus
E_2	Composite transverse modulus
E_x	Longitudinal modulus in x direction
E'	Flexural storage modulus
E''	Flexural loss modulus
L_l	Thickness of laminate

L_c	Crimp portion length of woven cell unit repeats
Ls	Straight portion length of woven cell unit repeats
T_g	Glass transition temperature
V_f	Fibre volume fraction
V_m	Matrix volume fraction
τ	Shear modulus

CHAPTER ONE

CHAPTER ONE

1 – 1 Introduction

The literature review in chapter two indicates that the fibres most widely used for composites today are those manufactured from E-glass. It has been the standard material for Fibre Reinforced Composites (FRC) with a usage approaching two million tonnes per year worldwide (Bader and Lekakou 1997). E-glass became available in various industrialised forms in order to accommodate the numerous manufacturing processes. During this boom it became apparent that the physical, chemical and dielectric properties of Glass Reinforced Plastics (GRP) were not sufficient to fulfil the specific needs of certain final applications. The aerospace sector was demanding higher performance material with regard to strength and modulus. These demands were met by R-glass. Subsequently a series of research programmes, including 200 types of glass were conducted in 1982 (Molinier, 1982), (Vetrotex, 1999).

Glass compositions of some fibreglass are illustrated in table (2 – 1). The strength of glass fibres when measured at room temperature is a function of the glass composition according to Loewenstein and Aslanova (Loewenstein and Dow 1968) and (Aslanova 1985). It can be seen from the results in table 4 – 1 that the highest strength is obtained from R-glass. This explains the use of such fibre in areas where a high resistance to working stress is required. (Molinier, 1982), (Vetrotex, 1999).

The literature review in chapter two emphasised the need for material, which was easy and convenient to handle in order to reinforce polymer matrices and properties to provide for a range of markets. Woven fabric reinforcement added a new dimension to the field of composites. The fabric pattern is often called the construction or fabric architecture, the essential construction requires only four weaving yarns: two warp and two fill. This basic unit is called the pattern repeat, (Dominguez 1987). Fabrics may be woven in a variety of patterns such as plain weave, twill weave, satin weave. The satin weaves represent a family of constructions with a minimum of interlacing.

The general requirement now is for composites to be of attractive structural materials enabling more cost-effective utilisation in the introduction of hybrid fabric in the world of composites.

Hybrid fabrics are those woven from two or more different types of fibre. Hybrid fabrics have also demonstrated weight savings, reduced notch sensitivity, improved fracture toughness, longer fatigue life and excellent impact resistance (Chou and Kelly 1980a).

The review further indicates that since 1982, no research work has been undertaken into utilisation of R-glass. This is possibly due to the high cost of R-glass production or the availability of E-glass at low cost in various industrialised forms to accommodate the numerous commercial needs. Meanwhile the demand for glass fabric woven material of higher mechanical performance has continued to grow in the aerospace sector. Interglas Technologies has recently designed a fabric using R-glass. It is a hybrid 8-harness satin woven fabric of E-glass in the warp and R-glass in the weft as compared with non-hybrid 8-harness satin woven fabric of E-glass both in the warp and the weft. The materials specification details are highlighted in chapter four.

The lack of experimental data and conclusions on R-glass prompted the setting up of a research programme at Bournemouth University in collaboration with Interglas Technologies, Sherborne UK. The results of this research programme using R-glass will provide a useful contribution expanding the field of glass fabric composites.

The aims of this research are to examine and highlight the significant differences in the properties of R-glass compared to those of E-glass in woven fabric composites and, specifically, to answer the following:

- Does R-glass complement E-glass in the hybrid and lead to improved properties?

- Does the fabric weave architecture significantly influence the micro- and macro-mechanical properties of the E- and R-glass composites?

- Is it possible to achieve higher mechanical performance without hybridisation?

The objective of the research is to determine the role of fibre hybridisation and fibre volume fractions on the damage mechanisms in glass fibre woven composites under different loading conditions.

Results of mechanical tests including ILSS, flexural, tensile and viscoelastic properties of glass woven composites are discussed in chapter five and summarised in chapter six.

Acoustic Emission (AE) was successfully employed on glass woven fabric composites during mechanical testing (ILSS, flexural and tensile). The AE ring down count complemented the stress-strain or load-displacement curves in order to contribute a better understanding of micromechanical failure of the composite. Features such as knee points and stress at breaking point for each stress-strain curve could be analysed accordingly through the use of AE zone classification. AE was used successfully to detect the damage caused by the different loading modes such as crack initiation, debonding, matrix damage, and fibre/matrix interfacial failure and fibre breakage of composite materials of woven fabric laminates.

In chapter five, a model has been developed derived from the damage events sequential process. The model is an experimental analysis model, supported by DMTA, AE, SEM and visual examination of specimen fracture surface. The damage event sequential process analysis has been used in relation to the outcome of a theoretical bridging model introduced by Ishikawa and Chou (Chou1992) as further development to the model. This work has shown that applying available test data into a mathematical model is an essential progression.

The DMTA is used to characterise the influence of fibre surface treatments in the glass woven composite and its interphase region. This is an issue of great importance; the interphase properties often dictate the overall mechanical performance and structural integrity of the composite.

The fabric weave architecture, which was chosen to investigate the hybrid effect, seems to have a major influence on the mechanical properties. Other weave hybridisation can be predicted from the outcome of the analysis which indicates higher mechanical performance (see further future work – chapter six).

One of the main aims of this research is to study material costs from an industrial point of view, and also to provide the designer with the necessary tools to develop the application. For example the cost of an E-glass bobbin is £ 7 while the cost of an R-glass bobbin is £ 49 (Vetrotex, 1999).

1 – 2 Objectives and Scopes of the Research

The main objective of this research is to determine the role of fibre hybridisation and the role of different fibre volume fractions in the mechanical properties of glass woven composites. Glass fibre woven fabric reinforced epoxy resin composites were used to investigate the following:

- Uniaxial tensile, flexural and interlaminar shear tests of non-hybrid E-glass woven fabric at four different fibre volume fractions in reinforced epoxy laminates.

- Uniaxial tensile, flexural and interlaminar shear tests on hybrid woven fabric composites in reinforced epoxy laminates. Tests were carried out in warp and weft directions and to be compared with non-hybrid fabric composites.

- The viscoelastic properties of the above composites were investigated in order to determine the role of fibre surface coating on the composites by using dynamic mechanical and thermal analysis (DMTA) tests.

- Acoustic Emission (AE) during testing and Scanning Electronic Microscopy (SEM) was employed to analyse the damage event sequential process after testing.

- Test results of the hybrid and the non-hybrid composites to be compared based on one to one for similar fibre volume fraction and specimen dimension for both the warp and weft.

- Test results of the hybrid at fixed fibre volume fraction to be compared with the non-hybrid at different levels of fibre volume fraction composites for similar specimen dimensions. This methodology can contribute to the understanding of the role of fibre hybridisation and that of different fibre volume fraction influence. The results deal with the comparison in the mechanical properties of glass woven fabric composites.

CHAPTER TWO

CHAPTER TWO

Hybrid Glass Reinforcement

2 – 1 Characteristics of Glass Fibre

The fibres manufactured from E-glass are so called because of their good electrical insulation properties. E-glass is by far the most common composition of glass used for fibre manufacture. It was initially produced for manufacture of composites in the 1930s; since then, and for the last thirty years in particular it has been the standard material for fibre reinforced composites (Bader and Lekakou 1997). There are a number of commercial compositions of glass fibre produced today. These are mainly based on silica (SiO_2) with additions of oxides of calcium, magnesium, boron, iron and aluminium (Hull 1996, Jones 1994, Mettes and Lubin 1969). Some of these compositions are shown in table (2 – 1).

In the production of glass fibres, various glass compositions are synthesised to provide the desired properties. For example, C-glass is chemical resistant, alkaline (more than 10%) and contains soda lime-silicate; A-glass is good for thermal and sound insulation and has a very low alkaline (less than 1%) content (Hull and Clyne 1996).

Generally, it should not be considered that there is only one glass for a given name. For example, the code "E" glass covers a multitude of variations around a theoretically standard composition (Molinier 1982). These variations depend on the origin of the vitrifiable raw material, the technological skill used by each manufacturer and the legislation existing in the manufacturing countries (for example anti-pollution) (Interglass Technologies 1999 and 1998).

The strength of glass fibres when measured at room temperature is a function of the glass composition according to Loewenstein (Loewenstein and Dow 1968). It has been detected that there was variation in fibre strength when fibres were taken from the virgin glass during the manufacturing of fibreglass. Aslanova reported strength measurements on glass fibres with various compositions, e.g. the strength for A, C and E glasses are 1.5, 2.0, 3.7 GPa respectively for these types of glasses, the modulus of elasticity varies relatively from 55-86 GPa (Aslanova 1985). The breaking stress values as mentioned were obtained with virgin filaments; filaments refers to the basic unit formed during spinning, which are gathered into yarn for use in the composite. Filaments usually are of extreme length and very small diameter, usually less than 25

μm. Designers are not directly interested in the properties of virgin filaments yet these values enable comparisons to be made between various fibres. However, it must be remembered that the properties of reinforced plastics, particularly the mechanical ones, are also dependent on the nature of the reinforcement, the standard of the manufacture, the resins used, the process and the yarn employed (ASM International 1987).

The other types of glass fibres including S-glass and R-glass, exhibit better mechanical properties than E- and C-glass, and both S-glass and R-glass have a high resistance to chemical corrosion. Glass mechanical properties of some types of fibreglass are presented in table (2 – 4).

Glass physical properties such as density and hardness for some glass fibre are illustrated in table (2 – 2). Glass thermal properties such as the softening point, strain, linear coefficient of thermal expansion, specific heat and coefficient of thermal conductivity are given in table (2 – 3).

2 – 1 – 1 Glass fibres manufacture

Glass fibres are manufactured as continuous filaments drawn from the molten glass raw material mixed in a furnace. Good mixing is very important to achieve the required homogeneous composition. The molten glass is then drawn under gravity through a series of bushings each having about 200 holes, each of which is typically in the range of 5-30 μm in diameter. The filaments are cooled and formed into bundles commonly containing between 200 and 2000 individual filaments. Since the drawn glass bundles are susceptible to abrasion and moisture attack, a fibre surface coating (known as a size) is applied. This size is generally applied in solution form and usually contains a polymer to coat and bind the filaments together in the bundle, a lubricant to reduce abrasion damage and increase handleability and a coupling agent which aids the filaments in adhering to the polymer matrix (Loewenstein 1983).

2 – 2 Fabric Structure

The first use of textile glass fibre on an industrial basis was around 1940 and this was for the insulation of electrical conductors used at high temperatures. It was the appearance of the thermosetting laminating resins, some years later, which gave continuous glass fibre its second application namely that of a reinforcement material.

This application increased extensively after the end of the Second World War, to an ever-greater number of thermosets and thermoplastics. This is the basis of the ever-increasing demand for glass fibre today. This remarkable expansion in the use of E-glass with high performance quality is the result of exceptional combinations of mechanical, electrical, dielectric and corrosion-resistant properties, e.g. glass-woven and glass-roving.

In the majority of cases fibres need to be processed into an intermediate form of reinforcement before they can be used in the production of composite structures. The type of reinforcement as chosen for a specific application is very important as it affects cycle times, determines fibre volume fractions, permeability and the final mechanical properties of the composite product. The list below describes some of the more common types of fabric reinforcement (ASM International 1987).

Chopped Strand Mat (CSM).
Continuous Random Mat (CRM).
Woven Fabric (WF).
Triaxial Fabrics.
Knitted Fabrics.
Braided Fabrics.
Three-Dimension Fabrics.
Non-Crimp Stitch Bond Fabrics

2 – 3 Glass Woven Fabrics

Fibres can be woven into many different types of weave patterns, widths, and thickness. The warp yarns, or ends lie in the lengthways (machine) direction of the fabric, whereas the filling yarns, or picks, lie cross-wise, at right angles to the warp yarn. Fabric construction is specified by the number of warp yarns per centimetre of fabric width and the number of filling yarns per centimetre in the length-wise direction. Therefore, fabric weight, thickness and breaking strength are proportional to the number and types of warp and filling yarns used in weaving.

Woven fabrics are widely used to reinforce polymer matrices, since they are easy and convenient to handle. The volume fractions of fibres are not high, because of the interlacing of fibres, yet the composite products have adequate properties for a range of markets.

2 – 4 Weave Pattern

The fabric design pattern often called the construction is the x, y co-ordinate system. The y-axis lies along the direction of the warp yarns and is the long axis of the fabric roll. The x-axis is the fill (weft) direction, that is, the roll width. The basic fabric weaves are few in number, but combinations of different types and sizes of yarns with different warp/fill counts allow hundreds of variations. The fabrics may be woven in a variety of patterns some of these weave patterns are presented in figure 2 – 1, (Interglass Technologies 1999 and 1998).

2 – 4 –1 Plain weave

Plain weave, which is the most highly interlaced, is therefore the tightest of the basic fabric designs and most resistant to in-plane shear movement. In a plain weave the warp and weft yarns are interlaced in a regular sequence of one under and one over (see figure 2 – 1). The plain weave demonstrates the greatest degree of stability with respect to yarn slippage and fabric distortion. The closely spaced yarns prevent sideways movement of yarns in the fabric, thus providing good distortion resistance and reproducible laminate thickness. The stiffness of the fabric in the warp and weft directions depends on the tightness of the weave and the properties of the yarn (Hofstee and Van Keulen 2001).

2 – 4 – 2 Basket weave

Basket weave, a variation of plain weave, has warp and fill yarns that are paired: two up and two down. The basket weave is less stable than the plain weave; it is more pliable and will conform more readily to simple contours.

2 – 4 –3 Twill weave

The twill weave interlaces one or more warp yarns over one and under two or more filling yarns in a regular pattern, e.g. in a 2×1 twill, weft yarns passes over one and under two warp ends (see figure 2 – 1). While in a 2×2 twill, the weft yarns pass over two and under two warp ends, producing a regular diagonal pattern in the cloth. Twill weave cloth has good drapability. This produces either a straight or a broken diagonal line in the fabric and consequently it has greater pliability and better drapability than both plain-woven and basket-woven fabric.

2 – 4 – 4 Satin weaves

The satin weaves represent a family of constructions with a minimum of interlacing. In these weaves, the weft yarns periodically skip, or float, over several warp yarns, as shown in figure (2 – 1). In the satin weave, there is only one interlacing point per pattern as repeated per yarn. The eight-end satin weave has one warp yarn interlacing over seven under one filling yarn in an irregular pattern, yielding to a pliable fabric that will readily conform to compound contours. Since this weave pattern allows a comparatively high yarn count per centimetre and fewer fibre distortions, it translates into better strength properties in all directions than a tighter weave, such as the plain weave.

The floating yarns that are not being woven into the fabric create considerable looseness or suppleness. The satin weave has excellent drapability that can produce a construction with low resistance to shear distortion and is easily moulded (draped) over compound curves as indicated in figure (2 – 2). This is one reason why the satin weaves are preferred for many aerospace applications, mainly for the aircraft wingroot area. Satin weaves can be produced as standard four, five, or eight-harness forms. Fabric woven with heavy warp yarns and fine filling yarns in long-shaft (such as the 8-end) satin weave patterns are called unidirectional fabric. These fabrics are characterised by a high strength contribution to composite in the heavy-yarn (warp) direction (Chou and Ko 1989).

Woven fibre reinforcements offer the following advantages compared with unidirectional reinforcements:

- Improved formability and drape
- Bi-directional reinforcement in a single layer
- Improved impact resistance
- Balanced properties in the fabric plane
- Enhanced through-thickness properties
- Elimination of interlaminar weaknesses, improved fracture toughness
- Yield constructions of tailorable thickness with enhanced through-thickness properties.

2 – 4 – 5 Hybrid fabrics

Hybrid fabrics are those woven from two or more different types of fibre (see figure 2 – 3), in contrast to fabric woven from a single type of fibre (Interglas Technologies 1999 and 1998). Combining fibre reinforcement allows the designer a considerable amount of flexibility. The hybridisation of glass fibres in composites provides higher material with a greater strength and modulus. The glass fibre composites can be improved by adding high-strength fibres (such as R-glass) with a greater strain-to-failure than the E-glass. Glass hybrid composites can be lubricated using conventional techniques. Hybrids usually have the same matrix and can be fabricated by the co-curing process (Chou and Ko 1989).

2 – 5 Types of Hybrid Laminates

Composites containing more than one type of fibre material are known as 'Hybrid'. The term 'hybrid' is commonly used to denote the incorporation of two different types of material into one single material, and the level of mixing can be either on a small scale (fibres, tows) or a large scale (layers, pultrusions, ribs). Hybrid composites are attractive structural materials for the following reasons.

- Firstly, they provide designers with the new freedom of tailoring composites and achieving properties that cannot be realised in binary systems containing one type of fibre dispersed in a matrix.

- Secondly, a more cost-effective utilisation of expensive fibres such as carbon and boron can be obtained by replacing them partially with less expensive fibres such as glass and Aramid.

- Thirdly, hybrid composites provide the potential of achieving a balanced chase of stiffness, strength and ductility, as well as bending and membrane-related mechanical properties.

Hybrids can be categorised into the following types:

2 – 5 – 1 Intraply

The different fibre materials are intimately mixed together and infiltrated with a matrix simultaneously. The hybrid in this case is described as intraply or intermingled as presented in figure (2 – 4a) (Chamis and Lark 1978) (Aveston and Kelly 1980).

2 – 5 – 2 Interply

Hybrid is made by bonding together separate laminae each containing just one type of fibre in a matrix, and is known as Interply (Chamis and Lark 1978) or interlaminated (Aveston and Kelly 1980) as indicated in figure (2 – 4b).

2 – 5 – 3 Interwoven

Hybrids consist of fabric reinforcements where each fabric contains more than one type of fibre and it can be termed as interwoven (Chou and Kelly 1980a) as presented in figure (2 – 4c).

2 – 5 – 4 Hybrid interface

An attempt is made to fabricate glass woven fabric composite laminates containing layers of different fibre surface treatments, based on the so-called 'hybrid interface' concept. The mechanical properties of hybrid laminates, including strength and elastic moduli are characterised and compared with those for non-hybrid laminates. The results show some improvements in tensile and bending strength when the laminates consist of hybrid layers containing low and high silane concentrations (Sham, Kim and Hamada, 1998).

2 – 6 Fibre Surface Treatments

When the fibre is made from a continuous filament, winding is the final process at the time of forming, and refers to the process whereby a continuous filament of fibre is wound on to a supporting form. Such a treatment is called a size such as a silane-coupling agent.

Silane coupling agents are hybrid molecules: a mixture of lubricant, binder, coupling agent and a greater part of demineralised water. The lubricant is added to prevent abrasive damage to filaments while handling because glass has a very high coefficient of friction. Antistatic agent hampers the build-up of static electricity during processing. The binder provides compatibility with specific resins or polymers. High mechanical strength and wet strength retention in composite materials can only be obtained when a high quality and durable glass-matrix bond exists (Plueddemann 1974). Silane coupling agents (Organo-functional) are designed to improve the performance of interfacial properties of glass fibre reinforced polymer matrix composites (Plueddemann 1974).

$$R\text{-}Si\text{-}X_3 + 3H_20 \rightarrow R\text{-}Si\text{-}(OH)_3 + 3XH$$

R is an Organo-functional group that is chosen to be compatible with the matrix resin to be employed. For epoxy matrices the functional group is often an amine or an amine slat and X is a group that is easily hydrolysable (Hull and Clyne 1996). Park and Kim studied surface treatment of carbon fibres; they reported that, increasing the surface functional groups on fibres increased composite mechanical behaviour. The study revealed that oxygen functional groups on fibres had a dominating effect on the interlaminar shear properties of the composite whereas the nitrogen-functional groups were not affected in this system (Park and Kim 2000).

For the treatment of fibreglass, it is required that the silane should be soluble in water and the dilute aqueous solution remains predominantly monomeric for at least one day in the treating bath. When dried on the glass surface, the coupling agent must condense to polysiloxane structures that retain a degree of solubility in order to be compatible with the resin.

Silane coupling agents are usually applied to glass fibre surfaces as part of the sizing resin, which is commonly in the form of an aqueous solution adjusted to pH4 with acetic acid. When comes into contact with the glass surface a layer of silane molecules is formed on the surface. Silane agents are intended to act as a protective coating for glass fibre surfaces and as a coupling agent to promote the adhesion with the polymer matrix. The silane agents are applied to the glass fibre surface as a size along with other components. A wide variety of organofunctional silanes have been developed, prominently by Plueddemann and co-workers. The silane hydrolyses during the preparation of the solution. A condensation reaction resulting in the

formation of oligomeric siloxanes (Plueddemann 1974a, 1991 and Pape and Plueddemann 1991) follows the hydrolysis of silanes to silanols. It is thought that fast hydrolysis is followed by a slow condensation process (Plueddemann 1974b) as the higher oligomers are probably not as good as the monomeric cilantro, at promoting adhesion (Plueddemann and Stark 1977). Hydrolysis of silanes, and the subsequent condensation reaction are dependent on the organofunctionality of the silane and the concentration and pH of the solution (Ishida et al. 1989a,b).

There are other modes of applying silanes such as dry blending used for mineral fillers, and the additive method in which the silane is added to the polymer phase. Silane diffuses and reacts to inorganic surfaces (Drown et al.1992, Cheng et al. 2001).

In order to enhance the bond between fibre and matrix, modified fibre surfaces need to be achieved by coating the fibres with silane reactive end groups (silane coupling agents) (Tesero and Wu 1991; Drzal 1985).

The rubber emulsion coating is a solution of different polymers such as polyurethane and polystyrene (Schlud and Lambla 1985), elastomer coating (Gerald et al.1998), PVAL (Park and Kim 2001) and Chromium complex, orthosilicates and titanates (Ahlstrom et al. 1995).

2 – 7 Interface

If the surfaces of two bodies come into intimate contact, the combination of two dissimilar faces in composite materials creates an interface between the two. In theory, this interface represents a 2D surface of contact between the components. To achieve efficient stress transfer, optimum adhesion is required between the matrix resin and the fibres. It is understood that, to attain good composite properties, it is necessary to transfer stress efficiently from the matrix resin to the load-bearing fibres in a given composite system. (Hull et al.1996). Hence the adhesion between fibre and matrix is a key consideration with respect to understanding the interfacial properties of composite materials. The theories of adhesion including wettability, inter-diffusion and chemical reaction covalent bonding, electrostatic inter-attraction, mechanical inter-locking and residual stresses are important interfacial adhesion phenomena in fibre reinforced composites.

The interfacial region of the composite will be affected not only by the composition of the coating, but also by its distribution on the glass fibre surface and in the composite matrix (Thomason 1995).

2 – 8 Interphase

It has been suggested recently that there is an existing three-dimensional region, interphase (or Mesophase) adjacent to the reinforcing fibre, where properties differ from both the fibres and the bulk matrix as represented in figure 5 – 27 (Drzal 1985), (Theocaris 1987). The properties depend on how this interphase is formed. It may be homogeneous and distinct or exhibit a composition, and hence a property and gradient which approaches that of the bulk matrix some distance away from the fibre. Traditionally, a two-dimensional surface of contact (interface) between fibre and matrix has been assumed to be responsible for the effective transfer of stress from matrix resin to load bearing fibres (Hull and Clyne 1996). It has been proposed that the interphase may be a chemical reaction zone, a diffusion zone, a nucleation zone, or a combination of them all (Ranade et al. 1997) and (Agrawal and Drzal 1996).

The interphase region possesses features such as: a finite dimension and thickness (Kim and Sham 2001), the bond mechanism to the fibres and bond mechanism to the matrix, properties of its own such as strength, modulus, Poisson's ratio, etc. (Drzal 1985) and (Thomason and Adzima 2001).

The influence of the interphase region on the mechanical properties of the composite has received wide attention. A good description of the mechanical properties of the interphase region between fibre and matrix allows a good prediction of the mechanical properties of the composite. The overall properties of a fibre-reinforced composite material are dependent upon the mechanical and chemical stability of the interfaces, or interphase, formed between the reinforcing fibres and the surrounding matrix (Ranade et.al. 1997) and (Agrawal and Drzal 1996).

Fibre/resin interface in composite materials is very important for material design because the **interphase** properties greatly affect the macroscopic mechanical properties of the composite. Various evaluation methods for interphase in composite materials have been proposed, such as

- Single-filament embedded tensile test,

- Pull-out test,
- Push-out test, etc.

It is considered that 'interphase' should mainly be divided into four types such as

1. Pure interphase between filament/matrix (Class I),
2. Fibre bundle interphase between filament/matrix (Class II),
3. Intersection interphase between two fibre bundles, which often appears in woven fabric (Class III) and
4. Interlaminar interphase in laminated composites (Class IV).

Each classified interphase is evaluated using various testing methods. This classification is one of the concepts to assist with the understanding of micro-macro interaction in composite materials (Hamada 1997).

Mathematical models take into account the two Mesophase layers (or interphase) formed between the main phases as boundary layers responsible for the quality of adhesion between phases (Theocaris 1987, 1988, 1990, 1992, 1995 and Theocaris et al.1997). The interphase layers are proposed for predicting the mechanical properties of sized fibre-reinforced composites. Several micro-mechanical models are developed to calculate the mechanical properties of composites; the experimental validation of these proposed models is often carried out on glass fibre/epoxy composites (Tirry et al. 1997).

2 – 9 Epoxy Resins

Epoxy resins are used extensively in composite materials for a variety of demanding structural applications. They are the most versatile of the commercially available matrices. They make it possible to obtain toughness, chemical and solvent resistance, mechanical responses, resistance to creep, and excellent adhesion to most fibres, heat resistance and excellent electrical properties. Epoxy resins have a broader range of physical and mechanical properties than unsaturated polyester and polyamides (Lee and Neville 1967).

Epoxy is the general classification for resins containing two carbons and one oxygen atom bonded in a ring. Such resins may be derived from many different starting materials such as phenol, bisphenol and multifunctional phenol (ASM International 1987)

Epoxy resins have superior strength and elastic properties with a lower shrinkage on curing. The strength of the interface bond between resin and fibre is also higher for epoxy resins. However, they have the disadvantage of a higher viscosity before curing, and epoxy is more expensive. Commercially available epoxy resins crosslink to a solid by reaction with a variety of hardeners. These hardeners may act as catalysts via catalytic action or become directly involved in crosslinking formation during the reaction by being absorbed into the resin chain. During curing, epoxy resins can undergo three basic reactions (Ashcroft 1993):

1. Epoxy groups are rearranged and form direct linkages between themselves.
2. Aromatic and aliphatic hydroxyl groups react with the epoxy groups.
3. Cross-linking occurs with the curing agent via various radical groups.

The glass fibre sizing system, containing a silane-coupling agent, results in a composite with a higher modulus, and a greater tensile strength, but a lower toughness compared with glass fibre without the silane-coupling agent (Drzal et al. 1991).

2 – 10 Acoustic Emission (AE)

Acoustic Emission testing procedures have been well established in codes of practice for monitoring damage processes and characterisation of composite structures. Because of the complex nature of the composite material, the fracture processes occurring in composites are very complex and difficult to study. Hence, AE techniques can be used advantageously to study the micro-fracture phenomena during straining of composites. The simplicity of its application, the acquisition of data in real-time and its potential for monitoring damage progression and accumulation make acoustic emission a useful experimental tool.

Non-destructive testing methods such as Ultrasonic, Radiography and Eddy currents are also commonly used for detection of flaws in composites. The AE technique on the other hand allows the characterisation of the initiation and growth of flaws by utilising the information supplied by the deformation, as the deformation propagates in the material.

2 – 10 – 1 Acoustic Emission in glass and glass fibre

Glass is a brittle material. Fracture occurs in the elastic portion of the stress-strain curve, where the slope is constant and equal to Young's Modulus. In comparison to glass, metals undergo a certain amount of deformation by plastic flow before failure. Plastic flow requires breaking bonds at one position, with subsequent movement of the atoms and bond formation at some other site. In glass, plastic flow is restricted. Hence, in an amorphous solid, such as glass, fracture rather than flow is the natural consequence of bond breakage (LaCourse 1972).

Glass exhibits a complex interdependence of strength on degree of surface damage, loading rate, temperature and nature of environment.

The recording of AE events shows that these correspond with the number of fibre breakages; failure modes can be identified. The large number of events occurring at final failure is usually associated with fibre breakage. In bending tests of single-fibre composites, AE parameters especially the peak frequency and its power energy obtained by a power spectrum analysis are useful in the interpretation of damage events. (Don and Roderic 1996). A transition of failure mode from fibre break accompanied by a matrix crack and debonding to buckling is observed when the stress in the embedded fibre changes from tension to compression. The debonding length is greatest near the loading point for the specimen with fibres near the tensile surface (Jinen et al.1997).

2 – 10 – 2 AE in composites

In composites, the stress waves are generated by a variety of actions involving cracking and separation in the fibres and the matrix. Material strain is required to release or generate the emissions; the simplest method to obtain an indication of AE activity is ring down counts (RDC). Appendix B gives more details on (RDC).

The AE signal in fibre-reinforced polymer (FRP) composites will be mainly from the matrix, the fibre and the interface between the matrix and fibre. Experiments using continuous glass fibre reinforced polyphenylene sulfide (PPS) composite, loaded in flexure, show that the first detectable AE signal is at about 0.3% strain level (Chen et al. 1992).

The acoustic emission (AE) technique appears to offer a very practical procedure for monitoring the failure processes in polymer matrix composites. Polymer matrix composites subjected to stress emit acoustic signals when micro-cracks occur, due to failure of the matrix, delamination, or fibre rupture. Moreover, this technique is more readily used in actual service conditions. An important aspect of the AE technique is that the information obtained is in real time. Once the instrumentation settings have been properly selected for a given assessment, the technique is very simple to utilise. On the other hand, AE by its nature is applicable only during proof loading. This may limit its usage in certain aeronautical and aerospace applications, although it is widely used to assess the integrity of composite structures in the chemical and automotive industries. For small-scale laboratory testing on well-defined samples, the AE technique can serve as a supportive test procedure for research into the failure process of new composites. It provides a non-destructive inspection of the material in order to locate and indicate the extent of non-visual damage.

A significant amount of research during the past two decades has addressed the viability of AE as a non-destructive test technique for composite materials.

Narisawa and Oba established a correlation between an acoustical signal and the fibre breakage by analysing the amplitude signals in a composite containing one or two fibres (Narisawa and Oba 1984). Mehan and Mullin first identified the possibility of correlating a specific failure from an acoustic signature (Mehan and Mullin 1971). They established the relevance of frequency spectral analysis to reconstruct the whole failure process. The problem in establishing a relationship between a specific failure mode and its acoustic signal is the simultaneous occurrence of different failure modes. Therefore, listening to noise in real-time using piezoelectric sensors makes it possible to give an interpretation of the events taking place in the material. Observations indicate that fibre-reinforced composites fail as a result of discontinuities generated by progressive damage that occurs during loading, making it possible to determine the integrity of composite materials (Arrington M. 1987).

The fibre and matrix dominated failure modes contribute to AE in composites. Matrix dominated failure modes include matrix cracking and ply delaminating (Ma et al. 1990). Failure modes for fibre include fracture and fibre micro buckling (Mittleman and Roman 1987). AE has also been employed by many researchers to probe the fibre-matrix interfacial failure between a fibre and a matrix (Netravali et al. 1991 and Bondt et al. 1993) and (Okoroafor et al. 1996). It is

important to identify and understand the AE characteristics of each of these modes individually in order to estimate flaw growth in relation to strength properties of composites (Choi and Lee 2001). Applications of AE of interest to research and industry are ongoing and the future in these areas appears unlimited.

In unidirectional composites matrix cracking and voiding are typically associated with the first signs of non-linearity on the stress-strain curve of a composite. Low AE activity corresponds with matrix damage i.e. cracking and voiding (Wevers 1997 and Kander 1991).

The intermediate AE activity corresponds with fibre-matrix interfacial damage in these composites. Debonding of fibres from the matrix resin typically leads to a decrease of the stiffness in the composite. The lowest level of intermediate AE activity could indicate shear lines initiating along the neutral axis. The highest level of intermediate AE activity indicates fibre-matrix damage and demonstrates a very small decrease in stiffness at the initiation of intermediate AE activity (Kander 1991 and Okoroafor et al. 1996). High AE activity indicates layer delaminations (Wang et al. 1995) or ultimate fibre damage and final breakage (Kander 1991).

Using two wide-band differential piezoelectric transducers allowed the location of the damage events to be determined by measuring the difference in the time-flight to each transducer for a given acoustic wave in the acoustic emission digitised signals location (Holford and Carter 1999).

A new methodology for the analysis of failure modes in composite materials by means of acoustic emission techniques has been developed. A single-carbon-fibre composite based on a polyester matrix has been used as a simple model. The occurrence of fibre-breakage during tensile loading tests has been observed by a polarised light microscope and concurrently detected by a resonant acoustic probe (Giordano et al. 1998).

Table (2 – 1) Glass compositions of some fibreglass*

	E-Glass	R-Glass	C-Glass	S-Glass
Silicon Dioxide (SiO_2).	52.4	60	64.4	64.4
Calcium Oxide (CaO).	17.2	9	13.4	-
Aluminium Oxide (Al_2O3)	14.4	25	4.1	25
Boron Oxide (B_2O_3).	10.6	-	4.7	-
Magnesium Oxide (MgO).	4.6	6	3.3	10.3
Sodium & Potassium OxideNa_2O & K_2O	0.8	-	9.6	0.3

* Data from (Hull and Clyne 1996), (Molinier, 1982), (Vetrotex 2000) and (Interglass Technologies, 1996, 1998).

Table (2 – 2) Physical properties of some fibreglass**

Physical Properties				
Properties	Unit	E-Glass	R-Glass	D-Glass
Density	g/cm^3	2.6	2.53	2.14
Hardness (Vickers 50g-15s)	-	5.6	6.2	
Sound Velocity	m/s	5680	5940	

**Data from (Vetrotex 2000)

Table (2 – 3) Thermal properties of some fibreglass*

properties	Unit	E-glass	R-glass	D-glass
Softening point(Littleton)	°C	840	986	769
Strain Point	°C	617	738	
Linear Coefficient of thermal expansion	m/m/°C	$5.3*10^{-6}$	$4.0*10^{-6}$	$3.0*10^{-5}$
Specific heat	J/g. °K	0.764 @ 20 °C 0.958 @ 200 °C	0.732 @ 20 °C 0.983 @ 200 °C	1
Coefficient of thermal conductivity	W/m. °K	1.0	1.0	0.8

*The glass fibre manufacturer (Vetrotex) provided these values in correspondence with author April 2000.

Table (2 – 4) Mechanical properties of some fibreglass**

	General Purpose Glass	Glass with resistance to acids		Glass with high mechanical performance	Dielectric glass	
	E Glass	A Glass	C Glass	R Glass	D Glass	Silica
Specific Gravity (g/cm^3) (filament glass)	2.59	2.46	2.45	2.53	2.14	2.2
Modulus of Elasticity (GPa) on filament	73	71	71	86	55	62-73
Breaking Stress (MPa) on virgin filament	3400	3100	3100	4400	2500	4000-5000

** Data from (Molinier, 1982), (Vetrotex 2000).

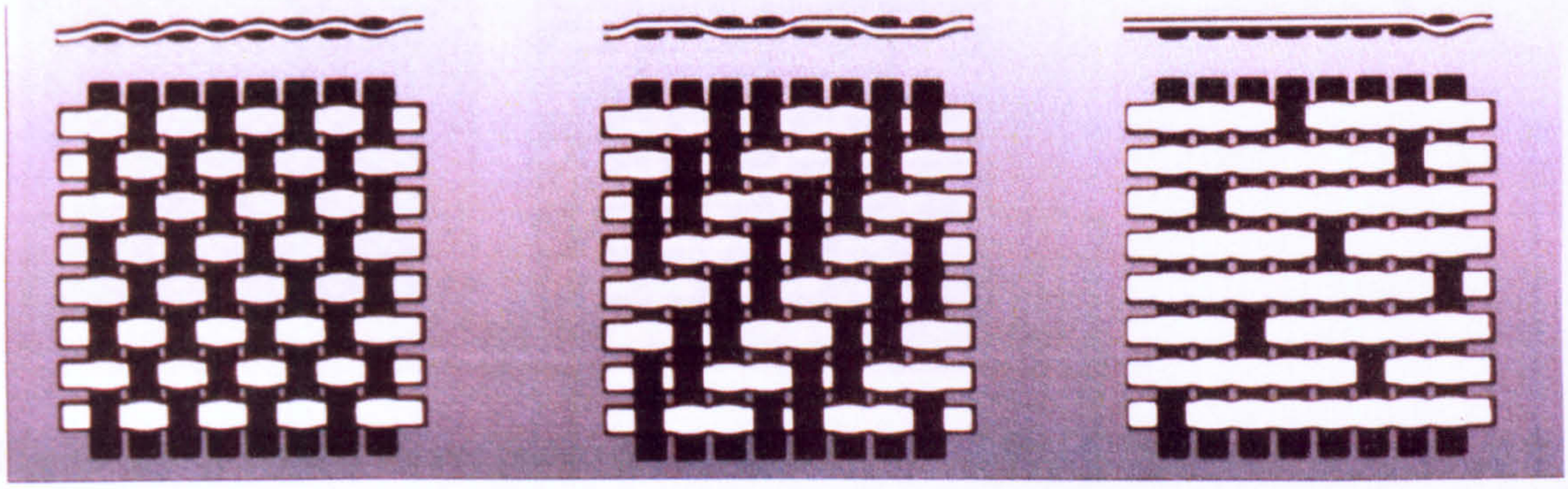

Plain weave Twill weave Satin weave

Figure (2 – 1) Three different weave patterns of fibre woven fabrics.

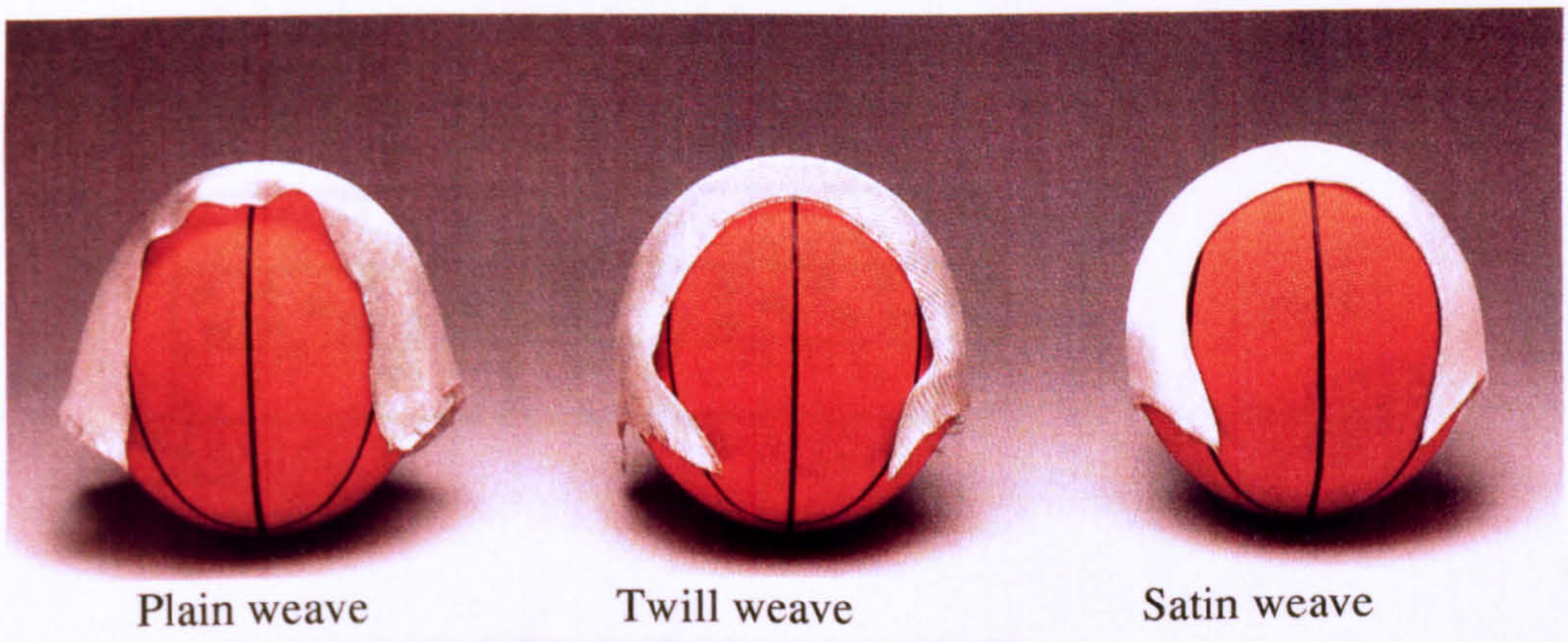

Plain weave Twill weave Satin weave

Figure (2 – 2) The difference in drapability between various weave patterns.

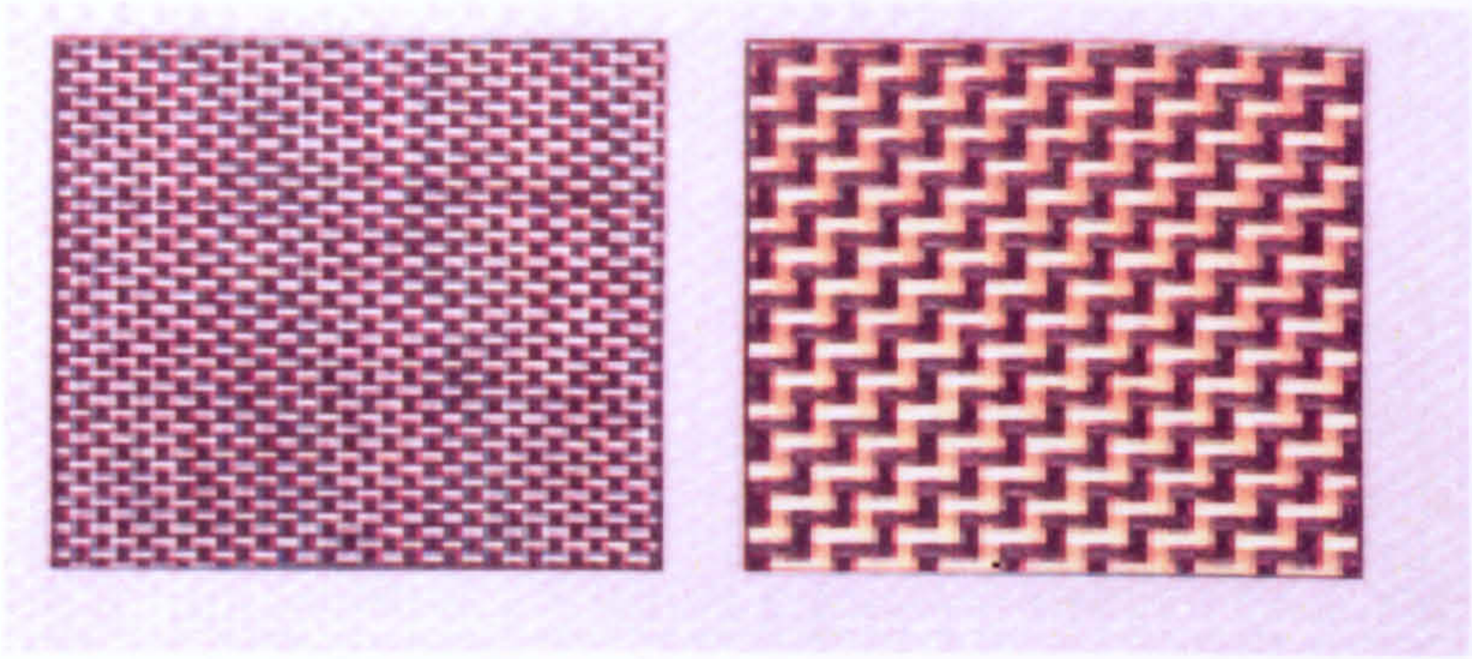

Figure (2 – 3) Hybrid weave patterns.

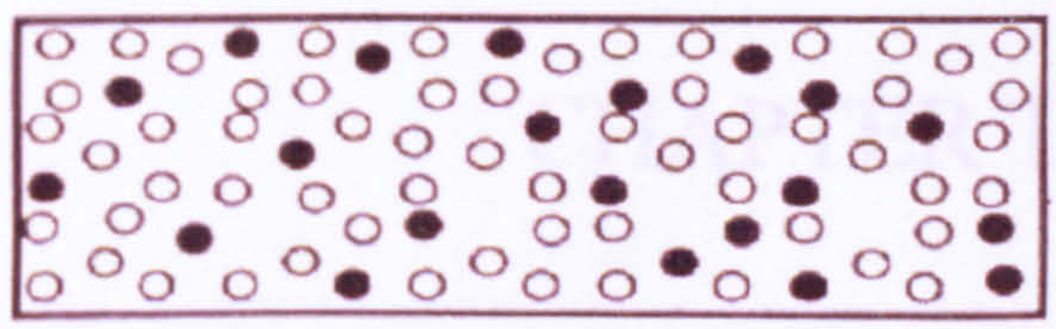

(a)

(b)

(c)

Figure (2 – 4) Three types of hybrid composites (After Chou 1996).
(a) Intraply or intermingled (b) Interply or interlaminated (c) Interwoven.

CHAPTER THREE

CHAPTER THREE

Mechanical Characterisation

3 – 1 Elastic Properties of Woven Fabric Composites

This section presents models which enable the elastic properties of woven fabric reinforced composite materials to be predicted. There are many models that have been developed to predict the elastic properties of composite materials based on continuous non-woven reinforcement. However, the number of these models which may be used to predict the properties of woven reinforced materials is small (Halpin 1984, 1994). For the purposes of this investigation, the theories and models that have been specifically developed to predict the elastic properties of thin laminated composites are the classical laminate theory and simple rule of mixture. The predictions of the models that are compared with the results of experimental data are discussed in chapter five.

3 – 1 – 1 Classical Laminate Theory (CLT)

In the Classical Laminate Theory it is possible to predict the macroscopic elastic properties of the laminate from knowledge derived from the individual lamina (layer) properties, and retrospectively to calculate the individual stress system within each lamina when the laminate is subjected to an applied loading. CLT treats individual laminae as macroscopically homogeneous, yet orthotropic in their elastic properties. The material constants such as stiffness do not vary with strain, the strains in the deformed plate are small, and also shear strains in planes perpendicular to the surface are assumed to be zero. The theory assumes that the laminate is in a state of plane stress, hence ignoring the interlaminar effects and the out-of-plane stress components. More details can be found in appendix A.

When the thickness direction properties significantly contribute to the response of the laminate to an externally applied elastic field, the classical plate theory breaks down (Chou 1992, Enie and Rizzo1970). The analysis is applicable to thin plies in which out-of-plane stresses and deformations can be neglected (Ashton et al. 1969), (Jones 1975), (Griffin et al 1981), (Enie and Rizzo 1970), (Whitney 1967) and (Rosen and Humphreys 1987). General lamination assumptions can be found in appendix A.

The classical thin laminated theory has been extended to take into consideration the effects of thermal and moisture diffusions, with particular emphasis on the transient behaviour. Because of the large differences in the magnitudes of the thermal conductivity and moisture diffusion coefficients, the thermal and hygroscopic problems can be solved separately and their linear elastic fields can be superposed to yield the stress concentrations due to transient thermal effects (Chou 1992).

The classical lamination theory has been applied to derive the constitutive equations for a cracking layer so as to describe laminate constitutive behaviour in the cracking process, in an analytical model of laminated composites with cracking layers (Wada, Motogi and Fukuda 2000).

The classical lamination theory describes the damage evolution in Fibre Reinforced Plastics (FRP) laminates with off-axis cracked plies in another analytical model for predicting the matrix crack which induces stiffness reduction of FRP laminates. With the predicted number of cracks, the variation of the laminate stiffness with the crack density is evaluated (Wada, Motogi and Fukuda 1999).

3 – 1 – 2 Software packages

Over the years many software packages have been developed to analyse elastic constants of the composite laminates. Attention is focussed on currently available design analysis procedures for fibre-reinforced polymer composites. Johnson describes some of the microcomputer programmes available to simplify laminate analysis (Johnson AF 1988, 1990 and 1995). The National Physics Laboratory (NPL) has also developed software to analyse laminates in the project entitled "predictive modelling of fibre reinforced polymer composites" (Broughton 1992).

Similar software to that of NPL is produced by SDRC in their "IDEAS" package. The SDRC software package gives the user the choice of using micro-mechanical theories for the property predictions. This implies that the user needs to be familiar with the different theories before using the software. In both the NPL and SDRC packages, the through-thickness properties whilst said to be important are not determined.

Some other software computer packages by Cirese (Cirese 1988), COMPO (Blankenship et al.1992) and a further commercial package called Mistra analyses the geometry of a unit cell of the material which is input by the user.

There are many software packages to determine mechanical properties of woven fabric composites. Stellbrink has developed the micro-mechanical software called Microlam to analyse laminated composite structures; this software can treat fabrics with different fibres in the warp and fill directions. However, Microlam assumes that both thread types in the same direction follow the same geometric shape. Some of the Microlam software inputs are related to the woven structural parameters and others are related to the fibre mechanical properties of the material. The software allows the user to select some of the fabric identification such as the fibre type, weaving pattern type (unidirectional, twill, satin etc.); details are given in chapter five, section 5 – 7.

The package will then calculate the strength of unidirectional or woven laminate plates, for example, and also predict the material properties of the laminate using the classical laminate theory in the calculation (Stellbrink 1996). The mechanical properties of woven laminate can theoretically be predicted and then compared to test results; details are given in chapter five.

3 – 1 – 3 The simple rule of mixtures

The geometry of thin, continuous fibre in a unidirectional array ensures that, when loaded in the fibre direction, the strains in the fibre and resin matrix are equivalent. For this reason the rule of mixture can be used with reasonable accuracy (Kelly and Nicholson 1971 and Vinson and Chou 1975), to predict the longitudinal modulus and tensile strength, i.e.

$$E_l = E_f V_f + E_m (1-V_f) \qquad (3.1)$$

and

$$\sigma_l = \sigma_f V_f + \sigma`_m (1-V_f) \qquad (3.2)$$

Where

E_l = composite longitudinal modulus

E_f = fibre longitudinal modulus

E_m = matrix modulus

V_f = fibre volume fraction

σ_1 = composite longitudinal tensile strength

$\sigma`_m$= matrix stress at fibre failure strain

σ_f= fibre strength

The rule of mixture strength prediction above is valid only where the matrix failure strain is greater than the fibre failure strain. This is the case for most practical polymer matrix composites.

A modified law of mixtures was used to predict the longitudinal Young's modulus for woven material composites (Johnson 1986).

$$E_1 = E_m (1-V_f) + \alpha E_f V_f \qquad (3.3)$$

The parameter "α" depends on the efficiency of reinforcement, which allows for slight fibre misalignment.

Theocaris modified the equation in (3.2) by introducing a third term to account for the modulus (E_i) of a third phase, called the (Mesophase) or interphase (Theocaris 1987).

$$E_1 = E_f V_f + E_m V_m + E_i V_i \qquad (3.4)$$

In a typical composite, both V_i and E_i are expected to be rather small. The longitudinal stiffness of the composite should be almost insensitive to the interface properties. Mathematical models, which take into account the two Mesophase layers (or interphase) formed between the main phases as boundary layers responsible for the quality of adhesion between phases, are proposed for predicting the mechanical properties of sized fibre-reinforced composites. Application of the models to an analysis of composites based on silane-coated glass fibres and epoxy resin are discussed by (Theocaris 1987, 1988, 1990, 1992, 1995 and Theocaris et al.1997).

The rule of mixture strength prediction is found experimentally to be a good approximation, as the above approach neglects the statistical nature of fibre strength, which results from the

distribution of flaws of varying severity within fibres. This mechanism considers that not all the fibres fail at a single stress level, allowing a progressively greater numbers of fibres to fail as the stress increases until a stress is reached at which point separation occurs. The statistical distribution of fibre flaws leads to a marked dependence of measured average strength on the length of fibre tested: the longer the fibre the greater the probability of encountering a severe flaw and the lower the average strength. In practice, the fibre strength is usually calculated as a strength measurement from the composite of the known fibre volume fraction (Chou 1992).

3 – 2 Woven Fabric Models

The three models that may be used to analyse the elastic properties of woven fibre composite are the mosaic model, a fibre undulation or crimp model and a bridging model that have been developed by Ishikawa and Chou (Ishikawa and Chou 1983b, Chou 1992).

3 – 2 – 1 Mosaic model

The mosaic model, a weave in its simplest form, see figure (3 – 1), idealises basically two layers of cross-ply lamina of a width equal to the thread width. This idealised laminate is simplified further by restricting the material, which is considered to be a single strip along each of the orthogonal weave directions. Figure (3 – 2) shows the strips within the unit cell of the materials, which are used in the parallel and series models. For the parallel model, it is assumed that a known force per unit length, applied uniformly across the sample cross-section, causes a state of uniform strain and curvature at the laminate mid-plane. This model is combined with the isostress and isostrain assumptions to predict the upper and lower bounds of the elastic moduli by using classical lamination theory. The mosaic model, however, does neglect the continuity and undulation of the fibres, and therefore only provides a "rough estimate" of the properties of fabric composite (Chou and Ishikawa 1989).

The overall fibre volume fraction increases with increase in the number of repeat cell units in woven cloth. This is because of the increase in the cross-ply region. Young's moduli increase with the increase in the number of repeats due to both the increases in the straight cross-ply region and overall fibre volume fraction (Naik 1994). This fact shows the relationship between the number of repeat units and Young's moduli of a woven composite and has been used in the

damage process analysis as part of the model developed (see the first application 5 – 5 – 2 in chapter five).

Using the mosaic model for simplifying woven fabric composites to account for the inter-yarn deformation, a one-dimensional analysis has been developed to predict the local elastodynamic and elastostatic behaviour. The analysis focuses on the unit cell of an orthogonal woven fabric composite, which is composed of two sets of mutually orthogonal yarns of either the same fibre (non-hybrid fabric) or different fibres (hybrid fabric) in a matrix material (Chen and Chou 2000).

3 – 2 – 2 Fibre undulation model

The second model deals with a fibre undulation or crimp model, as represented in figure 3 – 3. This model is concerned with the interlaced region of the woven fabric and considers fibre continuity and undulation in the loading direction within the unit cell. The model also considers the thread thickness, the length of undulation, and the angle of the threads as they weave around one another. Each cell contains regions of pure matrix and the overall fibre volume fraction can be different to the fibre volume fraction in the threads or yarns in such a model.

The model uses the unidirectional transformation equations to determine the thread properties due to the angle of undulation. The classical lamination theory is then used to determine the overall properties as with the mosaic model. Classical lamination theory is applicable for each tiny microscopic slice of the material of a certain width in the case of the hybrid weave figure (3 – 4).

Chou reports that the results for the moduli obtained from this model coincide exactly with the upper bound results from the mosaic model. This model is a 2D model and takes no account of fibre undulation in the transverse direction. It is reported that taking into account the existence of the yarn angle leads to a reduction of the effective elastic moduli (Ishikawa and Chou 1982b, 1983b) and (Chou 1992).

An analytical model to predict the moduli of a 2D woven fibre composite that takes into account voids in the structure has been developed by Farouk and is based on the undulation model. It is stated that the moduli predicted by this model are within 10% of the experimental values (Farouk et al. 1991).

3 – 2 – 3 Bridging model

The, 'bridging' model developed by (Ishikawa and Chou 1982b, 1983b, 1989) and (Chou 1992) considered interlaced regions in a satin weave composite that are remote from each other, (refer to figure 3 – 5). The bridging model is used to predict the properties of satin weave composites (Chou 1992). The bridging model is a combination of the mosaic model and the crimp model. The repeating cell of this model consisting of the central interlaced region where the undulation occurs, and four separate regions making up its surrounding area which is modelled as layers of cross ply lamina (the mosaic model). Regions II, III and IV act as bridges for the load transfer between regions V and I, while region III has an interlaced structure with an undulation filling yarn.

A three-dimensional view of the bridging model for 8-harness hybrid woven fabric is shown in figure (3 – 6) (Ishikawa and Chou 1983d).

The elastic properties of a woven fabric layer are functions of the fabric structure and material system used in the woven composites according to (Ishikawa et al.1985) and (Naik 1994).

A basic difference between hybrid and non-hybrid composites is that of material variation as well as geometric variation over the cell repeat units in the composite. The distributions of stress and strain over the laminate mid-plane vary with location in the hybrid fabric composite (Chou 1992). These two facts show the relationship between the elastic properties and the material used in a woven composite and have been used in a damage event sequential process model seen as the outcome from the bridging model (see e.g. the second application in chapter five - section 5 – 5).

In one of the published papers Ishikawa compares the theoretical and experimental results for the moduli of woven carbon fibre composites based upon the above models (Ishikawa et. al. 1985). Ishikawa agrees with Zhang and Harding (Zhang and Harding 1990) by stating that the fibre undulation ratio (h/a) is a very important parameter, which strongly affects the elastic moduli of plain weave composites. The values of the elastic moduli are also dependent upon the laminate ply number 'n', as neighbouring layers in a fabric that tend to suppress the warping of one another (Zhang and Harding1990). It has been found that as the undulation ratio increases, the value of E_x decreases (Chou 1992, Zhang and Harding 1990). It was also found that the in-plane shear modulus G_{xy}, is mainly influenced by the fibre volume fraction which decreases linearly

with 'n' (Ishikawa et al 1985). They also report that the mosaic model "shows particularly large discrepancies in the prediction of the moduli of plain-weave composites".

3 – 3 Mechanical Testing Characterisation

Mechanical testing as used in this study can be divided into destructive testing such as:

- Interlaminar Shear Strength (ILSS),
- Flexural and
- Tensile

And dynamic testing such as:

- Dynamic Mechanical and Thermal Analysis (DMTA).

3 – 3 – 1 Interlaminar Shear Strength (ILSS)

The short-beam test for the apparent interlaminar shear strength (ILSS) of composites is a simple test widely used in the composite industry. It is a three-point bending test on a specimen with a small span, which promotes failure by shearing the laminate. In transferring the shear load across the composite, the matrix plays the major role. For the ILSS test, the failure is mainly in the shear mode and ideally should occur in the mid-plane of the specimen. This is because the test method involves loading a beam under three-point bending with the span-to-depth ratio, L/h, chosen such that an interlaminar failure is induced along the centreline rather than a tensile failure on the bottom surface of the beam (Pagano and Pipes 1989). The ILSS failure depends upon the fibre/matrix adhesion level as well as the frictional effects or mechanical interlocking at the fibre/matrix interface (Park and Kim 2001, Schwartz, 1997). Good fibre/matrix adhesion is essential for the composite to perform well under shear loading. The ILSS test is used for assessing fibre surface treatments, fibre-resin compatibility as well as being used as a quality control method (Caldwell 1994).

Hayashi (1967) appears to be the first who investigated interlaminar shear stresses in an idealised laminate consisting of orthotropic layers separated by isotropic shear layers. Other important works were carried out by Bogy (1968), who investigated the singular behaviour of stresses at the intersection of a boundary and bonded dissimilar isotropic materials.

The finite-element formulation for cross-ply laminates as a two-dimensional problem was presented initially by (Foye and Baker 1971) and Herakovich proposed the two-dimensional finite-element formulation for laminates including off-axis layers (Herakovich et al. 1976).

Pipes and Pagano presented the first three-dimensional (numerical) analysis of interlaminar stresses in laminated composites (Pipes and Pagano 1970). Rybicki immediately followed the previous finite-difference solution by Pipes and Pagano with a three-dimensional finite element solution (Rybicki 1971). The free edge problem has also been investigated experimentally see (Pipes and Daniel 1971 and Herakovich et al.1984).

Some other interlaminar analytical solutions have been designed by Pagano (1978) (Rose and Herakovich, 1991), and a solution employing complex stress potentials and eigenfunction series by (Wang and Choi, 1982). The above historical/technical reviews are given by Herakovich, Pagano and Pipes (Herakovich 1998, Pagano and Pipes 1989)

The 2-D woven fabric reinforced composites often have poor interlaminar properties such as low interlaminar strength and toughness in comparison with their in-plane properties. Delaminations are considered to be one of the most common failure forms in such composites (Wang and Zhao 1995). The crack velocity of glass fibre composites was measured in a recent study by using the crack velocity and stress intensity relationship (Pauchard et al. 2001).

The weave patterns of glass fabrics have a strong influence on the interlaminar fracture behaviour of the woven composites. Wang and Zhao reported that the resistance of satin weave interlaminar stresses is much better than those such as in plain weave glass fabrics (Wang and Zhao 1995). Non-linearity and knee effects on stress-strain response were characterised in glass woven fabric epoxy reinforcement (Kumar et al. 2000).

The interlaminar shear strength is improved by increasing the matrix tensile strength. Because of better adhesion to glass fibres, epoxies in general produce higher ILSS values than vinylester and polyester resins in glass fibre-reinforced composites. For composites having lower fibre/matrix adhesion, the shear failure mode is dominated by interfacial failure more than for composites with higher fibre/matrix adhesion (Drzal and Larson 1994).

3 – 3 – 2 Flexural properties

Flexural strength is not considered an intrinsic property; however, the test is usually considered a good quality-control test (Wood and Langer 1987). Flexural test results are influenced by the span-to-depth ratio used in the test. The calculation of flexural strength and modulus depends upon specimen thickness squared; therefore the measurement of thickness is critical. Flexural stress distributions show little improvement over the classical laminated plate theory, hence, the requirement is to model the behaviour of thick laminates properly (Chou 1992). Stronger interfacial strength leads to an increase in flexural strength as reported by (Park and Kim 2001).

It was found that the mechanical properties of a composite with a high fibre volume fraction were more sensitive to the change of fibre-matrix adhesion than those in a low fibre volume fraction (Shiqiang and Lin 1999) and (Vallittu 1999).

The flexural strength in specimens reinforced with silanized glass fibre were significantly higher than those of un-reinforced specimens. The reinforcing effect increases with the increase in the glass fibres (Kaniej 2000), the laminate stiffness increased linearly with fibre volume fraction Thomason and Vlug 1996.

The flexural strength results correlated well with the level of interfacial shear strength. The interfacial shear strength could also be correlated with the level of fibre surface coverage given by the fibre coating (Thomason and Schoolenberg 1994).

3 – 3 – 3 Viscoelastic properties

Viscoelastic properties of composite materials can be examined by Dynamic Mechanical and Thermal Analysis (DMTA). The viscoelastic properties of composite materials dealing with matrices reinforced with spherical inclusions and continuous fibres were studied by Hashin (Hashin 1965b). Hashin showed that corresponding problems in elasticity could solve viscoelastic problems in composite materials fibres (Hashin 1969, and 1972). Examples of this are well known, and indicate that there are practical difficulties (Christensen 1971). This is due to the fact that very often the creep compliance or relaxation moduli of the constituents of a multi-component system are not known (Schapery 1967).

The work of Laws and McLaughlin on viscoelastic composite materials used a self-consistent

approximation. They analysed the creep compliance and numerical calculations performed on examples of composites containing spherical inclusions and continuous fibres (Laws and McLaughlin 1978).

(Chou and Nomura 1980 a, b) and (Nomura and Chou 1985) obtained the effective relaxation moduli based upon their work on effective elastic properties. Specific expressions of composite relaxation moduli are given in terms of the elastic and viscoelastic properties of the constituent phases, fibre volume fraction, and fibre aspect ratio.

Many researchers have employed dynamic mechanical analysis in characterising the interfacial properties of composite materials. Lewis and Nielsen observed differences in the amplitude of the tan delta signal depending on the concentration of filler additive in an epoxy matrix (Lewis and Nielsen 1970). An evolution of the temperature and time in concept of volume or mass of the interacting element was inter-related (Mezzenga et al. 2000).

The influence of the fibre volume fraction of the beads and their surface treatments was investigated by dynamic mechanical behaviour of epoxy/A-glass composites. The main difference between the different samples was observed in the rubbery modulus plateau (Shaterzadeh et al.1998).

DMTA can be used to characterise interfacial effects by measuring changes in the amplitude, peak broadness, and peak temperature of the tan delta signal. Other researchers have pointed towards the importance of restricted chain mobility, due to polymer-filler interactions, which can be detected by DMTA (Chua 1987), (Eckstein 1989) and (Jensen et al. 1998).

Dynamic mechanical analysis has also proved to be useful in studying the interfacial properties of laminated epoxy glass composite samples (Heise and Martin 1990). Paggoit has studied the effect of the third phase (the interphase) at the interface on fibre composite properties (Paggoit 1987).

It has been noted that dynamic mechanical testing can measure the glass transition temperatures (T_g) of a range of commercial and experimental coatings on glass fibres. Thomason discussed this, and was inquisitive to find out how the coating (T_g) can influence the formation of an interphase around the fibre. The (T_g) of a coating containing only epoxy resin was found to

decrease logarithmically with increasing layer thickness. This shows that, contrary to a recent suggestion, the effect is not due to preferential absorption of a curing agent (Thomason 1992).

Thomason pointed out that the interfacial region of the composite will not only be affected by the composition of the coating, but also by its distribution on the glass fibre surface and in the composite matrix (Thomason 1995). Thomason and Dwight presented and discussed a model to speculate how plots of atomic ratios could be used to estimate the surface coverage of the sizing on glass fibres and to obtain information on the sizing components. The glass fibres were coated with organic sizing (Thomason and Dwight 2000).

Haessler and his team studied the influence of the interface of differently treated glass fibres in epoxy resin composites by dynamic mechanical analysis. The results were compared with mechanical measurements of adhesion. It was found that the flexural storage modulus (E′) of the composites with improved interfacial bonding is increased over the whole temperature range investigated. Decrease of the magnitude of tan delta at the α-relaxation corresponded with an improvement of interfacial bonding. The behavioural differences could only be attributed to interfacial phenomena because the other parameters were kept constant. Dynamic mechanical analysis is an additional possibility for quantifying interfacial interactions (Haessler and Keusch 1999) and (Frenzel et al. 2000).

The samples of high viscosity epoxide composite are characterised by a lower cross-linked density. Conversely for low viscosity a high cross-linked density dynamic mechanical response characterises the epoxide composite samples (Kuzenko and Browing 1979) and (Armand Soldera, 1998).

3 – 3 – 4 Tensile properties

Herakovich discussed that the axial tensile strength of a unidirectional lamina is typically controlled by the ultimate fibre stress (Herakovich 1998). Kelly and Davies (1965) provided the analysis for predicting axial tensile strength as a function of fibre and matrix strengths, and the constituent volume fractions, assuming that the fibres are identical, continuous, aligned and uniformly spaced.

Tensile and flexural tests were carried out using graphite/epoxy composites with two different fibre surface conditions to identify the effects of fibre-matrix adhesion on the mechanical properties of composites in conjunction with the variation of fibre volume fraction (Shiqiang and Lin 1999).

The bond between the fibre and matrix in a hybrid ensures that both fibres continue to carry part of the applied load and to contribute to the overall stiffness after first cracking (Bunsell and Harris 1974). The transverse tensile strength decreases as the fibre content increases for glass fibre epoxy composites, and their results indicated that the transverse tensile strength is a sensitive test for assessing the interfacial bond strength. A strong correlation between tensile strength and interfacial strength (fibre surface treatment level) has been reported in several studies (Caldwell 1992).

Mar and Lin reported that the formation of longitudinal splitting in the unidirectional composites occurs as a consequence of one or more of the following failure mechanisms: transverse matrix cracking, fibre/matrix debonding (Mar and Lin 1979).

Rapid and extensive longitudinal splitting combined with fibre fracture was found to occur at a very late stage of tensile testing of unidirectional composites. Bader has reported that a low level of fibre surface treatment results in the classical brush-like failure (Bader 1993). Manders and Bader 1981 observed similar behaviour, which showed that the failure of glass/epoxy specimens during a tensile test was initiated by longitudinal splitting which progressed to total wearing down of the specimen to failure (Manders and Bader 1981). The slow propagation is dominated by transverse tensile stresses in the matrix, whereas, the fast growth is driven by shear stresses. It has been also reported by Wo1la and Goree that the longitudinal splits are initiated in a slow, stable manner at the crack tip followed by a rapid longitudinal split growth (Wo1la and Goree 1987).

Ahlstrom and Gerard studied the adhesion in E-glass fibres where they were subjected to various surface treatments with an epoxy matrix to evaluate the effect of the coating process. They reported that the tensile strength of the silane-treated glass fibre composite was higher than for the untreated fibres which is in compliance with reported data. An additional effect is observed for the elastomer-coated fibres, which present the highest tensile strength. This effect could be

attributed to an improved protection and/or elimination of the weakest filaments in the glass yarn during the treatment (Ahlstrom and Gerard 1995).

It has been shown that stress concentrations in unidirectional composites containing interfacial damage between fibres and matrix and lengths of damaged regions were influenced by interfacial shear strength (Qlng-Dun et al. 1997).

To improve the mechanical properties of fibre-reinforced polymer matrix composites, the hybrid systems based on unsaturated polyester and epoxy resins with different ratios were investigated (Park et al. 1998). The effects of a hybrid matrix system were evaluated by flexural, tensile and SEM experiments, Park observed that the hybrid system provided the maximum mechanical properties.

Tensile tests were conducted on a woven glass/epoxy laminate at varying fibre volume fractions in order to ascertain the relationship between the fibre content and failure mechanisms. The results suggest a brittle tensile failure in fibres of the woven laminate indicating that increasing of the fibre volume fraction leads to the likelihood of a matrix dominated failure mode (Okoli and Smith 1998).

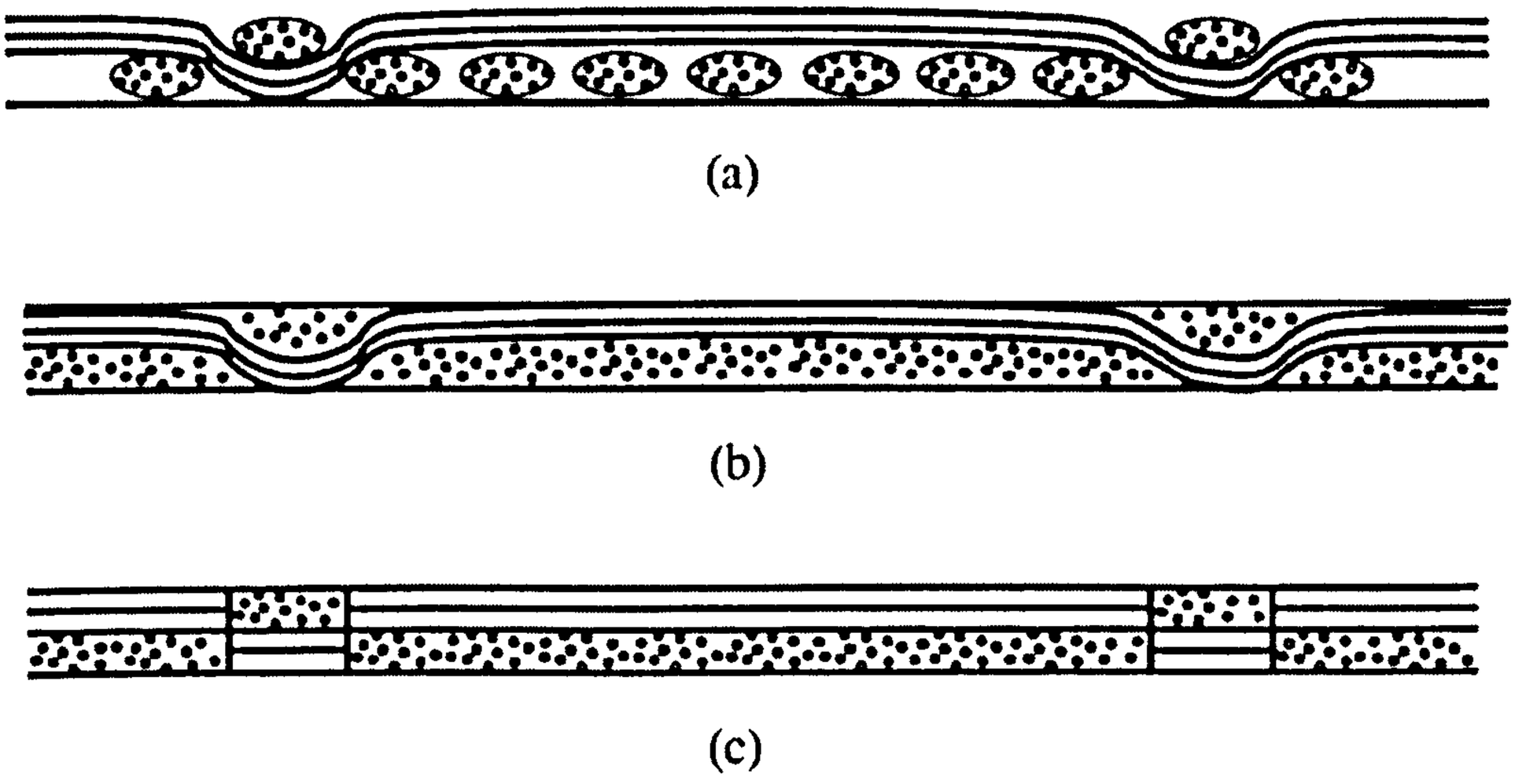

Figure (3 –1) Mosaic model for a unit cell of 8-harness satin (after Chou and Ishikawa 1983b).
(a) Cross-section of a woven fabric before resin impregnation;
(b) Woven fabric composite;
(c) Idealization of the mosaic model.

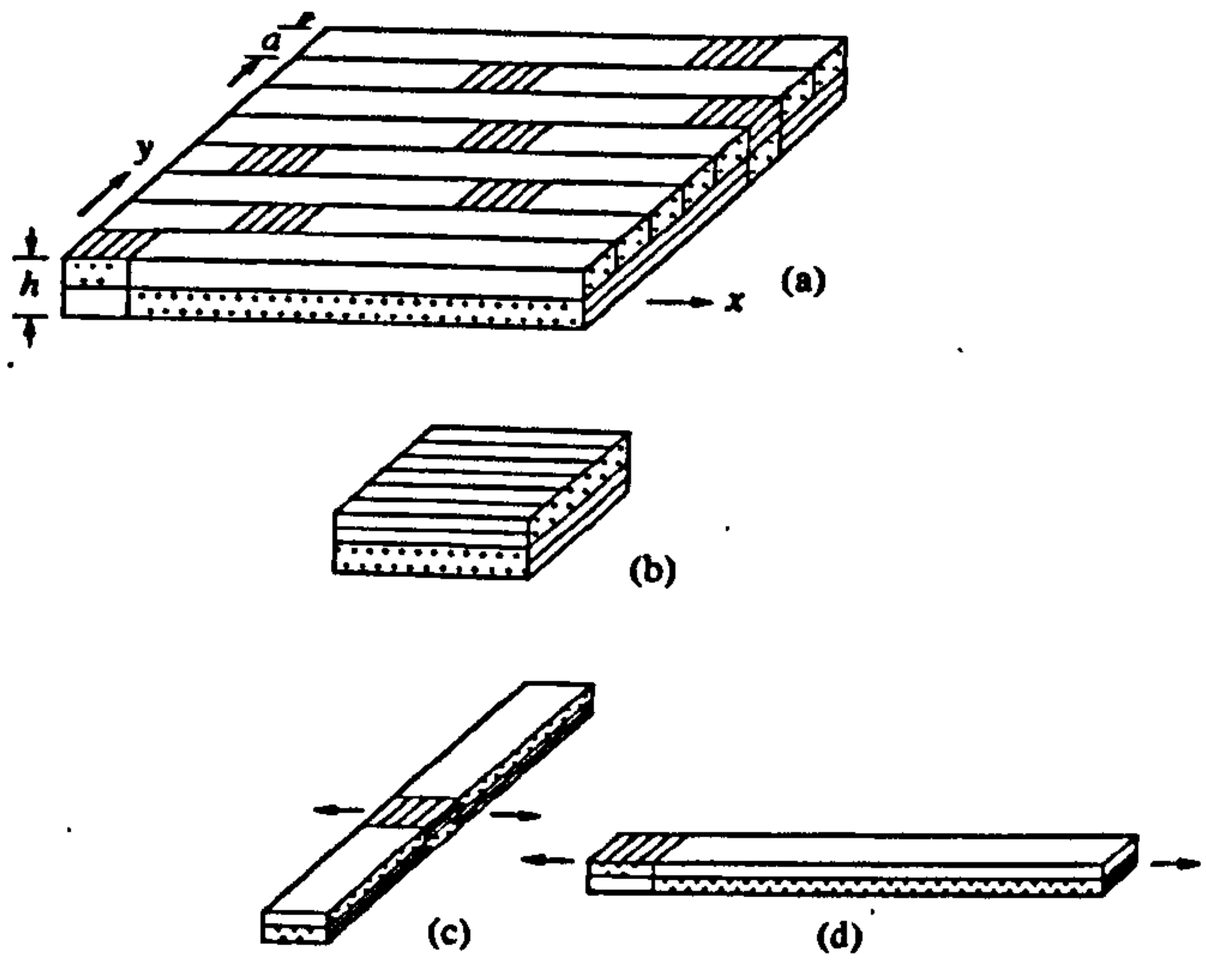

Figure (3 – 2) Mosaic model of 8-harness satin woven fabric (after Ishikawa and Chou 1983b)
a- Repeating region in an 8-harness satin composite;
b- A basic cross-ply laminate;
c- Parallel model;
d- Series model.

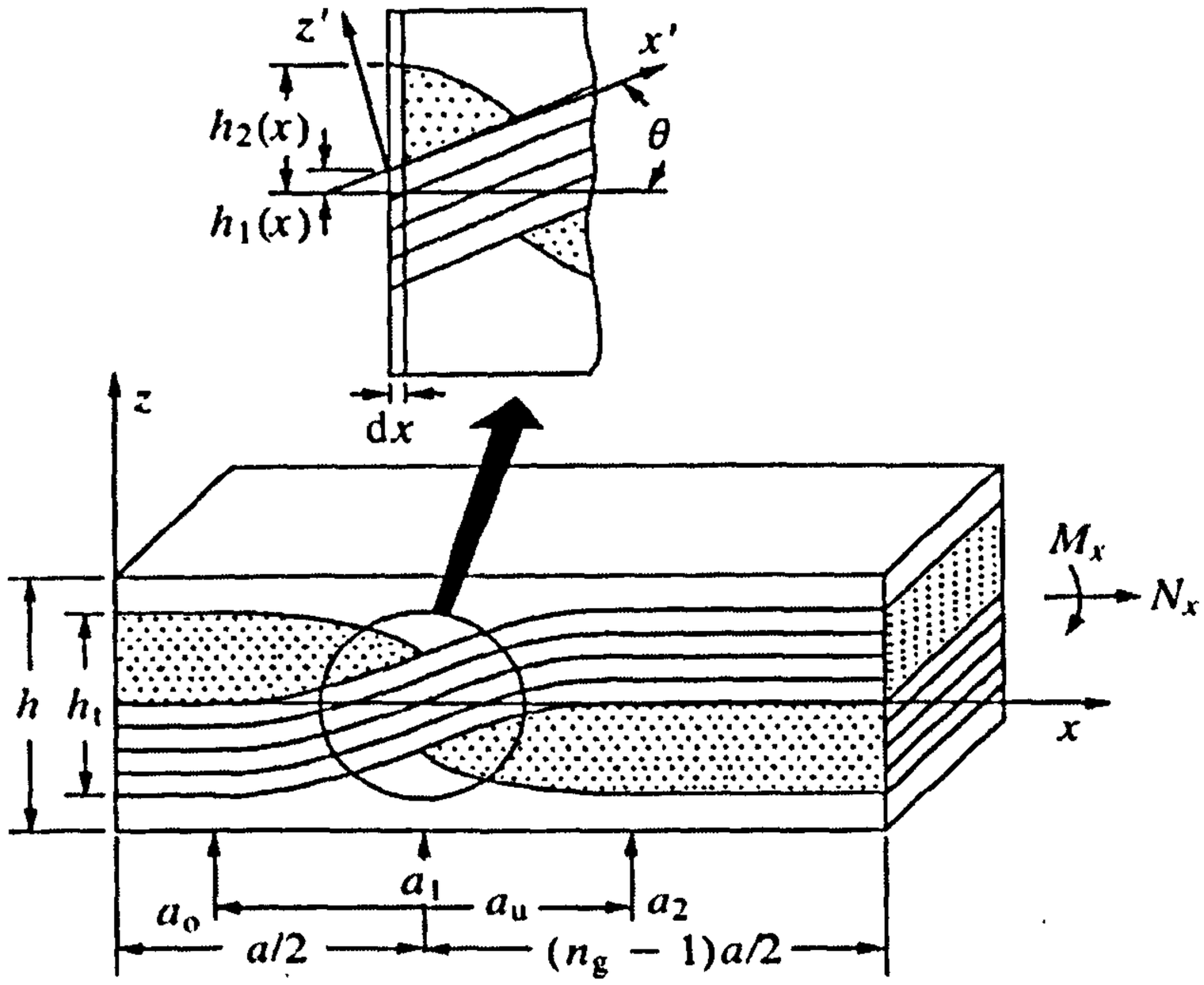

Figure (3 – 3) Fibre crimp model (after Chou and Ishikawa 1982b).

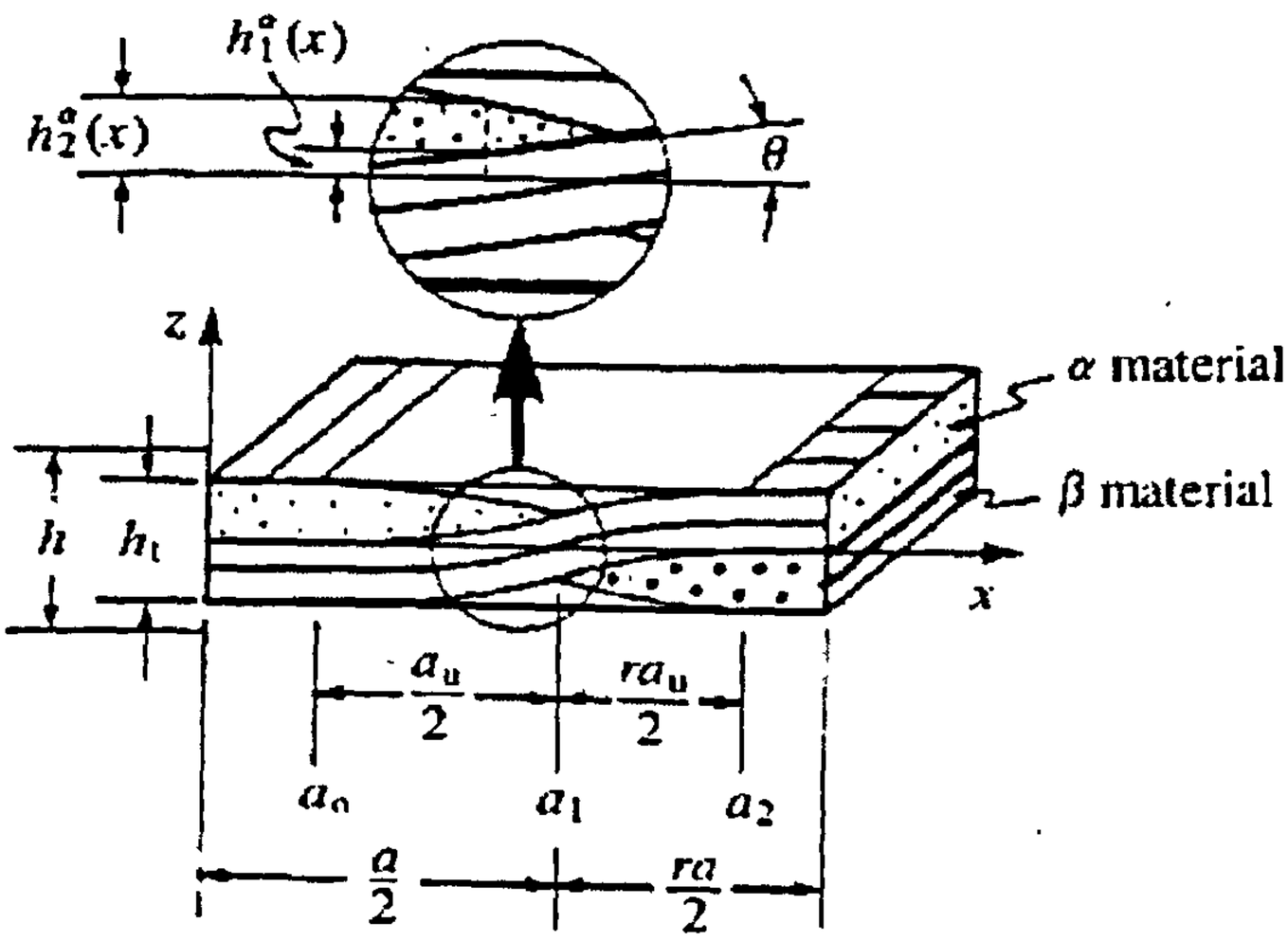

Figure (3 – 4) Fibre crimp model in hybrid woven fabric (after Chou and Ishikawa 1983d).

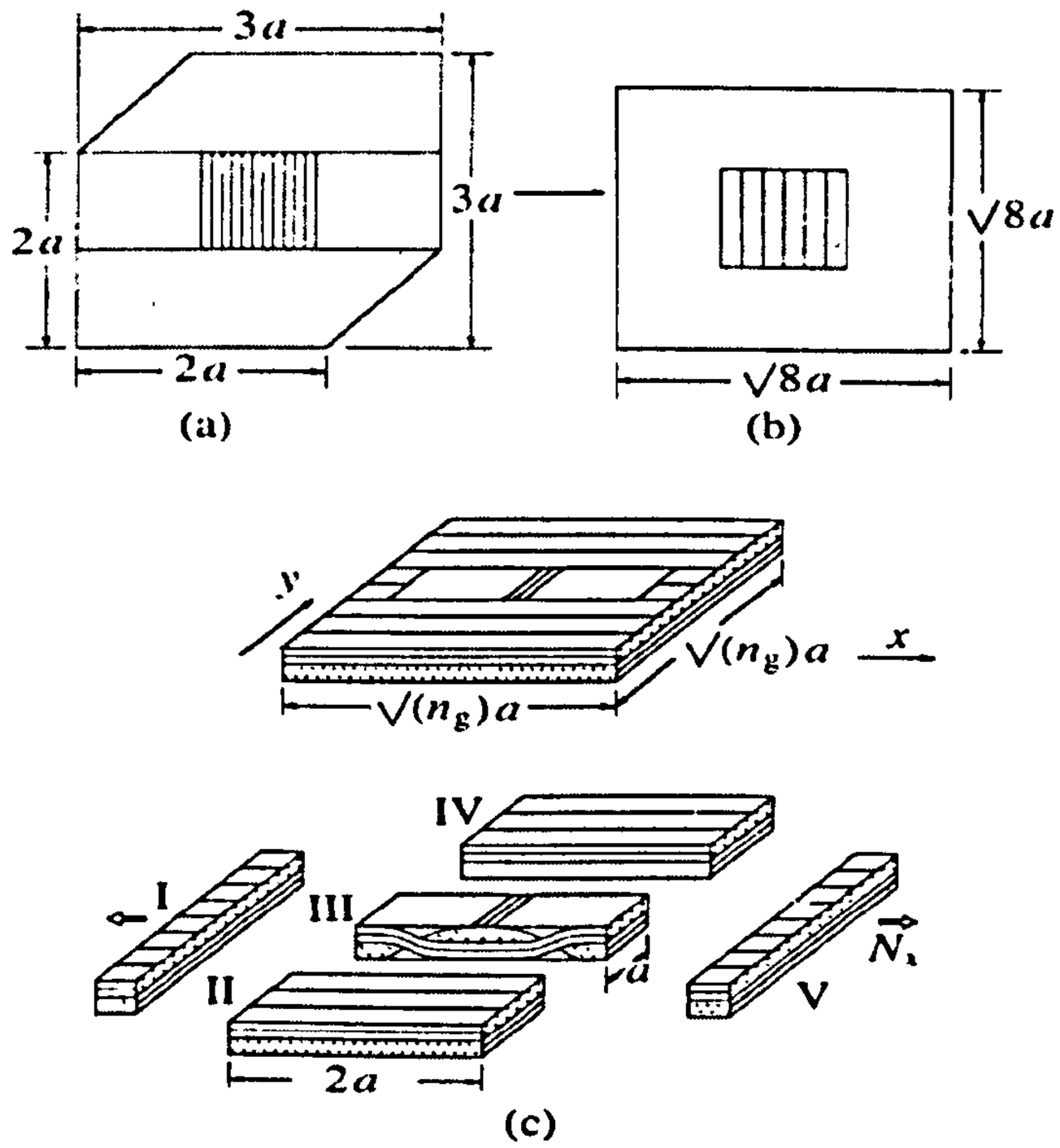

Figure (3 – 5) Bridging model of 8-harness satin woven fabric (after Ishikawa and Chou 1983b),
(a) repeating unit in an 8-harness satin composite,
(b) modified shape for repeating unit,
(c) idealization for the bridging model.

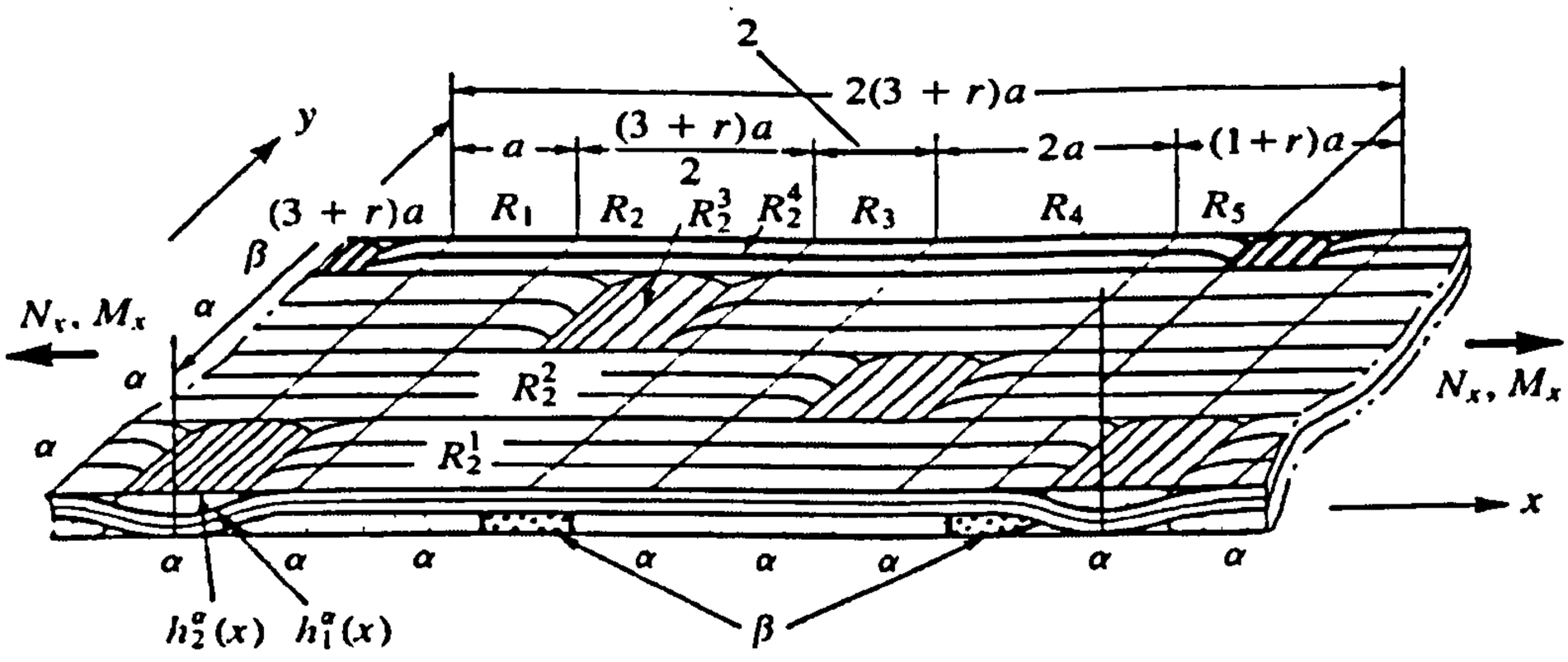

Figure (3 – 6) A 3D view of the bridging model for 8-harness hybrid woven fabric (after Ishikawa and Chou 1983d).

CHAPTER FOUR

CHAPTER FOUR

Experimental Details

This work deals with an investigation of fracture behaviour involving two different woven fabric composite materials. In this chapter, a description of the fibre, yarn, weave type, fibre coating details and the resin system reinforcement is given. The details of specimen preparation and test methods are explained. A description of techniques required to observe, record and classify the damage growth while testing such as AE, visual specimen examination (VSE) and scanning electronic microscopy (SEM) is presented.

4 – 1 Material Characteristics

The materials used in the experimental testing, supplied by Interglas Technologies, Sherborne UK, were: -

1. Non hybrid 8-harness satin woven fabric of EC9 68 TD22 in warp, EC9 68 in weft, SEM micrograph of the woven fabric see figure (4 – 1).

2. Hybrid 8-harness satin woven fabric of EC9 68 in warp and RC9 68 in weft.

Where E = E-glass, R = R-glass. C = continuous filament yarn. 9 = 9 micron diameter.
68 = 68 TEX i.e. 1000 m of yarn weighs 68g.
TD22 silane binder, resin compatible option used as fibre coating for both fabrics.

4 – 1 – 1 Yarn nomenclature

The yarn is composed of a specific number of filaments of glass of known diameter, typically 204 to 816 filaments, the weight of yarn in units of TEX (Interglass Technologies, 1999, 1998).

The advantages of the yarn are:
(i) High strength to weight ratio, approx. 68gm.TEX
(ii) Low elongation at break, approx. 3.5%
(iii) Perfect elasticity, no creep under sustained load
(iv) High electrical resistance

(v) Wide range of temperature resistance, -200C to +550C

(vi) Non absorption of moisture

(vii) Highly transparent

(viii) Non-flammable

(ix) Low chemical reactivity

The disadvantages were:

(x) Poor resistance to abrasion,

(xi) Poor resistance to flexing through acute angles.

The hybrid and non-hybrid fabrics of glass fibres used in the test consist of two systems of parallel yarns, the warp and the weft interlaced at ninety degrees to one another. The fabrics have identical or similar numbers of threads in both directions and the yarn count is generally the same. These are known as bi-directional fabrics. Greater mechanical strength and stiffness of laminate is due to limited thread deflection (crimp). The fabrics are more drapable and therefore better suited to shape components than plain weave fabrics.

The major features of hybrid and non-hybrid cloths were the same, i.e. both were eight-harness satin weave cloths, of similar weight. The two types of woven glass cloth were chosen, enabling not only general damage accumulation to be studied, but also the particular effect of the hybridisation of the yarns and fibre volume fraction on the behaviour of the laminates assembled.

4 – 1 – 2 Finishing

In order to achieve a strong bond between the glass surface and the resin, it is necessary to modify the un-reactive inorganic glass surface. Coupling agents known as **silanes** are used for this purpose. A silane can be considered as a double-ended molecule based on a silicon atom. On one side of the silicon atoms are ethoxy (OEt) or methoxy (OMe) groups and on the other are organic reactive groups, R_1: -

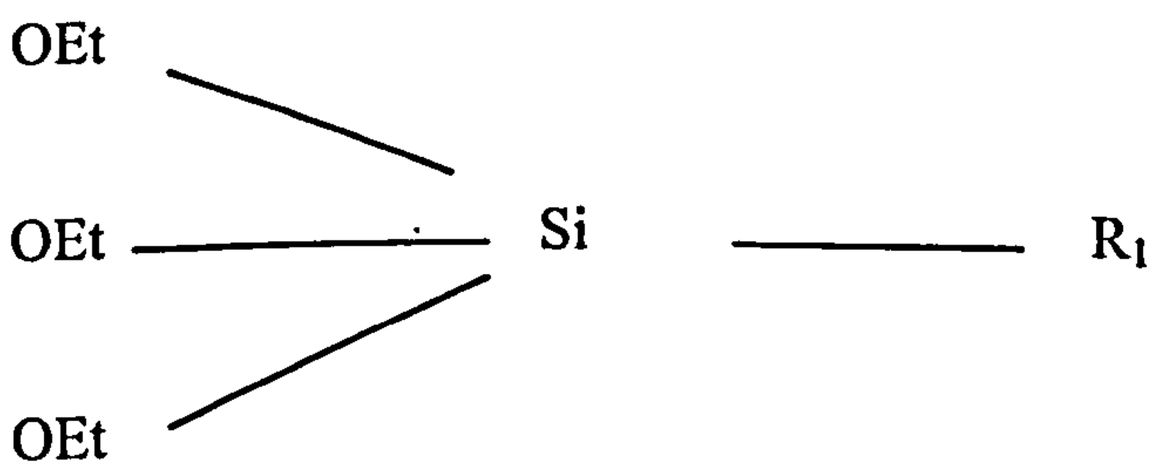

The silane is firstly dissolved in water when the OEt or OMe groups are hydrolysed to give: -

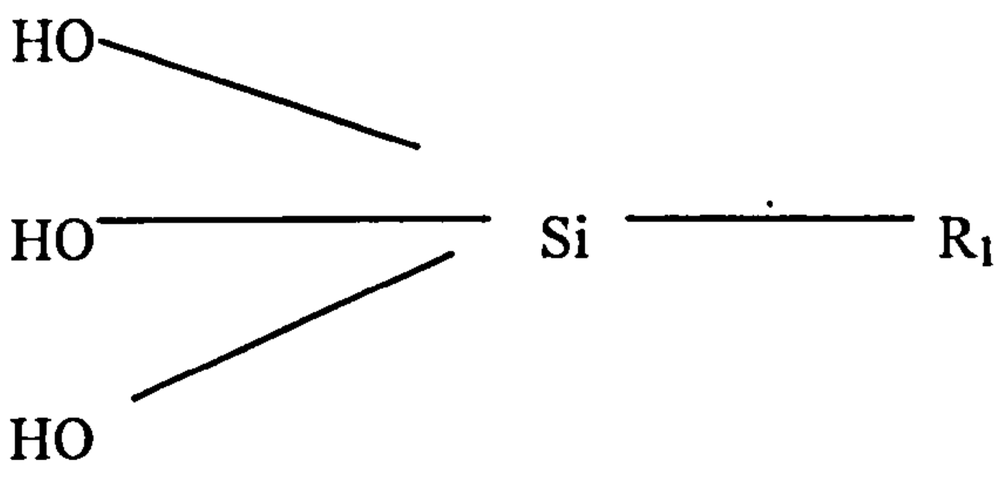

When heat-cleaned, the glass cloth is run through the silane solution so that hydroxyl groups on the glass surface react with the hydroxyl groups of the silane to form a Si-O-Si bond eliminating the water. This leaves the silane strongly bonded chemically onto the glass surface. This process has been used and explained by Interglass Technologies (Interglass Technologies, 1999, 1998).

4 – 2 The Matrix Resin System

The epoxy resin used in tensile, flexural, ILSS and DMTA testing laminates was produced by using **L20-SL set,** bisphenol A- (epichlorydrin) epoxy resin with cyclohexylamine hardener, from Bakelite. The resin specification is given in table (4 – 1). Both epoxy resins and hardener were supplied by Interglas- Technologies.

Epoxy is the general classification for resins containing two carbons and one-oxygen atom bonded in a ring. Such resins may be derived from many different starting materials such as phenol, bisphenol and multifunctional phonemic. The bisphenol-A is prepared as a result of the reaction of acetone and phenol. Since both phenol and acetone are readily available and the bisphenol-A is easy to manufacture, this material is comparatively inexpensive. This is one of the reasons why it is preferred that dihydric phenol be employed in epoxide resin manufacture. Since most epoxy resins are of low molecular weight and its colour is not particularly critical, the degree of purity of the bisphenol-A does not have to be great. Bisphenol-A with a melting point of 153° C is considered adequate for most applications whilst less pure materials may often be employed.

4 – 3 Test and Equipment

Tensile, flexural and ILSS tests were carried out on the following composites:

- Non-hybrid E-glass woven fabric composites (weft direction) with four different fibre volume fractions for the equal specimen dimension in order to investigate the effect of fibre volume fraction on glass woven composites.

- Hybrid (of R- and E-glass) and non-hybrid glass woven composites for the both warp and weft directions at similar fibre volume fraction (V_f) and equal specimen dimension in order to investigate the effect of fibre hybridisation on glass woven composites.

- Additionally tensile and flexural tests were carried out on neat epoxy resin.

4 – 3 – 1 Tensile test method

Tensile tests were conducted according to British Standard (BS) EN ISO 527-5 1997; (BS 2782: Part3: Method 326G: 1997) for woven composite laminates. The tensile test machine Zwick 50 could be loaded to 50 kN, using hydraulic grip with an extensometer for 100 mm extension, see figure (4 – 3 and 4 – 4). The tensile specimen was straight-sided and had a constant cross-section; sample dimensions were 250 mm long, 15 mm wide, and 1-mm thickness.

A test specimen was subjected to a longitudinal load at a speed of 2 mm/min, an extensometer with 100 mm extension being used to allow a force-extension curve to be drawn without inertia at the speed of testing. The requirements for the loading assembly permitted measurements of the load and deflection during the time of test period. Stress and strain values were calculated, with average and standard deviation adopted in calculations. Tensile stress was calculated using the following equation.

$$\text{Stress } (\sigma) = \frac{Load}{InitialArea} \qquad (4.1)$$

A tensile stress-strain curve along with the corresponding AE curve was used for damage accumulation analysis of the hybrid and non-hybrid composites.

4 – 3 – 2 Flexural test method (three-point bending)

Flexural tests were conducted according to BS EN 2746: 1998, on Testometric MICRO 350 using a three-point bending test jig, down-loaded across the width at a speed of 5 mm/min.

The jig was properly constructed and calibrated to achieve an approximately constant rate of relative movement between the loading nose and the supports. Figure (4 – 5) illustrates the test configuration. Dimensions of test specimens were 3 mm thickness, 15 mm width and 60 mm length. A test specimen was subjected to a three-point bending load. The requirements for the loading assembly permit measurements of the load and deflection during the time of the test period. Deflection was corrected by abstracting the machine deflection from reading deflection before calculating the values of strain, such that:

Corrected deflection = (Reading deflection) – (Machine deflection).

The stress and strain values are then calculated, the average and standard deviation, were adopted in calculations. Flexural stress was calculated using the following equation: -

$$\sigma_f = \frac{3FL}{2bh^2} \qquad (4.2)$$

where:

σ_f is the flexural stress, in MPa.

F is the load applied, in Newton.

L is the span, in mm.

b is the width of specimen in mm.

h is the thickness of specimen in mm.

The strain was calculated by the following formula:

$$\varepsilon_F = \frac{6dh}{L^2} \qquad (4.3)$$

where:

ε_F = is flexural strain in %

d = deflection in mm

h = thickness in mm

L = span length in mm

4 – 3 – 3 Apparent Interlaminar Shear Strength (ILSS) (short-beam method)

Interlaminar shear strength (ILSS) tests were conducted according BS EN ISO 14130: 1998, on Testometric MICRO 350, using a short-beam method, with a speed of 1mm/min. Figure (4 – 6) illustrates the test configuration. The ILSS test is similar in nature to the three-point loading method used to determine the cross-breaking strength of rigid materials. The loading assembly permits measurement of the deflection and load during the test. Deflection was corrected by abstracting the machine deflection from reading deflection before calculating the values of strain, such that:

Corrected deflection = (Reading deflection) – (Machine deflection).

The test specimen dimensions were 2 mm thickness, 10 mm width and 20 mm length; within the permissible range defined by the standard. The ILSS values were then calculated according to BS, using the following equation: -

$$\tau = \frac{3}{4} \times \frac{F}{bh} \qquad (4.4)$$

where:

F is the failure or maximum load, in Newton.

b is the width of specimen in mm.

h is the thickness of specimen in mm.

"Apparent interlaminar shear strength" is the term often used to describe the quantity measured. Hence, the results from different size samples or from tests under different conditions are not directly comparable; consequently the results obtained are not absolute figures.

4 – 3 – 4 Acoustic Emission analyser

Acoustic Emission (AE) monitoring used a Marandi 1004 with analysis equipment via a piezoelectric transducer during tensile, flexural and ILSS tests. Simultaneously AE parameters of the received signal were recorded in the form of ring down count (RDC). The RDC of acoustic emission was recorded as an analogue signal on the single channel by mean of a piezoelectric short-band transducer to give a classical representation of bar proportional to the rate versus time mode.

This methodology allowed investigation of the micro-mechanics failure process on woven composites. A short-band sensor was held in an improved clamp fixture as shown in figure (4 – 3). It was optimally aligned to ensure contact with the specimen. This arrangement was necessary due to

(1) limited space available on the specimen to hold the sensor (especially in the case of bending test), and

(2) The necessity to ensure that the sensor would not slip during the test.

Silicone grease (R5454-124 Silicon grease) was used as a coupling-agent between the sensor and specimen to reduce the peak amplitude of noise, and prevent it exceeding the threshold.

4 – 3 – 5 AE system calibration

Transducer calibration must be done in absolute units of displacement if it is to be correlated with dynamic phenomena. It is also necessary to calibrate the frequency response of the transducer. In this study the AE calibration of the AE system using a pencil lead breakage method has been followed. A 2H-pencil lead of 0.5mm diameter is usually applied. The lead field button is pressed repeatedly to protrude a definite length of lead and then it is made to break against an even surface to which the AE transducer to be calibrated is coupled. To obtain a repeatable constant AE source, the lead is broken at a fixed distance from the sensor, maintaining the same length and angle of contact of the lead with the surface. This method was adopted by Arved Nielsen and is sometimes called the Nielsen lead break method.

4 – 3 – 6 Scanning Electron Microscope (SEM)

The images generated by a SEM result from high-energy electrons striking a target in a fashion similar to that, which occurs in a conventional x-ray tube. Whereas the x-ray tube is specifically designed to produce x-rays, when the electrons strike the tube, the scattering characteristics of the target in a SEM vary with the target material. In most cases, where the target might be an engineering sample such as a fracture surface, the signals of greatest interest are the secondary and backscatter electrons. These vary with differences in surface topography as the electron beam sweeps across the surface. The scattering characteristics of the specimen are used to recreate the very high-resolution images that are readily associated with SEM work. Also of interest, however, is the field of x-rays that are emitted as a result of the electron bombardment (Bray and Stanley 1996).

In a preparation of the samples for the SEM inspection, samples were simply cut using a diamond wheel cutter. The samples were mounted on 10 mm square steel spools using double-sided adhesive carbon pads to hold them straight inside the SEM chamber and to protect them from damage. Therefore, the fracture surfaces were held towards the electron beam inside the chamber. Each sample was then gold plated in order to charge the electrons on the fracture surface. The plating was necessary because of the non-conductive nature of the composite samples since only conductive surfaces attract the electrons. This has enabled scanning of the enlarged fracture surfaces onto the SEM display for analysis. The scanning electron microscope utilised was a Phillips 505 model. Gold plating was carried out in an Agar Auto Sputter Coating machine. Black and white micrograph images of the fractured surfaces were scanned into the computer and then the images were produced digitally.

During scanning, the enlargement was adjusted to obtain a suitable image for fracture analysis. Depending upon the nature and severity of the fracture, the enlargement scale varied from 10 times to 1100 times the original fracture size. In order to display the fractures that could be seen easily from the surface of the sample, a low scale enlargement was employed, but for the images of fractures such as fibre/matrix debonding and fibre pullout, a larger scale was utilised to see the details of the fractured surfaces.

4 – 3 – 7 Dynamic Mechanical Thermal Analysis (DMTA)

Dynamic mechanical thermal analysis (DMTA) was conducted according to the British Standard BS 2782: Part 3 Mechanical Properties: Method 323B Flexural vibration – Non resonance method: 1996, ISO 6721-5: 1996. A Rheometric scientific dynamic mechanical analyser DMTA IV instrument was used for measuring the DMTA properties supported by Rheometric Scientific`s Orchestrator software on a windows platform incorporating a comprehensive multi-modular control and acquisition capability. Figure (4 – 7) illustrates the test configuration. A sinusoidal displacement is generated by the vibrator and applied to the specimen through moving clamps located close to the opposite ends of the specimen. The amplitude and frequency of the vibrator table displacement are variable and monitored by the transducer. The specimen is held at its centre by a second fixed clamp and thus undergoes sinusoidal flexural deformation.

The experimental tests, which were carried out under oscillating load, were monitored against time and temperature of oscillation, while the frequency of the sample was programmed at a constant 1.0 Hz throughout all tests. The DMTA tests involved with:

- Test on neat epoxy resin and four different fibre volume fractions of non-hybrid E-glass woven fabric composites.
- Tests on non-hybrid woven fabric composites of E-glass and hybrid woven fabric composites of E-glass in warp and R-glass in weft. Test were carried out for the both warp and weft directions at 42% fibre volume fraction.

The test was set up on a dynamic temperature ramp mode; the ramp rate was 3 C^{o}/min. and the soak time after ramp is 1sec. This applies a sinusoidal varying load, holding the frequency of the oscillation fixed at 1.0 Hz and strain 0.01%. The ratio of the amplitude of the stress and strain sine waves determines the storage modulus (elastic modulus) of the specimen, the phase angle between the two waves is called the loss angle and is a function of the internal friction of the material. A test specimen is subjected to a sinusoidal transverse force at a frequency of 1.0 Hz, significantly below the fundamental flexural resonance frequency. The amplitudes of the force and displacement cycles are applied to the specimen and these cycles are measured. The storage and loss components of the Young's complex modulus and the loss factor are calculated. The test fixtures for three point-bending have sufficient versatility to assure rigid, positive positioning of test samples in order to achieve accuracy of measurement.

Sepe contributed that the best dynamic mechanical analysis can be operated in a controlled stress or controlled strain mode, the primary value of the method in the dynamic experiment (Sepe 1999). In this mode of operation the DMTA instrument applied an oscillatory stress with controlled frequency, therefore similar methodology has been used in this study.

Dynamic modulus values using this method are a function of frequency rather than time; the stress function is sinusoidal. In perfectly elastic systems the applied stress and the resulting strain will be in the phase. For an ideal fluid the stress will lead the strain by 90^{0}.

Commonly, the glass transition is determined by measuring the specimen using either (tan delta) or loss modulus as a function of temperature. As the specimen goes through the glass transition,

the modulus drops by several orders of magnitude, and the loss modulus goes through a peak. The temperature at which the loss is at a peak maximum is defined as the glass transition temperature T_g.

4 – 3 – 8 The DMTA system calibration

The DMTA requires the following calibration tasks to be performed:

Removal of Fixtures: a calibration procedure instructs to remove all test fixtures. This means to remove the drive shaft attachment, frame and studs or clamps.

System Calibration: system calibration consists of the displacement, force, and spring calibrations, which must be performed in that order accordingly as mentioned by RSI Orchestrator guides.

Displacement calibration: displacement calibration ensures accurate displacement at the measurement head for a given commanded strain.

Force calibration: force calibration ensures the correct amount of force is applied to the measurement head. During this calibration step, the weight of the drive shaft is also measured.

Spring calibration: spring calibration calculates the spring constant of the drive shaft.

Cal check: cal check is provided to perform daily on abbreviated system calibration by performing only the spring calibration (rather than the full system calibration) and is recommended to be done daily.

Compliance calibration: as the measurement head deflects during testing, the instrument frame also moves due to its mechanical compliance. A small portion of this movement is measured along with the deformation of the sample. Compliance calibration subtracts the mechanical compliance of the instrument frame. This calibration can be helpful in obtaining accurate moduli when testing relatively thick, stiff samples.

Phase angle: phase angle calibration ensures accurate measurement of the phase angle between stress and strain

Tool mass calibration: tool mass calibration is a function that measures the mass of a test fixture, and adds this mass to the mass of the motor drive shaft. The inertia of the total mass is then calculated for use in compensating for inertia during testing. Inertia must be performed prior to the first time a test fixture is used to run tests. Subsequent use of the test fixture does not require tool mass calibration.

4 – 4 Porosity and Determination of Fibre Volume Fraction

4 – 4 – 1 Porosity

Pores are formed due to the extraction of volatile products of chemical reactions of hinder curing, solvents, air and moisture absorbed by the binder and reinforcing filler. These products, expanding when heated, form a system of open and closed pores, varying in shape and size. The effect of composite porosity is different, depending on the type of stress condition and strain direction (Gunyaev 1985).

The presence of porosity in a composite may involve a significant decrease in its mechanical characteristics by increasing the dispersion of their values. The presence of porosity also increases the sensitivity of the composite material to the external environment: increased absorption from humidity, decreased resistance to chemical products, etc. It will therefore be important to have an estimate of the proportion of porosity as a means of evaluating the quality of a composite. A high-quality composite material will contain less than 1% by volume of porosity, whereas a mediocre quality composite could have as much as 5% (Berthhelot 1999).

The presence of porosity is highlighted of the glass woven composite in figure 4 – 2. The method used to determine the volume of porosity content in woven glass fabric was the BS ISO 7822:1999. The magnitude of the void content is determined by rapid examination, using a microscope type Olympus BX 60, by applying one of the grids to each of the polished sections three times, examining a different field each time. Then all the fields, the number of points in each field, the number of fields for each section and the number of sections are examined in order to calculate the void contents (φ_v) as percentage by volume, using the following formula:

$$\varphi_v = \frac{N}{P} \qquad (4.5)$$

where

N is the total number of void points counted

P is the total number of points examined.

4 – 4 – 2 Determination of fibre volume fraction

The matrix burn-off technique has been used to determine the volume fraction of glass fibres within the test laminates using BS ISO 1172:1999. Two small samples (approximately 15 mm × 15 mm) were cut from two different regions of the laminate according to BS. Each sample was weighed before being placed in a ceramic crucible and covered with a lid, the weight of the crucible and the lid were known. The crucible was placed in the furnace at a temperature of 550^0 C for approximately 1 hour. With the absence of resin confirmed visually, the crucible was set aside to cool in the dry controlled temperature shelf-box. The crucibles were re-weighed after cooling.

The mass of the glass fibres (M_f) and the mass of the resin (M_m) within each sample were determined by simple subtraction.

Density of the E-glass was = 2.60 g/cm^3,

Density of the R-glass was = 2.53 g/cm^3

Density of the Epoxy resin was = 1.155 g/cm^3 (Vetrotex 2000).

The volume fraction (V_f) of the glass fibres in the composite was calculated using the equation:

$$V_f = \frac{\frac{M_f}{\rho_f}}{\left(\frac{M_f}{\rho_f} + \frac{M_m}{\rho_m}\right)} \qquad (4.6)$$

$$\text{Volume} = \frac{Mass}{Density} = \frac{M}{\rho} \qquad (4.7)$$

where:

M is the mass (or weight),

ρ is the density,

V_f is volume fracture of the glass fibre in the composite,

V_m is volume fracture of matrix.

4 – 5 Laminate Manufacture

The reinforcement for all laminates comprised of a number of woven fabric layers positioned in orthogonal alignment of warp and weft direction before the resin was applied by a hand lay-up process for each layer. In the case of hybrid fabric, the dominating fibre in the warp direction is E-glass, while the dominating fibre in the weft direction is R-glass. In the case of non-hybrid fabric, E-glass is in both warp and weft directions. This relative positioning was necessary to maintain a symmetrical stacking in the correct sequence within the laminate.

The procedure for the manufacturing of the laminates adopted a hand lay-up process. The resin to be used was weighed out and mixed thoroughly at room temperature. A thin layer of this resin was then spread on a sheet of silicone; a layer of glass cloth was then laid on the resin followed by another thin layer of the resin. The cloth was left until the resin had wetted all of the fibres; any entrapped air was removed by the application of gentle pressure with a roller. A similar procedure was followed for the remaining layers of the laminate.

Particular attention was paid to the orientation of the individual layers of wetted cloth to ensure that the sequence and symmetry of the finished laminate were correct. The composite laminates were cured in a heated press for 3 hours at 130 °C under pressure in order to achieve the correct thickness for relevant test samples. Post-curing proceeded in an oven at 80 °C for a further sixteen hours. Individual test pieces were then cut by an abrasive circular saw to get samples for the following investigations:

4 – 5 – 1 Investigating the effect of hybridisation

Laminates for **tensile** tests with **1 mm** thickness have **5 layers** of woven glass fabric achieving 48% fibre volume fractions of the composite.

Laminates for **ILSS** tests with **2 mm** thickness had **10 layers** of woven glass fabric achieving 48% fibre volume fractions of the composite.

Laminates for **flexural** tests with **3 mm** thickness had **15 layers** of woven glass fabric achieving 48% fibre volume fractions of the composite.

A similar procedure was adopted for both hybrid and non-hybrid fabrics for the purpose of comparison. The burn-off technique mentioned in section 4 – 4 determined fibre volume fractions of the composite.

In the specimen laminated from non-hybrid glass fibre fabric layers and epoxy resin reinforcement composites, it is essential to note that E-glass was in both weft and warp directions of the fabric. Consequently, the composite test specimen of non-hybrid glass fibre fabric contains only E-glass fibre. In the specimen laminated from hybrid glass fibre fabric layers and epoxy resin reinforcement composites, E-glass was in the warp direction and R-glass was in the weft direction of the fabric.

The weft direction of **hybrid** woven fabric laminates had the R-glass yarn in the normal direction with the loading axis. The weft direction of **non-hybrid** woven fabric had the E-glass yarn in the normal direction with the loading axis in ILSS and flexural testing. This allowed comparison of the two materials and constructions to be made.

In order to investigate the effect of hybridisation in the composites, test specimens for hybrid fabric were cut along the R-glass fibre in the weft direction and test specimens for hybrid fabric were cut along the E-glass fibre in the warp direction. The tests of hybrid and non-hybrid composites (weft direction) can be compared, as can the tests of the hybrid and non-hybrid composites in the (warp direction).

4 – 5 – 2 <u>Investigating the effect of fibre volume fractions in the composites</u>

Laminates of non-hybrid woven fabric made from E-glass in the weft direction with varying number of layers but constant laminate thickness were used in order to obtain different fibre volume fractions. These were as follows: -

Laminates made for **tensile tests** of 1 mm thickness having 4 layers of non-hybrid glass woven fabric achieved 38% fibre volume fractions (V_f) in the composite. Laminates of 1 mm thickness

having 5 layers achieved 48% V_f. Laminates of 1 mm thickness containing 6 layers achieved 56% V_f and finally laminates for tensile tests of 1 mm thickness containing 7 layers of non-hybrid glass fabric achieved 64% V_f in the composite.

Laminates of non-hybrid glass fabric made for **ILSS tests** of 2 mm thickness with 8 layers achieved 38% fibre volume fractions (V_f) in the composite. Laminates of 2 mm thickness containing 10 layers achieved 48% V_f. Laminates of 2 mm thickness and 12 layers achieved 56% V_f and finally laminates of 2 mm thickness and 14 layers of non-hybrid glass fabric achieved 64% V_f in the composite.

Laminates for **flexural tests** of 3 mm thickness with 12 layers of non-hybrid glass fabric achieved 38% fibre volume fractions (V_f) of the composite. Laminates of 3 mm thickness with 15 layers achieved 48% V_f. Laminates of 3 mm thickness with 18 layers achieved 56% V_f and finally laminates for flexural tests of 3 mm thickness with 21 layers of non-hybrid glass fabric achieved 64% V_f in the composite. The burn off technique mentioned in section 4 – 4 determined fibre volume fractions in the composite.

PAGE NUMBERING AS ORIGINAL

Table 4 – 1 Specification of the epoxy resin (L20-SL) system *.

Properties	Units	L20	SL
Density @ 25 ^{0}C	g/cm^3	1.155 -0.01	0.95-0.02
Viscosity @ 25 ^{0}C	mPa.s	900-150	90-10
Epoxide equivalent	g/equiv.	179	
Amine equivalent	g/equiv.		60
Volatile constituents/60 ^{0}C	%	<0.2	
Flexural strength	MPa	125	125
Tensile strength	MPa	56	55
Compressive strength	MPa	390	395
Elongation at break	%	10	9.5
Glass transition temperature (Tg)	°C	110	

* The manufacturer (Bakelite) provided these values in correspondence with author April 2000.

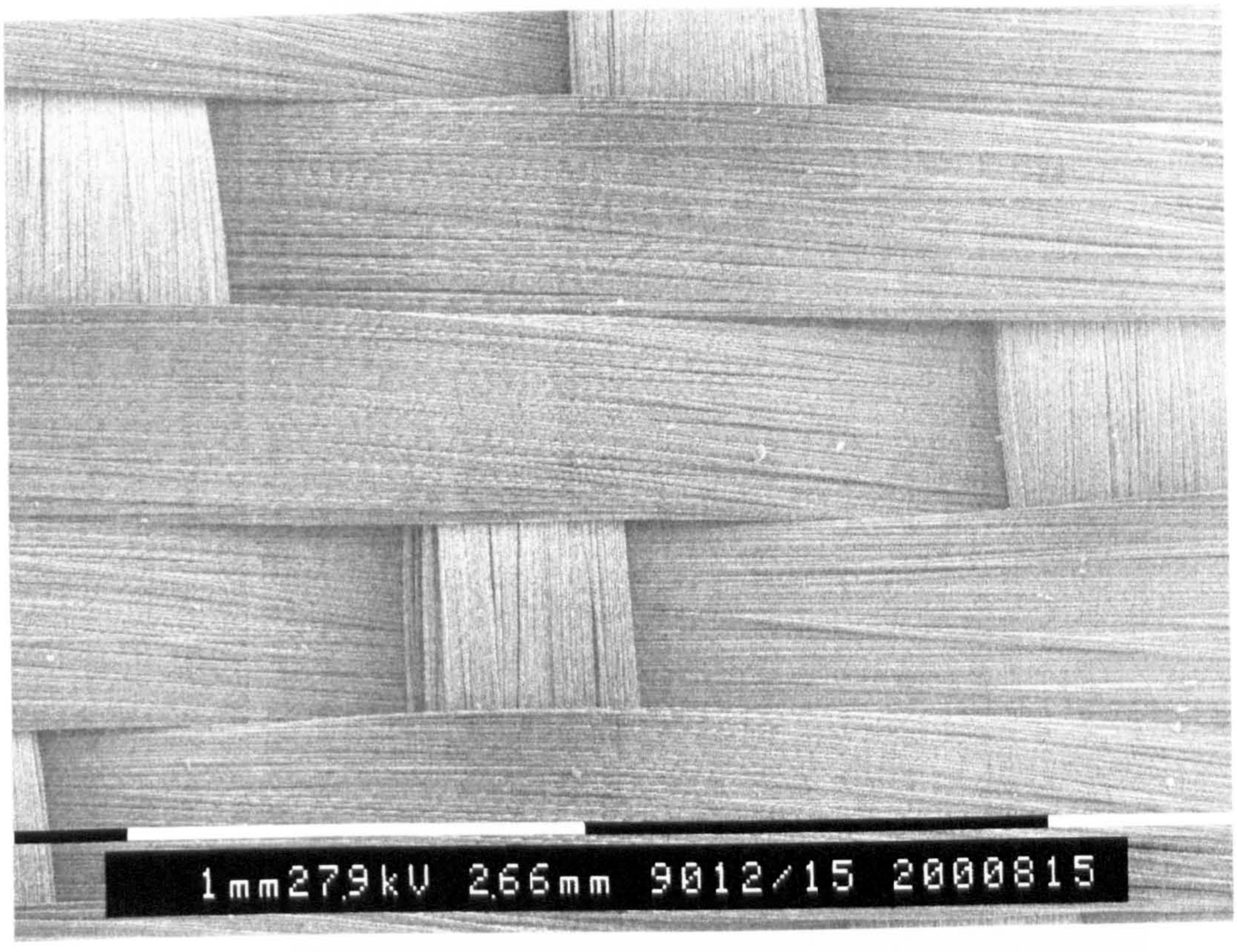

Figure (4 – 1) SEM micrograph of 8-harness glass woven fabric

Figure (4 – 2) the presence of porosity in the glass woven composite, an optical microscopy view of the through-thickness of glass woven composite specimen.

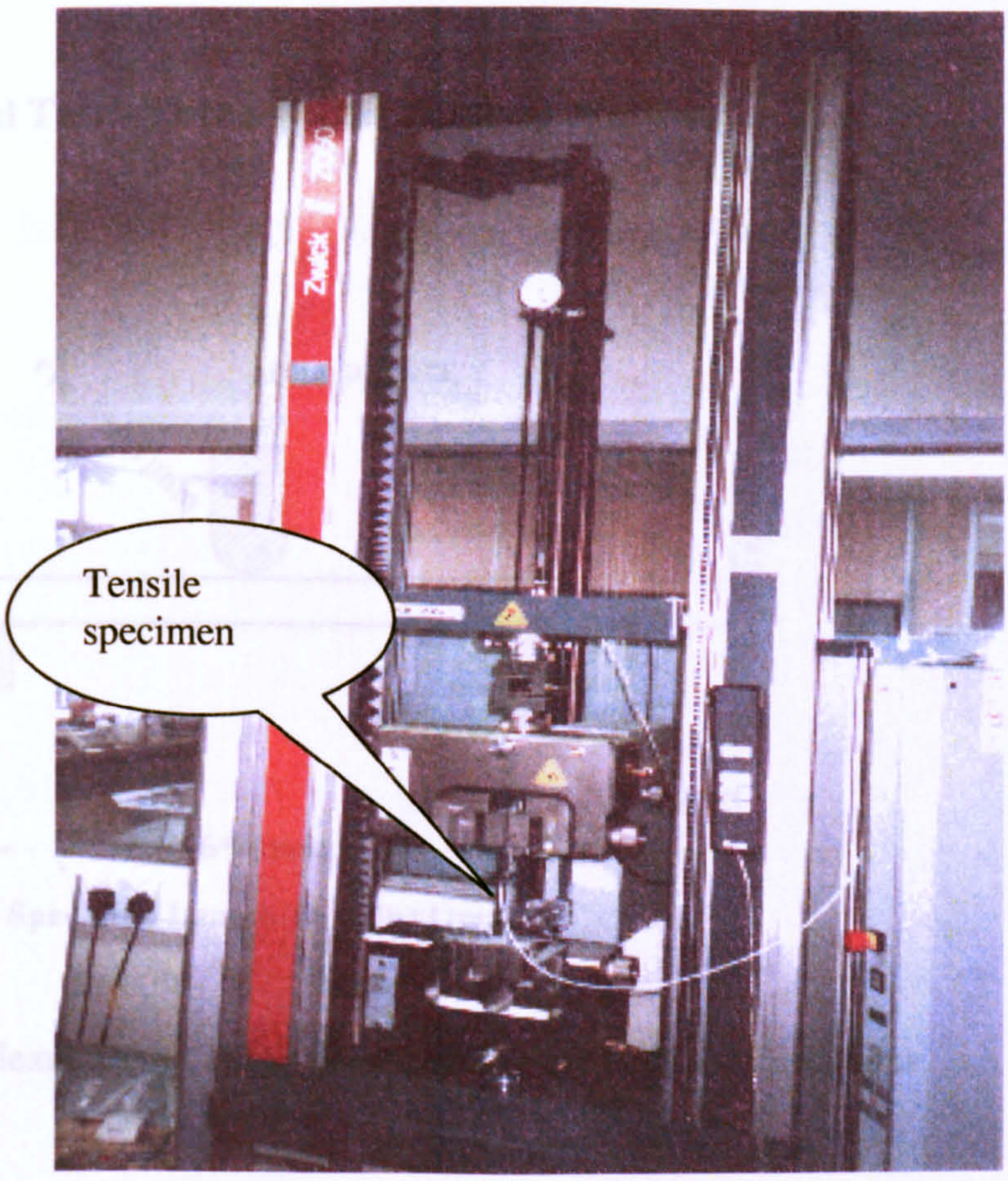

Figure (4 – 3) Zwick Z050 Tensile Testing Machine.

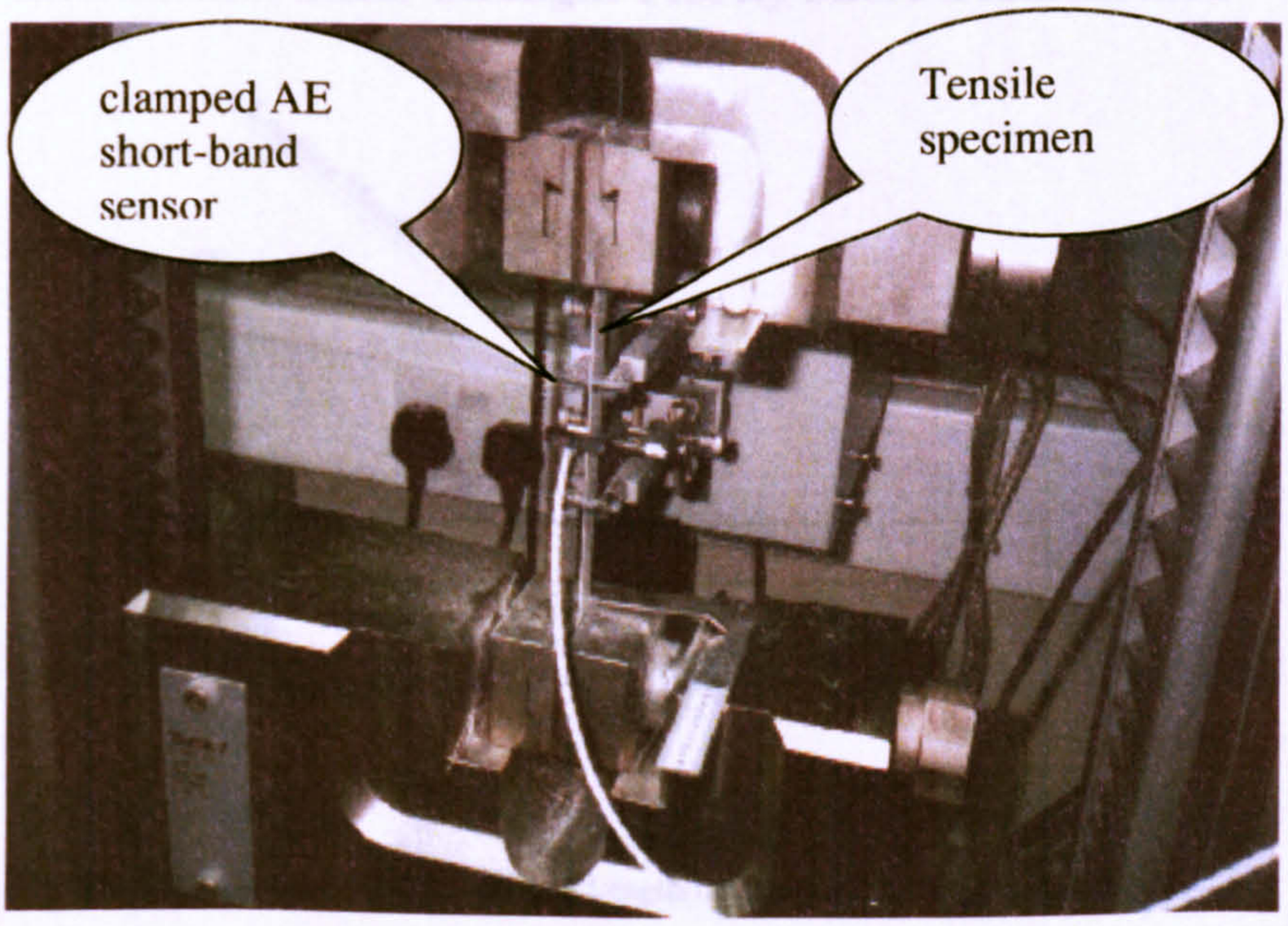

Figure (4 – 4) Tensile specimen fixed by hydraulic grip, extensometer for 100 mm extension and AE short-band sensor clamped on the specimen.

Flexural Test - Three-Points Bending Method

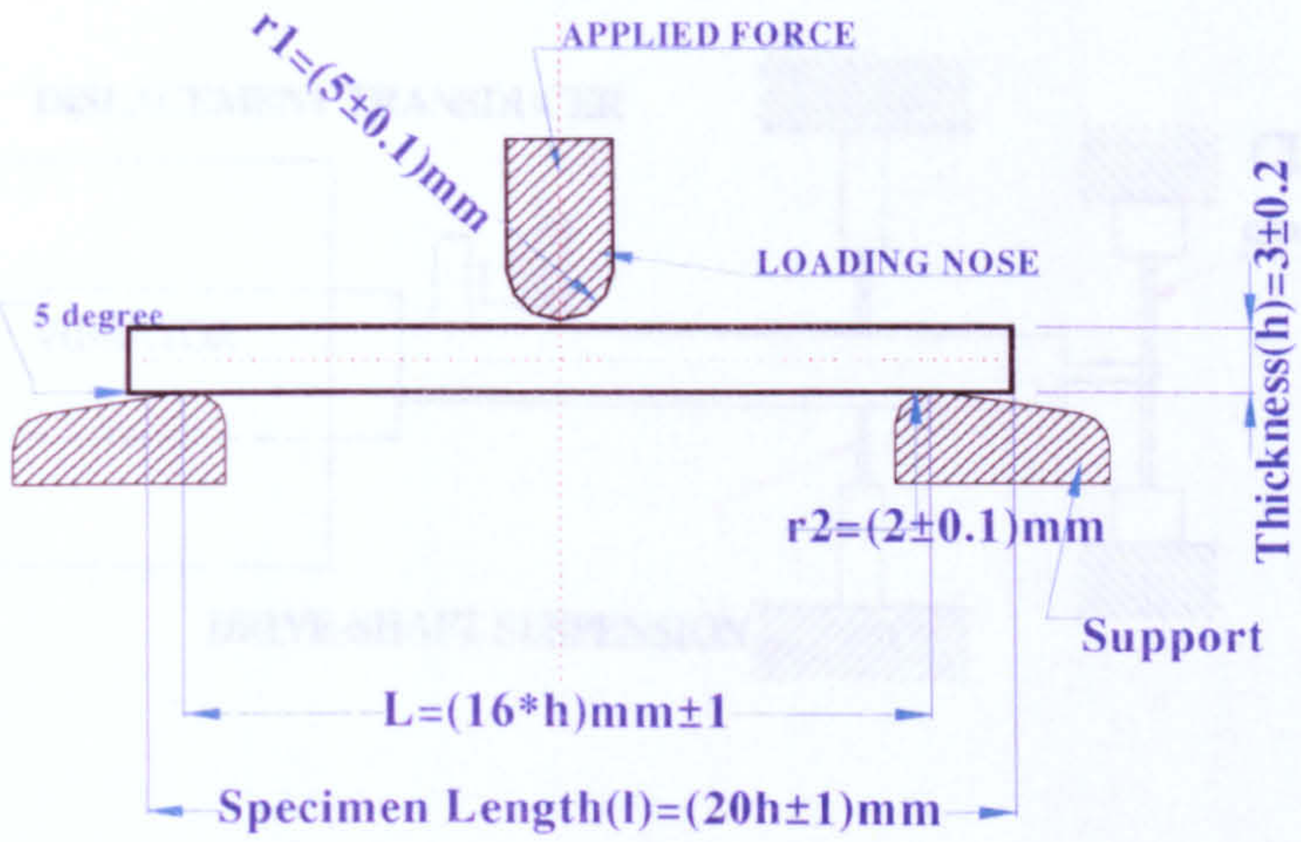

Figure (4 – 5) flexural test (Three-point bending method) configurations.

Interlaminar Shear Strength Test By Short-Beam method

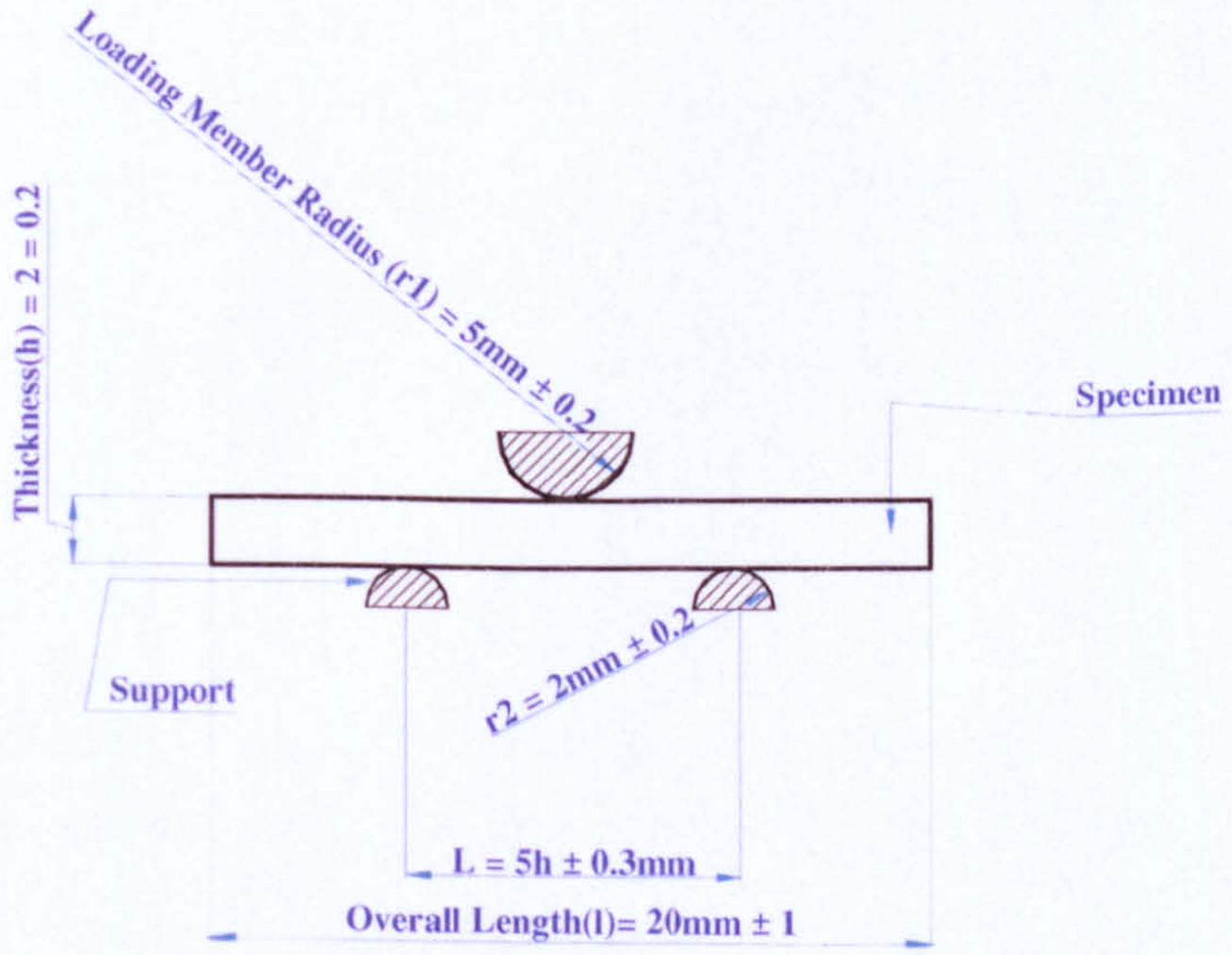

Fig (4 – 6) ILSS test (Short beam method) configurations.

Flexural Vibration - Non resonance method

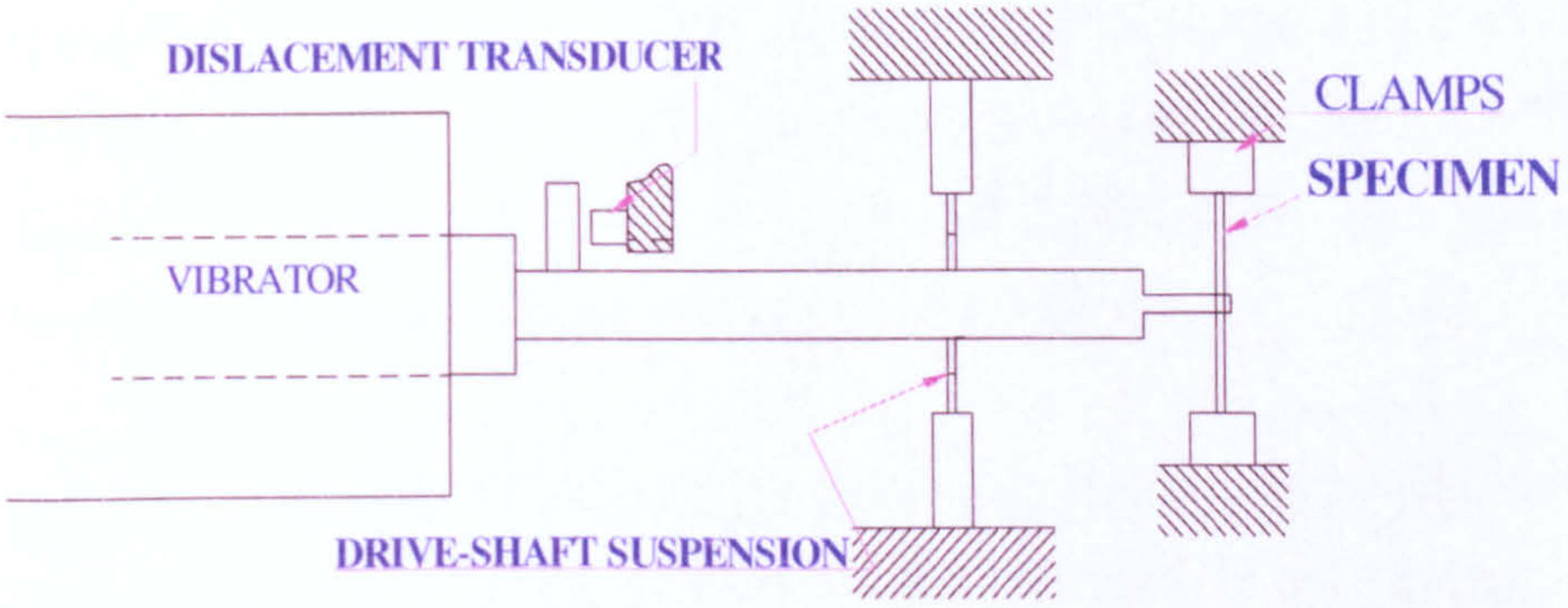

Figure (4 – 7) DMTA test configurations.

CHAPTER FIVE

CHAPTER FIVE

Results and Discussion

This chapter is divided into seven sections. The first four sections contain the results and discussion of Interlaminar Shear Strength (ILSS), flexural, Dynamic Mechanical and Thermal Analysis (DMTA) and tensile properties respectively. Each section deals with results and discussion from two different categories of experimental tests, (i.e. the non-hybrid and hybrid laminates) which have been carried out in this study.

Acoustic Emission (AE) was employed during ILSS, flexural and tensile tests. Scanning Electron Microscopy (SEM) of the specimen's fracture surface after testing assisted characterisation of the damage features.

The results are classified according to tests carried out, and, where appropriate, the mean and standard deviations of the results for sets of specimens are given in each category. The mean and standard deviations were used to categorise the variation of the results into significant or non-significant by using the t-test of probability; details are given in section six of this chapter.

The evaluation of the results has been discussed in section six of this chapter. The model of failure process and damage accumulation analysis in the glass woven composites is located in section five of this chapter. Microlam in-put and out-put details are located in section seven.

5 – 1 Section One: Interlaminar Shear Strength (ILSS) Results and Discussion

5 – 1 – 1 The results of ILSS test

The result of the ILSS tests on non-hybrid glass woven fabric reinforced epoxy resin composites with four different glass fibre volume fractions are set out in table (5 – 1), and are graphically presented in figure (5 – 1). The quantification of AE values during ILSS tests including four different glass fibre volume fractions is summarised in table (5 – 2). These results will demonstrate the effect of fibre volume fraction on ILSS in the composite.

The investigation of the ILSS test on hybrid and non-hybrid glass woven fabric reinforced epoxy resin composites at 48% V_f is studied for both warp and weft directions. The results are shown in table (5 – 3) and are graphically presented in figure (5 – 2). The quantification of AE values during ILSS testing including the hybrid and the non-hybrid for both warp and weft directions are summarised in table (5 – 4). These results will highlight the effect of fibre hybridisation on ILSS in the composite.

5 – 1 – 2 Discussion of the effect of fibre volume fraction on ILSS

The plot of ILSS in figure (5 – 1) allows the direct comparison of the value and performance of four different glass V_f composites. The shapes of load-displacement curves vary, and differ in their values of the ILSS strength at break point. The first set of composites with lowest fibre volume fraction at 38% V_f has the lowest shear strength value. The set of composites with highest fibre content at 64%V_f has the greatest shear strength value. The shear strength increases approximately by 10% from one fibre volume fraction to another in this investigation. The **knee point** appears on each load-displacement curve that exhibits varying values for each fibre volume fraction composite. The **knee point** and non-linearity response has been examined individually for each ILSS test (see figure 5 – 3).

The AE response and details including four V_f composites are shown in figure (5 – 1). The plot of AE provides two essential points of information: the starting point of actual deformation after a load is applied and continuous information concerning the damage sequential process during the test. It provides a clearer insight into the individual stages of the test depending on structure and morphology as well as about failure mechanisms taking place.

The AE **zones classification** technique has been used in this study in order to obtain the maximum information for different deformation levels during ILSS tests. The plots of ILSS load-displacement including its AE ring down count (RDC) curve in the figure (5 – 3) has been divided into three zones are as follows:

Zone A: The AE line parallel to the x-axis, until the AE onset point associated with the initial linear portion of ILSS load-displacement response, indicates that there is no AE activity in this zone. There was no existing record of **RDC** or any rise on the AE curve to define any plastic deformation of the composite specimen under ILSS loading in this zone. The Knee point of the

ILSS load-displacement curve is the first indication of non-linearity. The correlation between the AE onset point and the knee point of the load-displacement curve has also been examined carefully for each ILSS test. The explanation of non-linearity agrees with Wooh who showed that no macroscopic damage was found in the linear elastic region (Wooh et al. 1995).

Zone B: AE rise appears at the onset point, indicating the initiation of the first sign of damage in the construction of the composite material. Zone B has been determined from the continuous low level of AE ring down count recorded and it is believed this corresponds to matrix micro cracking. This is interpreted as being due to possible void formation in the composite and possible fibre/matrix interface failures.

Zone C: The AE ring down count continues rising almost linearly and progressively in zone C until specimen fracture. The higher **RDC** recorded corresponds to fibre/matrix interface damage which progressively increases to create **layer delamination** in the laminate.

The use of AE has been employed by Okoroafor, Netravali and Bondt to measure the fibre-matrix interfacial strength between a fibre and a matrix (see Netravali et al. 1991 and Bondt et al. 1993) and (Okoroafor et al. 1996). Wang observed high AE activity associated with layer delaminations (Wang et al. 1995). The **zone classification technique** of load-displacement and its relating AE curves have been utilised in this study to extract the maximum possible information from each variation in the damage events. The knee point of load-displacement and AE onset point relationship of woven glass fibre in the composites could be used and interrelated to the specimen fracture surface. The ILSS values and qualitative images of damage accumulation in woven composites are also interrelated.

The investigation of the ILSS test on non-hybrid glass woven fabric reinforced epoxy resin composites including four different glass fibre volume fractions have been studied carefully. The results show that the ILSS (τ) increases with the increase in overall fibre volume fraction due to an increase in the number of woven layers in the composite reinforcement. The representative figure (5 – 3) and the quantification of these values are summarised in table (5 – 1). The **AE** activities recorded a variation in the magnitude of the ring down count in each zone and distinct values corresponding to break points as summarised in table (5 – 2). It is essential to take into consideration that the higher the AE activity the greater the damage especially in relation to the interfacial bond and layer delamination.

It has been observed that the lower the V_f of the composite, the greater the values of ring down counts on the AE curve in each zone. AE activities monitored during ILSS (comparison view in figure 5 – 1), reveal that a higher V_f in the composite shows failure at lower displacement levels compared with those of low V_f composites. Therefore, the variations of the ILSS are considered to be due to differences in the overall fibre coating concentration and their interaction with the matrix caused by the variation of fibre volume fraction. This causes some changes in the overall fracture performance of the specimens. This is evidence that the variation in fibre volume fraction in the composites leads to a change in fracture performance and, presumably, refers to a change in the **interphase** mechanism. The interphase refers to a region between the bulk matrix and the glass fibres in the composite. Further details concerning the interphase phenomenon can be found in the DMTA analysis section three. Scanning Electron Microscopy (SEM) of the fracture surface of the specimen identifies variations in the damage performance for each individual composite.

It should be mentioned that the composite of 64% V_f was laminated with 14 woven layers. It should also be pointed out that the composite of 38% V_f was laminated with 8 layers only while the composite of 56% V_f was laminated with 12 layers and the composite of 48% V_f laminated with 10 layers.

The ILSS load-displacement together with its AE **rate** curves of woven fabric reinforced epoxy resin composite are represented in figure (5 – 4). The rate of the AE recorded and the number of peaks for each composite has been studied individually. The quantification of rate values for each composite is summarised in the table (5 – 2). It was observed that the number of peaks decreased with increasing fibre V_f in the composites, which clearly demonstrates a case of increased overall adhesion.

ILSS fracture performance of (four different Vf) woven composites was investigated by SEM. The objective of investigating the fracture surface of the test specimens after the ILSS test is to identify the damage performance for each individual composite.

The micrograph of SEM in figure (5 – 5) of non-hybrid glass woven fabric composite at 38% V_f exhibits the shear path with very little shear cusps and debris on the fibre surface indicating poor fibre/matrix interfacial bonding. The poor fibre/matrix interfacial bond causes the failure in the

matrix resulting in fewer fabric layers in the composites and high matrix volume fraction (V_m). The SEM micrograph shows a number of delamination paths in the composite.

The SEM micrograph in figure (5 – 6) of the ILSS fracture surface of non-hybrid glass woven composite at 48% V_f shows the shear fracture path with a small amount of irregular debris and shear cusps on the fibre surface indicating a weak fibre/matrix interfacial bond. The shear propagates through the composite primarily near the fibre/matrix interface. This infers a fragile matrix/fibre adherence. The SEM micrograph shows a number of delamination paths of shear fracture in the composite.

The SEM micrograph in figure (5 – 7) of the ILSS fracture surface of non-hybrid glass woven fabric composite at 64% V_f exhibits ILSS fracture with a single path and large number of hackles on the fibre surface. The large number of hackles indicates the ILSS path was shaped from a good fibre/matrix interfacial bond within the woven layer in the composite.

5 – 1 – 3 Discussion of hybridisation effect on ILSS.

The result in table (5 – 3) shows that the interlaminar shear strength (τ) of the hybrid composite is superior to the non-hybrid composite for the **weft** direction by approximately **12%** and for the **warp** direction by approximately **5%**. The shapes of load-displacement curves of the hybrid and non-hybrid composites in figures (5 – 2) vary and differ in their values of the ILSS (τ).

The **AE** response of the hybrid and non-hybrid composites shows that the knee points appearing on each load-displacement curve indicate individual values for each composite (see table 5 – 4). The **zone classification** methodology of plots has been followed in a similar manner to the previous section. An essential feature is that there is a distinct value in each zone and at breaks (the shear strength) for each composite. It can be seen that the AE of non-hybrid composite leads to an increase in the values of ring down count and rate compared to the hybrid composites in each zone.

The AE pattern recognition, including (figure 5 – 2) the selection and classification feature of hybrid and non-hybrid glass woven reinforced epoxy resin composites at equal fibre volume fraction, has been analysed in this section. The AE ring down count and rate in hybrid woven composites differentiates the hybridisation performance of the R-glass and E-glass while the

non-hybrid woven fabric contains only E-glass in the composites. The hybrid composites exhibited higher stress at the knee point and higher ILSS than the non-hybrid composites. The effect of hybridisation appears on the AE and load-displacement curves in each zone, details of the values are illustrated in table (5 – 4). This is an indication of greater shear fracture occurring in the non-hybrid composite, which is substantiated by the SEM micrograph showing a higher number of delamination paths and shear fractures as follows:

ILSS fracture performance of composites presented by the SEM micrograph in figure (5 - 8) shows the ILSS fracture surface of the **hybrid** glass composite **(weft direction)**. The ILSS fracture path and resin hackles along the shear path reveals that the crack path passes round the pocket of woven fibres indicating good fibre/matrix interfacial bonding. The debris and shear cusps are the result of the matrix failure, which dominated fracture along fibre bundles under the effect of undulations created by weaving.

The SEM micrograph in figure (5 – 6) of ILSS fracture surface of **non-hybrid** glass woven fabric composite at 48% V_f indicates a weak fibre/matrix bond as has been discussed in the previous section. The **number of delamination paths** of shear failure was higher in the non-hybrid composites than the number of delamination paths in the hybrid composites.

Theocaris has reported that the two Mesophase layers (or interphase) formed between the main phases as boundary layers dictate the quality of adhesion between phases. Their properties are thus critical for predicting the mechanical properties of sized fibre-reinforced composites (Theocaris 1987, Theocaris 1992, Theocaris and Stavroulakis 1997). The dynamic property results further provide the evidence of the effect of the interphase properties on the ILSS performance (see the DMTA analysis in section three of this chapter). Many researchers have observed similar behaviour. (Ranade et al. 1997, Agrawal and Drzal 1996) reported that the overall properties of a fibre reinforced composite material are dependent upon the mechanical and chemical stability of the interfaces, or interphase, formed between the reinforcing fibres and the surrounding matrix

The following results can be outlined from the above discussion:

- Table (5 – 1) shows the ILSS (τ) **increases with the increase of overall fibre volume fraction** in the composites. The increase in the number of layers in the composite leads to a

change in the interphase mechanism (properties) as explained by DMTA analysis in section three. The interphase property dictates the gross mechanical performance and structural integrity of the composite as a whole. Therefore the higher fibre volume fraction in composites produces greater interphase strength. A detailed specification concerning the interphase phenomenon can be found in chapter two – section (2 – 8) and section three of chapter five.

- The shear failure path in each set of laminates was the result of multiple matrix cracking and fibre/matrix debonding, which led to delamination path extension. The **number of delamination** paths of shear failure was higher in the low V_f composites than in high V_f composites. The SEM micrographs as shown provide a clearer view of the individual test failure mechanism in the composites.

- It has been observed that the declining glass V_f in the composite leads to growth in the magnitude of the AE ring down counts in each zone, (see figure 5 – 1). The number of peaks in the **rate** and the peak length decrease with increasing V_f in the composites. This clearly demonstrates a case of increased overall adhesion, (see example plot of the rate in figure 5 – 4).

- The AE values obtained (table 5 – 2) correspond to different levels of micromechanical failure. An example would be matrix failure, which results in a number of fibre-matrix interfacial failures including layer delamination. The AE activities monitored during ILSS, leads to the conclusion that higher levels of V_f in the composite show failure earlier or at less deflection values than those of low V_f composites (see figure 5 – 1).

- Table (5 – 3) shows the ILSS (τ) of non-hybrid composites compared with those of hybrid composites for both weft and warp directions. The chemical composition of R-glass fibres differs from that of E-glass (See the chemical composition of each glass in table (2 – 1). It is believed that differing fibre composition influences the fibre-coating distribution on the R- and E-glass fibres. This could lead to different micro- and macro-mechanical performance between the hybrid and non-hybrid composites. Therefore, the hybrid composite had higher interlaminar shear strength in composites compared to the non-hybrid composite. The dynamic property result further provides the evidence of the effect of the fibre treatment

distribution on the composite performance (see the DMTA analysis in section three of this chapter).

- The AE curves of hybrid and non-hybrid glass woven fabric reinforced epoxy resin composites vary both in form and magnitude. The AE activity reveals that both composites were brittle. The hybrid composite exhibits higher toughness than the non-hybrid composites. Therefore the hybrid composite could absorb more energy with a sustained crack growth stability through crack surface bridging and crack tip blunting.

- It is observed that ILSS of the hybrid composite leads to a reduction in the magnitude of ring down count in each zone compared with that of the non-hybrid composite. The variation in AE ring down counts values at ILSS indicates accumulated damage events were higher in the case of non-hybrid compared with hybrid composites. The higher the AE activity, the greater is the damage. The hybrid composite exhibits less delamination when observed by SEM.

Table 5-1 ILSS Test Results of Non-hybrid Glass Woven Composites (including **Four Different Fibre Volume Fractions).**

ILSS Test Results of Non-hybrid Glass Woven Fabric Composites **at Different Fibre Volume Fractions.**							
Test	Fibre Volume Ratio (%)	No. of Plies in 2mm Thickness	Load (N) @ Knee Point	ILSS (Mpa)		Load (N)	
			Mean	Mean	Std.Dev.	Mean	Std.Dev.
Non-hybrid @38%	0.38	8	296.10	18.11	1.80	480.80	15.00
Non-hybrid @48%	0.48	10	370.13	23.29	2.10	598.60	18.80
Non-hybrid @ 56%	0.56	12	476.90	27.42	2.41	769.20	22.10
Non-hybrid @ 64%	0.64	14	516.28	29.13	2.67	831.10	24.70

Table 5-2 **AE** Patent representing **ILSS** of Non-hybrid Fibre Glass Woven Composites including Four Different **Fibre Volume Fractions**

AE Patent representing **ILSS** of Non-hybrid Fibre Glass Woven Composites at Four Different **Fibre Volume Fraction**							
				Zone B		AE at Finial Fracture	
Laminates	Thickness (mm)	Fibre Volume Fraction (%)	No. of Plies in 2mm Thickness	Corr. Of Knee & Onset Points	RDC	RDC	AE Rate (Highest peak)
Non-hybrid @38%	2.0	0.38	8	yes	3.36E+04	2.80E+05	3.60E+04
Non-hybrid @48%	2.0	0.48	10	yes	2.35E+04	1.96E+05	2.60E+04
Non-hybrid @ 56%	2.0	0.56	12	yes	1.98E+04	1.65E+05	2.10E+04
Non-hybrid @ 64%	2.0	0.64	14	yes	1.58E+04	1.32E+05	1.70E+04

Table 5-3 Comparison **ILSS** Test Results between Non-hybrid and Hybrid Woven Composites

ILSS Test Results of **Non-hybrid** Woven Composites							
Test	Fibre Volume Ratio (%)	No. of Plies in 2mm Thickness	Load (N) @ Knee Point	ILSS (MPa)		Load (N) @ Final Fracture	
			Mean	Mean	Std.Dev.	Mean	Std.Dev.
Non-hybrid **(Weft)**	0.48	10	370.13	23.29	2.17	598.00	18.80
Non-hybrid **(Warp)**	0.48	10	377.20	23.52	2.64	610.00	18.85
ILSS Test Results for **Hybrid** Woven Composites							
Hybrid **(Weft)**	0.48	10	447.30	26.49	2.86	715.00	20.00
Hybrid **(Warp)**	0.48	10	411.20	24.92	2.65	660.00	19.00

Table 5-4 AE Patent representing ILSS of Non-hybrid and Hybrid Glass Woven Composite

AE Patent representing **ILSS** of Non-hybrid and Hybrid of Glass Woven Composites						
			Zone B		AE at Finial Fracture	
	Laminates	Fibre Volume Fraction (%)	Corr. Of Knee & Onset Points	RDC	RDC	AE Rate
Non-hybrid	(Weft)	0.48	yes	2.35E+04	1.96E+05	2.60E+04
	(Warp)	0.48	yes	2.22E+04	1.85E+05	2.70E+04
Hybrid	(Weft)	0.48	yes	1.68E+04	1.40E+05	2.20E+04
	(Warp)	0.48	yes	2.16E+04	1.80E+05	2.65E+04

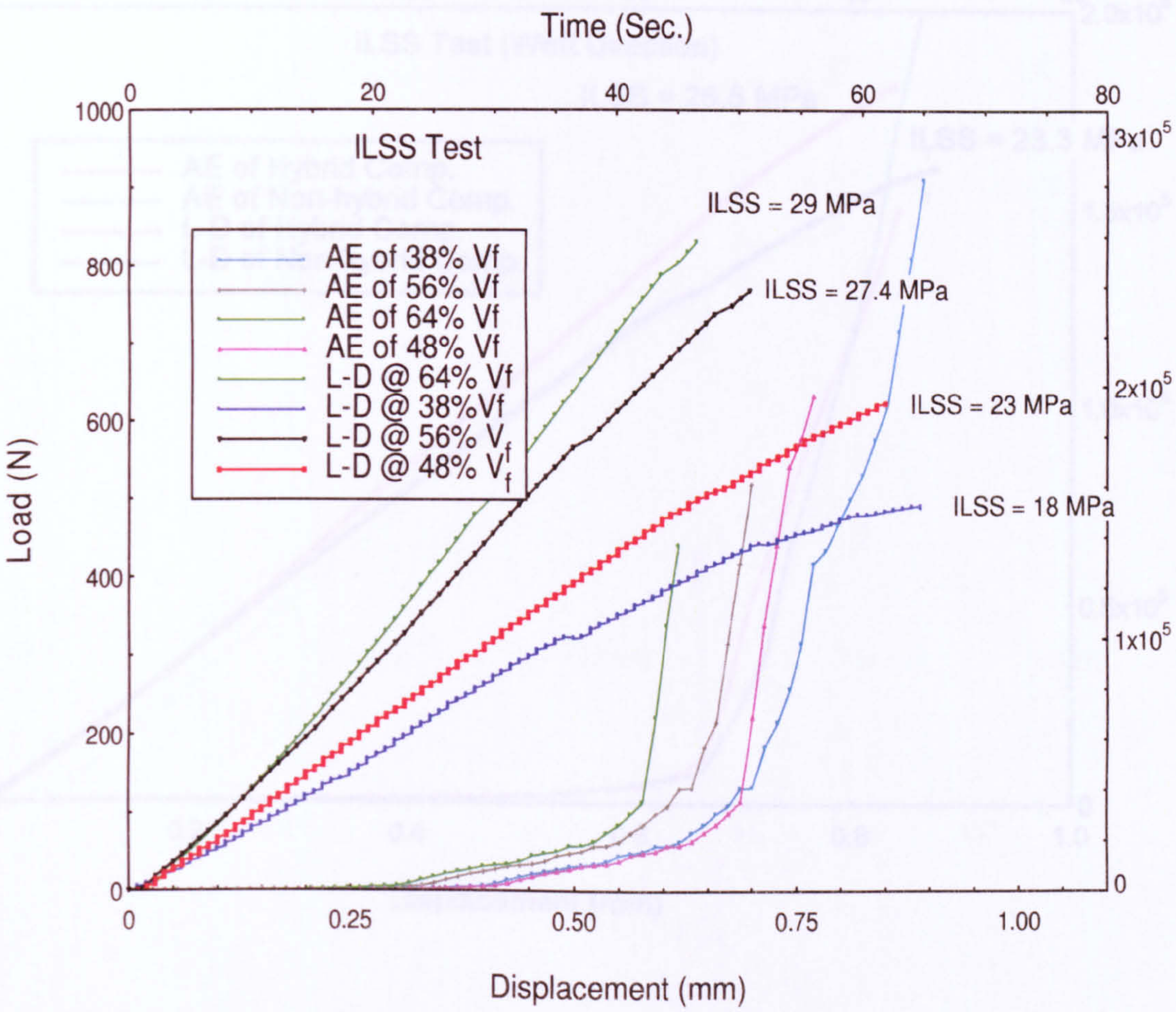

Figure (5 – 1) ILSS plot of Load-Displacement and its RDC curves of **Non-hybrid** glass woven fabric reinforced epoxy resin composites including **four different fibre volume fractions**.

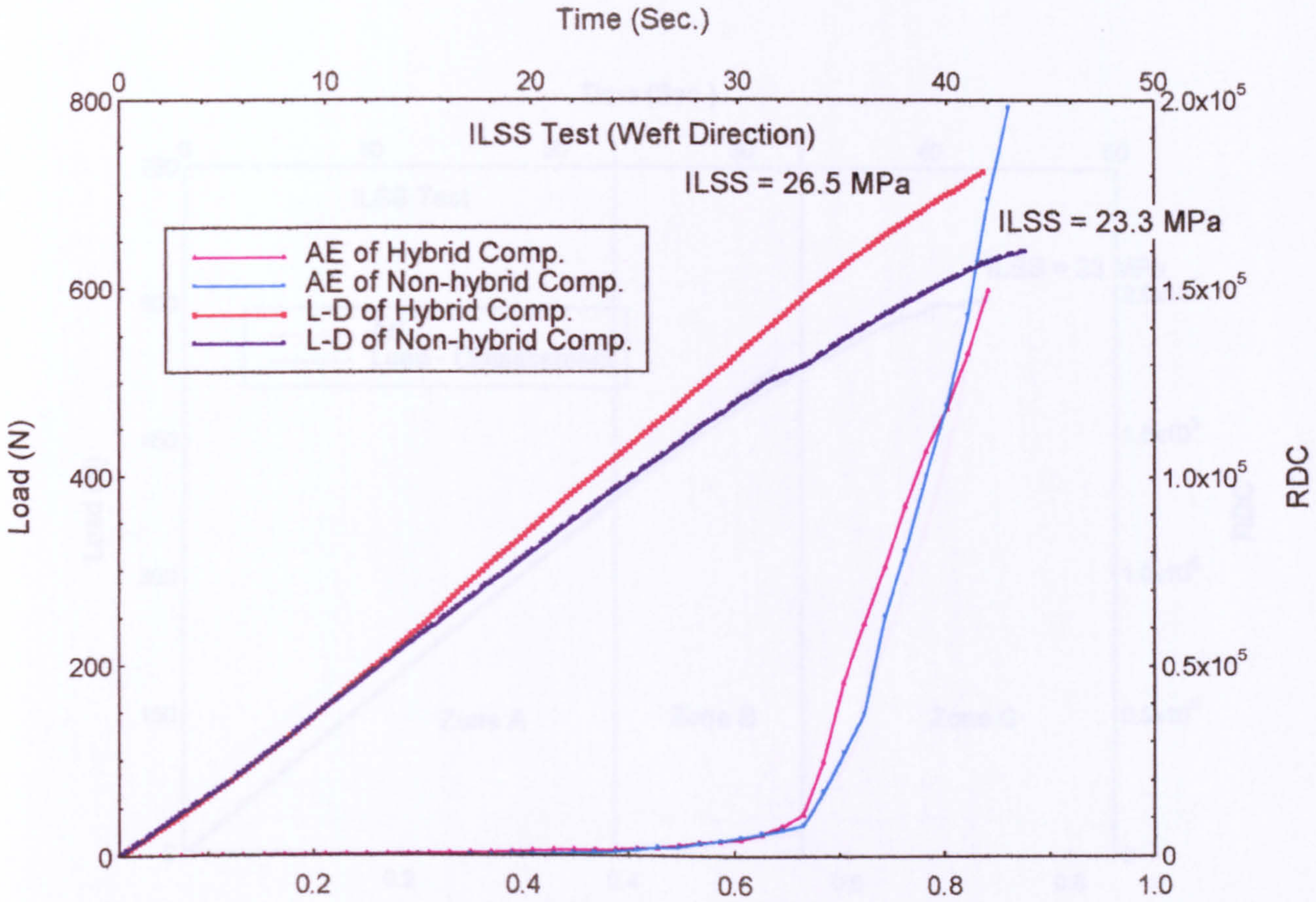

Figure (5 – 2) ILSS plot of L-D and its RDC curves of **Hybrid** and **non-hybrid** glass woven reinforced epoxy resin composite for **weft direction** at 48% V_f.

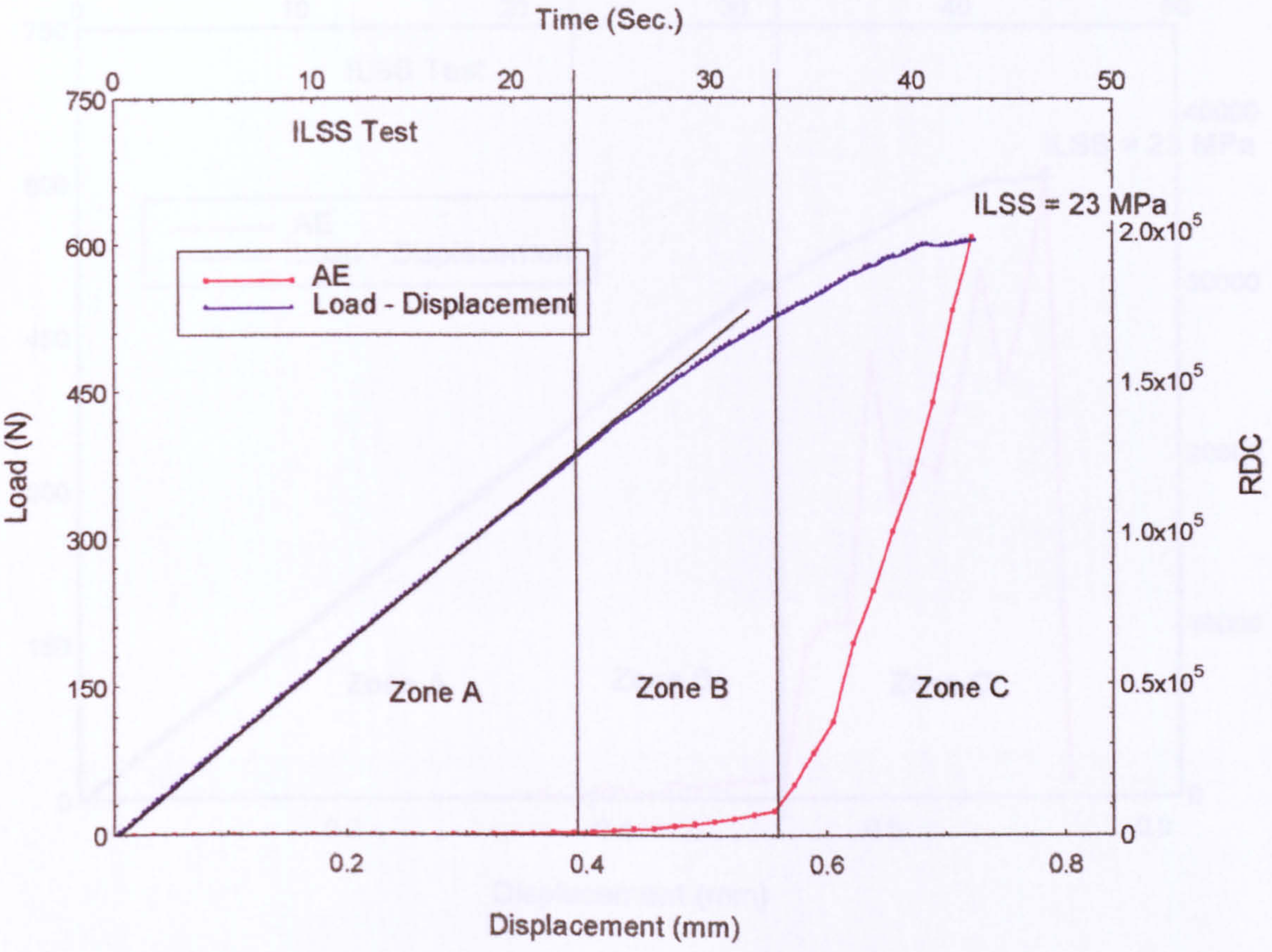

Figure (5 – 3) the **zone classification technique** used in the ILSS plot of **Load-Displacement** and its AE **ring down count** curves of non-hybrid glass woven reinforced epoxy resin composite.

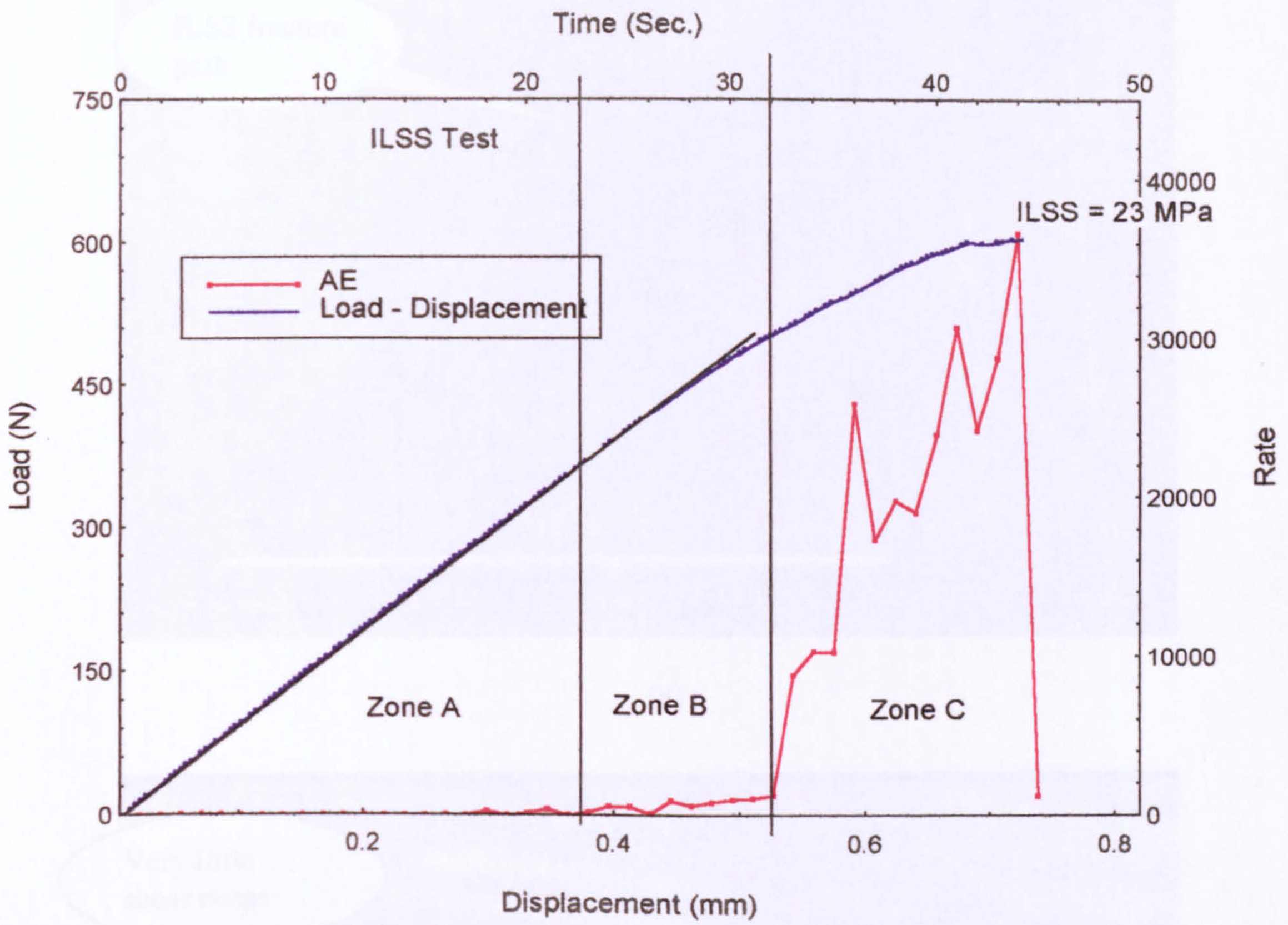

Figure (5 – 4) the **zone classification technique** used in the ILSS plot of **Load-Displacement** and its AE-**rate** curves of non-hybrid glass woven-reinforced epoxy resin composite.

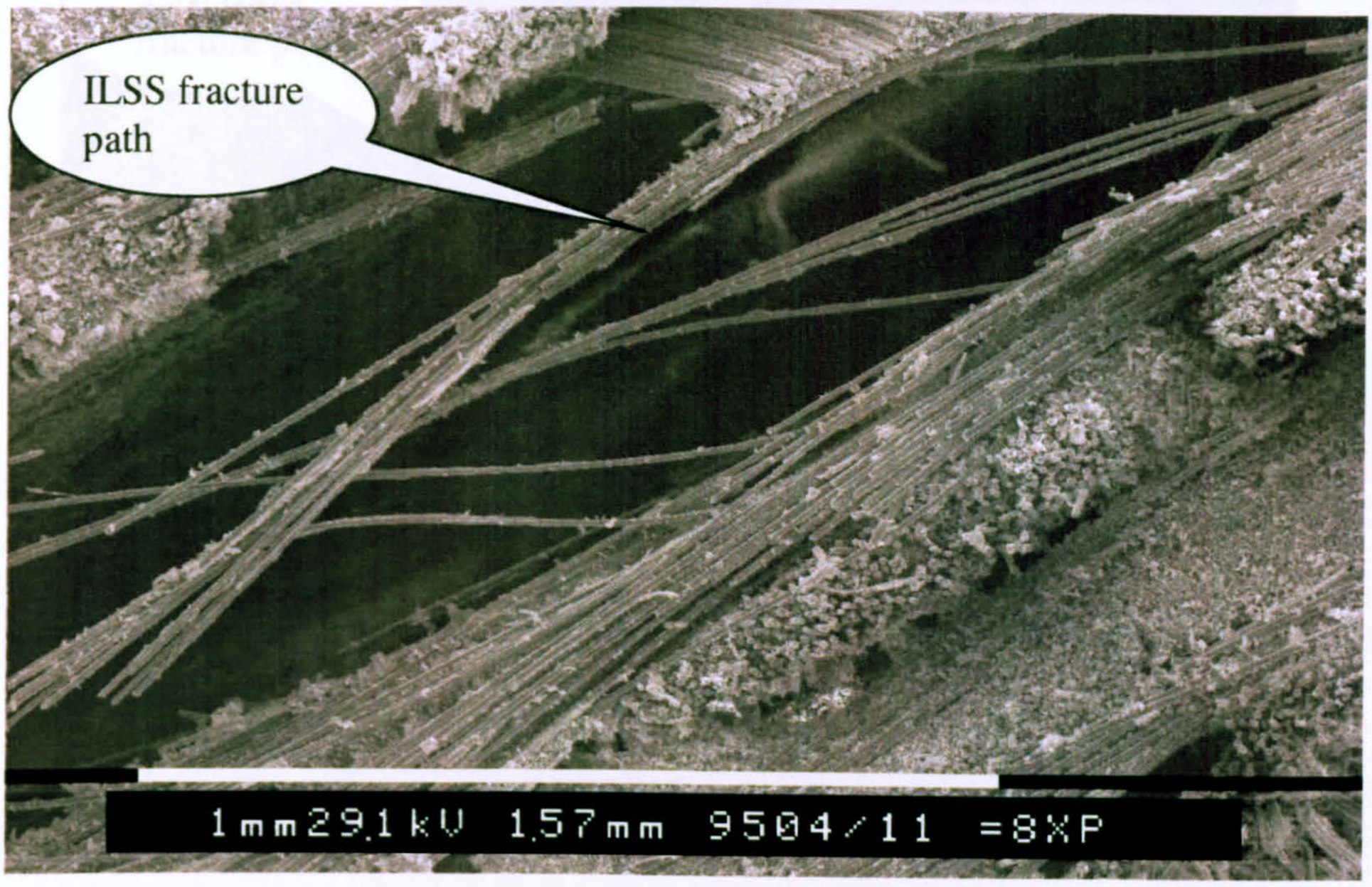

(a)

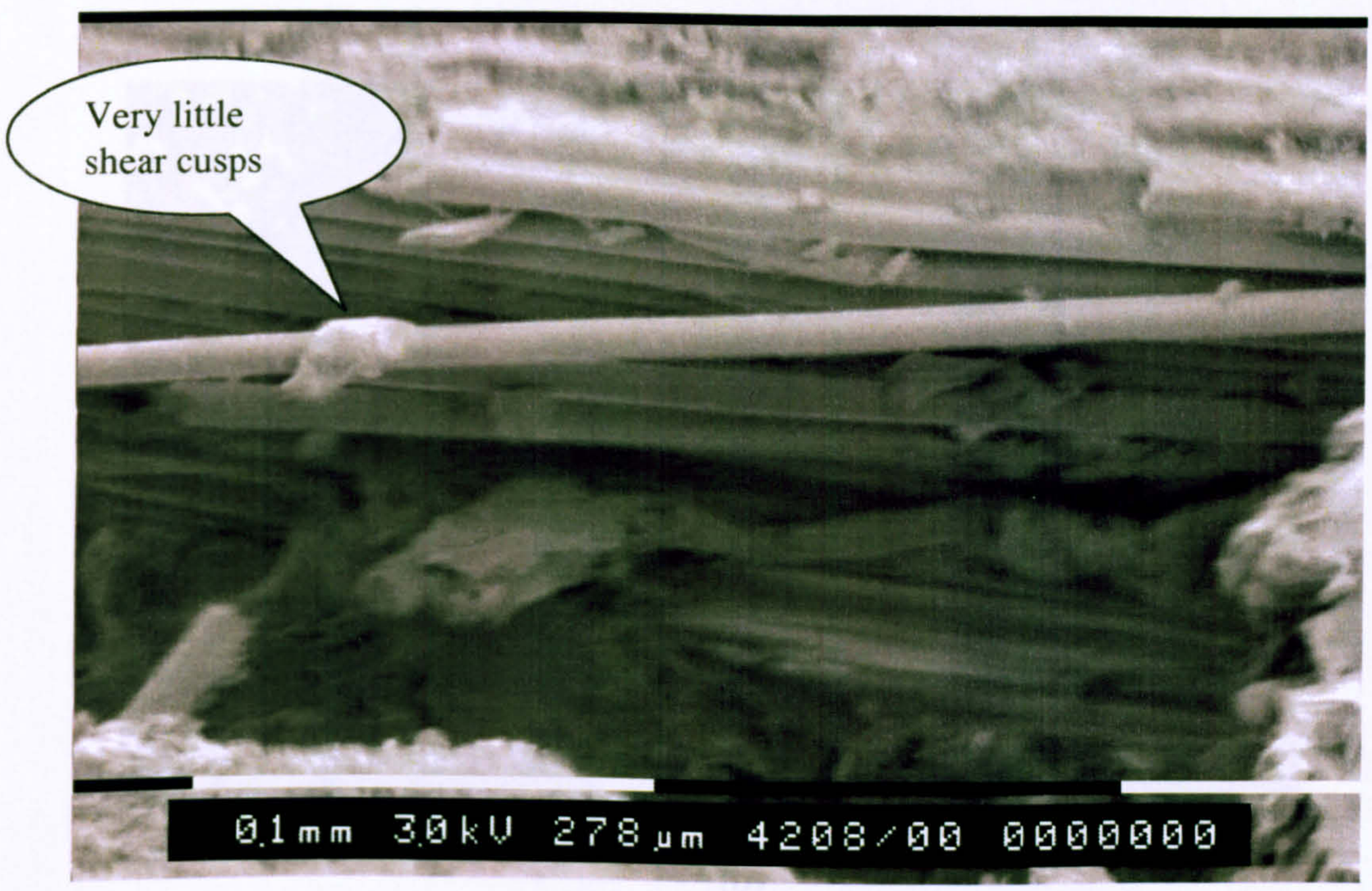

(b)

Figure (5 – 5) SEM micrograph of ILSS fracture surface of Non-hybrid glass woven fabric composite at **38%** V_f shows (a,) 85x view of the ILSS fracture path. (b) 500x very little shear cusps on the fibre surface indicating poor fibre/matrix interfacial bond.

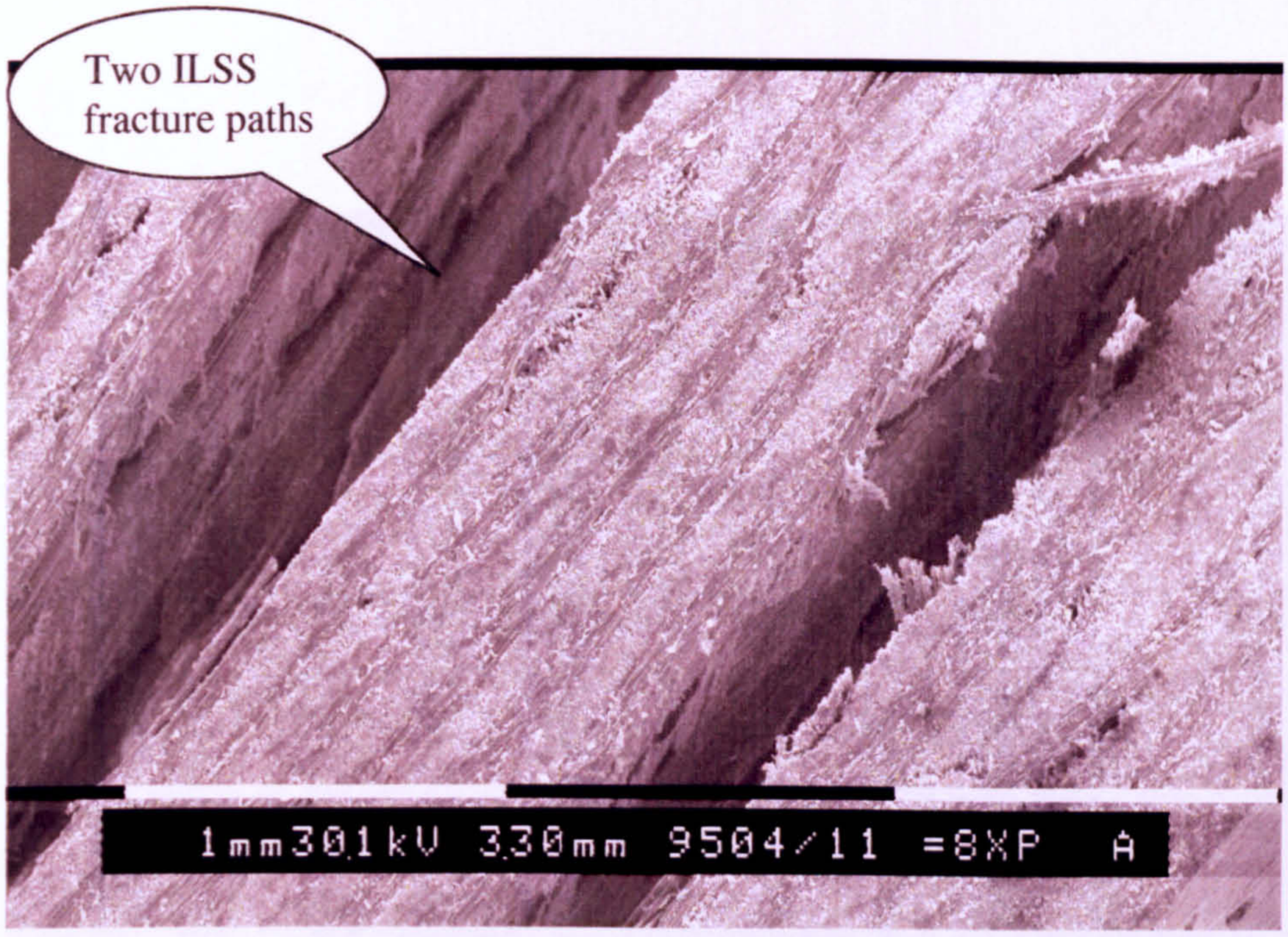

(a)

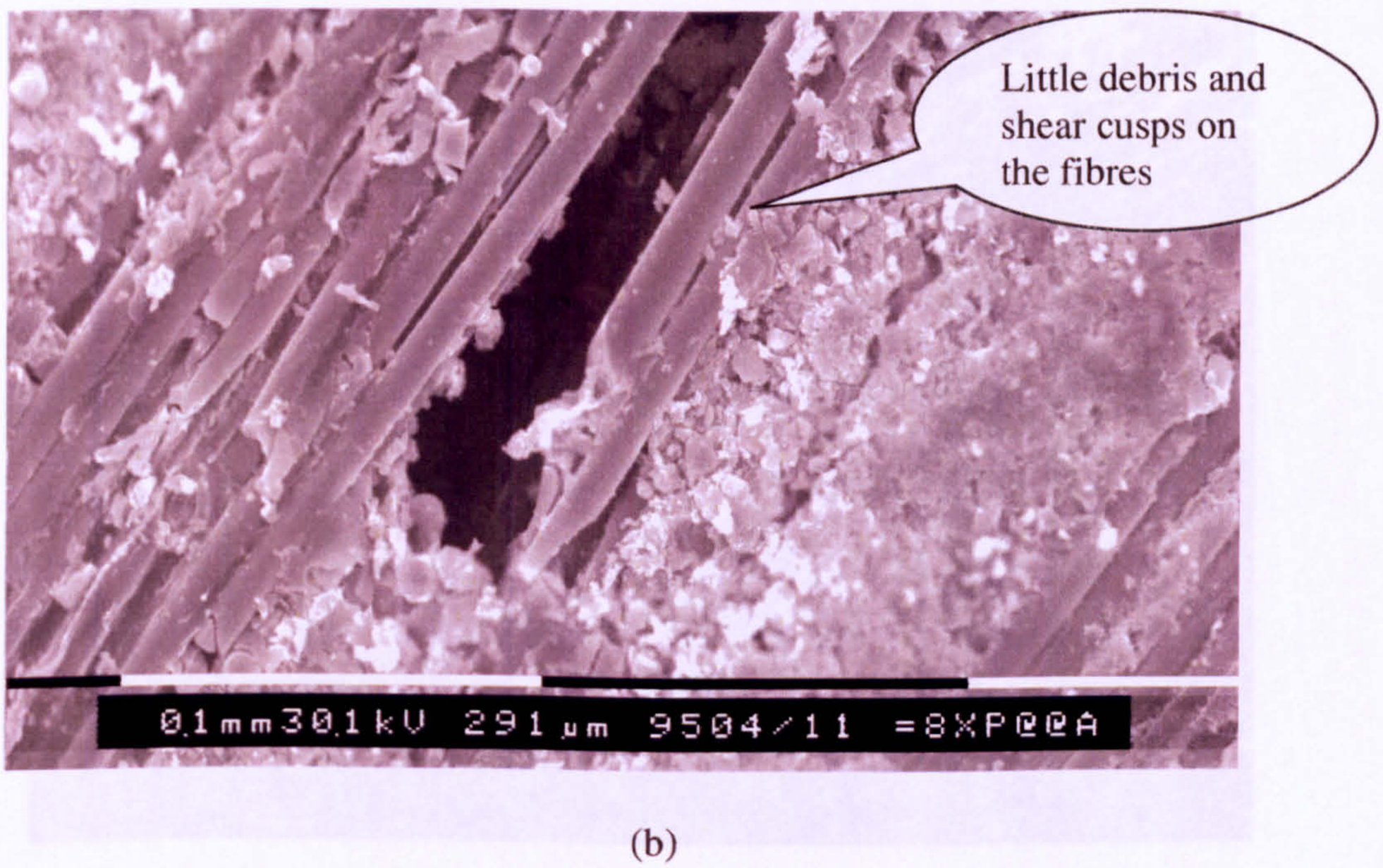

(b)

Figure (5 – 6) SEM micrograph of ILSS fracture surface of **Non-hybrid** glass woven fabric composite at **48%** fibre volume fraction shows (a) 40x view of the ILSS fracture path. (b) 420x higher magnification shows small debris and shear cusps on the fibre surface indicating weak fibre/matrix interfacial bond.

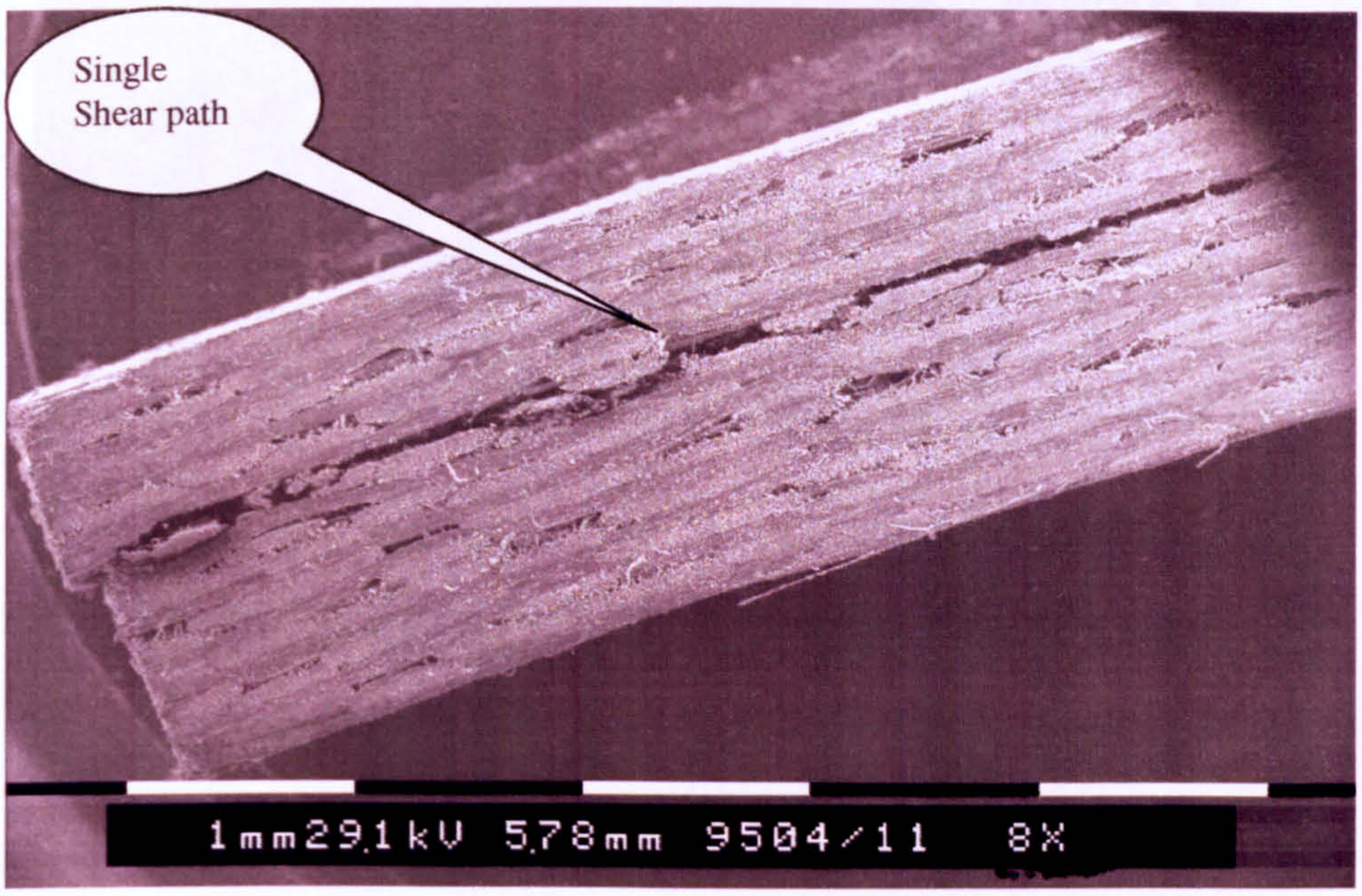

(a)

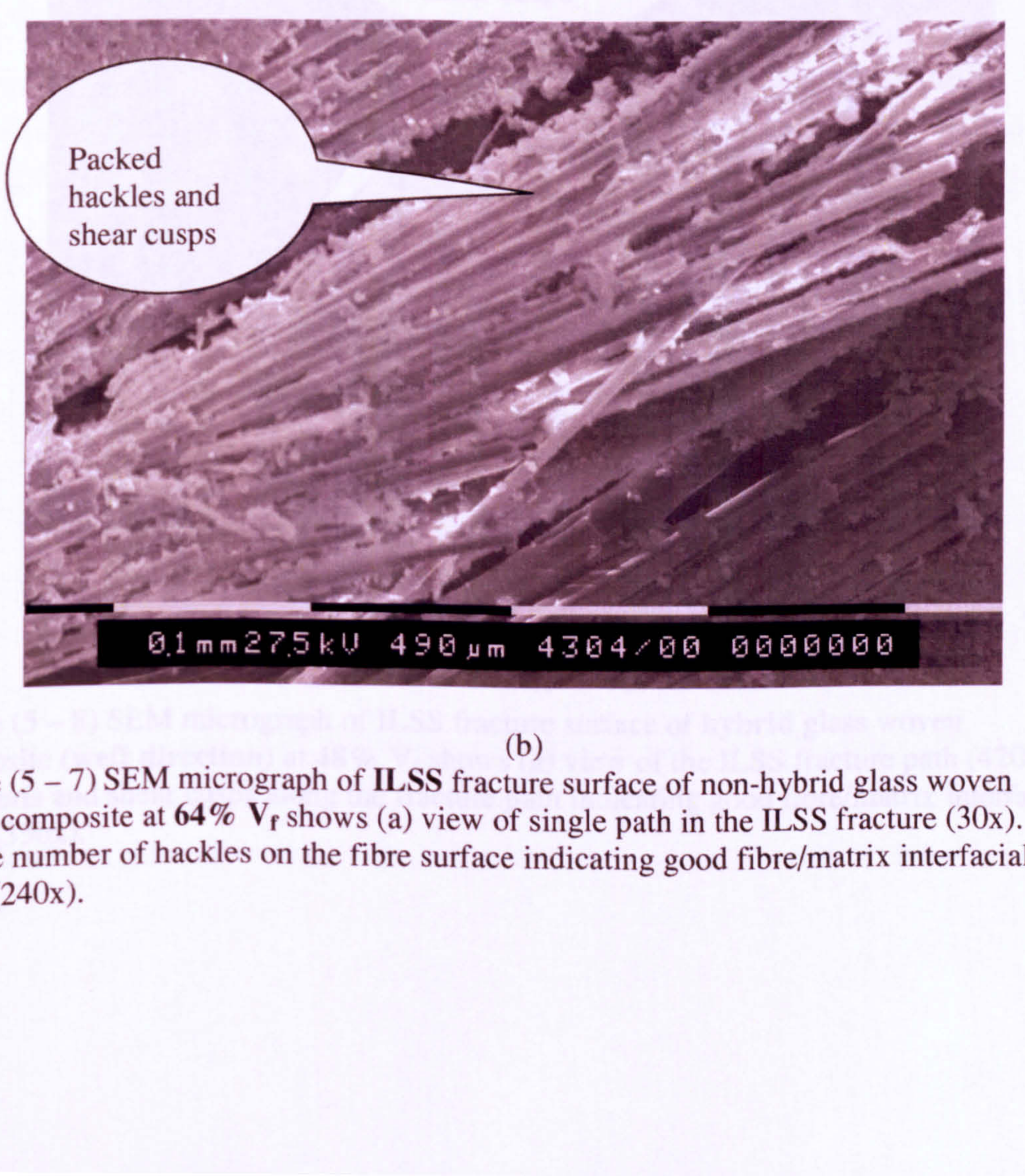

(b)

Figure (5 – 7) SEM micrograph of **ILSS** fracture surface of non-hybrid glass woven fabric composite at **64% V_f** shows (a) view of single path in the ILSS fracture (30x). (b) a large number of hackles on the fibre surface indicating good fibre/matrix interfacial bond (240x).

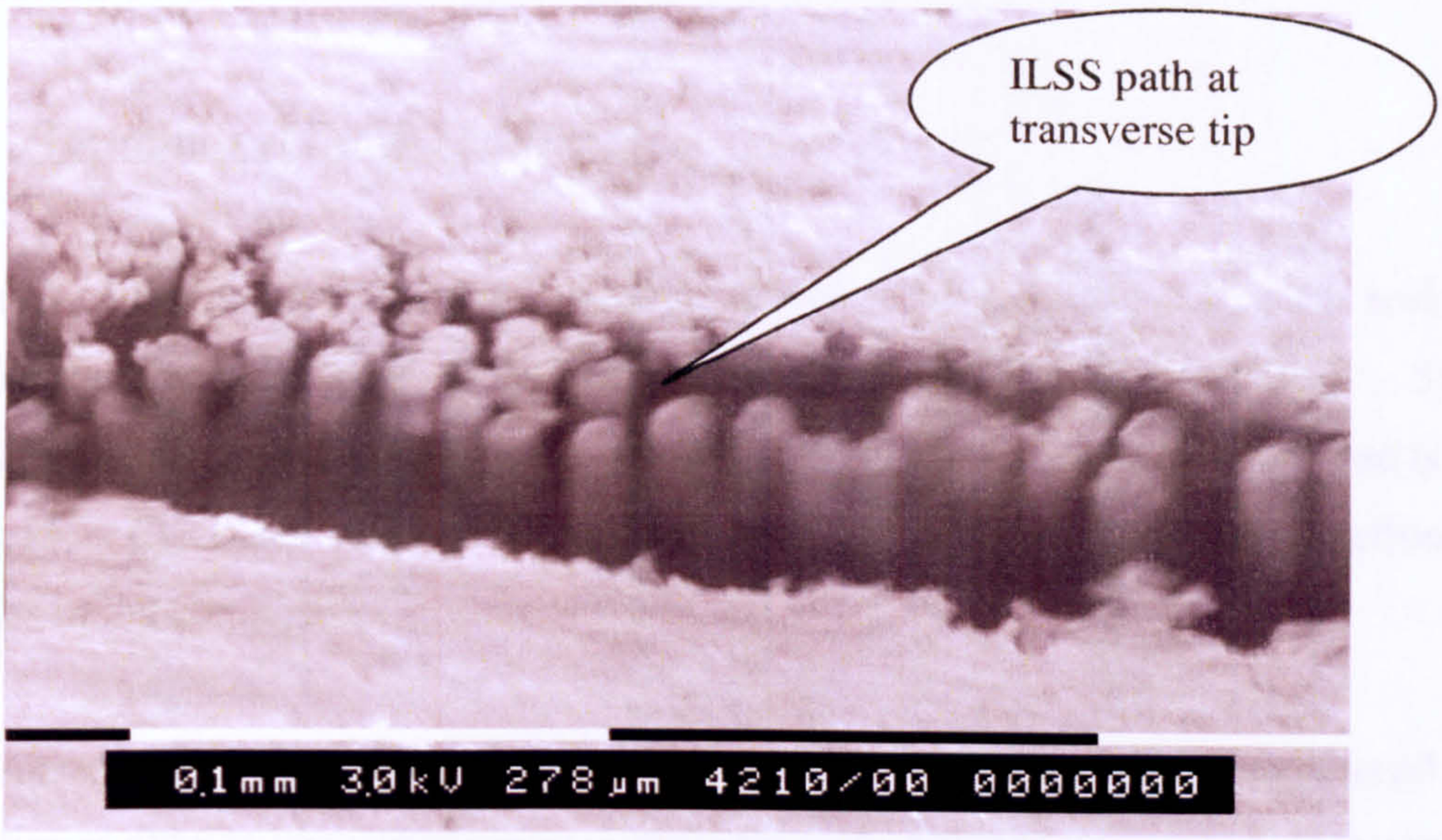

(a)

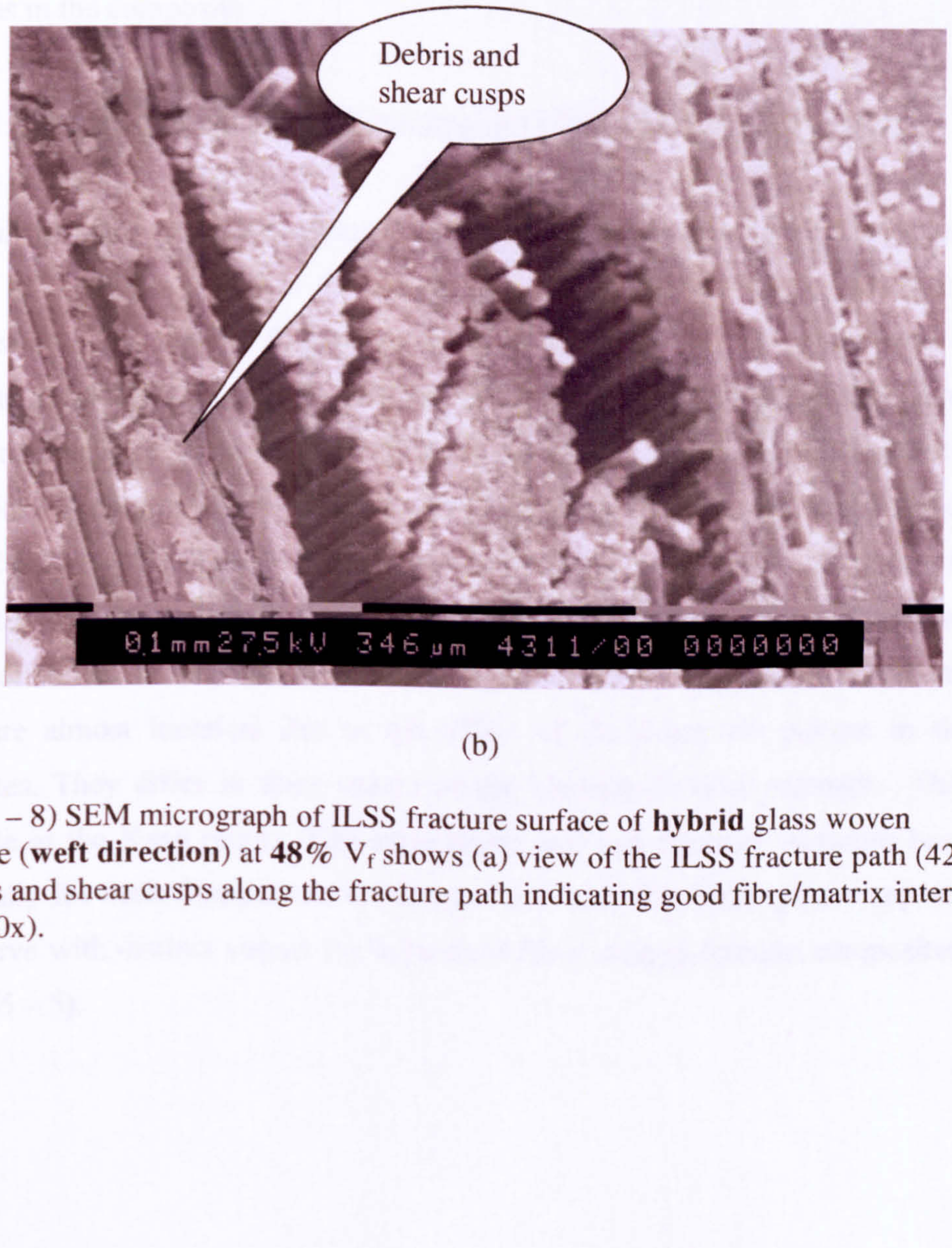

(b)

Figure (5 – 8) SEM micrograph of ILSS fracture surface of **hybrid** glass woven composite (**weft direction**) at **48%** V_f shows (a) view of the ILSS fracture path (420x). (b) debris and shear cusps along the fracture path indicating good fibre/matrix interfacial bond (350x).

5 – 2 Section Two: Flexural Properties

5 – 2 - 1 The results of flexural tests

The results of flexural tests on non-hybrid glass woven fabric reinforced epoxy resin composites including four different glass fibre volume fractions are set out in table (5 – 5). They are graphically presented in figure (5 – 9). The relative AE ring down count and rate is summarised in table (5 – 6). These results will highlight the effect of fibre volume fraction on flexural properties in the composite.

The results of the flexural test on hybrid and non-hybrid glass woven reinforced epoxy resin composites at 48% V_f are summarised in table (5 – 7). They are graphically presented in figures (5 –10 and 5 – 11). The relative values of AE activities monitored during the flexural tests are summarised in table (5 – 8). These results will reveal the effect of fibre hybridisation on flexural properties in the composite.

5 – 2 – 2 Discussion of the fibre volume fraction effect on flexural properties.

The result in table (5 – 5) confirms that the flexural strength significantly increases with the increase of V_f. This is due to the increase in the number of woven layers of the composite reinforcement. The highest flexural modulus is achieved by the highest fibre volume fraction composite at 64% V_f, and the lowest flexural modulus is achieved by the lowest fibre volume fraction composite at 38% V_f. The flexural strength increases from 38% to 48% V_f and from 48% to 56% V_f (both by approximately 23%). However the flexural strength increase only a 7% from 56% V_f to 64% V_f, which further shows the limitation effect of V_f reinforcement in the composite. The plot of flexural tests in figure (5 – 9) allows a direct comparison of the values and performance of four different fibre volume fraction composites. The stress-strain curve shapes are almost identical due to the effect of the 8-harness pattern in the woven fabric composites. They differ in their values of the ultimate flexural strength. This is particularly noticeable at the Knee points. The **knee point** and non-linearity response has been examined individually for each flexural test (see figure 5 – 12). The knee points appear on each stress-strain curve with distinct values for individual fibre volume fraction composites as summarised in table (5 – 5).

AE activity monitored during the flexural tests including the four different V_f non-hybrid E-glass woven composites are presented in figure (5 – 9b). The AE zones classification technique (figure 5 – 12) has been used in a similar methodology to that in the previous section in order to obtain the maximum possible detail for failure process analysis. The quantification of **AE values** is summarised in table (5 – 6).

The stress-strain trends of four V_f composites are presented in figure (5 – 9a) and the corresponding AE curves presented in figure (5 – 9b). The correlation between the AE onset point with the knee point of the flexural stress-strain curve has been evaluated individually for each flexural test. The values are recorded in table (5 – 6). The RDC provides the two lowest values of 56% V_f and 64% V_f, and the highest two records for composites of 48% V_f and 38% V_f. It was found, after careful study of the rate for each composite, that the number of peaks decreases with increase of V_f in the composites (see the example plot of the rate in figure 5 – 13).

The high level of AE ring down count was recorded due to low V_f in the composites. This clearly reveals that the greater damage, such as fibre pullout and fibre rupture, is associated with the low V_f composites. This is shown by the SEM micrograph of the flexural fracture surface. The SEM micrograph further reveals that the interlaminar cracking and fibre buckling dominates in the high V_f composite.

The flexural fracture performance of four different V_f composites were investigated by SEM. The SEM micrograph in figure (5 – 14) shows the flexural specimen of the non-hybrid E-glass woven composite of **low composite V_f** illustrating:

(a) through-thickness view indicating the fracture surface dominated by tensile failure.
(b) fibre bundle pullout.
(c) rear view of matrix deformation resulting in curved plates of resin.
(d) fibre bundle fractures formed in the undulation region of woven fabric.

The SEM micrographs in figure (5 – 15) show the flexural specimen of non-hybrid E-glass woven fabric composite of **high composite V_f** and indicate:

(a) through-thickness view of the fracture surface dominated by shear side of the three-point bend and buckling of fibre under the effect of weaving formed by beam compressive stress.
(b) shear path propagated from the midpoint of the specimen towards the end of the specimen.
(c) matrix crack propagation tending to form a shear path due to the fibre-rich region.

(d) fibre bundle pullout occurring in the high V_f in the undulation region near the transverse fibres.

The flexural load imposes tensile, compressive and shear stresses on different locations within a structure. The top surface is in compression, the bottom in tension and the shear is through-thickness. The change in flexural strength (σ_f) is attributed to differences in the failure mode and the fibre/matrix adherence. It was indicated in the ILSS section that the higher the fibre volume fraction, the greater the ILSS in the composite. The greater interfacial strength leads to an increase in flexural strength (σ_f). This means the fibre/matrix interaction depends on the number of woven fabric layers in the composites. In other words, the fibre/matrix adhesion was dependent upon the fibre surface treatment concentration and interaction in the composites as a result of fibre volume fraction variation.

In the composites where there is the strongest interface bond, there is a significant increase in the flexural strength due to a change in the failure mode from an interface-initiated mode to a predominantly tensile (or compression) mode. This observation may be explained in terms of the non-uniform stress distribution across the thickness of the specimen in three-point bending where the principal stress directions vary according to their distance from the surface.

5 – 2 – 3 Discussion of the fibre hybridisation effect on flexural properties.

The results show the UFS (σ_f) of the hybrid composite in the weft direction are superior to non-hybrid composites by approximately 19%. This variation is considered to be significant by the t-test (as discussed in Appendix C). The result of the weft direction test further shows the modulus of hybrid composites is superior to the modulus of non-hybrid composites. The shapes of stress-strain curves (in the weft direction) are different, and are distinct in their values (see figure 5 – 10). The Knee points of the stress-strain curves follow a similar pattern. A higher stress was recorded at the knee point of the hybrid composite when compared to the non-hybrid composite. The AE activities of the hybrid composite show a significant reduction compared with the non-hybrid composite and this mainly related to the number of damage events. The SEM micrograph reveals that fibre rupture is primarily associated with non-hybrid composites and layer delamination in the hybrid composite (see figures (5 – 14) and (5 – 16)).

The AE ring down count during the flexural test for both hybrid and non-hybrid composites is shown in figure (5 – 10). The zone classification methodology of AE (figure 5 – 12) has been followed in order to analyse the damage progress throughout the AE activities in a similar manner to the previous section. The correlation between the AE onset point with the knee point of the flexural stress-strain curve has been identified for both hybrid and non-hybrid composites. It can be seen that the hybrid glass fibre woven in the composite reduces the magnitude of the ring down counts compared with the non-hybrid composites during the flexural test (in the **weft direction**). Consequently the rate of the non-hybrid was higher compared with that of the hybrid composite. This was found after individual and careful study of the rate for each composite (see rate plot e.g. in figure 5 – 13). The values of AE of hybrid and non-hybrid woven fabrics are summarised in table (5 – 8).

The AE (weft direction) curve shapes of hybrid and non-hybrid glass woven reinforced epoxy resin composites differ in their values. These values represent the effect of a fibre hybridisation on the mode failure, as well as micromechanical failure progress in the composite. This refers to the fibre bundle pullout and fibre rupture in the non-hybrid composite, whereas the hybrid composite shows buckling, limited bundle pullout and shear cracking, as shown by the SEM micrograph (figure 5 – 16). The variation in **AE** ring down count values at ultimate flexural fracture refers to generated damage events and were higher in the case of non-hybrid compared with the hybrid composites.

The performance of flexural fracture surface investigated by SEM. The SEM micrograph in figure (5 – 16) shows the flexural specimen of **hybrid** glass woven fabric composite in the **weft direction**, and indicates:

(a) view of through-thickness with the shear side dominating the fracture surface starting from the midpoint and continuing towards the edge of the specimen and a buckling of fibre under the effect of weaving as result of compressive stress,

(b) shear pockets next to the transverse fibre bundle around fabric undulation, created by weaving,

(c) in higher magnification, evidence of a good fibre/matrix adhesion in the hybrid near the transverse fibre bundle fracture and matrix crack propagation tending to form a shear path along resin-rich regions,

(d) matrix-rich region next to the R-glass fibre bundles that caused the shear fracture.

The SEM micrograph in figure (5 – 14) of a **non-hybrid** glass woven composite flexural specimen (weft direction) has been discussed for a low V_f composite in the previous section. The fracture of non-hybrid composites (weft direction) is dominated by the tensile failure mode promoted by fibre rupture. Conversely, the fracture of hybrid composites (weft direction) is dominated by ply delamination and is accompanied by matrix cracking.

The SEM evidence shows that the variation in the results were due to differences in the overall fibre properties and their fibre coating interaction with the matrix, causing some changes in the overall fracture performance of the specimens.

In figure (5 – 11) the stress-strain curves shape of hybrid and non-hybrid composites (warp direction) appear similar to each other. The results show almost identical values of the UFS (σ_f) for both hybrid and non-hybrid composites in the warp direction. Knee points appear on each stress-strain curve exhibiting similar values of flexural stress. Fracture performance of the flexural specimens of hybrid and non-hybrid woven composites in the warp direction were similar to each other see figure 5 – 14. The fracture surface dominated the tensile side of the three-point bend specimens. The fibre rupture and matrix deformation was shown to be the result of the tensile failure mode. The RDC and rate of hybrid and non-hybrid glass woven composites warp direction, show similar performance as recorded in table (5 – 8).

The result indicates no improvement of flexural strength in the warp direction. The difference between the hybrid and non-hybrid composites is that the hybrid composite is composed of R-glass and E-glass, whereas the non-hybrid composite contains the E-glass only. It is essential to mention that the R-glass was in the weft direction of the hybrid weave, whilst the E-glass was in the warp direction. Therefore, there was significant improvement of flexural properties in the weft direction but no improvement in the warp direction.

From the above discussion the following results can be identified:

- The lowest level of ultimate flexural strength (UFS) value was associated with the lowest fibre volume fraction composites. The lowest fibre volume fraction contains the lowest number of layers. The composite containing a higher number of layers exhibited higher stress-to-fail. Conversely, the composite containing the lowest fibre volume fractions had the lowest level of flexural stress-to-fail.

- The fractures of the low V_f composites were dominated by tensile failure mode and accompanied by matrix cracking and fibre rupture. The fracture of high V_f composites was dominated by ply delaminations accompanied by matrix cracking.

- The lower the glass fibre volume fraction in the composite the higher is the magnitude of the AE ring down count at each zone as shown in figure (5 – 9b). Consequently the rate was higher, see the representative plot in figure (5 – 13). It was found, after careful study of the rate that the number of peaks and peak length decrease with the increase of V_f in the composites. This clearly demonstrates a case of overall increased failure events in the low V_f composites and a case of overall decreased failure events in the high V_f composites.

- A comparison of AE activities monitored during flexural tests for differing V_f is shown in figure (5 – 9b). The figure reveals that in the low fibre volume fraction composites, the failure appears earlier or at less strain than in those of high V_f composites. This is clearly due to the greater stiffness and higher resistance to flexural stress caused by the high V_f in the composite.

The result indicates no improvement of flexural properties in the **warp direction** and a significant improvement in the weft direction. The variation in UFS (σ_f) of hybrid and non-hybrid composites in the **weft direction** can be summarised as;

- The lower ultimate flexural strength (σ_f) values were associated with non-hybrid composites. The hybrid composites exhibited higher σ_f. This clearly demonstrates the case of increased flexural strength and the subsequent adhesion bonding in the composite promoted by fibre properties.

- The non-hybrid composites are dominated by a tensile failure mode accompanied by matrix cracking and fibre rupture. The hybrid composites are dominated by ply delamination accompanied by matrix cracking.

- The hybrid composite exhibited a higher modulus than the non-hybrid composite, demonstrating the case of increased overall stiffness in the composite. It has been noticed that the non-hybrid composites show failure at less strain than those of hybrid composites.

The AE activities monitored during the flexural test, (figure 5 – 10) shows the hybrid composite having more resistance to the flexural stress than the non-hybrid composite.

- It was observed that the non-hybrid composite shows a higher magnitude of ring down counts on the AE curve at each zone compared with the hybrid composites (figure 5 – 10). The rate consequently was higher as shown by the number of peaks recorded (see the representative figure 5 – 13). This is clearly another demonstration that an increased overall composite flexural property appears to be promoted by fibre properties.

Table 5-5 **Flexural** Test Results of Non-hybrid Glass Composites including Four Different **Fibre Volume Fractions.**

Flexural Test Results of Non-hybrid Glass Woven Fabric Composites **including Four Different Volume Fractions.**									
Test	Fibre Volume Ratio (%)	No. of Plies in 3mm Thickness	Mean Stress (MPa) @ Knee Point	UFS (MPa)		Strain (%)		Mean E-Modulus (GPa)	
				Mean	Std.Dev.	Mean	Std.Dev.	Mean	Std.Dev.
Non-hybrid @38%	0.38	12	141.82	279.41	16.45	2.30	0.16	14.85	1.62
Non-hybrid @48%	0.48	15	190.45	380.50	19.69	2.18	0.09	18.83	2.11
Non-hybrid @ 56%	0.56	18	234.44	458.62	21.48	1.82	0.08	22.97	2.84
Non-hybrid @ 64%	0.64	21	251.23	488.55	23.91	1.45	0.06	25.63	3.23

Table 5 - 6 AE activities during Flexural tests of Non-hybrid Composites including Four Different Fibre Volume Fractions

AE activites during **Flexural** test of Non-hybrid Fibre Glass Woven fabric Composites including Four Different **Fibre Volume Fractions**						
			Zone B		AE at Finial Fracture	
Laminates	Thickness (mm)	No. of Plies in 3mm Thickness	Corr. of knee & onset Points	RDC @ end of zone B	RDC@ ultimate fracture	Highest Peak in the Rate
Non-hybrid @38%	3.00	12	yes	1.54E+05	7.70E+05	4.00E+04
Non-hybrid @ 48%	3.00	15	yes	1.09E+05	5.45E+05	3.48E+04
Non-hybrid @ 56%	3.00	18	yes	8.20E+04	4.10E+05	2.10E+04
Non-hybrid @ 64%	3.00	21	yes	4.10E+04	2.05E+05	1.80E+04

Table 5-7 Comparison **Flexural** Test Results between Non-hybrid and Hybrid Glass Woven Composites

Flexural Test Results of **Hybrid** Woven Composites									
Test	Fibre Volume Ratio (%)	No. of Plies in 3mm Thickness	Stress (MPa) @ Knee Point	UFS (MPa)		Strain (%)		Mean E-Modulus (GPa)	
			Mean	Mean	Std.Dev.	Mean	Std.Dev.	Mean	Std.Dev.
Hybrid (Weft)	0.48	15	272.50	434.67	22.78	2.10	0.03	21.13	2.89
Hybrid (Warp)	0.48	15	245.32	394.06	21.26	2.30	0.03	19.42	2.23
Flexural Test Results of **Non-hybrid** Woven Composites									
Non-hyb. (Weft)	0.48	15	190.45	380.50	19.66	2.18	0.09	18.83	2.11
Non-hyb. (Warp)	0.48	15	239.68	388.19	21.16	2.40	0.05	19.17	2.21

Table 5-8 **AE** activities during **flexural** tests of Non-hybrid and Hybrid Woven Composites

AE Patent representing **flexural** test of Non-hybrid and Hybrid Glass Woven Composites						
			Zone B		AE at Finial Fracture	
	Laminates	Fibre Volume Fraction (%)	Corr. of knee & onset Points	RDC @ end of zone B	RDC@ ultimate fracture	AE Rate
Hybrid	Weft	0.48	yes	8.20E+04	4.00E+05	1.80E+04
	Warp	0.48	yes	9.61E+04	5.25E+05	3.82E+04
Non-hybrid	Weft	0.48	yes	1.09E+05	5.45E+05	4.08E+04
	Warp	0.48	yes	9.56E+04	5.24E+05	3.45E+04

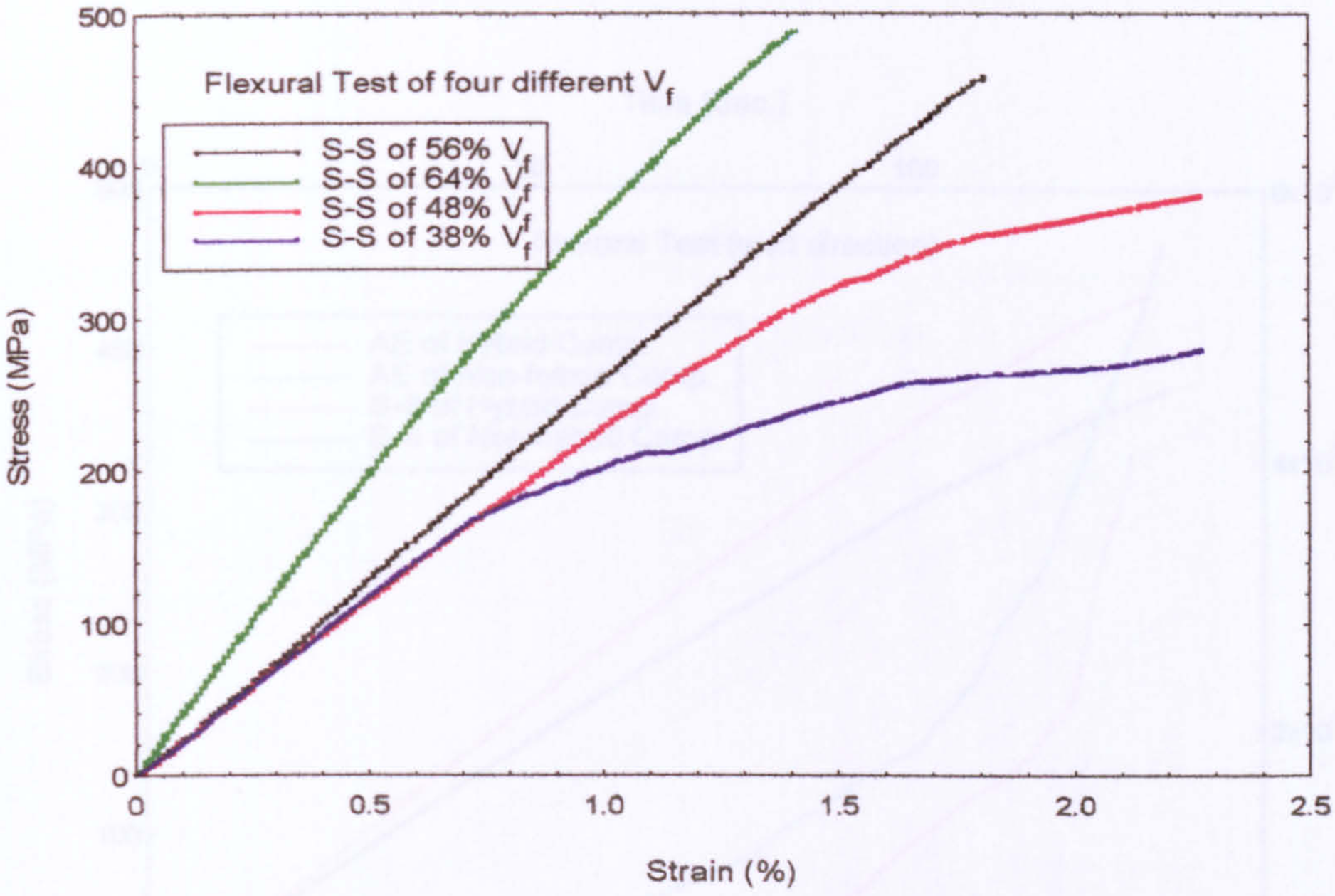

(a)

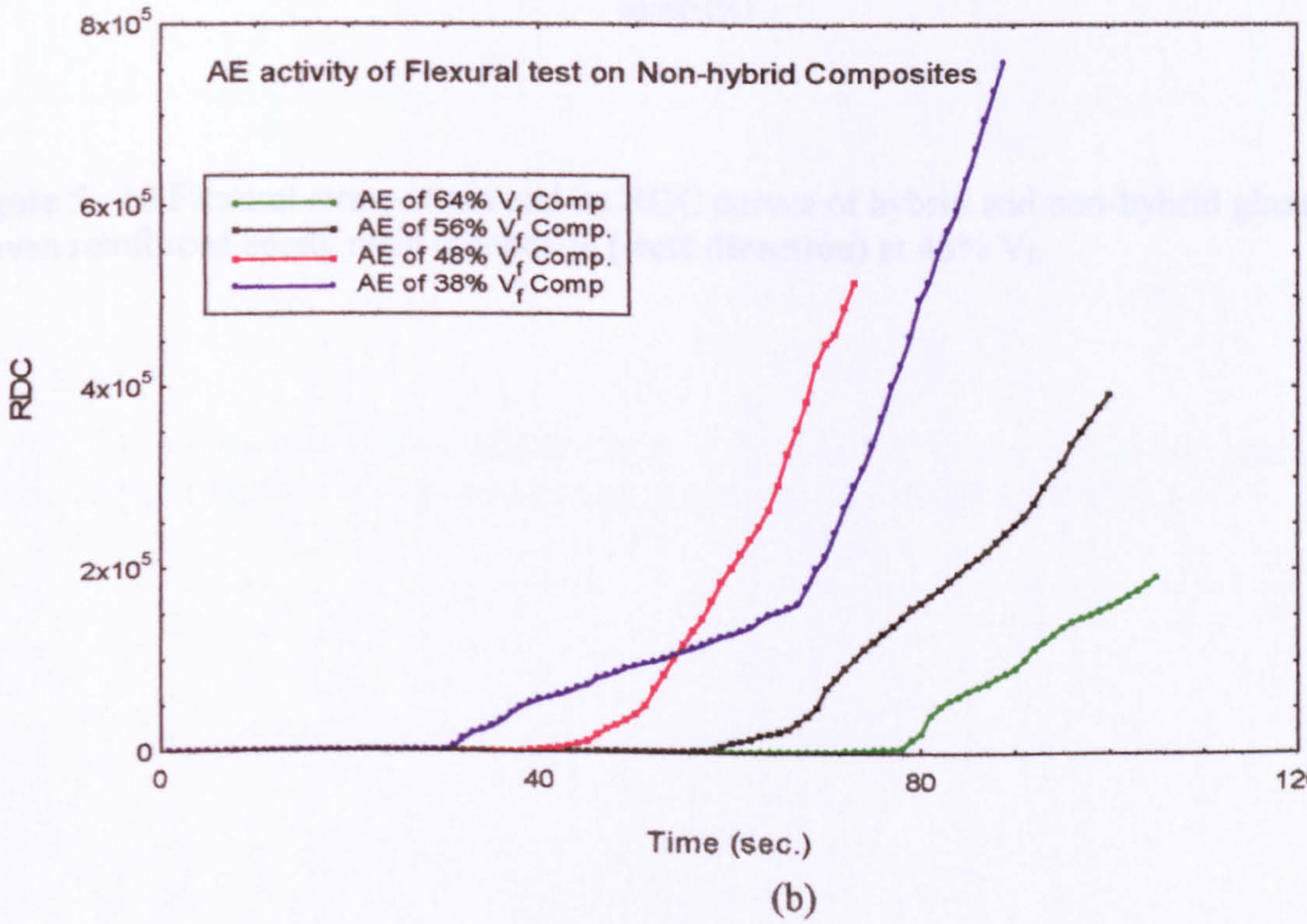

(b)

Figure (5 – 9) (a) flexural stress-strain curves of non-hybrid woven reinforced epoxy resin composite including four different fibre volume fractions. (b) the corresponding RDC activity curves of the stress-strain curves of (a).

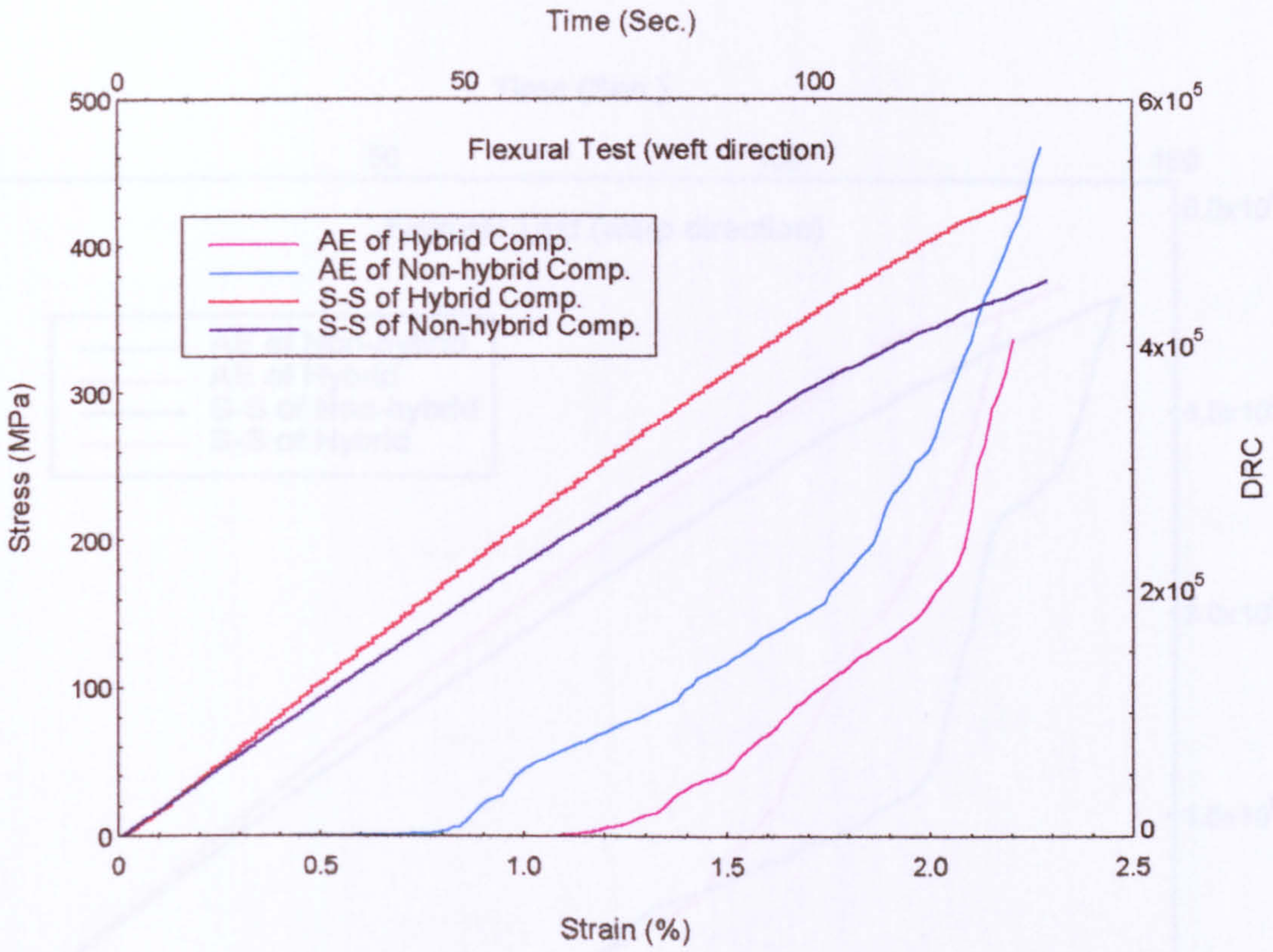

Figure 5 –10 Flexural stress-strain and its RDC curves of hybrid and non-hybrid glass woven reinforced epoxy resin composite **(weft direction)** at 48% V_f.

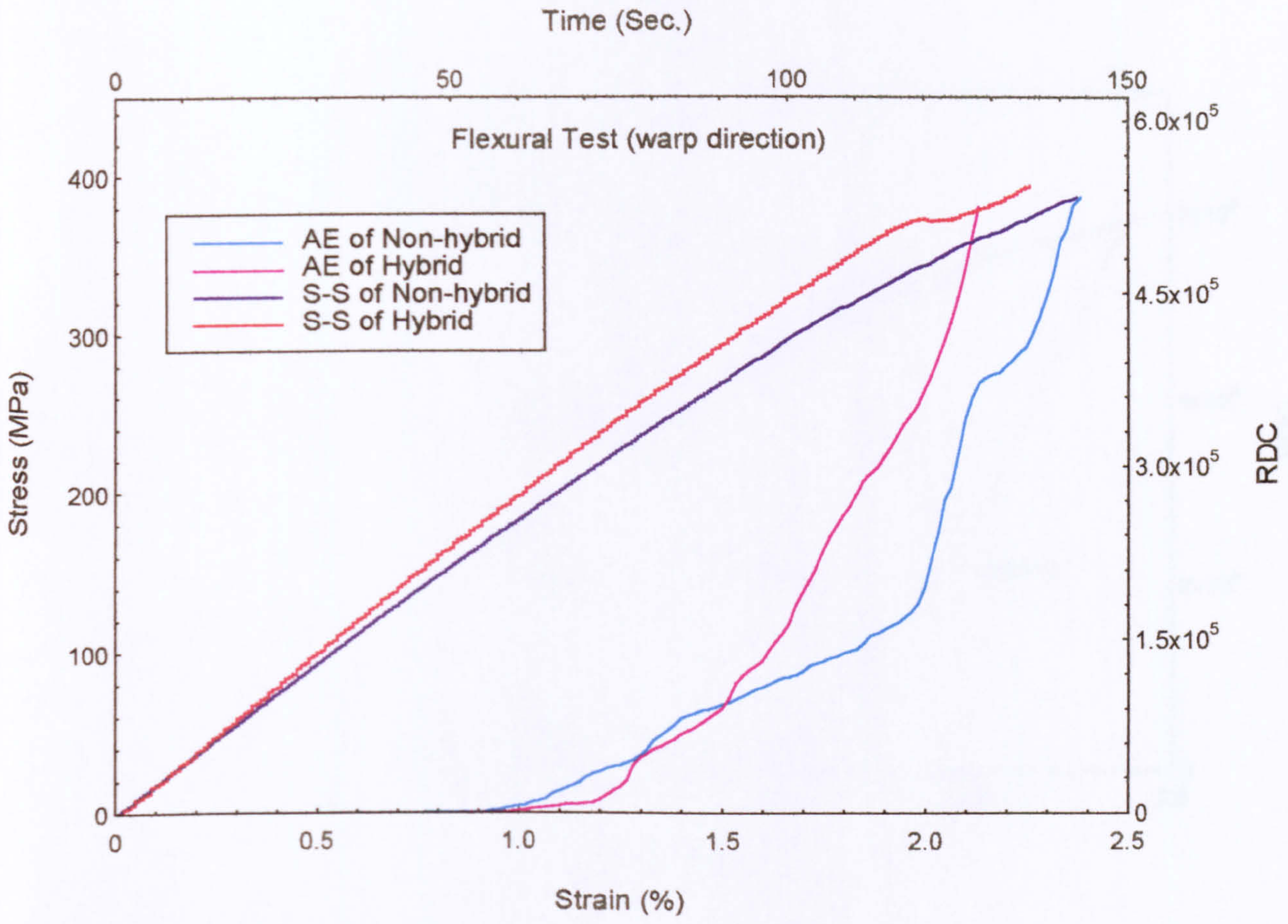

Figure (5 – 11) Flexural stress-strain and its RDC plot of hybrid and non-hybrid glass woven fabric reinforced epoxy resin composite **(warp direction)** at 48% V_f.

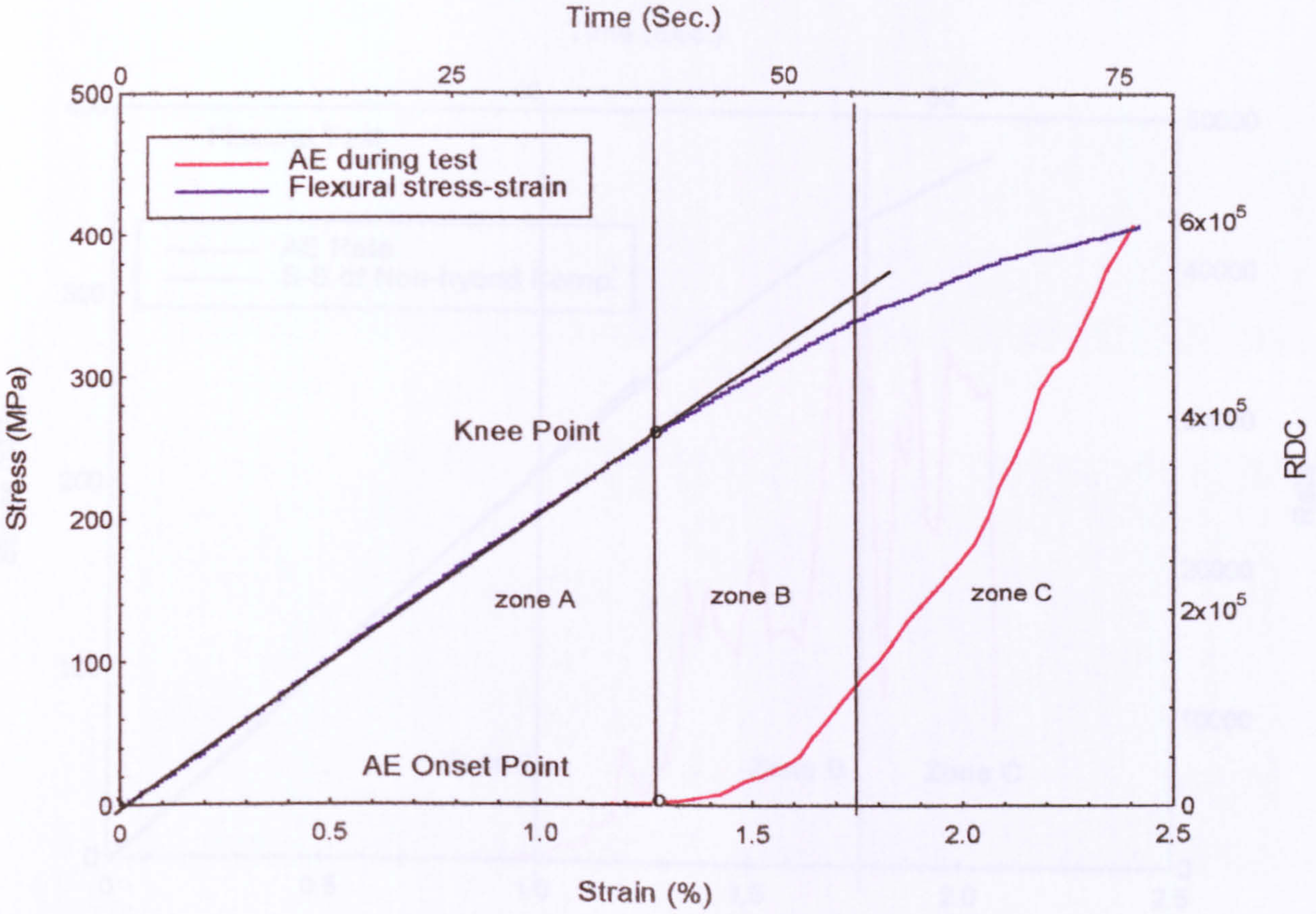

Figure (5 – 12) **Zone classification technique** used in the flexural stress-strain and its RDC curves of glass woven fabric reinforced epoxy resin composite.

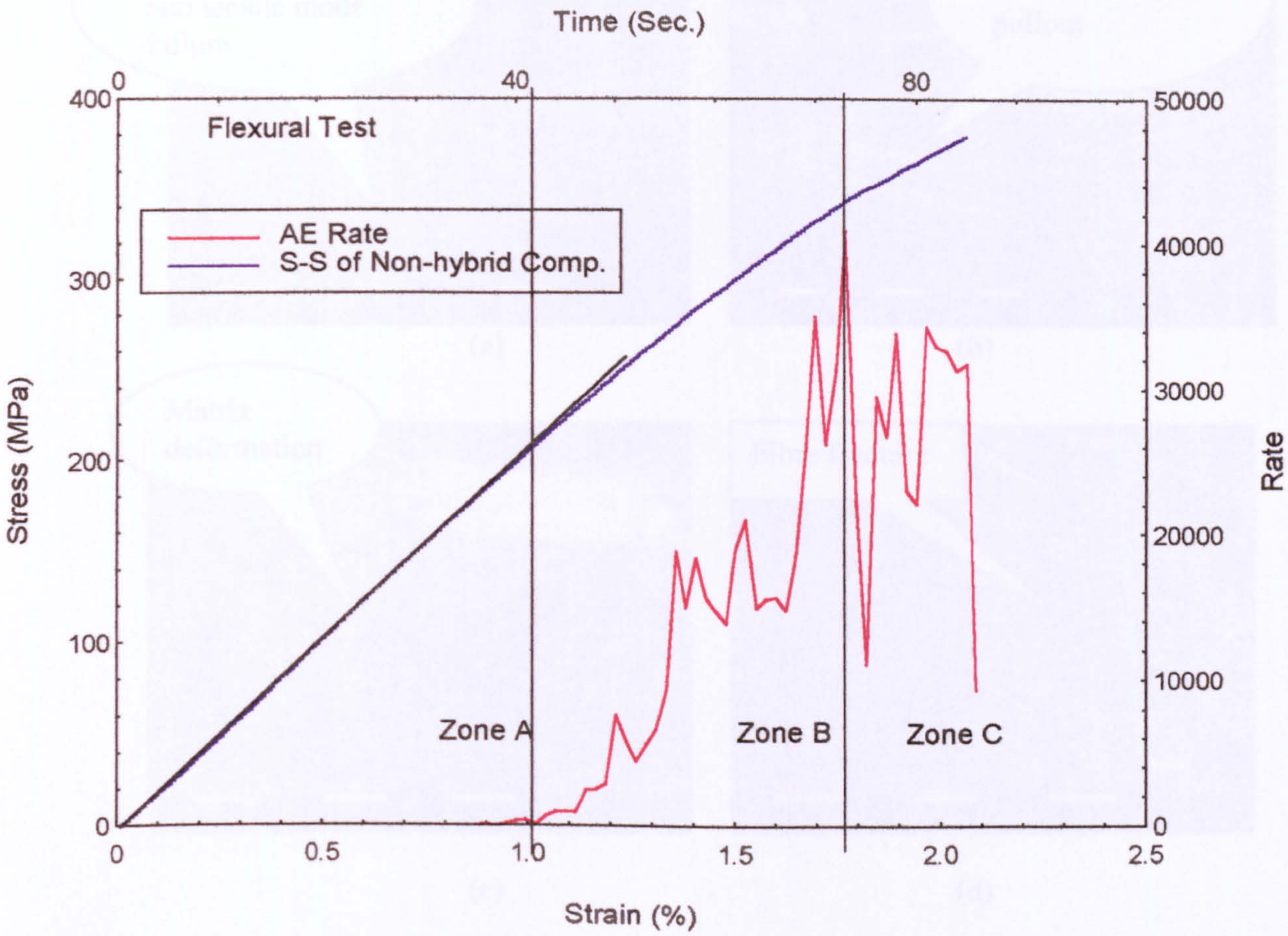

Figure (5 – 13) **Zone classification technique** used in the flexural stress-strain curve and its AE rate of glass woven fabric reinforced epoxy resin composite.

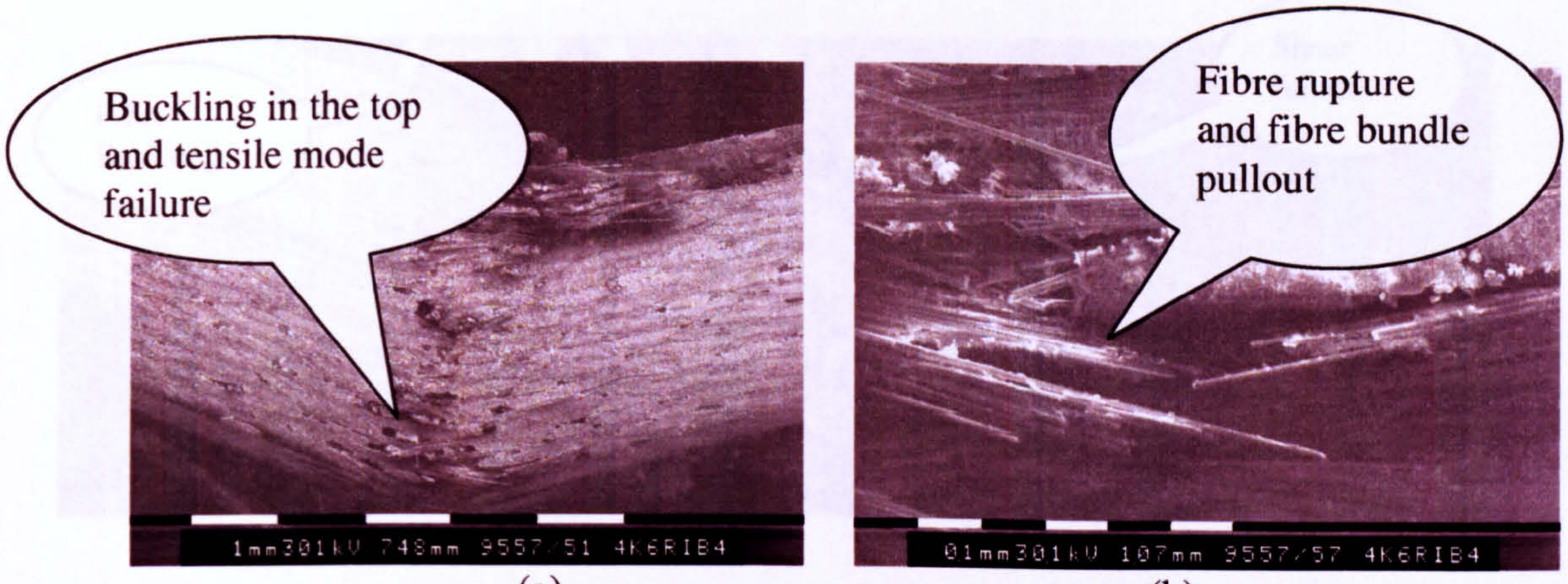

Figure (5 – 14) SEM micrograph of flexural through-thickness fracture surface of non-hybrid E-glass woven glass fabric composite at 48% fibre volume fraction shows. a- (80x) tensile mode failure. b- (200x) fibre bundle pull-out. c- (60x) backside view of the specimen shows the matrix deformation in the crimp area. d- (100x) fibre fracture.

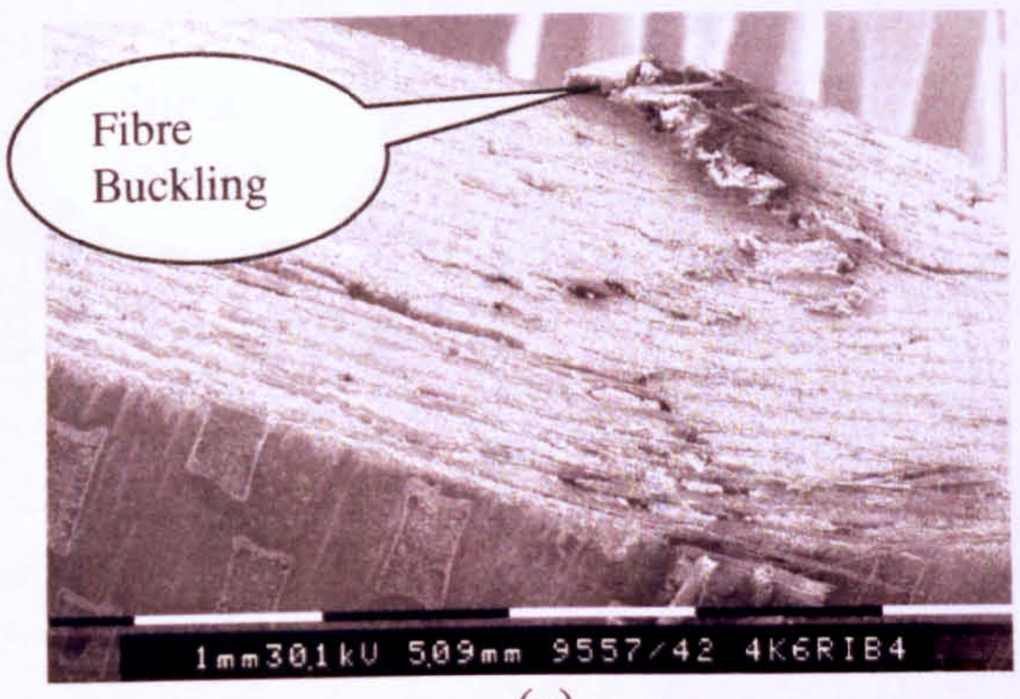

(a)

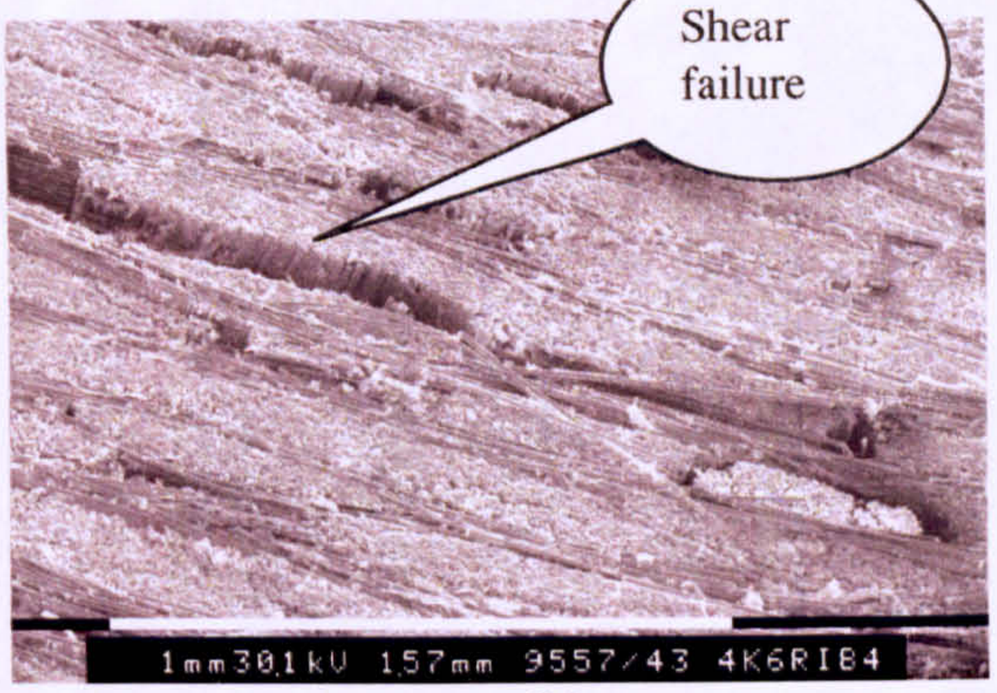

(b)

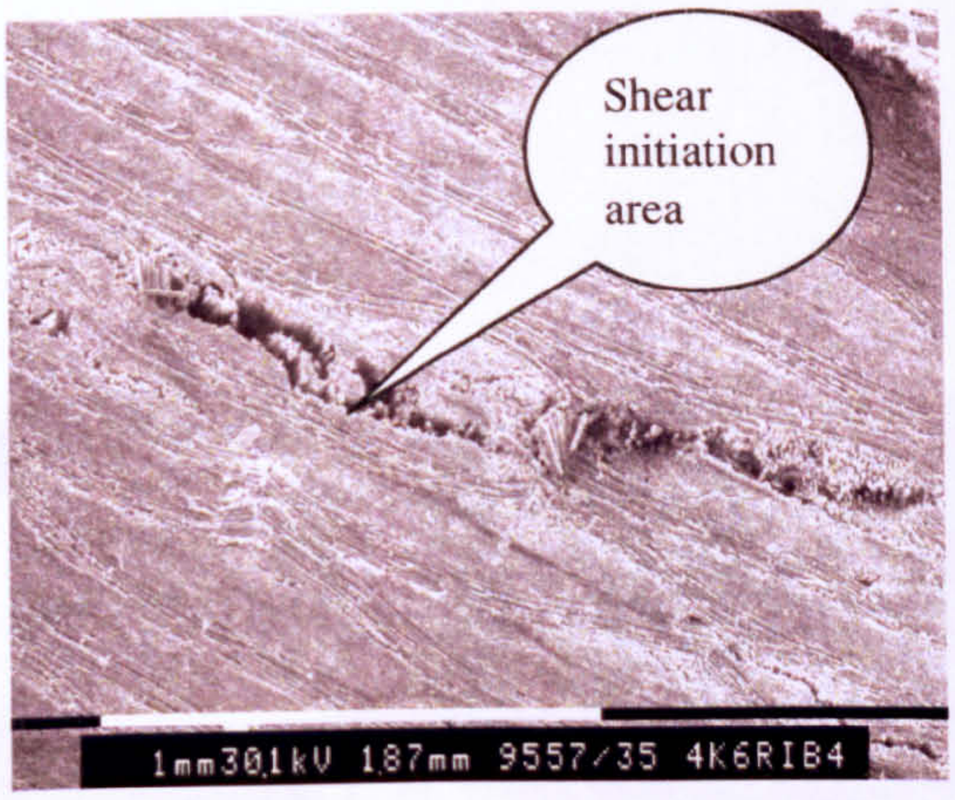

(c)

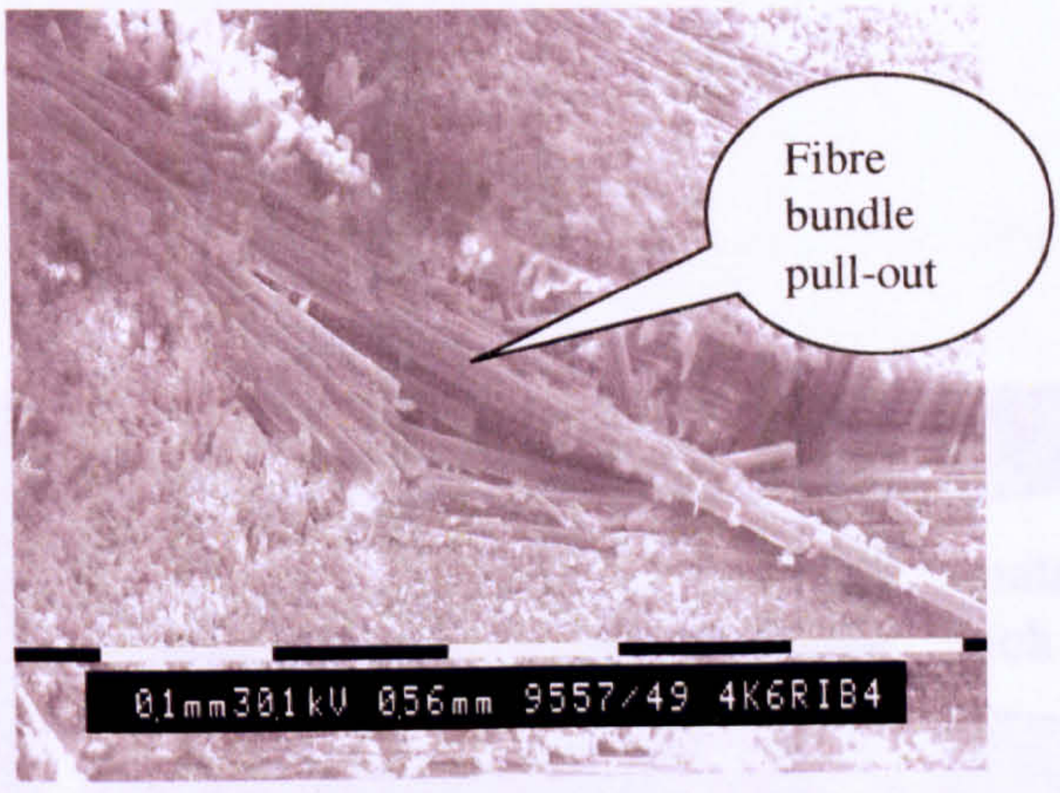

(d)

Figure (5 –15) SEM micrograph of flexural through-thickness fracture surface of E-glass woven glass composite at 56% V_f shows a- (30x) shear failure. b- (30x) shear failure path. c- (30x) fibre-rich area in shear path. d- (200x) fibre pull-out due to fibre concentration.

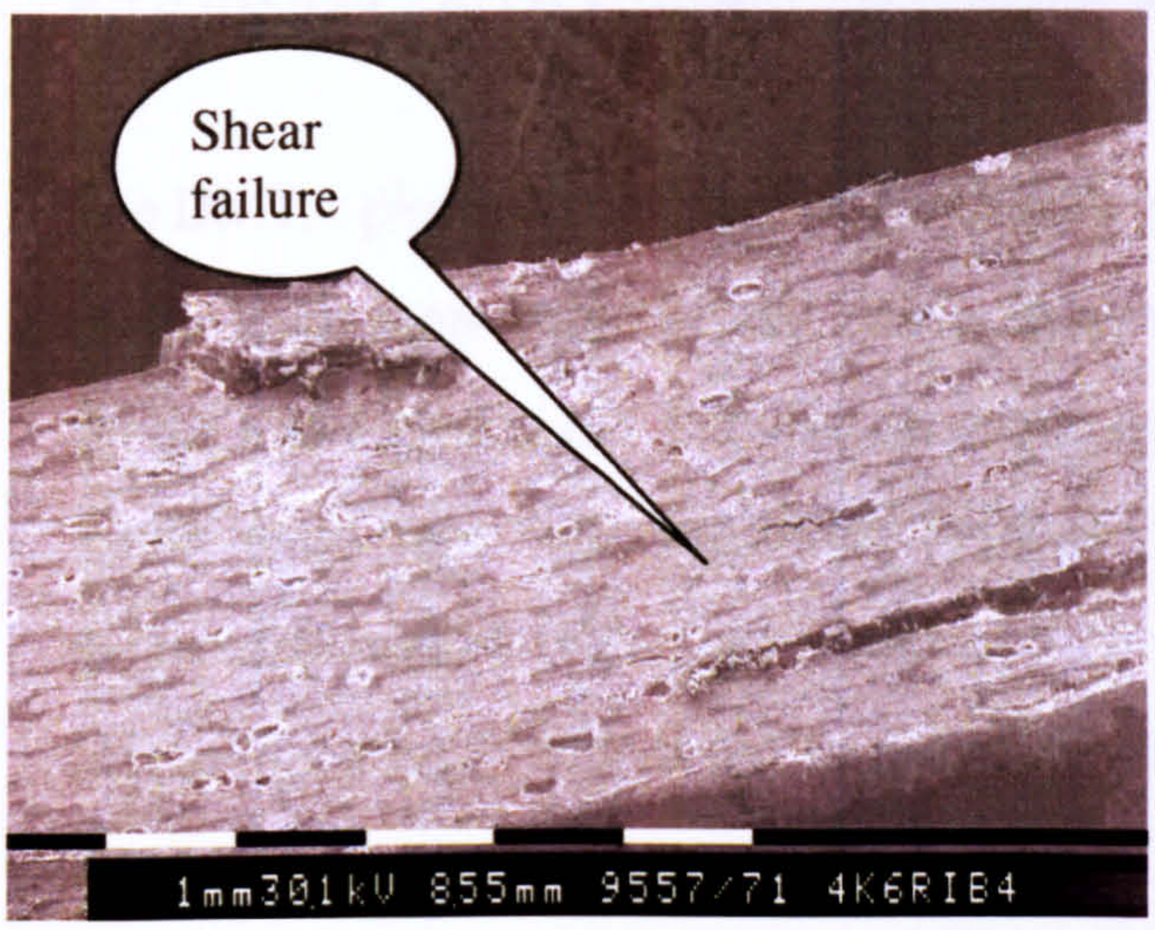

(a)

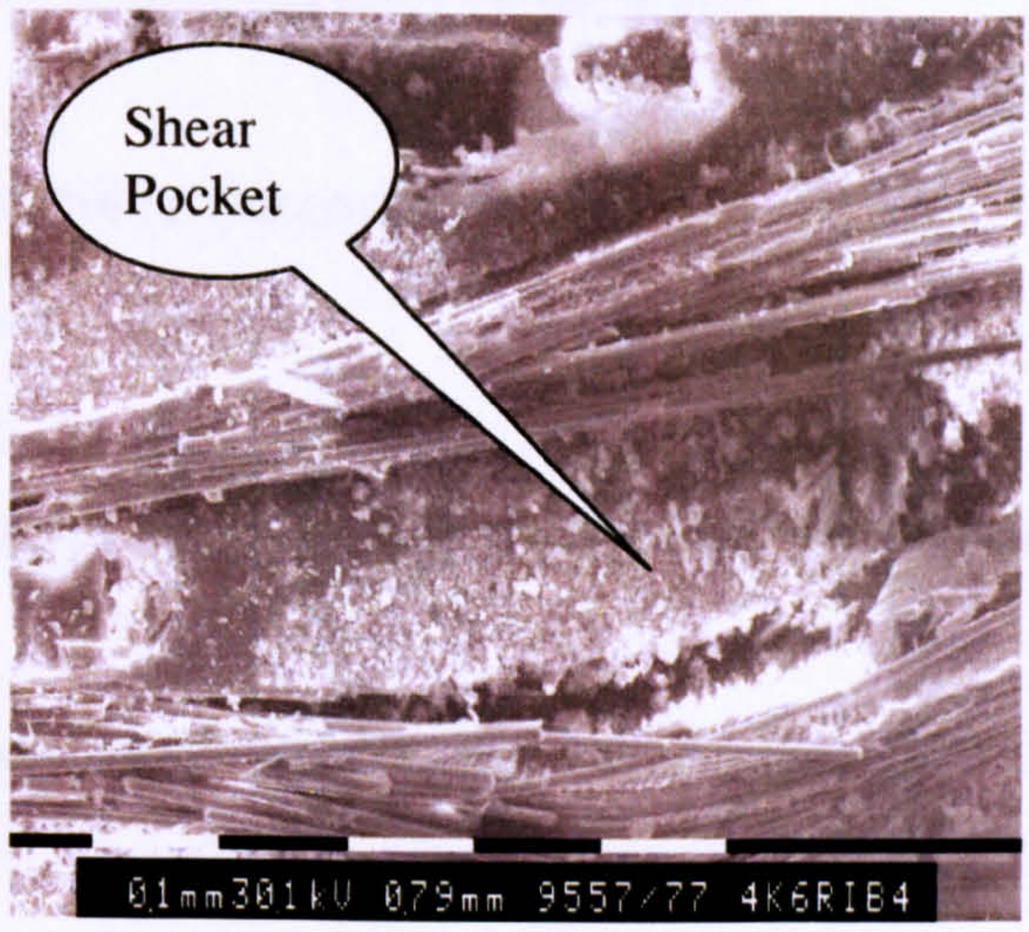

(b)

(c)

(d)

Figure (5 – 16) SEM micrograph of **flexural** fracture surface of **hybrid** glass woven composite **(weft direction)** at **48%** V_f shows a- (100x) through-thickness fracture surface. B- (100x) shear pockets around fabric undulation created by weaving. c- 400x transverse fibre bundle in the fracture surface. d- (140x) matrix-rich area caused shear fracture.

5 – 3 Section Three: Dynamic Mechanical and Thermal Analysis (DMTA)

The DMTA plots provide the following information on the composite:

(a) the storage modulus (i.e. the elastic response),

(b) the loss modulus (i.e. the viscous response),

(c) the glass transition temperature (T_g), the (T_g) is taken, in this study, to be the temperature of the maximum peak of the loss modulus,

(d) tan (δ), delta (δ) stands for the out of the phase angle between stress and strain.

5 – 3 – 1 The results of DMTA tests.

The results of the DMTA tests include the data from neat epoxy resin and four different fibre volume fractions of non-hybrid glass woven reinforced epoxy resin composites and are summarised in table (5 – 9). The results are graphically presented in figures (5 – 17), (5 – 18) and (5 – 19). These results highlight the effect of fibre volume fractions on DMTA properties in the composite.

The results of the hybrid and non-hybrid glass fibre woven fabric reinforced epoxy composites tests at a similar fibre volume fraction of 48% V_f are given in table (5 – 10). They are graphically presented in figures (5 – 20) and (5 – 21). These results highlight the effect of fibre hybridisation on DMTA properties in the composite.

5 – 3 – 2 Discussion of composites fibre volume fraction effect on DMTA properties

The loss moduli curves figure (5 – 17) represent the neat epoxy resin and three E-glass woven reinforced epoxy resin composites that contain different fibre volume fractions. The shape of the loss moduli (E``) curves were identical, but distinct values of the glass transition temperature (T_g) for each fibre volume fraction composite is summarised in table (5 – 9).

The glass transition temperature (T_g) is considered to be a maximum peak of the loss modulus. The glass transition temperature of the epoxy set (L20-SL) was determined in this research to be

approximately 110.30 °C compared with 110 °C obtained by the manufacturer as shown in table (4 –1). The epoxy is an example of a cross-linked system and has distinct temperature-dependent behaviour. However, in general these materials all have a well-defined glass transition temperature that produces the typical behaviour of a storage modulus.

The glass fibre in the woven fabric reinforcement is a typically inorganic material with very high softening points (840 °C) for E-glass as shown in table (2 – 3). This is well above the temperature at which organic polymers such as epoxy resins degrade. This reveals the fact that glass fibres are purely elastic systems while the epoxy resins and fibre glass/epoxy interphase are viscoelastic.

The composite with 38% V_f gave the highest T_g value (approximately 140.96 °C) and the composite at 56% V_f had the lowest T_g of (approximately 121.62 °C). The fibre surface treatment concentration varied with the number of woven fabric layers in the composites. In other words, the fibre surface treatment concentration varied when varying the fibre volume fraction. This indicates that the crosslinking option of the epoxy system is consequently dependent on both the fibre coating and matrix volume fraction variation. Therefore, the epoxy/glass fibre composites exhibit distinct temperature-dependent behaviours. The higher the fibre volume fraction in the composites, the more tightly is the crosslinking mobility between the matrix and fibre surface treatment. This can be used as evidence that the glass transition temperature of composites depends on fibre volume fraction. The V_f is reflected in the matrix crosslinking mobility, the fibre surface treatment concentration and its interaction in the composite. Therefore, it is believed that the variation in glass transition temperature of glass woven composites is caused by the fibre surface treatment concentration in the composite.

This shows that the silane/sizing interaction with the epoxy matrix produces a material with different properties than the bulk matrix. This is termed interphase. The fibre coating concentration affected the fibre/matrix interphase formation and consequently the fibre/matrix adhesion, composite shear and flexural strengths. (Al-Moussawi et al. 1993, Larson and Drzal 1994) reported that the interphase has a lower T_g than the bulk matrix, the interphase modulus is generally higher than the modulus of the bulk matrix. In this particular system, the T_g of the composite declines as the V_f increases.

The plots of **tan delta** in figure (5 – 19) allow the direct comparison of the value and performance of the neat epoxy resin and three different V_f non-hybrid E-glass woven/epoxy composites. The high tan delta value implies that once the deformation is induced, the material will not recover its original shape. It is considered to be soft and pliable. The values of tan delta for each composite are summarised in table (5 – 9).

The α-relaxation refers to the main relaxation rising to peak maximum in the tan (δ) or loss moduli curves. The α-relaxation peaks in the tan (δ) curves for the composites with higher V_f is broader than that of lower V_f composites. However, the peak positions moved to a lower-temperature region with an increase in fibre volume fraction. The decrease in tan delta magnitude at the α-relaxation is associated with an improvement of interfacial bonding according to Haessler and Keusch (1999). This could assist in explaining the ILSS improvement with an increase in fibre volume fraction as discussed in section one.

The tan delta curves follow closely the loss modulus curve. The rapid rise in the tan delta curve coincides with the rapid decline in the **storage modulus** (E′) up to the maximum peak. The storage moduli of the composite shown in figure (5 – 18) are reduced by 3-4 orders of magnitude. The reductions in the storage modulus depend on the fibre volume fraction in the composite (see table 5 – 9). After this stage, the storage moduli continue declining very similarly for each composite. Once the glass transition was completed the loss modulus and tan delta dropped back to the level close to the pre-transition values. The storage modulus can represent a comparison of the plastic material and load-bearing capability for different volume fraction composites. This explains the tensile property improvement.

DMTA scans of epoxy resin materials and resin/fibre glass woven with different fibre volume fraction counterparts show that the increase in room temperature properties is only a small part of the improvement. The highest values of storage moduli determined for the glass fibre reinforced composite at 64% V_f is not only higher at the T_g and α-relaxation but also over the entire temperature range. The low storage modulus indicates that an applied load easily deforms the material.

5 – 3 – 3 Discussion of the fibre hybridisation effect on viscoelastic properties in the composite

In figure (5 –20), the loss moduli plot shapes were identical, possibly due to the effect of the 8-harness pattern in the woven fabric composites. They differ in their values of the glass transition, T_g showing individual values for each composite. The result shows that the glass transition temperature of the hybrid composite (approximately 119.7 °C) has a lower value of T_g than the non-hybrid composite (approximately 130.22 °C).

The difference between the hybrid and non-hybrid composites is that the hybrid composite is composed of R-glass and E-glass whereas the non-hybrid composite contains E-glass only. Glass fibre is a typically inorganic material with very high softening points (840 °C) for E-glass and (986 °C) for R-glass. This is well above the temperature at which organic polymers like epoxy resin degrade. It is therefore believed that the variations in the T_g of hybrid and non-hybrid composites depend on the fibre surface treatment concentration or its distribution in the composite. The fibre properties influence its surface treatment distribution and its concentration in the composites. Consequently it is believed that the glass transition temperature (T_g) of hybrid composites is lower than the T_g of non-hybrid composites due to fibre surface treatment concentration in the composite. This variation can therefore be due to the concentration of fibre surface treatment on the glass fibre surface and later its interaction density with matrix.

The result further emphasises that the storage moduli values of the **hybrid** composite are higher compared to those of the **non-hybrid** composite. The tan delta values of the hybrid are less than those of non-hybrid composites. Any change in the mobility of the composite structure will appear as a peak in the loss modulus and the tan delta curves as well as a step reduction in the storage modulus. The reduction in tan delta magnitude of the hybrid is associated with an improvement of interfacial bonding and ILSS compared to those of the non-hybrid.

The magnitude of tan (δ) and log (E′) plots in figure (5 – 21) as well as the α-relaxation allow a good comparison of the hybrid and non-hybrid glass woven fabric/epoxy reinforcement. The peaks in the tan (δ) curves for the hybrid composite have a similar shape to the non-hybrid composite. However, the peak positions of hybrid composite move to lower-temperature regions

when compared to the non-hybrid composite. The logarithmic storage moduli scale of y-axis shows the hybrid composite drops by 5-6 in order of magnitude while the non-hybrid composite drops down by 4-5. This variation which, occurs before and after glass transition is related to different properties of the fibres in the woven material. The storage modulus (E′) curve, figure (5 – 20), shows a similar pattern to log (E`). The storage modulus can represent a comparison of the plastic material and load-bearing capability for hybrid and non-hybrid at similar fibre fraction composites. The values of DMTA parameters of hybrid and non-hybrid composites are illustrated in table (5 – 10).

This can be used as evidence that the variation of T_g in the composites is dependent on the region of fibre surface treatment interaction with the matrix and is called interphase. The interphase possesses features such as a finite dimension and thickness (Kim and Sham 2001). It has been suggested that the interphase may be a chemical reaction zone, a diffusion zone, a nucleation zone, or a combination of them all. Thomason compared between 1995 – 2001 a number of techniques to probe the interphase region in the glass fibre / epoxy matrix composite. He stated that the thickness of the interphase region is about (1μm) surrounding the fibre.

The visualisation of the three-dimensional interphase in figure (5 – 22) shows two possible interpretations. The interphase region with spatially varying properties promotes fibre surface treatment around the single fibre in the micro level (fibre). The figure further shows the possible number of fabric interlayers that are imposed by glass fibre surface treatments, matrix and fibres constituents in the composites at the laminate level (interlayer). The two interpretations can be interrelated, however, the relationship between the two levels, is obvious.

The interphase material created by interdiffusion of silane sizing is either more ductile or more brittle than the bulk matrix material. Therefore, the interphase in the composite can be divided accordingly into a ductile form (e.g. the low V_f non-hybrid composite) or a brittle form (such as the hybrid and high V_f non-hybrid composite). This is in concurrence with literature, see (Chua et al 1987) and (Drown and Drzal 1992).

The interlaminar shear, flexural and tensile strengths are increased as the principal effects of fibre surface treatment and its concentration on composite properties.

The following results can be gathered from the discussion:

- The T_g of composite declines from approximately (140.96 °C) for a low V_f composite to approximately (121.64 °C) for a high V_f composite table (5 – 9). This variation in the T_g refers to the variation of the glass fibre treatment concentration as a result of V_f variation in the composites.

- It is further shown in table (5 – 9) that the T_g of a composite at 64% V_f rises to approximately 125.9 °C compared with 121.6 °C for a composite of 56% V_f. This indicates the limitation which V_f can mutually be imposed in the composites. This change in the T_g can contribute to the limitation of V_f effect on mechanical property improvement (such as ILSS and flexural properties). Further detailed discussion concerning the limitation phenomenon can be found in section six.

- The higher the V_f level in the composite, the lower the magnitude of tan delta at the α– relaxation. The lower the magnitude of tan delta the higher is the improvement of interfacial bonding (ignoring the V_f limitation effect).

- The higher the V_f in the composites, the higher is the crosslinking mobility. This leads to a higher level of interaction consistency in the composite. In other words, there is more crosslinking density in the composite. This variation is due to the variation in silane and matrix concentration resulting from the variation of V_f in the composites.

- Therefore, the fibre/matrix adhesion and consequently the tensile, interfacial bond and flexural property relies on the fibre surface treatment concentration in the composites. In other words the matrix cross-linking density and fibre/matrix networking is a result of the number of fibre layers in the composite.

- It is shown in table (5 – 10) that the T_g of hybrid composite is less than the T_g of non-hybrid composite by approximately 10 °C. This is a result of the variation in the concentration of glass fibre surface treatment and its interaction in the composites.

- The result further shows that the magnitude of the tan delta at the α-relaxation of the hybrid composites is lower compared with those of the non-hybrid composites. The lower magnitude of tan delta leads to an improvement of interfacial bonding and ILSS of the hybrid compared to the non-hybrid composites.

- The distribution of fibre surface treatment in the composites can generate different levels of interphase properties. This appears to be promoted by the crosslinking mobility in the composites that is performed at different levels of interaction consistency in the composite.

- The glass fibre shows a purely elastic system while the epoxy resins and fibre glass/epoxy interphase are viscoelastic.

Table 5-9 **DMTA** results of non-hybrid glass woven composites including epoxy resin and four different fibre volume fractions

DMTA results of non-hybrid composites including four different fibre volume fractions												
	Room Temp.	**Tg**	Test end Temp.	Room Temp.	**Tg**	Test end Temp.	Room Temp.	**Tg**	Test end Temp.	Room Temp.	**Tg**	Test end Temp.
Fibre Volume Ratio (%)	0.38			0.48			0.56			0.64		
Temp (Celsius degree)	27.18	140.96	200.00	27.18	130.22	200.04	27.18	121.64	200.34	27.18	125.91	200.36
Mean Storage Modulus E′(Pa)	1.28E+10	1.20E+10	6.81E+09	2.05E+10	1.59E+10	1.24E+10	2.48E+10	1.67E+10	1.18E+10	2.55E+10	2.31E+10	1.91E+10
Mean Loss Modulus E″(Pa)	3.42E+08	1.32E+09	1.90E+08	2.94E+08	1.12E+09	3.50E+08	2.82E+08	1.02E+09	5.85E+08	3.86E+08	8.52E+08	7.53E+08
tan_delta	0.023	0.110	0.028	0.014	0.070	0.028	0.012	0.053	0.050	0.015	0.037	0.030
Log E′(Pa)	10.17	10.05	9.83	10.31	10.20	10.09	10.38	10.22	10.07	10.41	10.36	10.28

DMTA result of 100% Epoxy resin			
	Room Temp.	**Tg**	Test end Temp.
Temp (Celsius degree)	27.18	110.17	200.42
Mean E′(Pa)	2.76E+09	7.67E+08	2.59E+07
Mean E″(Pa)	9.64E+07	2.15E+08	6.83E+05
tan_delta	0.046	0.630	0.026
Log E′(Pa)	9.32	8.89	7.41

Table 5-10 **DMTA** results of hybrid and non-hybrid glass woven composites (**weft** direction) at 42% fibre volume fraction.

DMTA results of hybrid and non-hybrid glass woven composites						
	Hybrid (Weft dir)			**Non-hybrid** (Weft dir)		
Fibre Volume Ratio	0.48			0.48		
	Room Temp.	Tg	Test end Temp.	Room Temp.	Tg	Test end Temp.
Temp (Celsius degree)	27.18	119.70	200.77	27.18	130.22	200.04
Mean Storage Modulus E′ (Pa)	2.23E+10	1.74E+10	1.12E+10	2.05E+10	1.59E+10	1.24E+10
Mean Loss Modulus E″(Pa)	3.43E+08	1.45E+09	4.87E+08	2.94E+08	1.12E+08	3.50E+08
tan_delta	0.017	0.051	0.043	0.014	0.070	0.028
Log E′ (Pa)	10.30	10.24	10.05	10.31	10.20	10.09

Table 5-11 **DMTA** results of hybrid and non-hybrid glass woven composites (**warp** direction) at 42% fibre volume fraction.

DMTA results of hybrid and non-hybrid glass woven fabric composites						
	Hybrid (Warp dir)			**Non-hybrid** (Warp dir)		
Fibre Volume Ratio	0.48			0.48		
	Room Temp.	Tg	Test end Temp.	Room Temp.	Tg	Test end Temp.
Temp. (Celsius degree)	27.18	117.26	200	27.18	128.42	200
Mean Storage Modulus E′(Pa)	2.07E+10	1.68E+10	1.24E+10	1.99E+10	1.45E+10	1.10E+10
Mean Loss Modulus E″(Pa)	3.50E+08	1.33E+09	4.70E+08	2.38E+08	1.14E+09	3.03E+08
tan_delta	0.017	0.079	0.038	0.012	0.087	0.027
Log E′ (Pa)	10.35	10.23	10.10	10.30	10.16	10.04

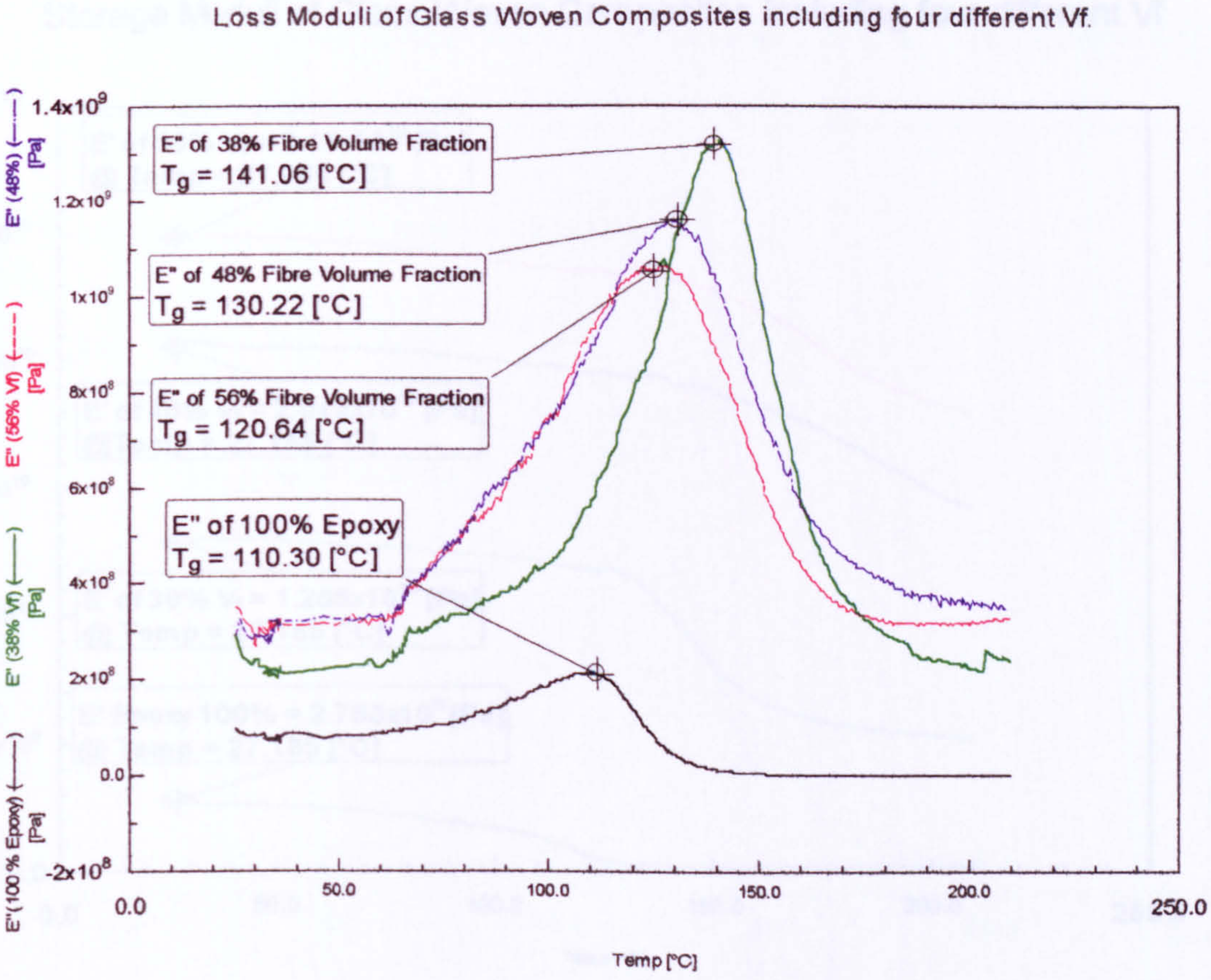

Figure (5 – 17) loss moduli plot of the non-hybrid glass woven reinforced epoxy resin composites including four different fibre volume fractions.

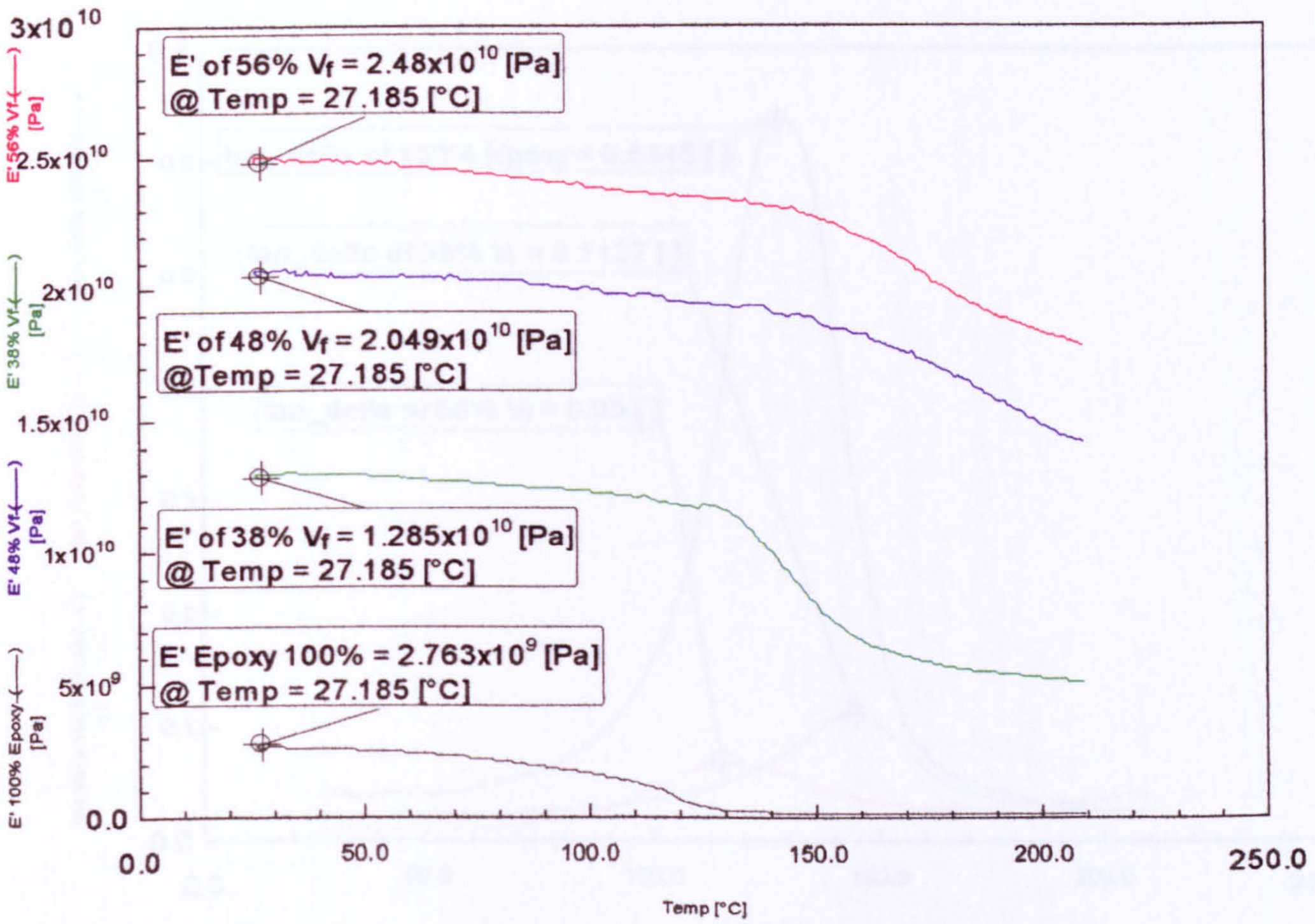

Figure (5 – 18) the storage moduli plot of non-hybrid glass woven fabric reinforced epoxy resin composites including four different fibre volume fractions.

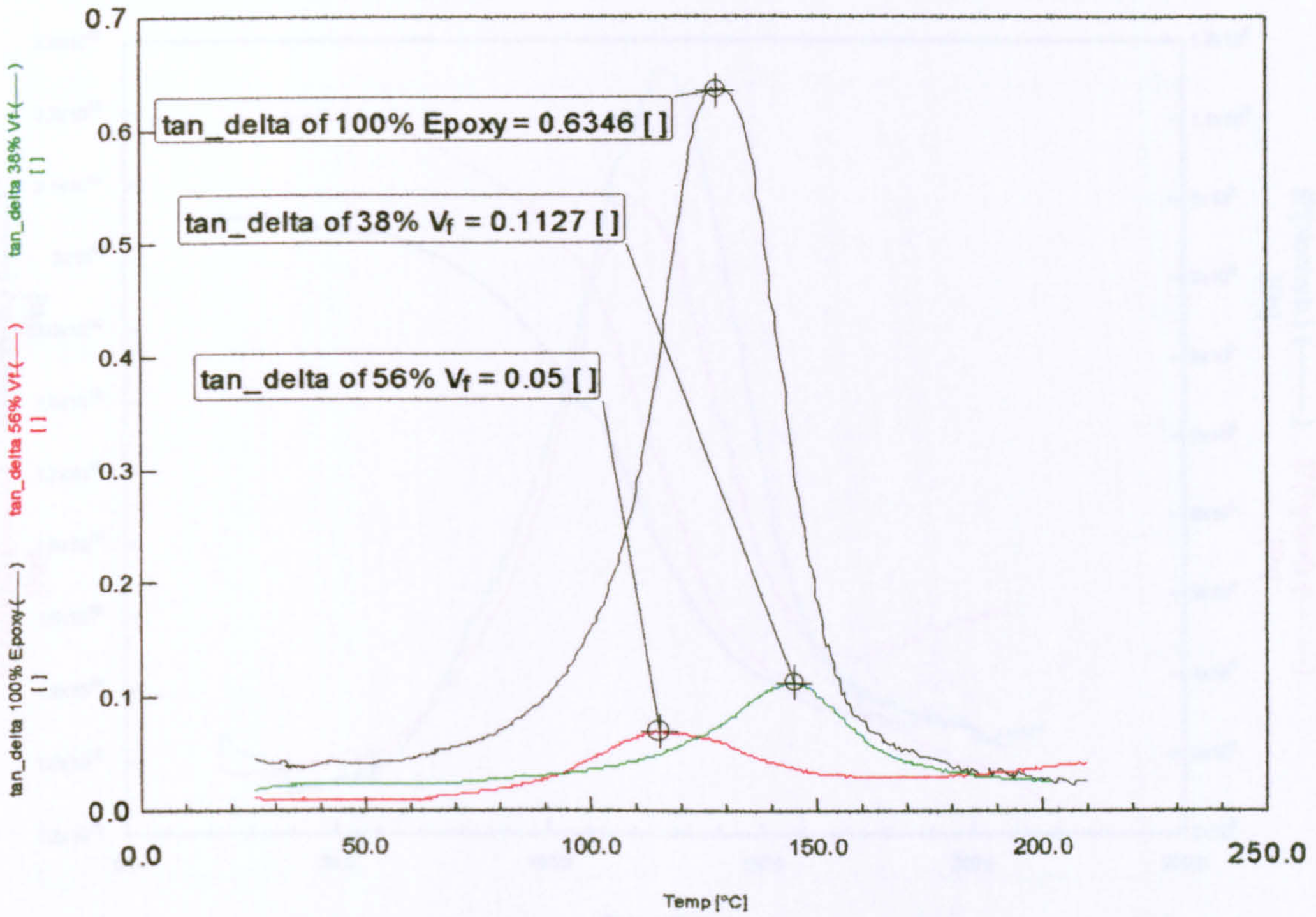

Figure (5 – 19) the tan delta plot of non-hybrid glass woven fabric reinforced epoxy resin composites including three different fibre volume fractions.

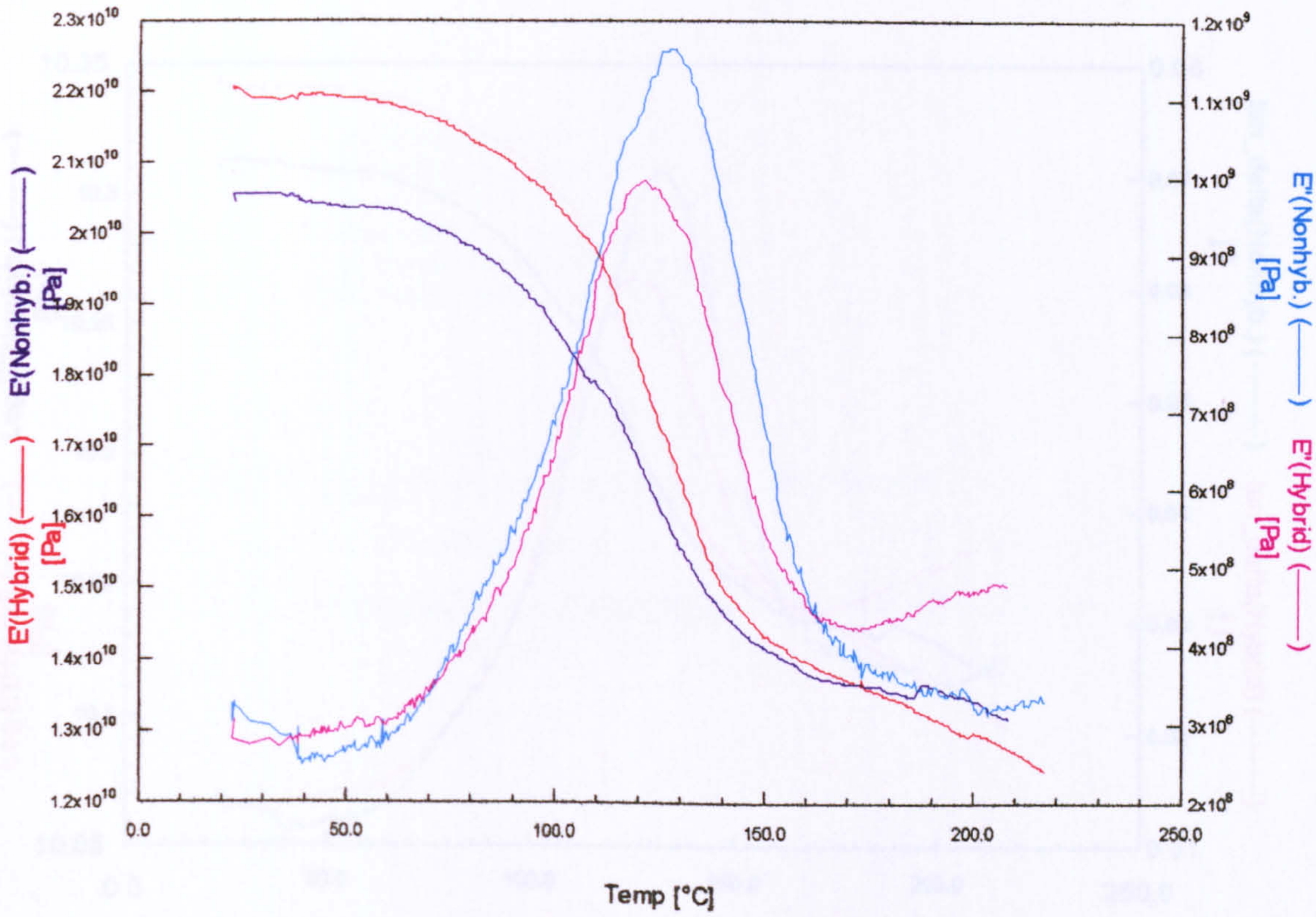

Figure (5 – 20) DMTA of hybrid and non-hybrid glass woven reinforced epoxy resin composites (weft direction). Plot of loss and storage moduli at 48% V_f.

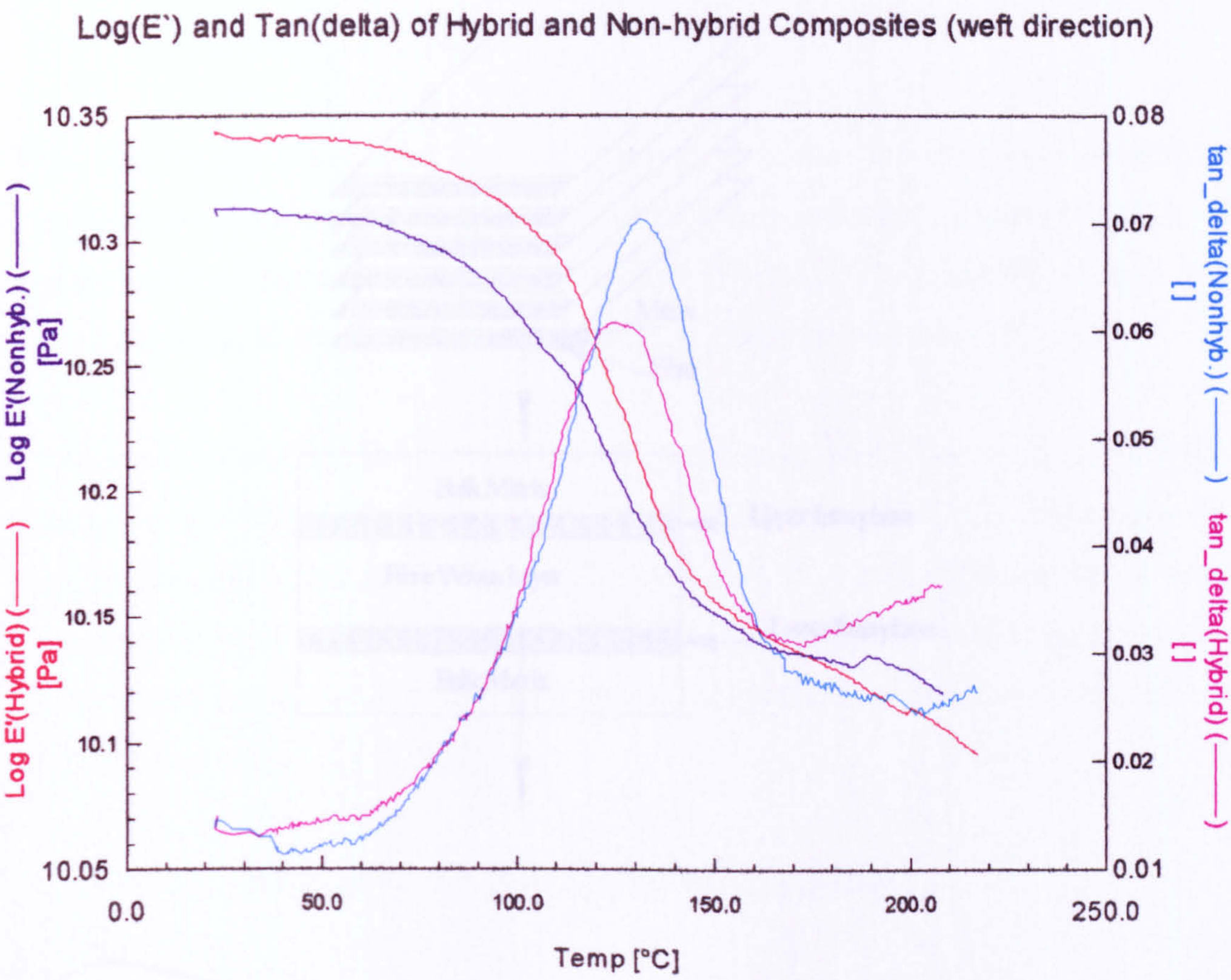

Figure (5 – 21) DMTA of hybrid and non-hybrid glass woven composites (weft direction); plot of tan (δ) and log (E′) curves at 48% fibre volume fraction.

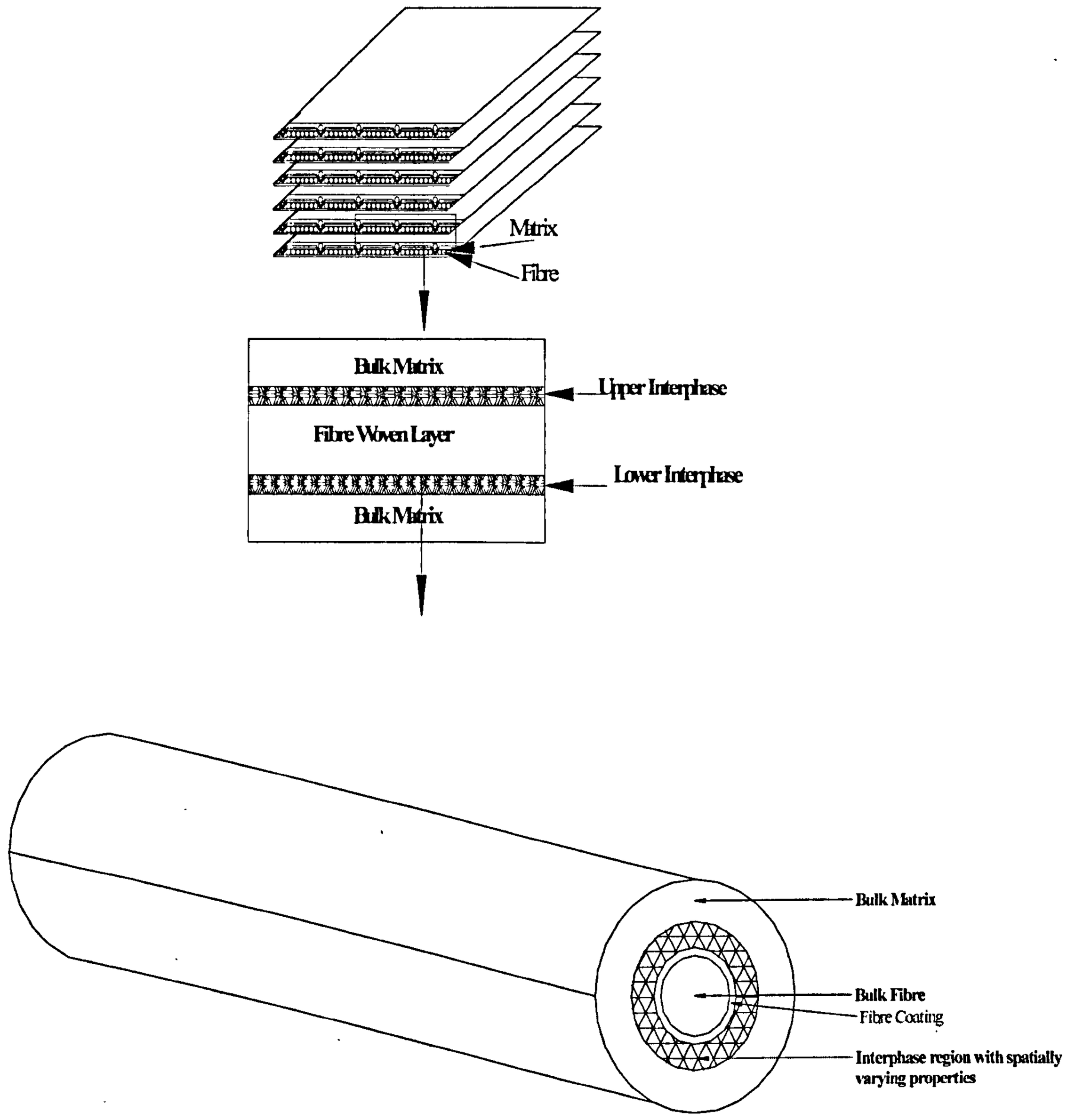

Figure (5 – 22) Visualisation of three-dimensional interphase. The interphase layer promoted by the number of woven layers in the composites, in the laminate level, as a result of interaction with spatially varying properties elevated by glass fibres surface treatment, in the micro (fibre) level.

5 – 4 Section four: Tensile Properties

5 – 4 – 1 The results of tensile tests

The results of the tensile test on non-hybrid glass woven fabric reinforced epoxy resin composites including four different glass V_f are summarised in table (5 – 12). The results are graphically presented in figures (5 – 23) and (5 – 24). The quantification of AE values during tensile tests including four different glass V_f is given in the table (5 – 13).

The result of the tensile tests on hybrid and non-hybrid glass woven reinforced epoxy resin composites, weft and warp directions are set out in table (5 – 14). The results of weft direction are graphically presented in figures (5 – 25) and (5 – 26). The results of warp direction are graphically presented in figures (5 – 27). The quantification of AE ring down count (RDC) and rate, including the hybrid and non-hybrid composites for both weft and warp directions, are summarised in table (5 – 15).

5 – 4 – 2 Discussion of the effect of V_f on tensile properties

Figure (5 – 23) shows a comparison of four V_f composites including the stress-strain and the corresponding AE **ring down count** curves. The stress-strain curves are similar in shape, but differ in their values of the ultimate tensile strength. The result further shows that the highest magnitude of ultimate tensile strength (UTS) was associated with the highest level of fibre volume fraction at 64% V_f composite. The lowest values of UTS was associated with the lowest level of V_f in the composite at 38% V_f. The appearance of two knees on each stress-strain curve having distinct values for each composite is due to differences in fibre volume fractions.

In figure (5 – 24) a comparison of four V_f composites including the stress-strain and the corresponding AE **rate** curves are presented. It has been observed that the number of peaks of the rate, including the peak length, decrease with increasing V_f in the composites. This clearly reveals the high damage associated with the low V_f in the composites.

The tensile moduli and strengths were higher than the flexural moduli and strengths for all woven glass/epoxy composite investigated in this project (see tables 5 – 5 and 5 – 12). It is believed that the higher tensile strength is attributed to the differences in the critically loaded

volume of tensile and flexural specimens. In flexural tests, only the outer fibres at the mid-span, the beam, are loaded up to their maximum stress, whereas under the tensile loading, the whole composite volume is critically loaded, yielding a higher probability of strength.

AE activities including four V_f glass woven composites, the representative plots of stress-strain, together with the corresponding AE curves for the woven glass composite at 48% V_f, are shown in figure (5 – 28). The stress-strain curve in the plot, shows that the non-linear shape of the curve is due to the non-linear response of the matrix material. Two knees appear on the stress-strain curve of glass woven fabric reinforced epoxy composites. The first knee point is visible in the stress-strain curve at less than 1 % strain. The moduli of elasticity are usually obtained from the initial linear portion of the stress-strain curve. The correlation between the first knee point and the acoustic emission onset point has been indicated and examined to evaluate the failure process analysis objective. The zone classification technique of stress-strain corresponding AE curves has been utilised in this study in order to obtain the maximum possible information from a group of samples. The use of zone classification technique divides the plots in figure (5 – 28) into three zones as follows:

Zone A: a portion of the AE curve, between the origin and the onset point, is associated with the initial linear portion of stress-strain response until the first knee point portends the first indication of non-linearity. The RDC reading in this zone exhibits that there is no existing record of any rise in the curve to define plastic destruction of the composite specimen under tensile loading. The correlation between the AE onset point with the first knee point of the stress-strain curve has been examined carefully for each individual tensile test.

Zone B is defined as the distance between the first and second knee points under the second linear portion of the stress-strain curve. The AE rise appears instantaneously at the onset point indicating the initiation of the first destructive damage in the construction of the composite material. The AE curve then rises up gradually consistent with existing regions of uniform strain, which may fail simultaneously with continuous tensile stress drops. The low **RDC** values of AE recorded in this zone are believed to correspond to the matrix cracking and damage due to possible voids in the composite.

The AE curve in the first half of zone B indicates matrix damage progressively including fibre/matrix interface damage initiation. The AE curve in the second half of zone B rises more

rapidly with higher RDC recording indicating fibre/matrix interface damage progressively increasing. The interfacial failure grows rapidly as it reaches a critical size, followed by matrix continuous cracking and possibly failure in the fibre-matrix interphase region. The interphase failure refers to the failure in a region between the bulk matrix and the fibre woven layer in the composite. The formation of matrix damage is due to a number of fibre-matrix interfacial damages resulting from a multi-microcrack.

Zone C: The AE continues to rise linearly from the second knee point until final tensile specimen failure occurs. The AE in this zone recorded the highest level of ring down counts in the life history of the composite test. This corresponded to the recording of higher emission results from the continuing destruction of the composite specimen under tensile loading. The high emission presumably corresponds to fibre debonding in the off-axis of the laminate, layer delamination, fabric weaving distortion and fibre rupture. A more detailed discussion of the damage sequence and zone classification can be found in section five, the damage event process model.

The explanation of non-linearity agrees with Wooh who showed that no macroscopic damage was found in the linear elastic region (Wooh et al. 1995), while the use of AE has been employed to analyse the damage event in unidirectional composites (see Wevers 1996, Kander 1991, and Mittleman and Roman 1987). In this study the zone classification technique of stress-strain and its relating AE curves have been utilised to extract the maximum possible information from each variation, in the interpretation of the damage event sequence. Thus the stress-strain knee point and AE onset point relationship of woven glass fibre in the composites could be investigated in some detail. The stress values and qualitative images of damage accumulation in woven composites are also interrelated.

It was noticed that the lower the glass fibre volume fraction in the composite the greater is the magnitude of AE ring down count at each knee point (see figure 5 – 23). The higher the AE activity the greater is the damage. Furthermore, the lower the fibre volume fraction in the composite the higher the AE activity recorded at the ultimate tensile fracture accompanied by the layers delamination and fibre rupture. Low AE activities at knee points and ultimate tensile fracture recorded for high V_f composites refers mainly to fibre yarn debonding and weave distortion. The high AE activity at ultimate tensile fracture recorded for lower V_f composite refers mainly to the fibre yarn debonding in the off-axis of the laminate, layer delaminations, and

fibre rupture. The values represent different micromechanical failure as indicated by the SEM and visual examination of the tensile fracture surface. The failure sequence in all four laminates follows a similar pattern. Furthermore the AE distinct value is reflected in the curve pattern promoted by sequential damage events. This damage mainly occurs next to the second knee point. The stress values at knee points and their corresponding RDC reveal that the different fracture mechanisms generated are due to the variation in the interphase properties of composites. The interphase property is a function of the variation in the fibre volume fraction.

The **visual examination** of tensile specimens after tests is examined individually so as to observe the failure mode of each test and each specimen. The mode of failures can be divided into the following categories: -

Tensile failure mode (1) - This mode of failure is associated with low fibre volume fraction in the composites. The specimen of non-hybrid E-glass woven composite at 38% V_f in figure (5 – 29a) shows the tensile specimen split into two pieces. This includes a complete longitudinal fibre rupture and matrix deformation. Some fibre bundle debonding in the transverse-axis is created by weave crimp in the composite. The fibre rupture indicates poor tensile properties in the loading axis and poor interlaminar shear strength (ILSS).

Tensile failure mode (2) - This mode of failure is associated with lower intermediate V_f composites. The tensile specimen of the non-hybrid E-glass woven fabric composite at 48% V_f in the figure (5 – 29b) shows the specimen broken into two pieces. The fracture includes signs of fibre bundle pull out and complete longitudinal fibre rupture. A complete matrix deformation and fabric delamination including fibre bundle pullout in the longitudinal axis can be seen. The delamination in the off-axis direction is affected by the weave construction of the fabric in the composite. The fracture mode indicates intermediate tensile properties and ILSS.

Tensile failure mode (3) - This mode of failure is associated with high-intermediate V_f composites. The tensile specimen of the non-hybrid E-glass woven composite at 56% V_f as shown in figure (5 – 30a), remains coherent. The fracture surface shows a change in the alignment of the specimen as a whitening area that is approximately at a 30^o angle to the loading axis. The length of fracture (whitening area) in the specimen is between 50 – 60 mm. Some signs of woven fabric delamination occur including fibre bundle debonding in the off-axis direction affected by the weave construction of the fabric in the composite. This indicates high

tensile properties and very good performance of ILSS in such composites. The specimen after fracture shows signs of stability, indicating very good composite reinforcement.

Tensile failure mode (4) - This mode of failure is associated with high V_f composites at 64% V_f. The tensile specimen of non-hybrid E-glass woven fabric composite as shown in figure (5 – 30b), remains coherent. This includes a change in the specimen alignment to approximately 45° angle to the loading axis. The length of fracture (with wide whitening area) in the specimen is between 40-50 mm. This indicates that such a high V_f employed in the composite reinforcement was not as good as the previous composite reinforcement at 56% V_f. There are signs of woven fabric layer delaminations including fibre bundle debonding in the off-axis affected by undulation created by weaving.

The **SEM** micrograph in figure (5 – 32) shows the fracture surface of non-hybrid glass woven fabric composite of 38% V_f, which indicates:

(a) Brittle fibres were mainly ruptured rather than pulled out. The few shear cusps of the epoxy resin on the glass fibre surface indicate poor fibre/matrix adhesion.

(b) Poor fibre/matrix interfacial bond. The failure seems to have occurred at the fibre/matrix interface. The fibre/matrix interface failure followed by some obvious fibre breakage and fibre pullout could have produced the final failure. The fibre/matrix adhesion is comparatively low in these composites. This is because the composites hold a low level of strength and modulus promoted by the low V_f of the composite.

The SEM micrograph of the fracture surface at 48% V_f composite in figure (5 – 33) displays

(a) The presence of surface debris and shear cusps of the matrix on the fibre surface. This indicates an intermediate interfacial strength between fibres and matrix compared with the previous composite. The figure exhibits brittle fibres mostly pulled out rather than ruptured under the effect of undulation created by weaving.

(b) A layer delamination in the through thickness side.

The SEM micrograph of the fracture surface at 56% V_f composite in figure (5 – 34) shows

(a) A change in the specimen alignment occurred due to the multiple fibre bundles debonding in the damage location. The misalignment of the laminate left whitening mark on the specimen surface.

(b) An obvious weave distortion in the specimen surface. The weave distortion refers to the general distortion in the weave repeat unit. Furthermore the micrograph shows fibre debonding and a layer delamination.
(c) A higher magnification of (b) indicates some fibre rupture at crimp curvature.

The SEM micrograph in figure (5 – 35) displays the damage location of 64% V_f composite,
(a) shows the change in the specimen alignment is a result of multiple matrix cracking,
(b) shows the crack propagation along the interface at the edge of woven fibres, the crack path passes round the pocket of woven fibres,
(c) shows the fracture of fibre bundles under the effect of undulations created by weaving. The elevated fracture shows a tortuous curved failure path that is possibly related to a brittle interphase formed in the composite.

The VSE and SEM micrograph along with the AE used in this study were interrelated to the micromechanics of the damage events sequence occurrence. This will be used in damage sequence modelling (see section 5 – 6).

5 – 4 – 3 Discussion of fibre hybridisation effect on composite tensile properties

The result shown in table 5 – 14 indicates that the ultimate tensile strength (UTS) of the hybrid composite for the weft direction is superior to the non-hybrid composite by approximately 20 %. The Young's modulus and UTS values show that the hybrid composite is stiffer and greater in strength than the non-hybrid composite.

AE activities of weft direction: the non-hybrid glass woven composite in the weft direction displays a higher magnitude of RDC and rate compared to the hybrid composite. The results of RDC and rate activities during the tensile tests are summarised in table (5 – 15) and graphically presented in figures (5 – 25) and (5 – 26) respectively. The shapes of stress-strain curves are identical, but differ in magnitude. Two knees appear on each stress-strain curve having different values. The two knee points divide the curves into three linear portions. The appearance of two knees on each stress-strain curve with distinct values for each composite is due to the different fibre mechanical properties of R-glass and E-glass. This shows the hybridisation effect on composite properties. The zone classification technique has been utilised as discussed in the above section. The features at the knee points and ultimate tensile strength in each curve possess

distinct values. A higher magnitude of the AE at ultimate tensile fracture was recorded for the non-hybrid composite. The higher the AE activity the greater is the damage. The damage refers mainly to layer delamination and fibre rupture. A lower value of AE was recorded for the hybrid composite. This is because of the fibre debonding in the off-axis of the laminate, and fabric weaving distortion including specimen misalignment. The AE activity represents different micromechanical failure mechanisms as indicated by the SEM and visual examination of tensile fracture surface.

The visual specimen examination shows the tensile mode failures of the **hybrid** composite weft direction in figure (5 – 30) and the **non-hybrid** composite in figure (5 –29b). The hybrid specimen after fracture remains coherent and shows signs of stability, indicating good composite reinforcement. The non-hybrid composite shows a specimen split into two pieces and indicates signs of complete longitudinal fibre rupture and fibre bundle pullout. The visual specimen examination of the non-hybrid composite has been discussed in the previous section.

The SEM micrograph in figure (5 – 36) shows:

(a) The initiation of the fibre/matrix debonding on the fracture surface of the **hybrid** composite at 48% V_f.

(b) The presence of surface debris and shear cusps of the matrix on the fibre surface indicates a good fibre/matrix bond. It is believed that the presence of surface debris and cusps of the matrix on the fibre surface possibly lead to layer delamination. The regular hackle pattern dominating the fracture surface is left by fibres after shear failure. The SEM micrograph further shows a change in the specimen alignment resulting from multiple fibre debonding. It is believed that a well-developed interphase has been formed by the hybrid woven composites. The SEM micrograph figure (5 – 32) of a tensile specimen of **non-hybrid** woven glass fabric composite (weft direction) at 48% V_f has been discussed in the previous section.

The stress values at knee points and UTS including its corresponding RDC reveal that the different fracture mechanisms generated are due to differences in the interphase properties of the composites. The visual specimen examination and SEM evidence suggest that the variation in the results is due to differences in the interphase property. The interphase property generated by fibre coating and their interaction with the matrix is revealed by DMTA. The fibre coating is influenced by the fibre properties and causes the changes in the overall fracture performance of the specimens.

The results in table (5 – 14) show the UTS of the hybrid are close to non-hybrid composites in the (**warp direction**). The results in table (5 – 15) show that the AE ring down count value of the non-hybrid E-glass woven composites are close to the magnitude of the AE ring down count of the hybrid composites during the tensile test. The results indicate no improvement of tensile strength in warp direction.

The shapes of the stress-strain curves in figures (5 – 27) are identical. The damages sequence in hybrid laminates follows a similar pattern of non-hybrid laminates (in warp direction). The AE ring down count in figure (5 – 27) of the composite warp direction represents the performance of E-glass in both the hybrid and non-hybrid glass woven composites. Therefore, the features at knee points and ultimate tensile strength for each curve have similar values. The zone classification technique has been followed and discussed in the previous section. The final reading of RDC on the AE curve as recorded in table (5 – 14) identifies the fibre rupture occurrence in both composites.

The visual specimen examination indicates that the tensile mode failures of the hybrid and non-hybrid composite warp direction are similar to each other (see figure 5 – 30b). The SEM micrograph of the fracture surface of non-hybrid and hybrid glass woven composites (warp direction) at 48% V_f is similar (see figure 5 – 32). Thus the work in this particular investigation shows no effect of hybridisation on the composite warp direction.

The main difference between the hybrid and non-hybrid composites is that the hybrid composite is composed of **R-glass** and **E-glass** whereas the non-hybrid composite contains E-glass only. It is essential to mention again that the R-glass was in the weft direction of the hybrid weave while E-glass was in the warp direction. Therefore there was significant improvement of tensile properties in the weft direction, which did not occur in the warp direction. The failure sequence for both laminates follows a similar pattern due to the effect of 8-harness woven fabric composites having individual values for contrary failure mechanism on stress-strain and AE curves.

From the above, the following results can be identified:

- The tensile strength (σ) and tensile modulus increases with increasing overall fibre volume fraction in the composites see table (5 – 12). This is due to the increase in the number of layers. This clearly demonstrates the effect of V_f on tensile properties.

- The tensile specimen of high V_f composites remains coherent despite changes in the specimen alignment with the whitening area on the specimen. Conversely, the tensile specimens of low V_f composites splits into two pieces and include signs of complete longitudinal fibre rupture. This indicates the greater tensile strength is associated with high V_f composites compared to those of low V_f composites.

- The AE activities monitored during tensile tests indicate that the high V_f composites were more brittle than the low V_f composites. It has been observed that the higher the glass V_f in the composite the lower the AE activity. This comparison is presented in figures (5 – 23 and 5 – 24). This clearly demonstrates a case of increasing overall fibre strength promoted by fibre volume fraction of the composite.

- The higher level of UTS (σ) and tensile modulus is associated with the **hybrid** composite in the **weft direction** compared to the non-hybrid composite see table (5 – 14). This is due to the presence of the R-glass, in the hybrid composite (weft direction). The result shows the level of UTS (σ) and tensile modulus of the hybrid composite and non-hybrid composite **(warp direction)** are close to each other. This is due to the presence of the E-glass in the warp direction for both composites. This clearly demonstrates the variation effect of fibre mechanical properties on the tensile property of the composite.

- The tensile specimen of the hybrid composite **(weft direction)** remains coherent in one piece with a change in the alignment. The tensile specimen of the non-hybrid split into two pieces indicating complete longitudinal fibre rupture. This indicates the tensile strength of the hybrid is superior to that of the non-hybrid. Meanwhile the tensile specimen of the hybrid and non-hybrid composites **(warp direction)** broke into two pieces. This indicates no improvement of tensile strength in the warp direction.

- The hybrid composites (weft direction) showed greater toughness performance as compared to non-hybrid composites (compare views in figures 5 – 25 and 5 – 26).

- The AE activities level of the non-hybrid composites (**weft direction**) is higher compared with the hybrid composites (see figure 5 – 25). Conversely the AE activities show that the hybrid and non-hybrid composite (**warp direction**) hold close values (see figure 5 – 27). This clearly is another demonstration of R-glass strength and its resistance to tensile stress in the composites.

Table 5-12 **Tensile** Test Results of Non-hybrid Glass Woven Fabric Composites including four Different **Fibre Volume Fraction.**

Tensile Test Results of Non-hybrid Glass Woven Fabric Composites at Different Fibre Volume Fractions.										
Test	Fibre Volume Ratio (%)	No. of Plies in 1mm Thickness	Stress @ Second Knee point (MPa)		UTS (MPa)		Strain (%) @ UTS		Mean E-Modulus (GPa)	
			Mean	Std.Dev.	Mean	Std.Dev.	Mean	Std.Dev.	Mean	Std.Dev.
Non-hybrid @38%	0.38	4	331.49	20.86	414.33	30.32	3.55	0.22	22.46	2.02
Non-hybrid @48%	0.48	5	400.50	23.19	501.90	33.71	4.25	0.34	25.56	2.22
Non-hybrid @ 56%	0.56	6	460.31	25.17	577.81	36.59	3.68	0.26	28.29	2.47
Non-hybrid @ 64%	0.64	7	508.33	27.84	642.55	40.47	3.28	0.27	30.79	2.56

Table 5-13 AE Patent during tensile test of Non-hybrid Composites including Four Different **Fibre Volume Fractions**

AE Patent during tensile test of Non-hybrid Fibre Glass Woven fabric Composites including Four Different Fibre Volume Fraction							
			AE @ Knee Points			AE @ Finial Fracture	
Laminates	Fibre Volume Ratio %	No. of Plies in 1mm Thickness	Corr. Of first Knee & Onset Points	RDC @ Second Knee	Rate @ Second Knee	RDC	Rate
Non-hybrid @38%	0.38	4	yes	60000	54000	1306214	67000
Non-hybrid @48%	0.48	5	yes	50000	40000	1137395	50000
Non-hybrid @ 56%	0.56	6	yes	44000	18000	969616	27000
Non-hybrid @ 64%	0.64	7	yes	39000	7000	851057	12900

Table 5-14 Comparison of Tensile Test Results between Non-hybrid and Hybrid Glass Woven Composites

Tensile Test Results of **Non-hybrid** (E-Glass) Woven **Composites**										
Test	Fibre Volume Ratio (%)	No. of Plies in 1mm Thickness	Stress @ Second Knee (MPa)		UTS (MPa)		Strain (%) @ UTS		Mean E-Modulus (GPa)	
			Mean	Std.Dev.	Mean	Std.Dev.	Mean	Std.Dev.	Mean	Std.Dev.
Non-hybrid (weft dir.)	0.48	5	400.50	23.19	501.90	33.71	4.25	0.34	25.56	2.22
Non-hybrid (warp dir.)	0.48	5	428.12	22.13	536.96	32.17	4.04	0.30	27.19	2.31
Tensile Test Results for **Hybrid** (E-Glass in Warp, R-Glass in Weft) Woven **Composites**										
Hybrid (weft dir.)	0.48	5	483.12	25.16	609.29	36.57	4.74	0.39	30.18	2.61
Hybrid (warp dir.)	0.48	5	430.48	22.56	542.49	32.80	4.06	0.29	27.88	2.41

Table 5-15 AE Patent representing **Tensile** activity of Non-hybrid and Hybrid Glass Woven Composite

AE Patent representing **Tensile** of Non-hybrid and Hybrid Glass Woven Composites							
				AE @ Second Knee		AE @ Finial Fracture	
	Laminates	Fibre Volume Fraction %	Corr. Of Knee & Onset Points	RDC	Rate	RDC	Rate
Non-hybrid	Weft	0.48	yes	50000	40000	1137395	50000
	Warp	0.48	yes	48000	35000	965816	48000
Hybrid	Weft	0.48	yes	39500	25000	837942	35000
	Warp	0.48	yes	47000	34600	953816	46000

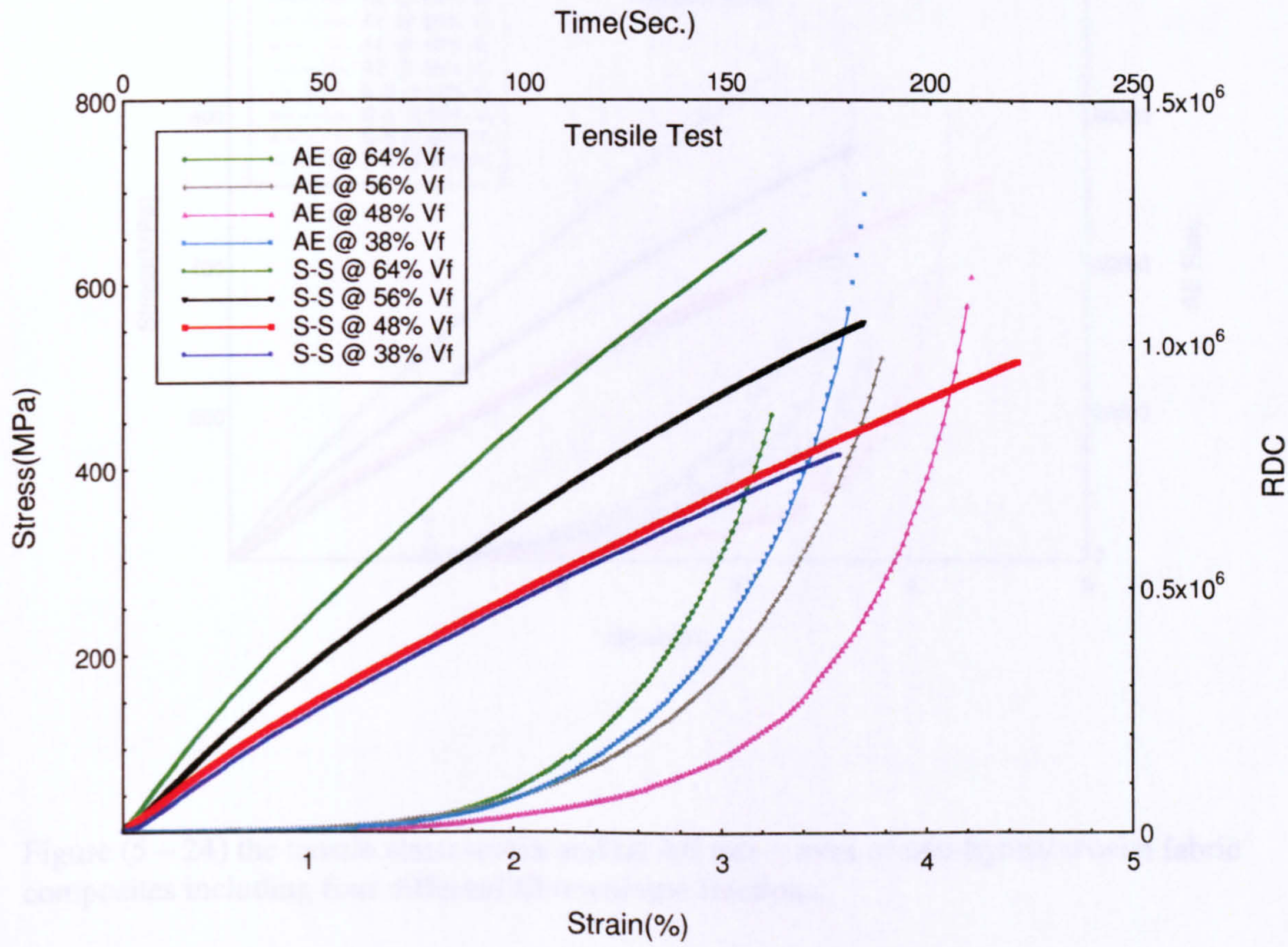

Figure (5 – 23) the tensile stress-strain and its AE ring down count activity curves of non-hybrid woven composites including four different fibre volume fractions.

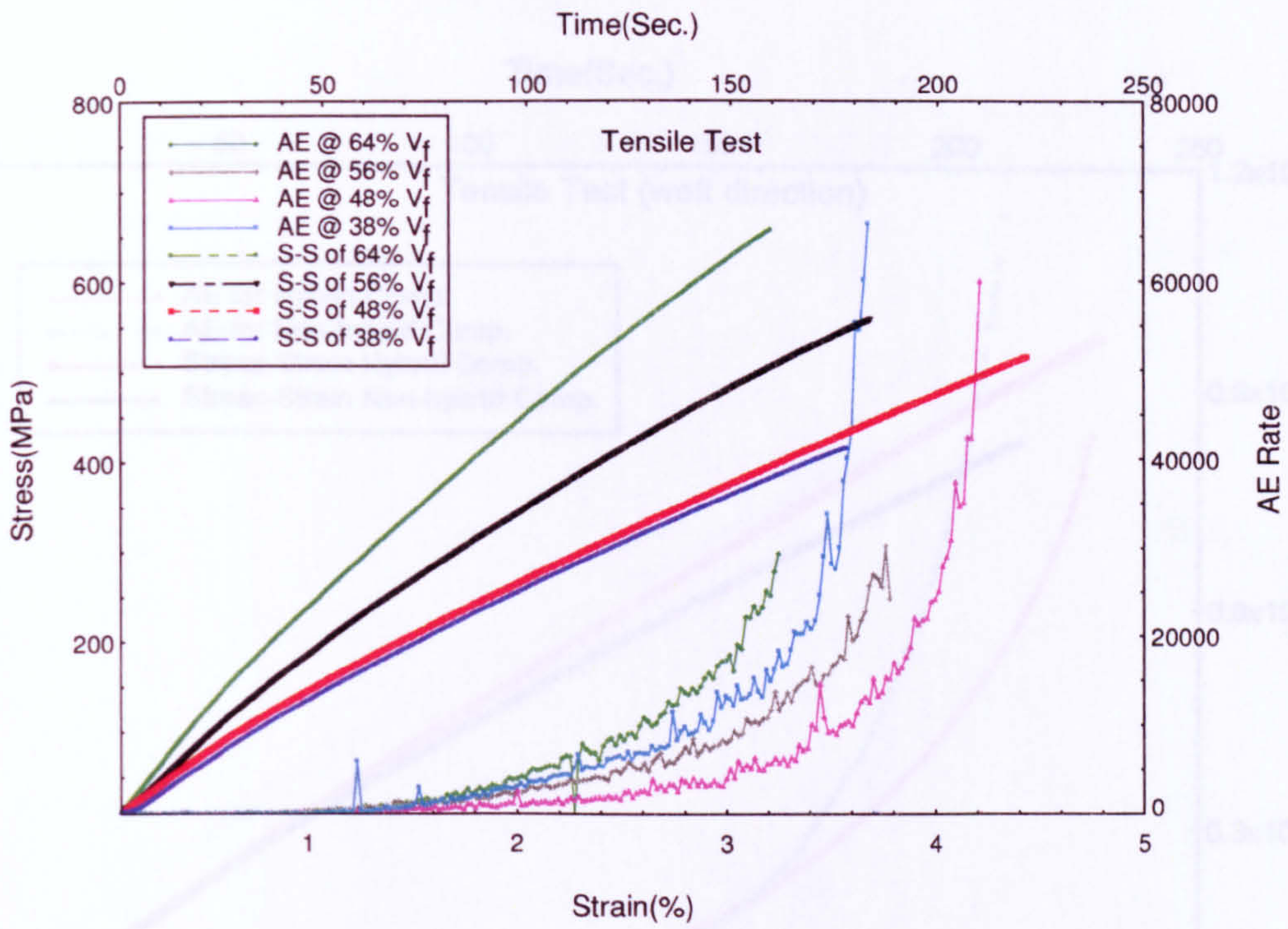

Figure (5 – 24) the tensile stress-strain and its AE rate curves of non-hybrid woven fabric composites including four different fibre volume fractions.

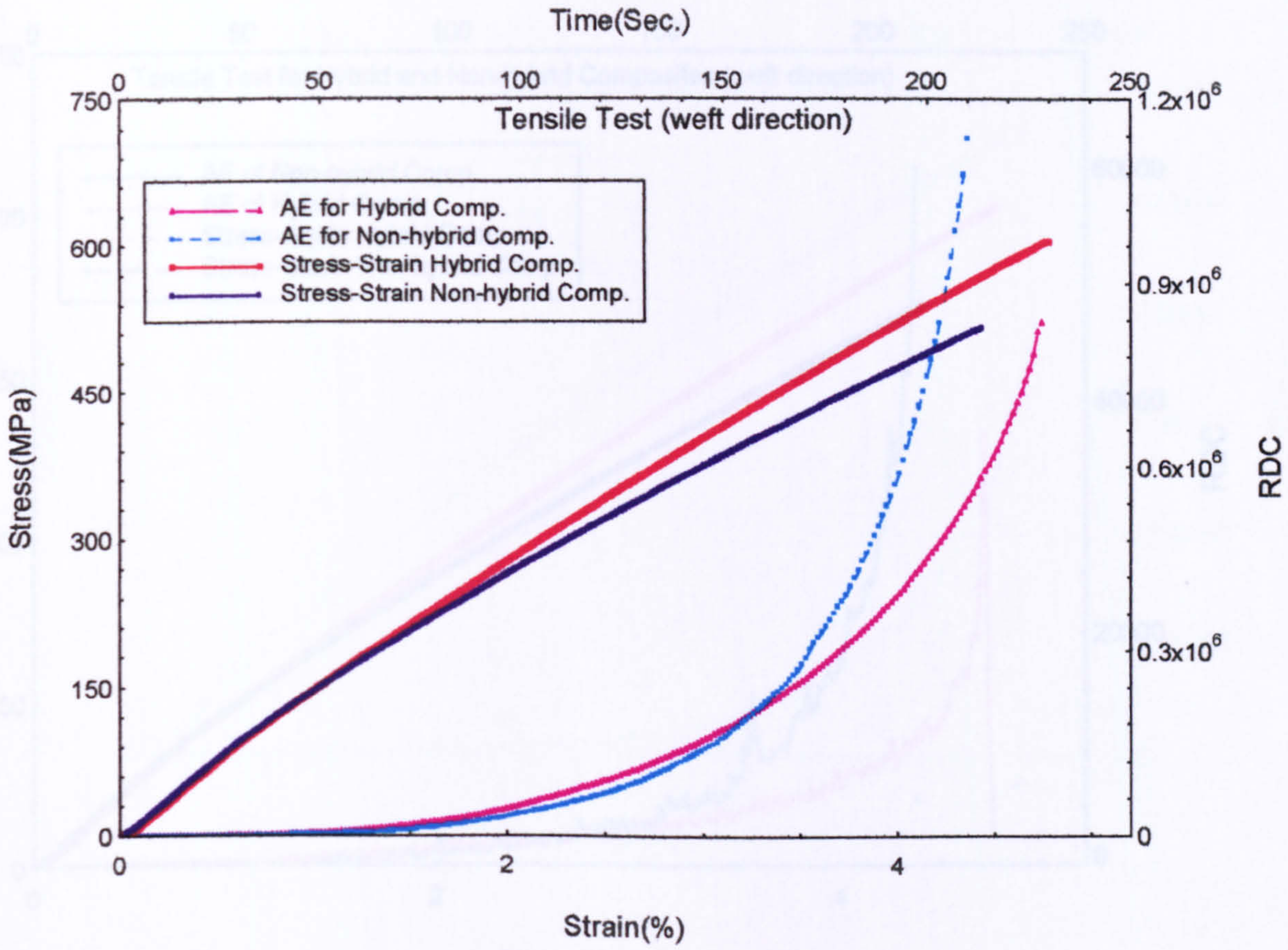

Figure (5 – 25) The tensile stress-strain curve of hybrid and non-hybrid woven fabric composites **(weft direction)** at 48% V_f, and its AE ring down count activity.

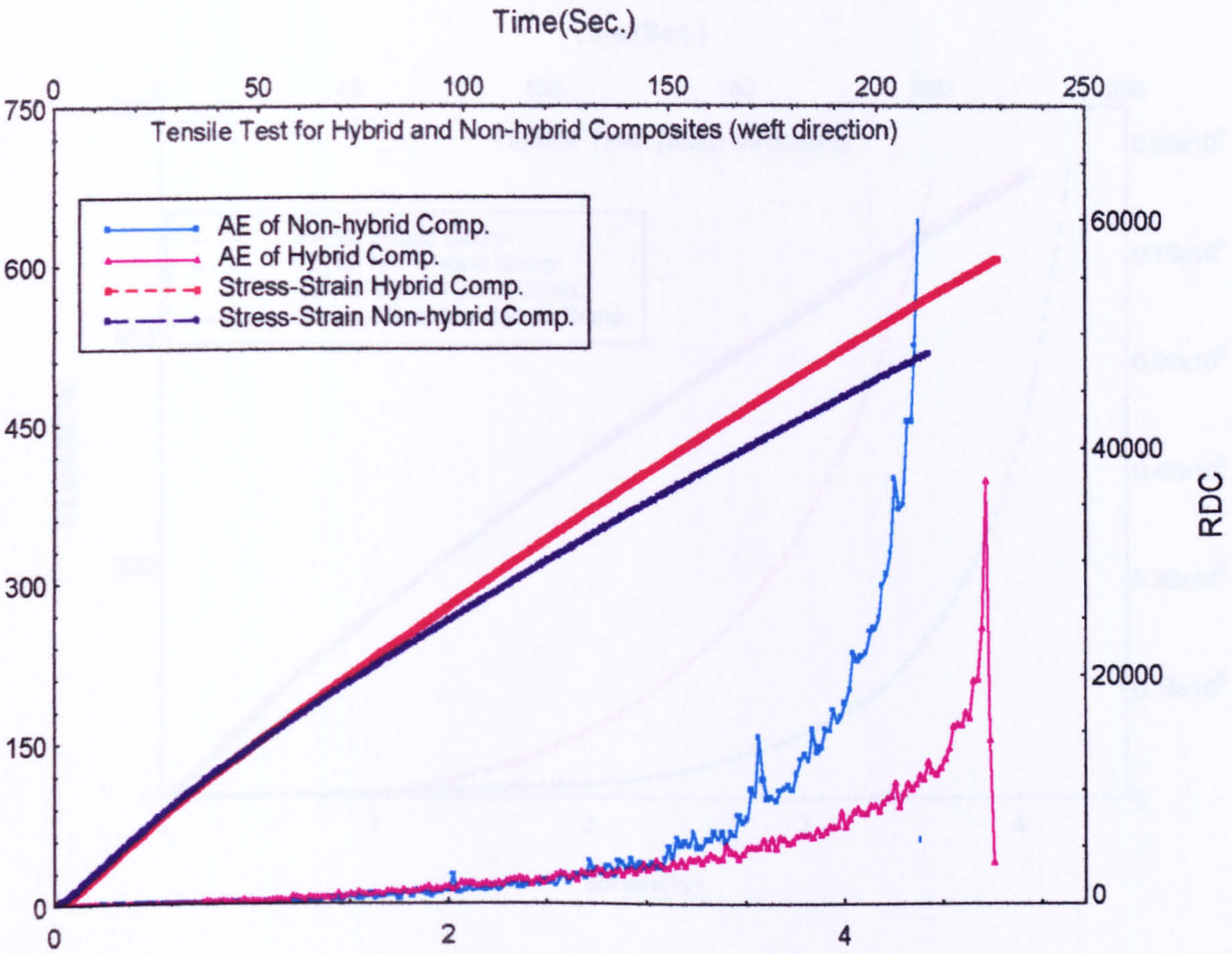

Figure (5 – 26) The tensile stress-strain and its AE rate curves of hybrid and non-hybrid woven fabric composites (weft direction) at 48% V_f.

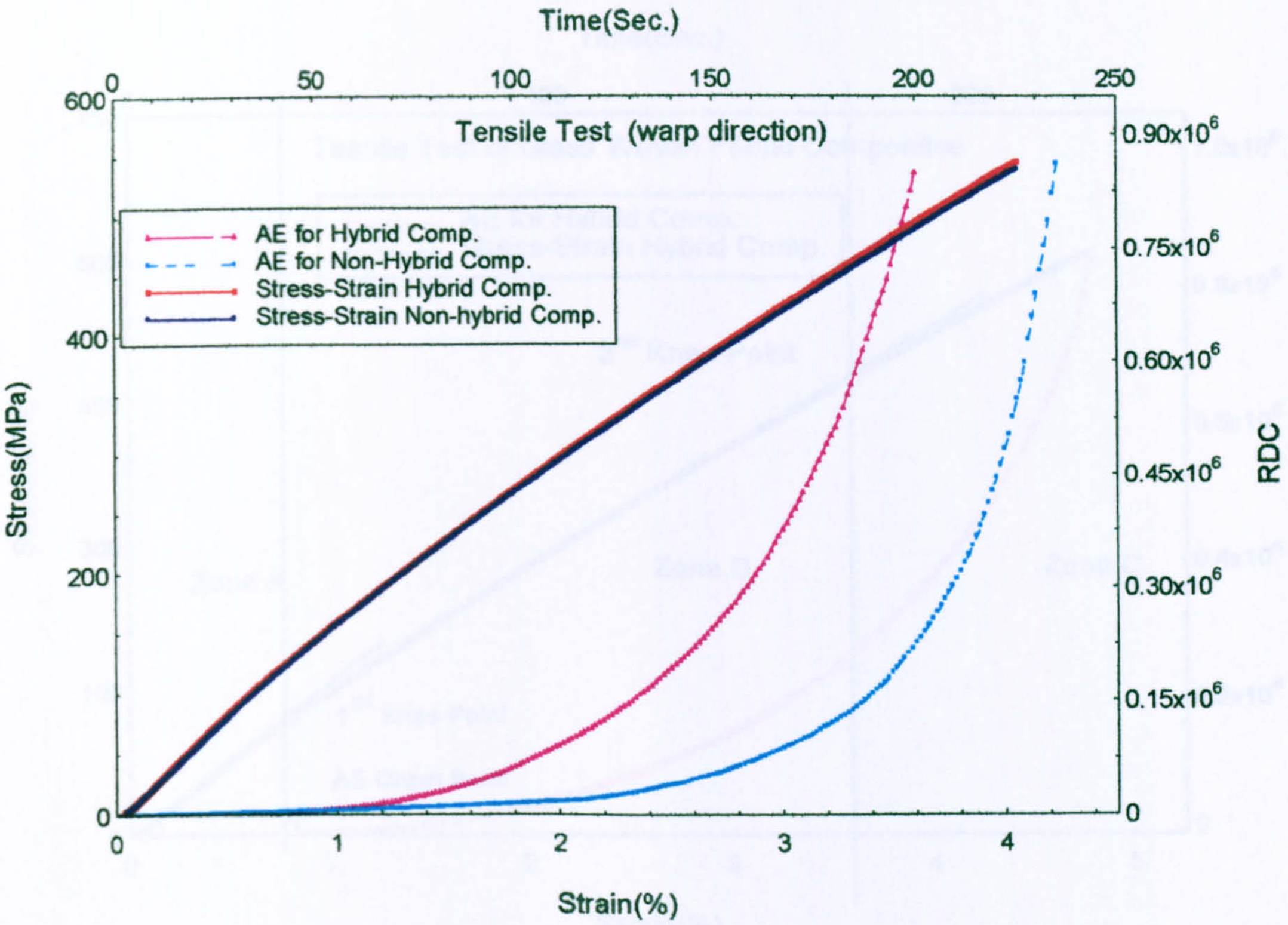

Figure (5 – 27) the tensile stress-strain and its AE ring down count activity curves of hybrid and non-hybrid woven fabric composites (warp direction) at 48% V_f.

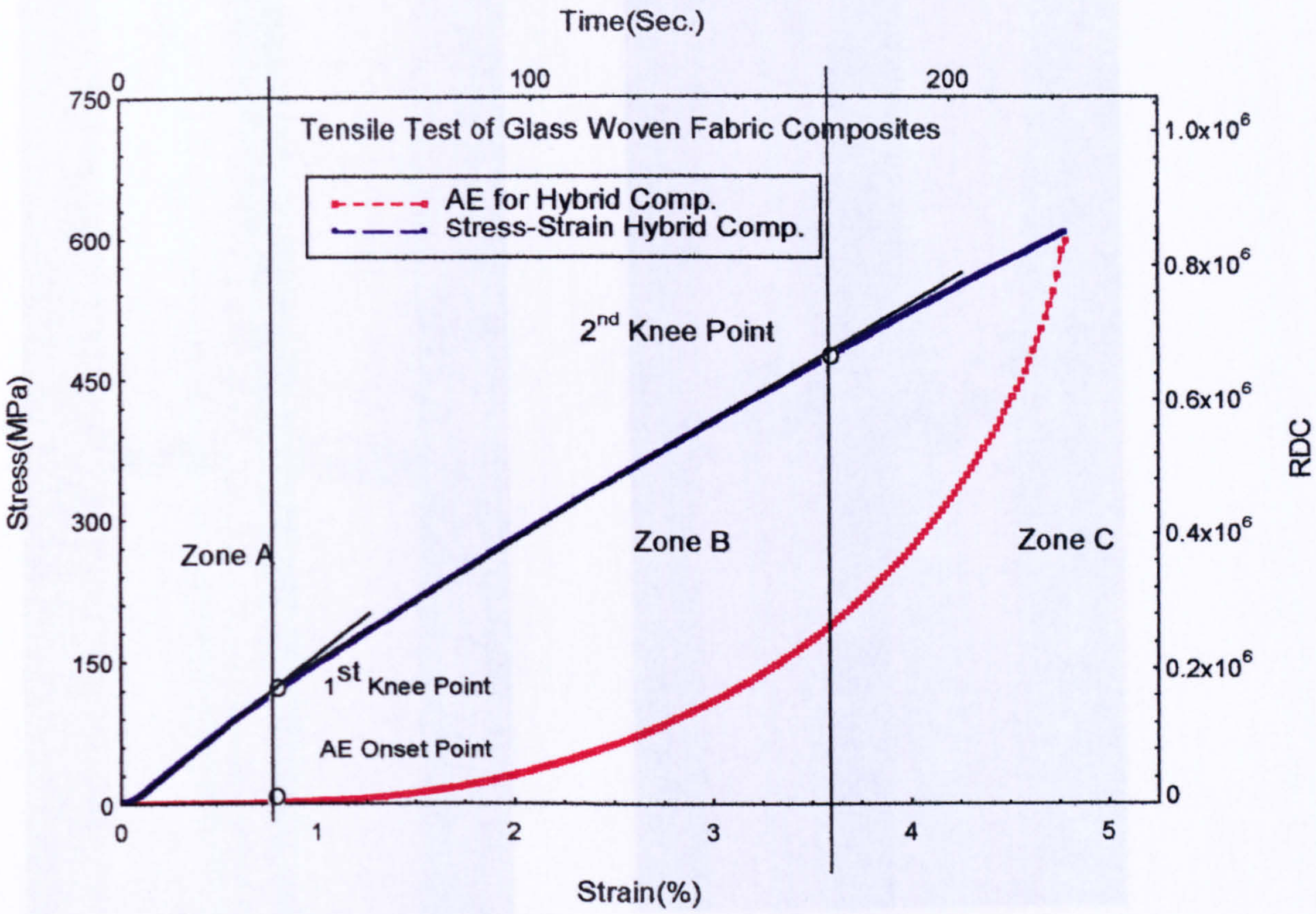

Figure (5 – 28) the **zone classification technique** used in tensile stress-strain and its AE curves of glass woven fabric reinforced epoxy resin composite.

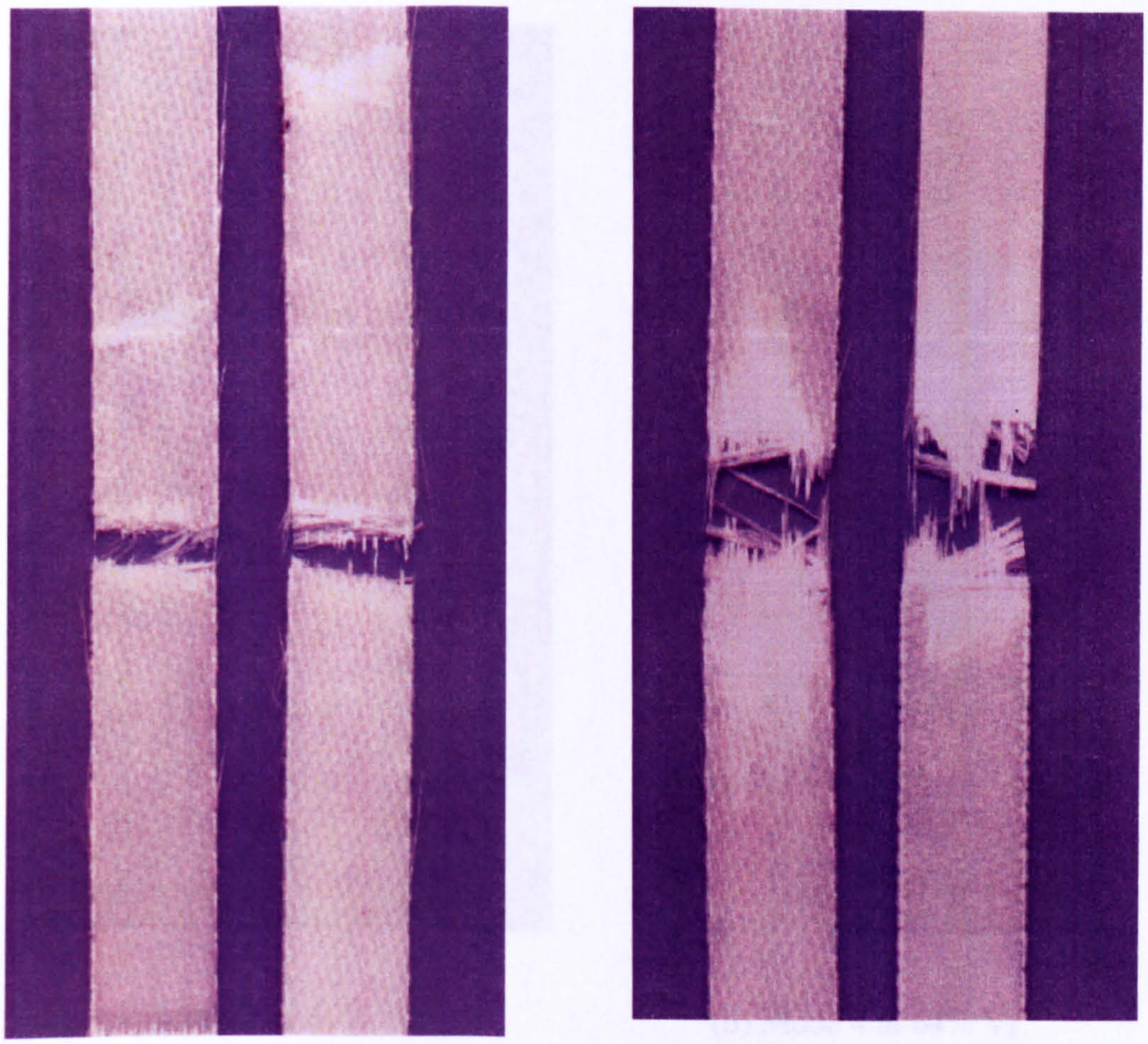

(a) Mode1 at 38% V_f (b) Mode 2 at 48% V_f

Figure (5 – 29) Tensile specimens after test of non-hybrid glass woven fabric reinforced epoxy resin composites; (a) Tensile failure mode1 at 38% V_f, (b) Tensile failure mode 2 at 48% V_f.

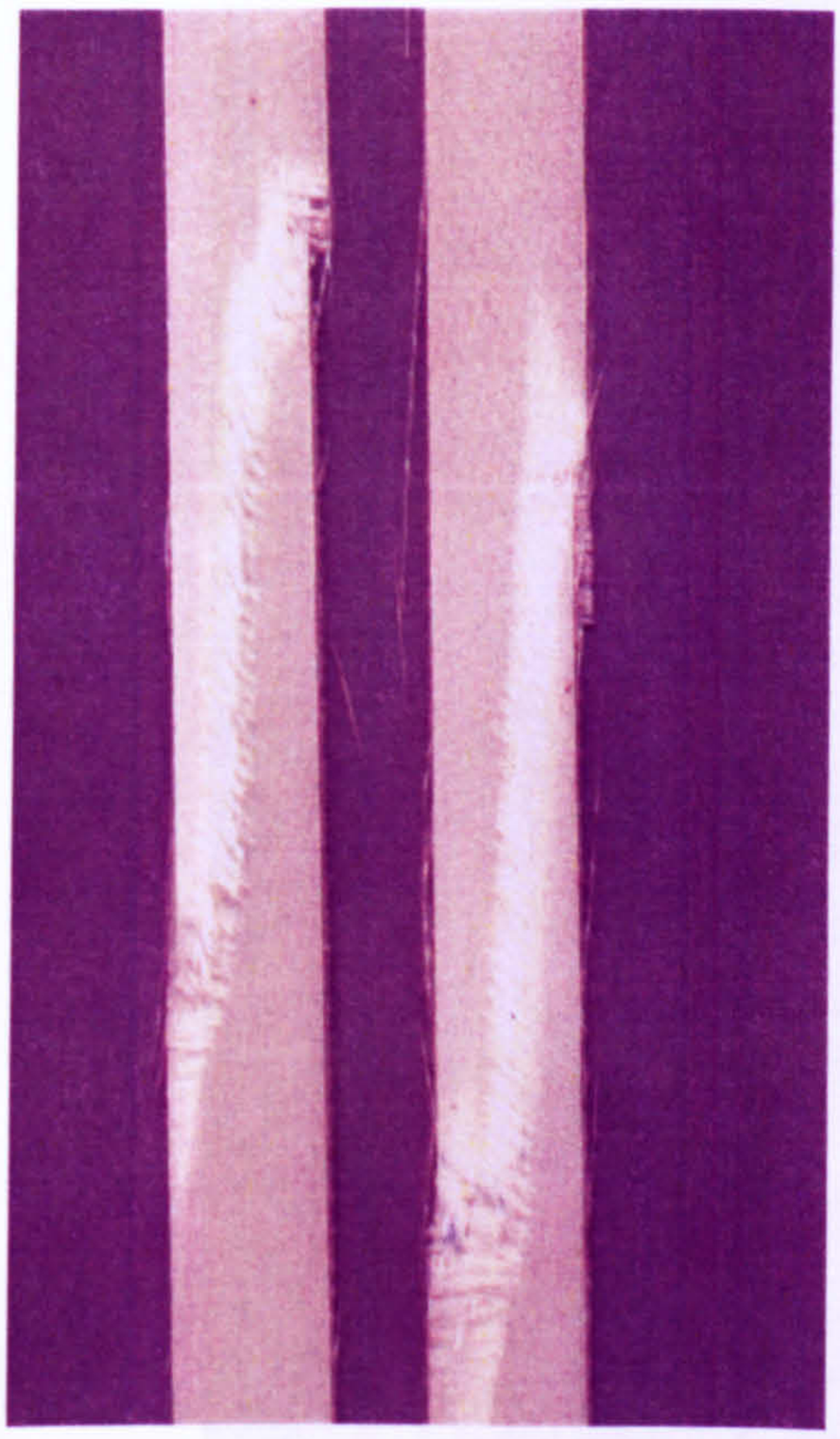

(a) Mode 3 at 56% V_f

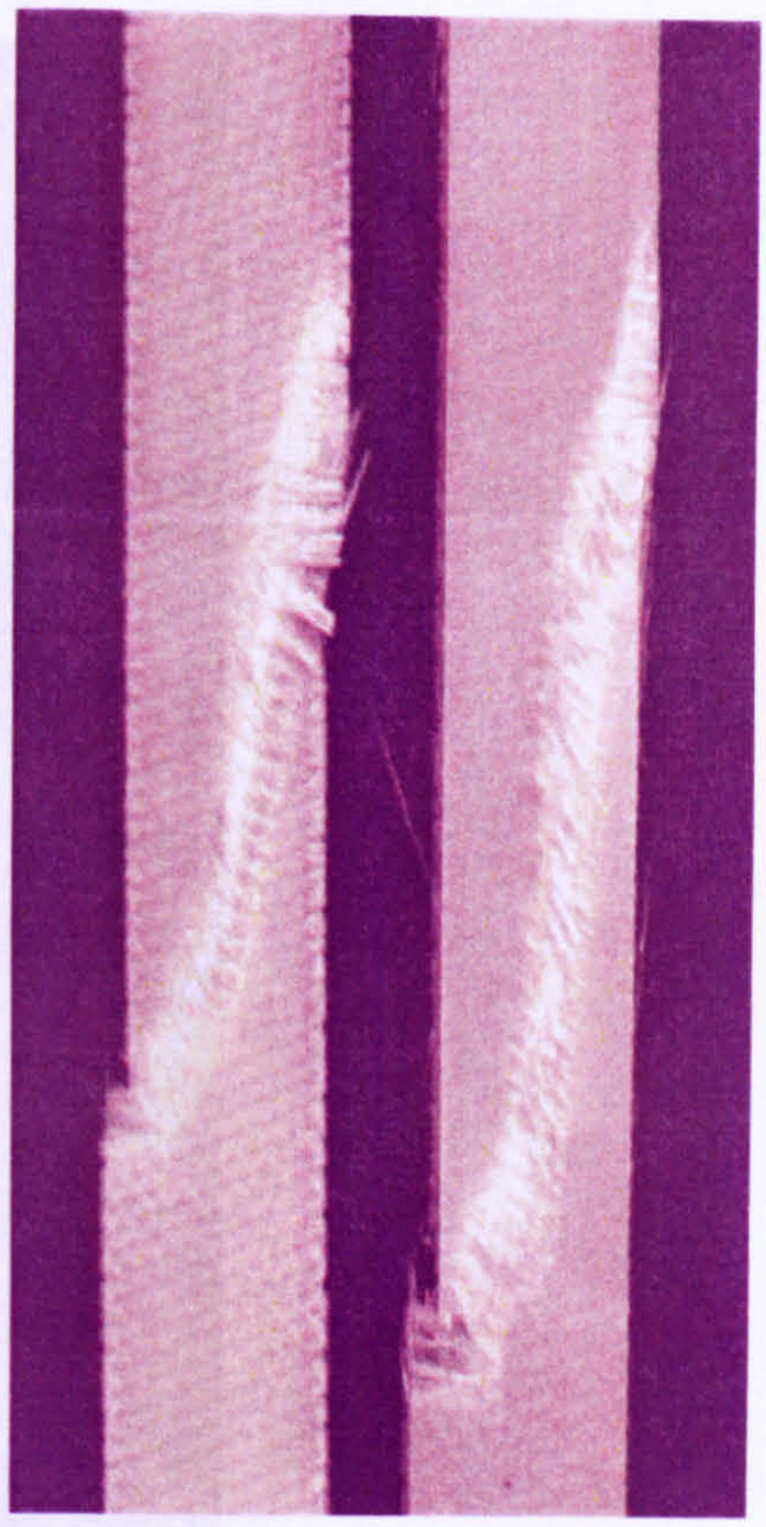

(b) Mode 4 at 64% V_f

Figure (5 – 30) The tensile specimens after test of the non-hybrid glass woven fabric reinforced epoxy resin composites, (a) Tensile failure mode 3 at 56% V_f, (b) Tensile failure mode 4 at 64% V_f.

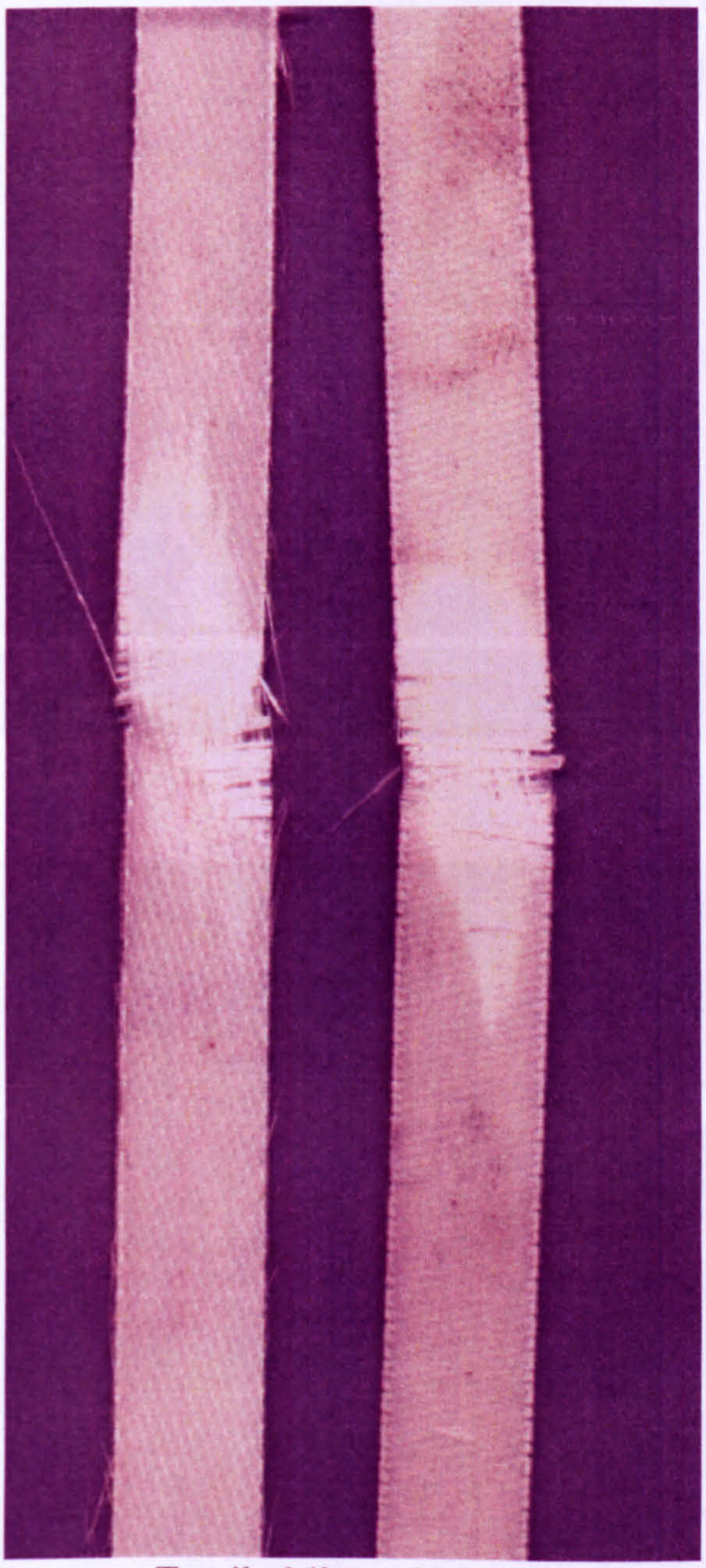

Tensile failure of **hybrid**

Figure (5 – 31) The fracture surface of the tensile specimen of the hybrid glass woven fabric reinforced epoxy resin composites at 48% V_f (**weft direction**).

(a)

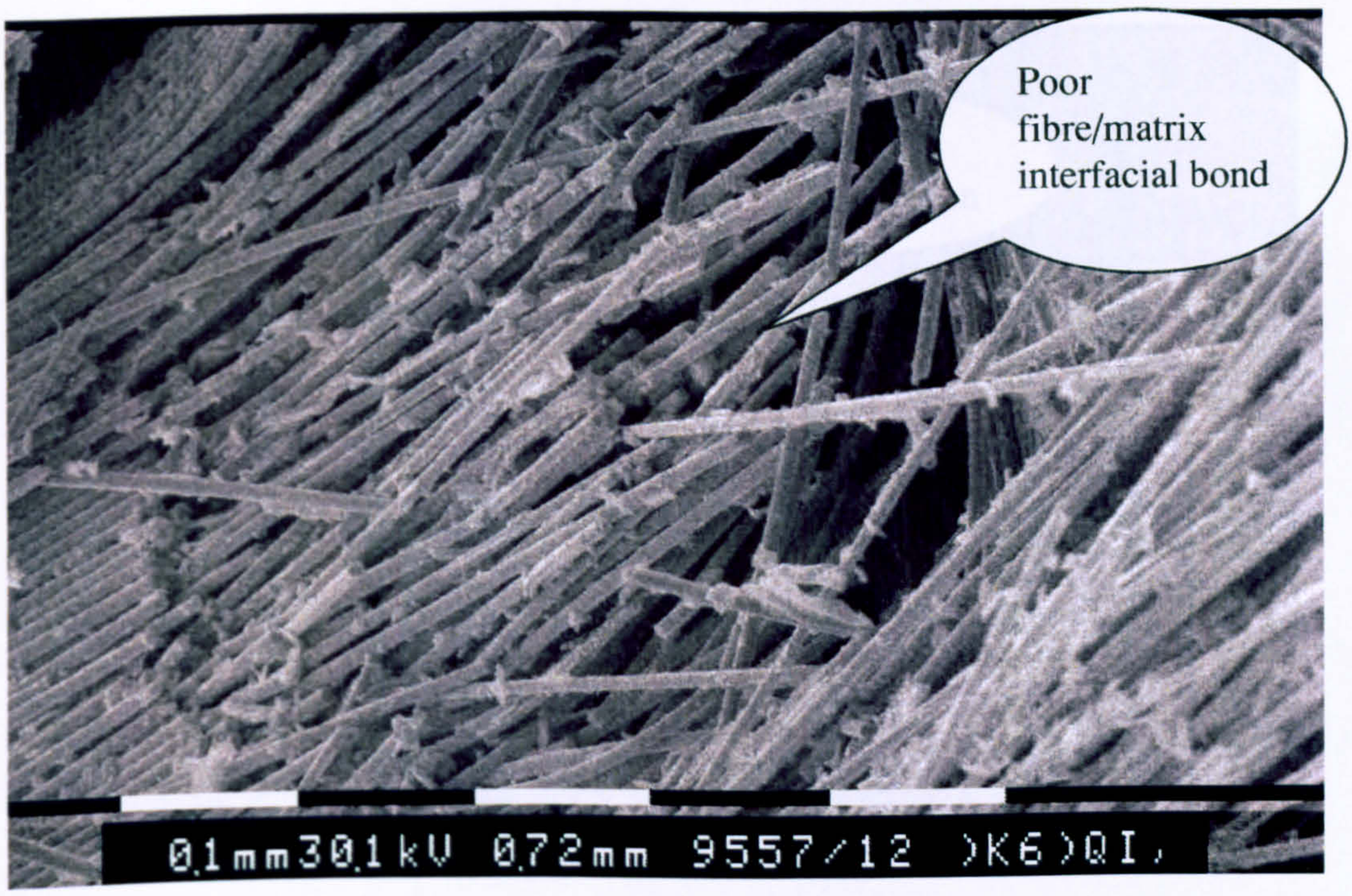

(b)

Figure (5 – 32) SEM Micrograph of the fracture surface of the **non-hybrid** glass woven composite at **38%** V_f shows:
a- (105x) brittle fibres mostly ruptured rather than pull-out
b- (210x) poor fibre/matrix interfacial bond and weave repeat unit deformation.

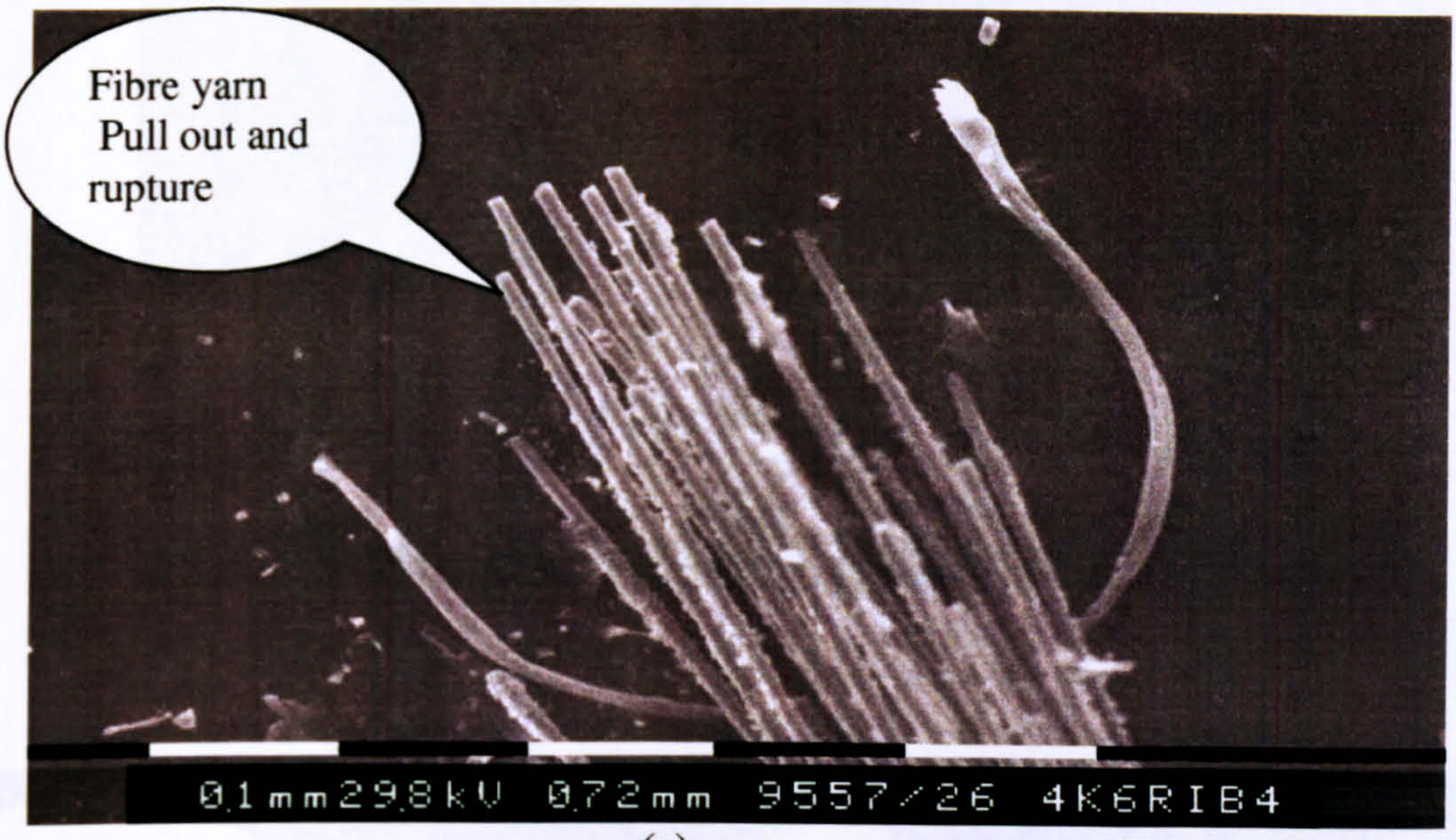

(a)

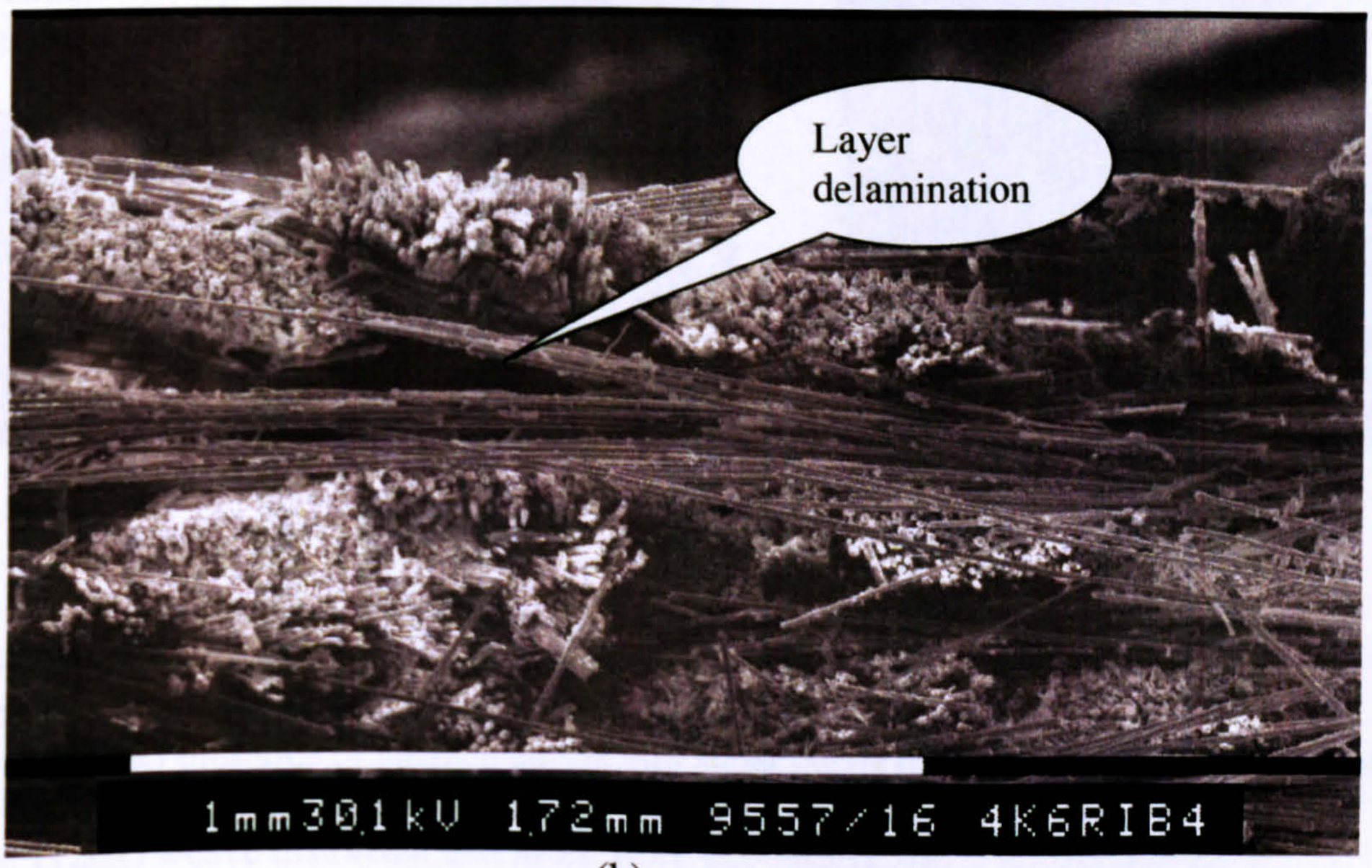

(b)

Figure (5 – 33) SEM Micrograph of the tensile fracture surface of the **Non-hybrid** glass woven composite at **48%** fibre volume fraction shows

a- (220x) brittle fibres mostly pull-out rather than rupture under the effect of undulations created by weaving.

b- (90x) layer delamination.

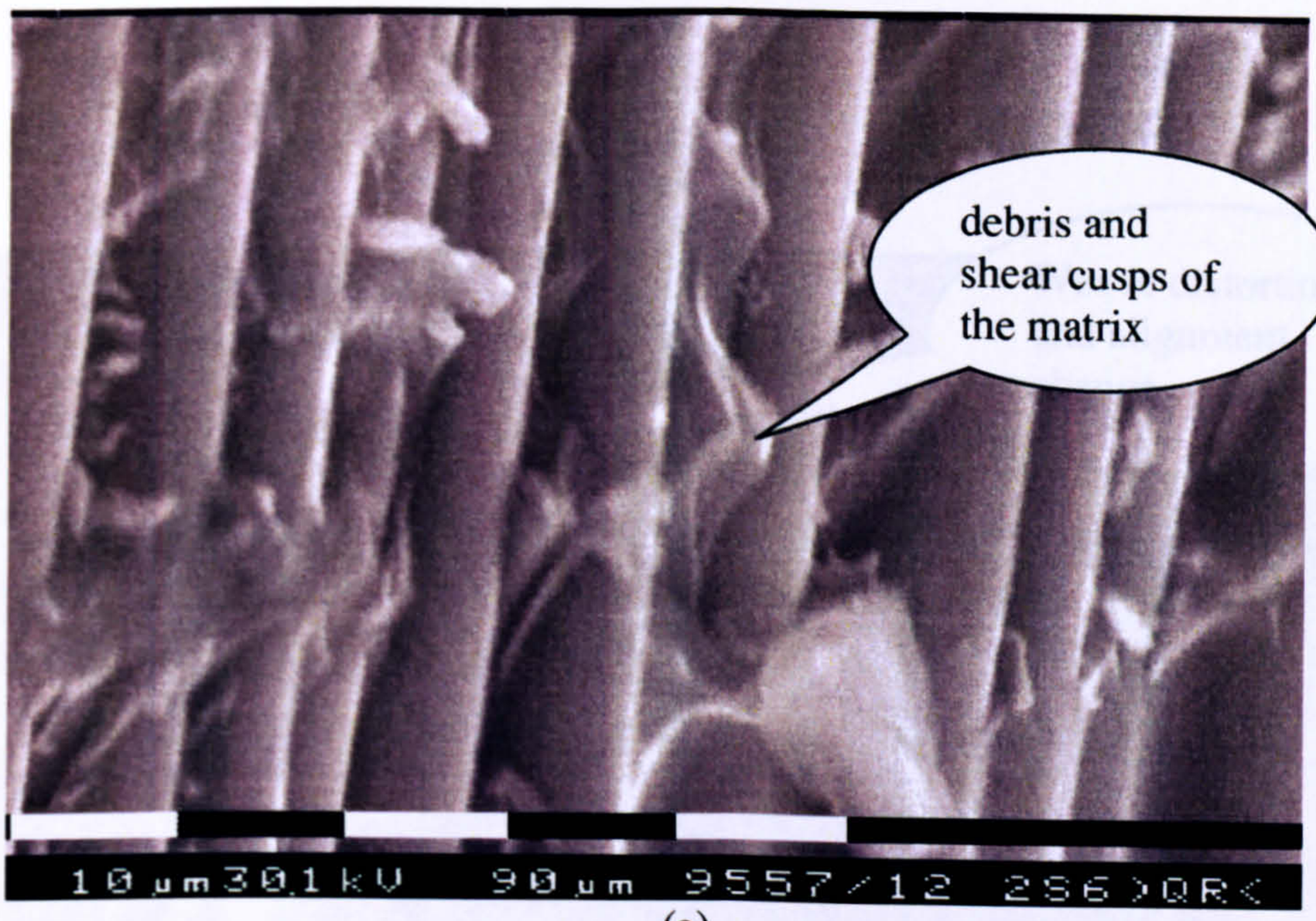

(a)

(b)

(c)

Figure (5-34) SEM Micrograph of tensile fracture surface of **non-hybrid** glass woven composite at 56% fibre volume fraction shows

a- (1000x) presence of surface debris and shear cusps of the matrix on the fibres exhibits good interfacial bond.

b- (120x) weave distortion and multi fibre debonding and layer delamination

c- (200x) fibre rupture at undulation curvature in the higher modification of b.

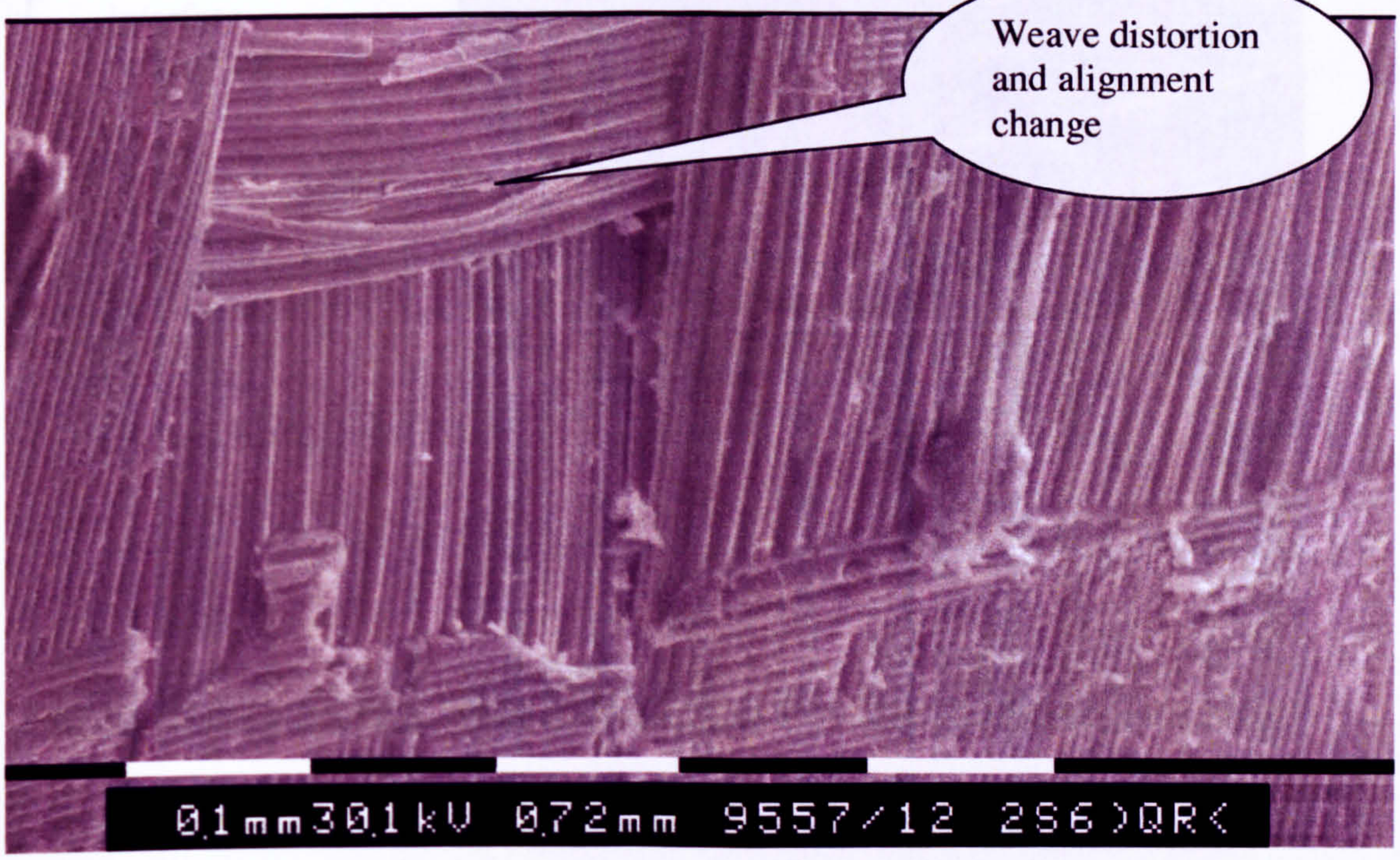

(a)

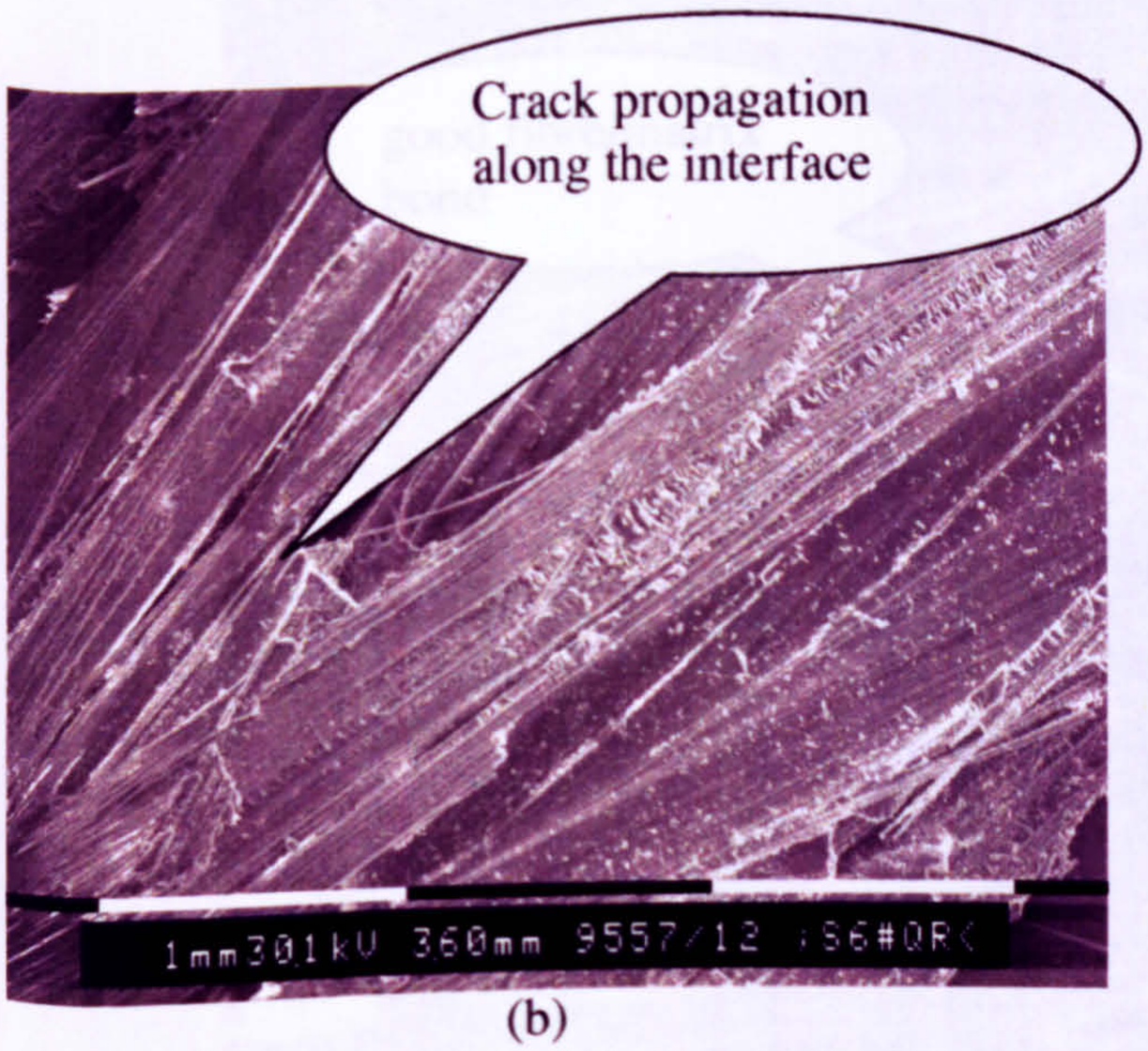

(b)

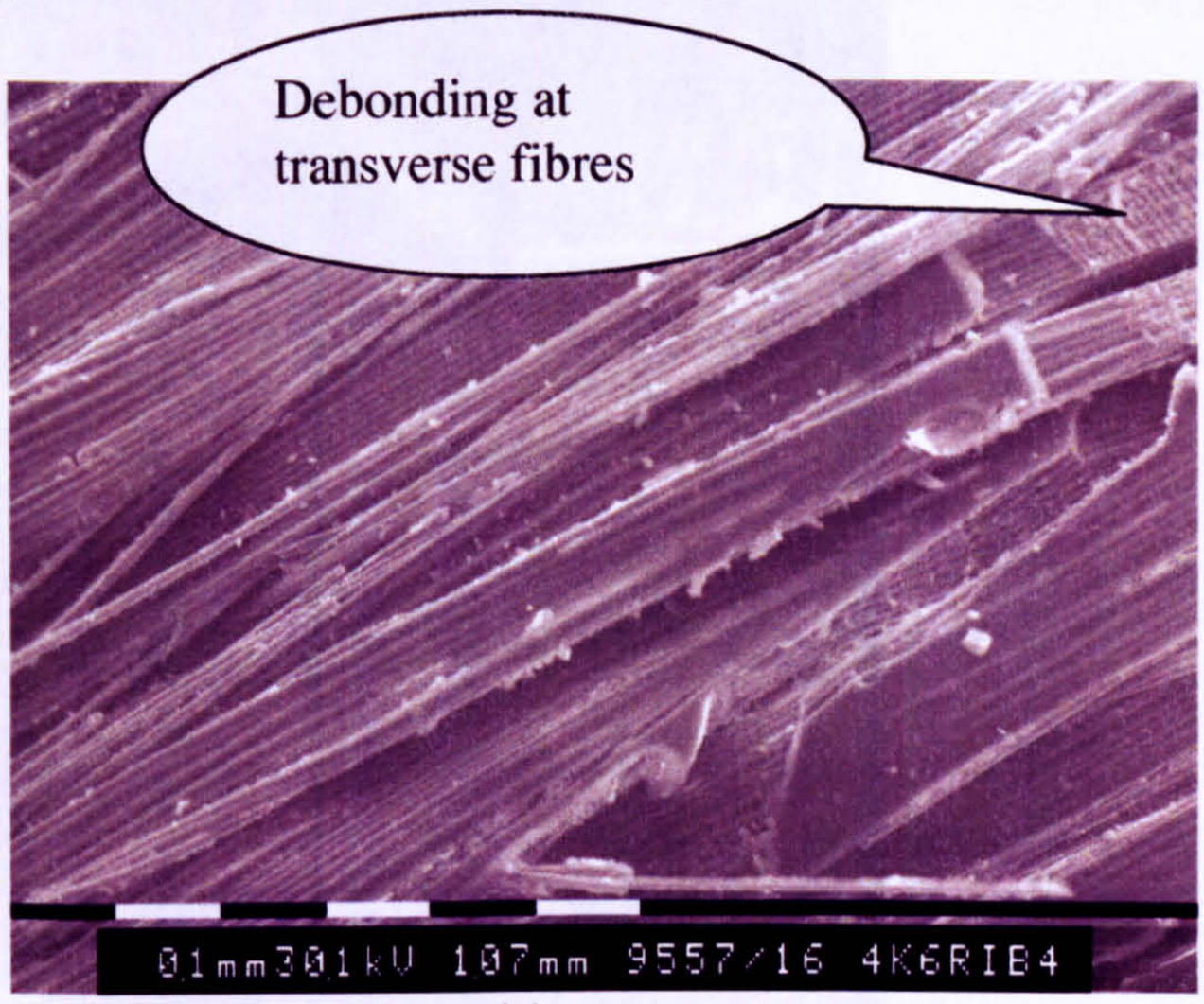

(c)

Figure (5 – 35) SEM Micrograph of the non-hybrid glass woven fabric composite at 64% V_f shows

(a) (210x) change in the specimen alignment as result of multiple matrix cracking.
(b) (270x) Crack propagation along the interface when it meets woven fibres, the crack path passes round the packet of woven fibres.
(c) (400x) Debonding of fibres bundles under effect of undulations created by weaving.

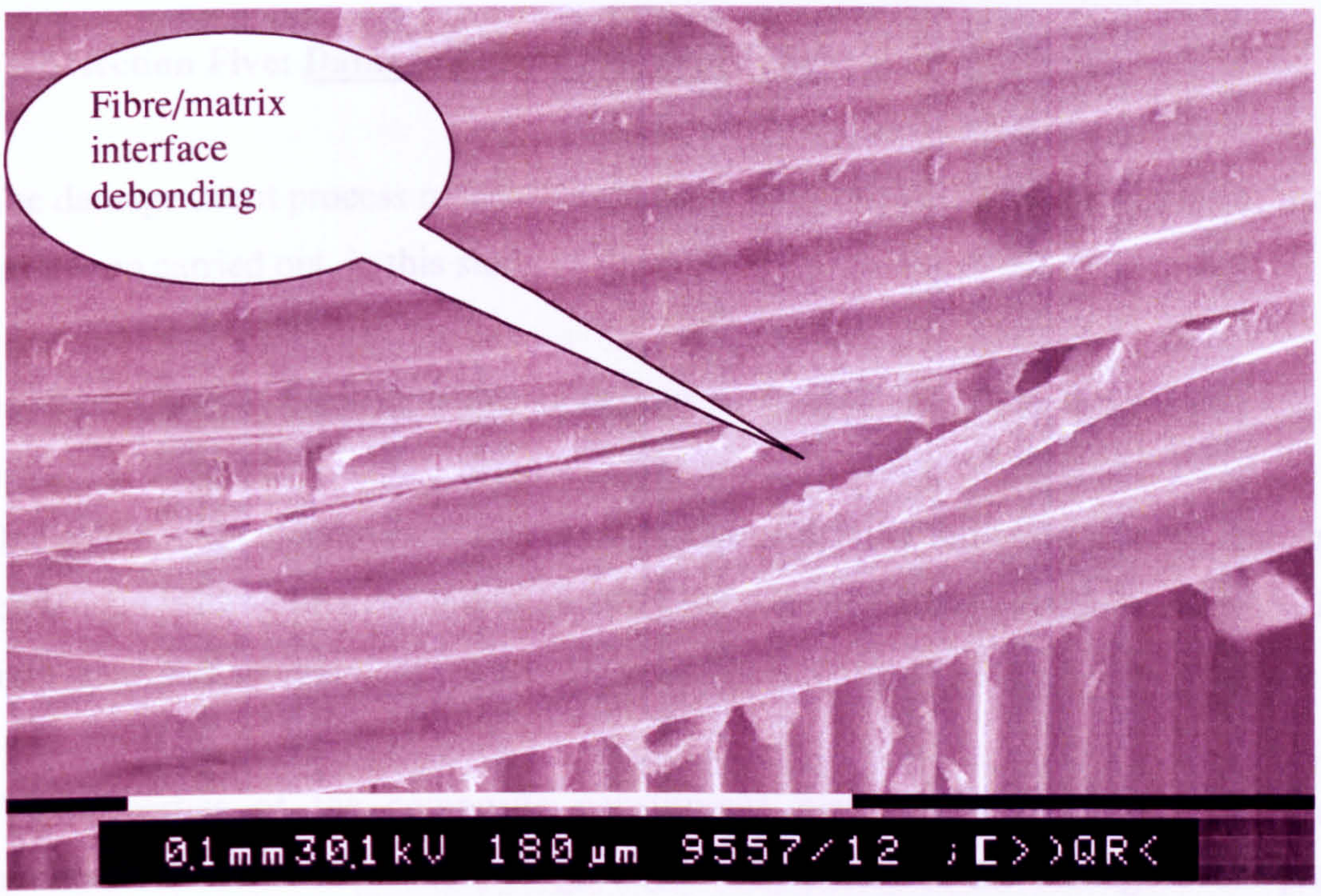

(a)

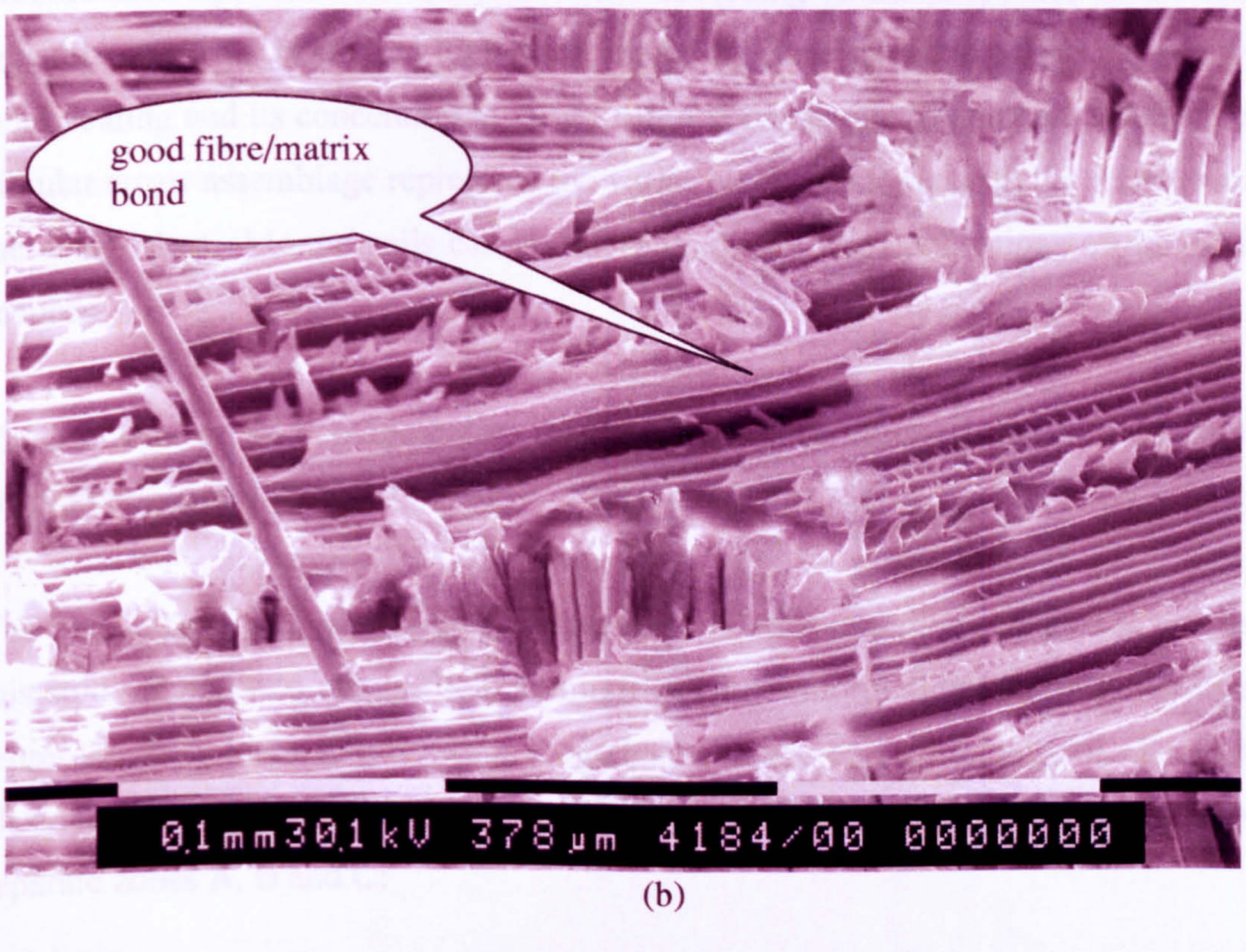

(b)

Figure (5 – 36) SEM Micrograph of the fracture surface of the **hybrid** glass woven fabric composite at 48% V_f shows

a- (810x) fibre/matrix interface debonding initiation,

b- (400x) presence of surface debris and shear cusps of the matrix on the fibre surface, indicating good fibre/matrix bond.

5 – 5 Section Five: Damage Events Process Model

The damage event process model section deals with two different categories of modelling, which have been carried out, in this study:

5 – 5 – 1 Damage event sequence modelling

One of the main objectives of this study is to identify the initiation of each damage event during the tensile loading process and to quantify the type of damage event in order to classify it in the right stage and category.

The properties of the composite constituents play an important role in quantitative and qualitative event classification. Figure (5 – 37) describes the damage event process for glass woven composites during the tensile loading. The closed circular arrow represents damage process data input into the analysis model according to the properties of the tensile specimen constituents. The constituent properties, including fibre properties, fibre volume fraction and the fibre coating and its concentration vary from one composite to another. Hence the design of the circular arrow assemblage represents the variation of data input with the constituent properties of the composites. More details can be interpreted from the applications of the model in the next section.

The sequence of the damage events for the woven glass composite system during the tensile test is summarised as follows:

The zone classification technique of stress-strain corresponding AE curves has been utilised in this study in order to obtain the maximum possible information from a group of samples. The representative plots of stress-strain, together with the corresponding AE curves for the woven glass composite, are shown in figure (5 – 28). It is possible to divide the curves into three separate zones A, B and C:

Zone A, corresponds to the linear portion of the stress-strain curve. During this stage no AE signal was detected.

Zone B corresponds to the area between the first and second knee points. The damage initiation starts from the end of the first linear portion of the stress-strain curve. The first knee point coincides with the onset of the AE ring down count. The AE onset point was considered to show the beginning of the stress wave corresponding to a damage initiation such as matrix micro-crack. There is then a gradual process of matrix failure and fibre/matrix interfacial damage, which eventually occurs over a long period of time. The entire woven composite specimen tested in this study undergoes this process at 50% of ultimate tensile stress. The maximum recorded ring down count (RDC) in zone B was 0.25×10^6. The progress of matrix-micro crack leads to matrix fracture, which results in premature fibre/matrix debonding as the stress continues to drop. The SEM micrograph, in figure (5 – 36a), shows a case of such debonding.

The sequence of the damage events within **zone B** of the stress-strain plot in figure (5 – 28) can be identified by the following:

1. matrix micro crack
2. fibre/matrix debonding
3. matrix fracture

The deformation in **zone C** can be divided into two different levels:

The first level is the prelude to ultimate fracture. The process to ultimate fracture is a continuation of damage events represented by the second knee point of the stress-strain curve. The second knee point reveals that the damage progresses from matrix failure to different fracture mechanisms, such as higher levels of interfacial fracture, which are associated with higher stress levels. This is a gradual process of failure, which eventually occurs over a short period of time when woven composite specimens undergo about 75 % of the ultimate tensile stress. The fibre/matrix debonding roughly coincides with the end of zone B and beginning of zone C. Crossing the second knee point during continued stress on the specimen, leads to complex failure, such as weave repeat unit distortion (see figure 5 – 33b) and damage in the yarn form (see figure 5 – 34a).

The weave repeat unit refers to the pattern of the woven fabric. The woven fabric used in this investigation was 8-harness satin weave. The yarn form deformation refers to the damage in the yarn form construction. The destruction of weave unit promotes the initiation of fabric deformation. The SEM micrograph, in figure (5 – 35c), shows the effect of weave undulation on the fracture surface. The weave repeat unit's distortion could lead to transverse yarn debonding

and layer delamination as detected by SEM micrograph and visual specimen examination, as shown in figures (5 – 33b) and (5 – 30). The yarn debonding in transverse direction and layer delamination refers to a higher level of fabric deformation.

The AE activities recorded a variation in the magnitude of the AE ring down count corresponding to the second knee point for each individual composite. The second knee point values, and the corresponding RDC values, reveal that there is a variation in the damage mechanisms generated as a function of the variation in the constituent properties of the composites. The variation in the constituent properties of the composites generates a variation in the interphase properties. This is responsible for the variation in the values of knee points and the corresponding AE values.

The second level deals with initiation of ultimate fracture. These failures are associated with fabric deformation, such as transverse yarn debonding and layer delamination. The evidence from the SEM micrograph, in figures (5 – 35b and 5 – 34b) and visual specimen examination in figure (5 – 30), detected such failure. This type of failure occurs in the second part of zone C as a consequence of previous damage. This type of failure was associated with a high level of tensile stress and a higher level of AE records and activities. This damage process of woven fabric failure ultimately occurs over a relatively short period of time and the woven composite specimen undergoes this at 90% – 95% of ultimate tensile strength and the record of RDC, in figure (5 – 28 – zone C), is expected to be over 0.7×10^6.

The damage events process within **zone C** of the stress-strain plot in figure (5 – 28) can be identified by the following:

1. interfacial fractures
2. weave repeat unit destruction
3. yarn form deformation
4. yarn debonding in the transverse direction
5. layer delamination

The ultimate fracture, which occurs in the end of zone C, can be divided into two modes:

1. Specimen splits into two pieces and fibre fracture occurs.
2. Specimen alignment distortion.

In the first case, where the specimen splits into two pieces, complete fibre rupture occurs and no existence of the bridging in such composites is indicated (see figure 5 – 29). In the second case, the change in the specimen alignment (or specimen alignment distortion) occurs when the specimen does not split into two pieces and thus represents a case of bridging in the composites as indicated in figures (5 – 30 and 5 – 31). This will be discussed later in more detail in the bridging validation section, which will help to clarify the model by using two applications.

A **quantitative and qualitative** relationship is established in this model so as to obtain further details of the damage event identification as presented in figure (5 – 38). The **quantitative** values of viscoelastic properties, for example, such as storage modulus, loss modulus, the glass transition temperature (T_g) and (tan δ) have been calculated using DMTA. In addition the quantitative values of ILSS and flexural tests were used. The **qualitative** views of the fracture surfaces are represented by SEM and visual specimen examination (VSE). The AE profile represents the **life history of the damage process** during the testing. The model correlates the AE profile with quantitative values and qualitative views in order to identify the damage event and the level of failure. The relationship between quantitative values and qualitative images of damage accumulation in woven composites assembled in this model is shown in figure (5 – 38).

The significance of this relationship highlights the necessity of using, simultaneously, different tools in the damage event sequence analysis as mentioned earlier. The applications of the quantitative and qualitative relationship have been presented in the next section of bridging criteria validation.

5 – 5 – 2 The Bridging Validation Modelling, The objectives of bridging validation is to identify the damage event process in order to classify the bridging support that can prevent the catastrophic failure by splitting the specimen into two pieces. This bridging phenomenon has been presented mathematically by Ishikawa and Chou (Chou 1992) and was discussed in chapter two.

Application (1) the objective of this application is to study the effect of the fibre volume fraction in the composite on bridging validation. In other words, it aims to identify the damage event sequence of the low and high fibre volume fraction in woven glass composites to facilitate the implementation of bridging support.

Young's moduli increase with the increase in the number of cell unit repeats due to increases in the straight portion and cross-ply region of the weave (Naik 1994). The increase in the fibre volume fraction leads to an increase in the number of cell unit repeats of woven fabric. **This fact could establish a relationship between the Young's moduli and the number of the cell unit repeats in the woven composite.**

The results of the tensile test of non-hybrid glass woven fabric reinforced epoxy resin composites, using four different glass fibre volume fractions, are summarised in table (5 – 12) and are graphically presented in figure (5 – 23). The highest magnitude of Young's modulus and ultimate tensile strength (UTS) was associated with the highest level of fibre volume fraction at 64% V_f in non-hybrid woven composite. The lowest values of Young's modulus and UTS were associated with the lowest level V_f in the non-hybrid composite at 38% V_f.

The variation in the Young's modulus and UTS were interrelated with the variation in fracture mechanisms generated due to the variation in the fibre volume fraction. **Therefore a relationship could be established between the variation of damage sequence mechanisms and the number of cell unit repeats in the composite.**

The **visual examination** of a tensile specimen of a low V_f composite (figures 5 – 29a,b) reveals that the specimen failed due to the fibre fracture, indicating that **no bridging** was involved. The shape of the tensile mode failure, which split into two pieces, showed signs of complete longitudinal fibre rupture and complete matrix fracture. Furthermore, the evidence from the SEM micrograph in figure (5 – 32) indicates brittle fibres and that most ruptured rather than being pulled out and poor fibre/matrix interfacial bond. The ILSS of the 38% V_f composite was (approximately 18.1 MPa) and flexural strength was (approximately 279.4 MPa). This represents a case of low V_f composite, whilst the ILSS of the 64% V_f composite was approximately 29.13 MPa and flexural strength was approximately 488.5 MPa. Therefore, the ILSS of the low V_f composite sustained higher shearing failure and a transfer of high stress concentration across the interface compared with those of high V_f composite. The initial damage sequence of the low V_f composite seems to engross fracture of individual fibres at weak points. As each fibre breaks, redistribution of stress occurs, leading to additional stresses on neighbouring fibres associated with a local stress magnification effect. Thus, there is an increased probability that the fracture will occur in the closely adjacent fibres.

The highest V_f composite possesses the highest ILSS value and indicates good fibre/matrix adhesion. The result denotes that the increase in flexural strength and modulus and interlaminar shear strength is due to the increase of fibre volume fraction in the composites. The ILSS and flexural properties have been discussed earlier in this chapter.

The **visual examination** of the tensile specimen of a high V_f composite in figure (5 – 30) displays the appearance of good bridging. The figure exhibited debonding under the effect of undulation created by weaving, as well as layer delamination on the fracture surface leading to a change in the alignment of the specimen. Furthermore, the evidence from the SEM micrograph in figures (5 – 34 and 5 – 35) display debonding, as well as layer delamination at the fracture surface. The tensile specimen therefore remains integral whilst including a change in the alignment of the specimen of approximately $30^{\circ} - 45^{\circ}$. The length of fracture (white area) on the specimen was between 40-70 cm. It should be pointed out that the composite of 38% V_f was laminated with only 4 layers and that the composite of 49% V_f was laminated with 7 layers. The visual examination of a tensile specimen of the high V_f composites in figure (5 – 30) shows that delamination was found to affect only the outer layers of the laminate. The fracture surface of the low V_f composite in figure (5 – 29a) exhibited complete layer delamination and gives the impression that the delamination occurs in the early stage of the second knee point.

Thus, a relationship between the fracture surface performance and the number of cell unit repeats is obvious. An increase in the number of cell unit repeats could prevent catastrophic failure by splitting the specimen into two pieces.

Application (2) the objective of this application is to study the effect of fibre hybridisation in the composite on bridging validation, in other words, to identify the damage event sequence of the hybrid and non-hybrid woven glass composites that facilitate bridging support.

The bridging considered by Chou, as a basic difference between hybrid and non-hybrid composites is the material variation over the cell unit repeat in the composite. Moreover the distribution of stress and strain over the laminate mid-plane varies with location in the hybrid fabric composite (Chou 1992). **This fact could establish a relationship between the stress and strain distribution over the laminate mid-plane and material location over the cell unit repeat.**

The results of the tensile tests on hybrid and non-hybrid glass woven reinforced epoxy resin composites at 48% fibre volume fractions (in table 5 – 14) are graphically presented in figure (5 – 25). The variation in the E-Modulus of the non-hybrid and the hybrid composites shows the hybrid is stiffer and greater in strength than the non-hybrid composite. The result shows the UTS of hybrid composites is superior to non-hybrid composites (weft direction) by approximately 21%. The stress values of the non-hybrid are 345 MPa and for the hybrid composite 419 MPa at the second knee point. The variation in the stress values at the second knee point is believed to be due to the variation in the interphase properties of the composites as a function of the variation in fibre hybridisation. This clearly produces a modification in the damage sequence mechanisms.

Therefore a relationship could be established between the variation of damage sequence mechanisms and material location over the cell unit repeat. The difference between the hybrid and non-hybrid composites from the material point of view is that the hybrid composite is composed of R-glass and E-glass whereas the non-hybrid composite contains E-glass only.

The **ILSS** of the non-hybrid composite was 23.3 MPa and flexural strength 361.50 MPa, whilst the ILSS of the hybrid composite was 26.5 MPa and flexural strength 430.67 MPa. The result, which is statistically significant, as obtained by the t-test, for flexural strength denotes that the increase in flexural strength and modulus and interlaminar shear strength is due to the fibre hybridisation in the composites. The ILSS of the non-hybrid composite appears to promote higher shearing failure in the matrix region and the transfer of high shear load across the composite compared with the hybrid composite. As each fibre breaks, redistribution of stress occurs, leading to additional stresses on neighbouring fibres associated with a local stress magnification effect. Thus, there is an increased probability that the fracture will occur in the closely adjacent fibres. The value of hybrid composite ILSS is higher in value and is characterised by good fibre/matrix adhesion. The **flexural** test is thus shown to be able to differentiate between the properties of hybrid and non-hybrid composites.

The **visual examination** of the hybrid tensile specimen in figure (5 – 31) exhibited good bridging and the SEM micrograph in figure (5 – 36) shows the presence of surface debris and shear cusps of the matrix on the fibre surface, indicating a good fibre/matrix bond. The visual examination of the non-hybrid tensile specimen in figure (5 – 29a) exhibited fibre fracture indicating that no bridging was involved. The appearance of the tensile mode failure in the non-

hybrid composite, which split into two pieces, showed complete longitudinal fibre rupture and complete matrix fracture. Furthermore the evidence from the SEM micrograph in figure (5 – 33), indicates (a) that fibre bundles fractured, and that most were pulled out rather than ruptured under the effect of undulations created by weaving and (b) layer delamination.

The relationship between the fracture surface performance and material location over the cell unit repeat is obvious. The fibre hybridisation over the cell unit repeat of the woven fabric could prevent catastrophic failure by splitting the specimen into two pieces.

The above two applications highlight the relationships between the number of cell unit repeats of the woven fabric and the material properties over the cell unit repeat and fracture surface performance of the tensile specimen. These relationships could validate the principle of the bridging model, such that, the elastic properties of a woven fabric layer are functions of the fabric structure and material system used in the woven composites according to (Ishikawa et al. 1985) and (Naik 1994).

Moreover, the **AE** activities also recorded a variation in the magnitude of the AE ring down count corresponding to the second knee point for each individual composite. The quantification of AE values is summarised in table (5 – 13). The higher the fibre volume fraction in the composite, the lower the AE activity recorded. The higher the AE activity the greater the damage. This is due to the layer delamination at the second knee point. This occurs in the 38% V_f composite, whilst the composite of 64% V_f prevents similar delamination. The knee point's values and its corresponding RDC values reveal the different fracture mechanisms generated due to the variation in the interphase properties of composites as a function of the variation in the fibre volume fraction. The lower the fibre volume fraction in the composite the higher the AE activity recorded at ultimate tensile fracture, possibly due to fibre rupture.

The **AE** activities also show that non-hybrid glass fibre woven in the composite leads to growth in the magnitude values of ring down counts compared to the hybrid composites during tensile tests. The **AE** ring down counts of hybrid and non-hybrid composite (weft direction) values is summarised in table (5 – 15). The AE activities also recorded a variation in the magnitude of the ring down count corresponding to the second knee point for both hybrid and non-hybrid composites. The higher AE activity, the greater the damage, which is caused mainly by layer delamination towards the second knee point in the non-hybrid composite. The hybrid composite

exhibits less delamination. The variation in **AE** ring down count values at ultimate tensile fracture illustrates accumulated damage events and were higher in the case of non-hybrid compared with hybrid composites. This is mainly due to fibre bundle pullout and fibre rupture.

Furthermore, the magnitude of **(tan δ)** for 38% V_f composite was measured to be approximately 0.110 and the value of the T_g was approximately 141 °C while the magnitude of tan (δ) for 64% V_f composite was measured to be approximately 0.037 and the value of the T_g was approximately 126 °C. This indication reveals that strong interfacial bonding is associated with high fibre V_f composite. The T_g magnitudes decreased with increasing fibre volume fraction in the composites; the highest T_g was for the 38% V_f composite. The T_g of the composite clearly influences the formation of the interphase surrounding the fibre. The magnitude of **(tan δ)** for the non-hybrid composite at 48% V_f was measured at 0.070 and the value of T_g were 130.2 °C. The magnitude of tan (δ) for the hybrid composite at 48% V_f was measured at 0.051 and the value of the T_g was 119.7 °C. This magnitude of tan (δ) indicates that strong interfacial bonding is associated with hybrid composite, as discussed in the DMTA section. The T_g can be considered to be a function of fibre surface treatment concentration, i.e. a component of R-glass in the hybrid. The T_g of the composite was influenced by the formation of an interphase around the fibre.

The flowchart in figure (5 – 39) is designed for quality control purposes to ensure a satisfactory woven glass composite. Designers must be familiar with the effect of the interphase structure of the individual composite and the DMTA data, specifically the function of tan (δ) and T_g as the critical parameters promoted by data. This allows the increase in efficiency of composite reinforcements, and eliminates any possible poorly reinforced composite. The RDC values under tensile tests are correlated with the tan delta from DMTA and the extraction of results must be performed mechanically by a classification of bridging conditions. The flowchart is made up of three essential data: the tan (δ), the RDC and the classification of the bridging condition. On one hands the tan (δ) parameter enables the depiction of acceptable fibre/matrix adhesion and on the other the AE activities determine the acceptable damage event level in the composite. The bridging condition dictates the performance of any possible fracture in the woven glass composite. Quality control can be used together with figure (5 – 39) to ensure that the research objective i.e. a satisfactory fabric weave architecture and hybridisation effect can be considered more simply.

Summary of the section

Two applications have been discussed to emphasise that bridging can prevent catastrophic failure by cutting the specimen into two pieces such as in cases of high V_f and hybrid composites.

The ILSS test promotes failure by shearing the laminate; the shear failure mode is dominated by interfacial failure, while the matrix plays a major role by transferring the shear load across the composite. Good fibre/matrix adhesion is essential for the composite under shear loading. The ILSS test is therefore used for assessing fibre-resin compatibility. The flexural test is used for assessing fibre volume fraction and fibre properties. This is in agreement with the literature Chamis (1974, 1987), Caldwell (1992), Drzal and Larson (1994), ASM International (1987) and Kaniej (2000).

The viscoelastic property is influenced by the effect of fibre coating distribution or the fibre coating concentration in the composite. The quantitative values of viscoelastic properties of composites such as the magnitude of tan (δ) represent the quality of the interfacial bond in the composite. The fibre surface treatment concentration can influence the T_g of the composite, which influences the formation of an interphase around the fibre.

The ILSS, viscoelastic and flexural properties of the composites could contribute to the interfacial and fibre constituents leading to improved understanding of the damage event processes under the tensile test for individual composites. This includes the evidence provided from the SEM micrographs and visual specimen examination, and the use of quantitative-qualitative relationships to identify the damage events. The damage sequence analysis, indicated in this study, has not, it would appear, been mentioned in previous research.

The construction of the damage event sequence for the glass woven composite system during the tensile test is illustrated by the circular arrow assemblage in figure (5 – 37), and considers the variation in the quantitative values and qualitative images of damage accumulation of woven composites. This model could present new methodology to identify and classify the damage event sequence as follows:

- The model employs different tools in assembly such as AE, SEM, VSE and DMTA, which is

a new technique.

- The zone classification technique of stress-strain and its relating AE curves has been utilised in this study so as to ascertain the maximum possible information from each experiment, and is considered to be a new technique in the identification of damage event sequence of woven composites.

- The relationship between quantitative values and qualitative images of damage accumulation in woven composites is also considered to be a new methodology in the identification of damage event sequence as assembled in figure (5 – 38).

- The implementation of bridging validation on the tensile specimen is considered to be a new application in the investigations of tensile properties.

- A flowchart in figure (5 – 39) is designed for quality control purposes to ensure a satisfactory woven glass composite.

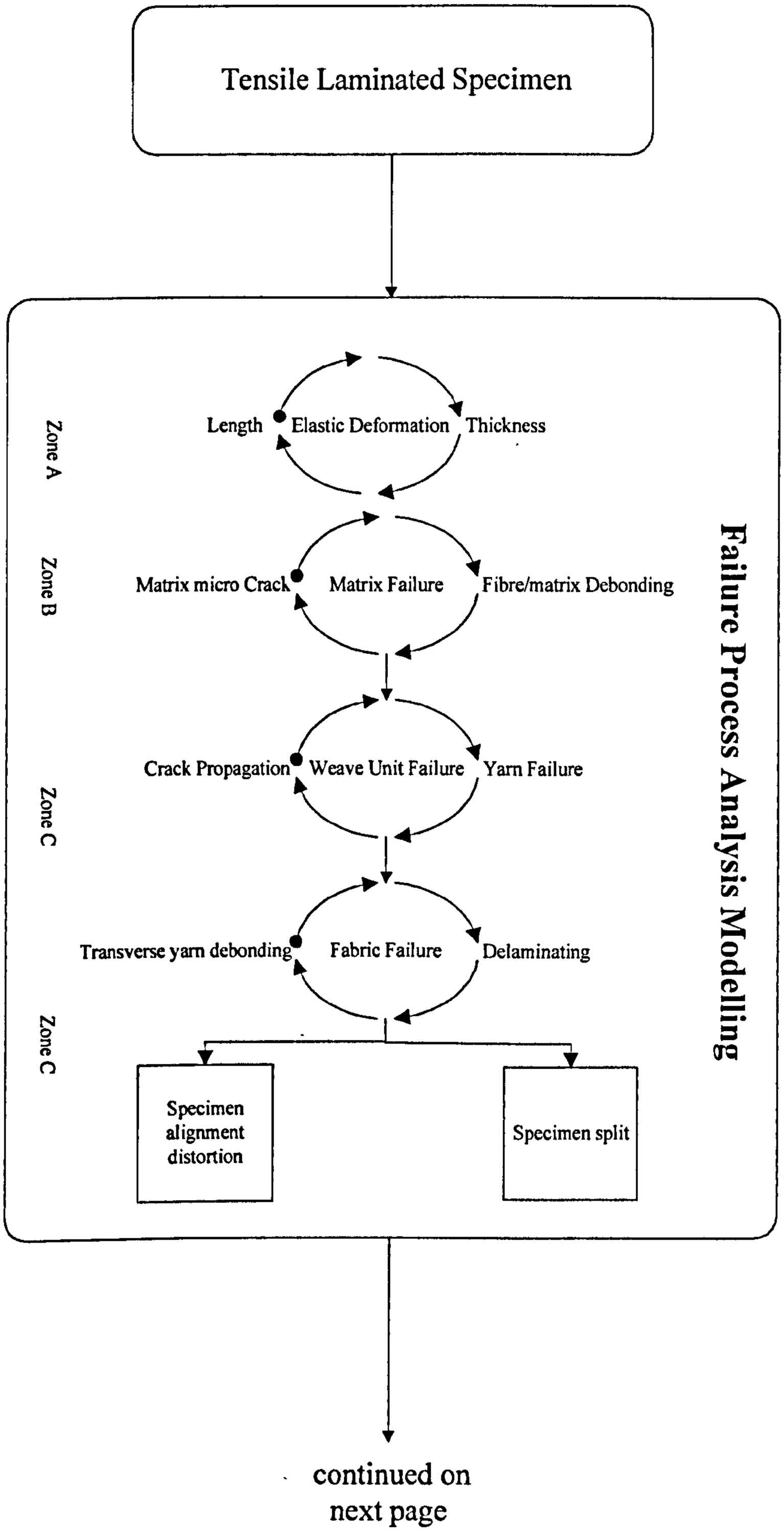
Tensile Laminated Specimen
Stage 1
Failure Process Analysis Modelling
Zone A
Length
Elastic Deformation
Thickness
Zone B
Matrix micro Crack
Matrix Failure
Fibre/matrix Debonding
Zone C
Crack Propagation
Weave Unit Failure
Yarn Failure
Transverse yarn debonding
Fabric Failure
Delaminating
Zone C
Specimen alignment distortion
Specimen split
continued on next page

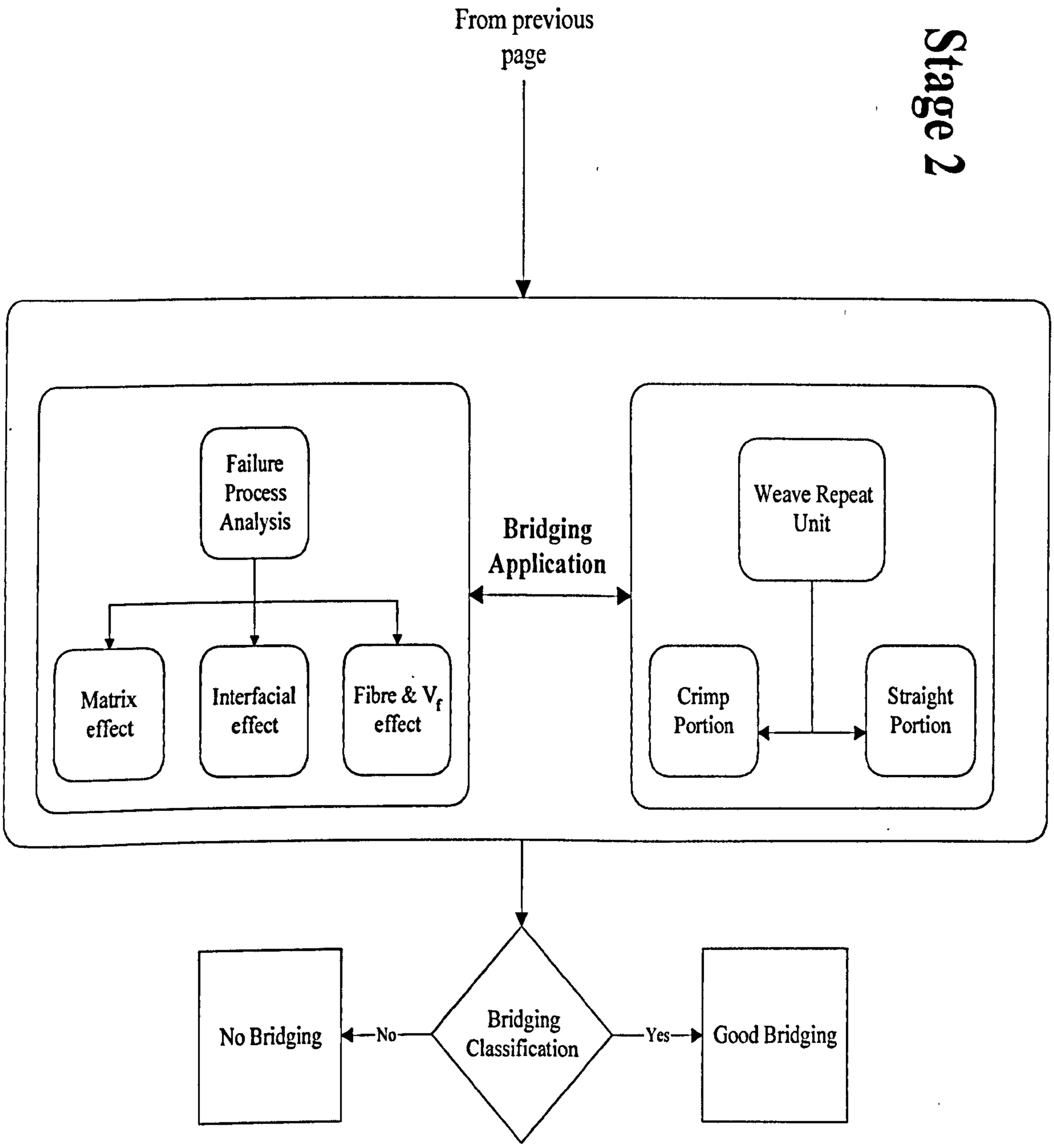

Figure (5 – 37) The damage events process modelling during tensile test of glass woven fabric composites.

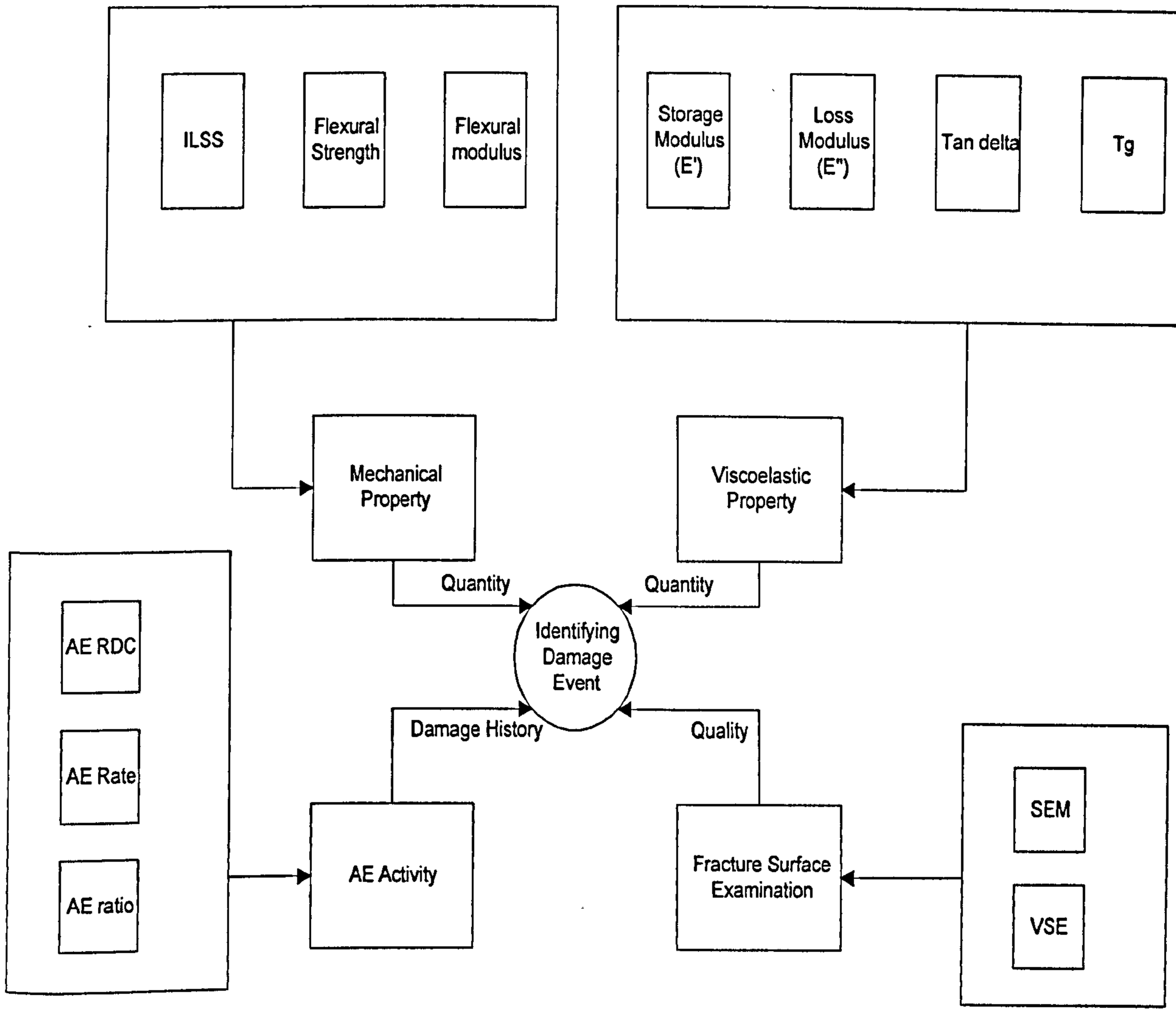

Figure (5 – 38) Damage event identification of glass woven reinforced epoxy resin composites.

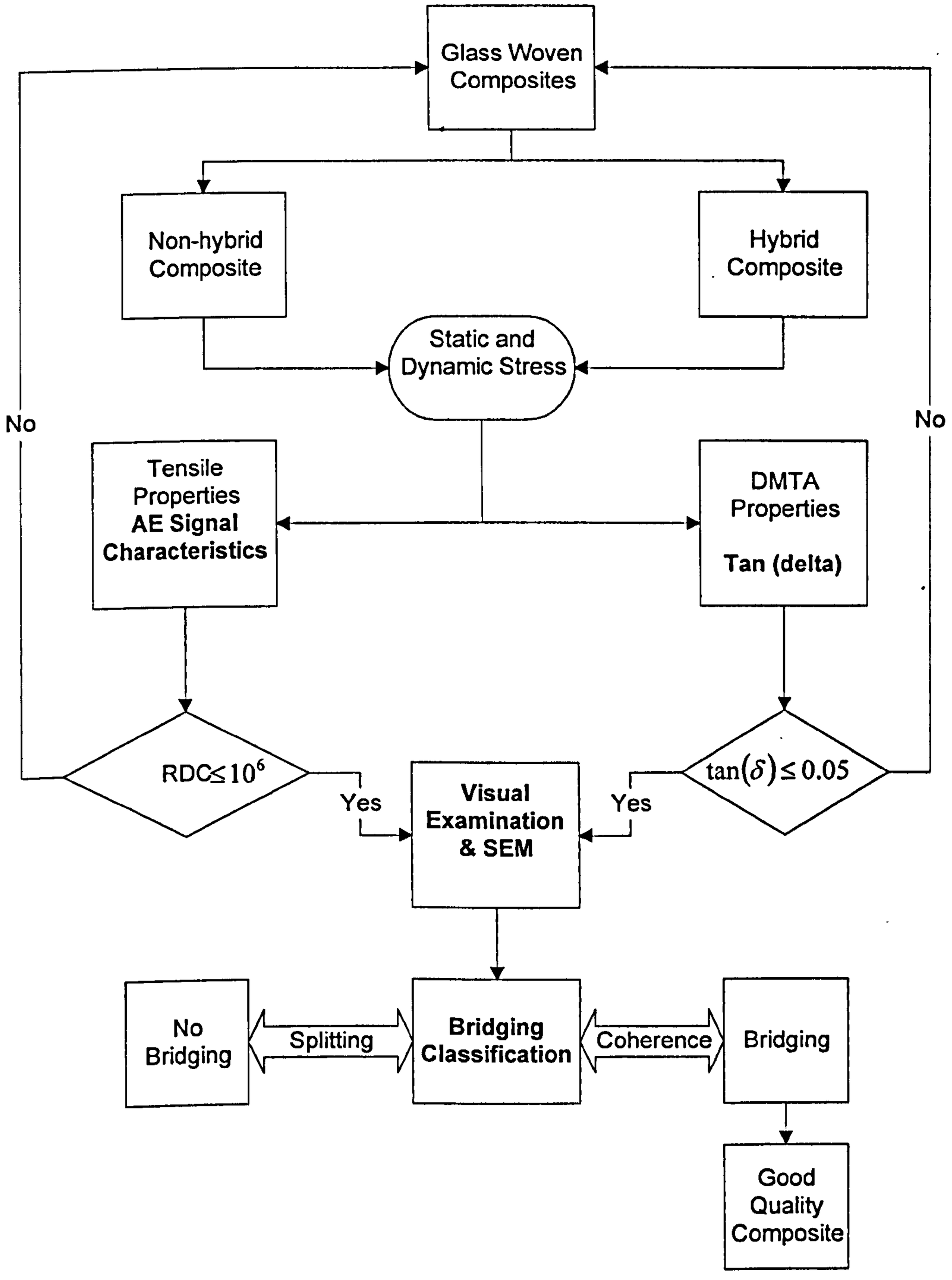

Figure (5 – 39) flow chart of reinforcement quality control in the glass woven composites.

5 – 6 Section Six: Evaluation of the Results

5 – 6 – 1 The correlation of experimental results with DMTA

The comparison of test results for flexural moduli and ILSS of non-hybrid woven composites at different fibre volume fractions with the values obtained from DMTA are laid out in table (5 – 16). The DMTA values refer to the values of storage moduli, glass transition temperature (T_g) and tan (δ). A similar comparison for identical fibre volume fraction between the hybrid and non-hybrid glass woven composites values are set out in table (5 – 17).

The relation between the glass transition temperature (T_g) and ILSS corresponding to four V_f composites is presented in figure (5 – 40). These V_f composites are selected from the experimental results. The figure shows the linear increase of ILSS among the first three V_f composites and linear decrease of the corresponding values of the T_g. The figure further shows that the T_g for the 56% V_f composite was approximately 122 °C rising to approximately 126 °C for the 64% V_f composite. This relation further indicates the limitation effect of V_f on ILSS in the composite. The limitation effect was obvious in the case of 64% V_f which was clearly excessive for the composite. Therefore, the composite of 64% V_f cannot be the optimum composite. Similar relations between the glass transition temperature (T_g) and UFS were established including the V_f limitation effect and are presented in figure (5 – 41). The V_f limitation effect has been considered whilst discussing the ILSS and flexural results.

The V_f limitation effects are mainly due to the limitation of crosslinking between the epoxy resin and glass fibre surface treatments. The glass transition temperature (T_g) as determined by DMTA reveals the role of fibre surface treatment concentration in each composite. This explains the role of fibre surface treatment on the mechanical properties of the woven composites. It is therefore considered that the fibre surface treatment concentration of the glass woven fabric composite influences the ILSS and flexural properties. The DMTA can contribute some more advantages: it is a non-destructive test, several elastic constants such as storage and loss moduli, and tan (δ) over a range of temperatures can be found in a single experiment. The DMTA test is capable of producing accurate results, and can improve the interpretation of the destructive test.

The reduction of the glass transition temperature (T_g) values as a function of fibre surface treatment concentration due to the increment of V_f in the composite leads to a good correlation with the increases of ILSS in the experimental results. The experimental results show that the ILSS (τ) increases with the increase of overall fibre volume fraction in the composites. Moreover, a similar trend for tan delta could be observed, the reduction in tan delta magnitude is associated with an improvement of interfacial bonding in the composites due to the increment of V_f in the composite, see tables (5 – 16) and (5 – 17).

The storage modulus (E`) represents the capability of load bearing for each composite, this correlates with the values of UTS of the composites. The UTS level of the hybrid composite for example was superior to the UTS of the non-hybrid composite, hence agreeing with the storage modulus (E`) values of DMTA.

The values of the storage modulus (E`) of DMTA were close to the values of the flexural modulus obtained from the flexural mechanical test, which show good correlation between the two tests.

The relation between the T_g and both ILSS and UFS reveals the V_f limitation effects on the mechanical properties of the composites and this relation should be considered in the application of the rule of mixtures. The rule of mixture application on the tensile modulus and UTS does not show the V_f limitation effects, for example. The results of the tensile modulus and UTS are examined by the rule of mixtures as presented in figure (5 – 42); the figure exhibits a linear dependence on the fibre volume fraction composites. This implies that the rule of mixture is applied to these cases. When the fibres in woven fabric composites are identical, continuous, aligned and uniformly spaced, the rule of mixture then provides the tool for predicting the axial tensile and flexural strength as a function of fibre and matrix strengths, and the constituent volume fractions. This corresponds to the literature (Herakovich 1998).

5 – 6 – 2 Classification of the results between significant and non-significant

The results of ILSS, tensile and flexural properties have been tested by the t-test of probability (see the details of t-test method in appendix C). The values of tensile and flexural strength of the hybrid and non-hybrid composites for similar V_f exhibit significant variation in properties see table (5 – 18). The ILSS indicates insignificant variation for similar V_f in the composite and

similar specimen dimensions between the hybrid and non-hybrid composites. The values of tensile and flexural strength of the non-hybrid including four different fibre volume fraction composites exhibit significant property variation. In the other words, the tensile and flexural strengths exhibit significant improvement for each fabric layer added in the composite laminate body for similar specimen dimensions.

Table 5-16 DMTA results correlated with experimental results (role of composite Vf)

	direction	Fibre Volume Ratio (%)	Mean Flexural Modulus (GPa)	ILSS (MPa)	Tan (delta)	Mean Storage Modulus @ Room Temp. (GPa)	Tg (Celsius degree)
Non-hybrid Composites	Neat Epoxy		2.40	-	0.2800	2.09	110.17
	weft	0.38	14.85	18.106	0.1098	14.70	140.96
	weft	0.48	19.83	23.288	0.0705	20.52	130.22
	weft	0.56	22.97	27.421	0.0530	24.01	121.64
	weft	0.64	25.63	29.131	0.0370	25.11	125.91

5-17 DMTA results correlated with experimental results (role of fibre hybridisation)

	direction	Fibre Volume Ratio (%)	Mean Flexural Modulus (GPa)	ILSS (MPa)	Tan (delta)	Mean Storage Modulus (GPa)	Tg (Celsius degree)
Non-hybrid Composites	weft	0.48	19.83	23.24	0.0710	19.93	130.22
	warp	0.48	20.17	23.52	0.0871	20.52	128.42
Hybrid Composites	weft	0.48	21.13	26.49	0.0510	21.30	119.70
	warp	0.48	20.43	24.92	0.0787	20.67	117.26

Table 5-18 t-test of Tensile, ILSS and Flexural Test Results Hybrid and Non hybrid (Weft Direction)

t-test of Tensile, ILSS and Flexural Test Results Hybrid and Non-hybrid (Weft Direction)			
	UTS (MPa)	UFS (MPa)	ILSS (MPa)
Mean Hybrid	609.29	430.67	26.488
Mean Non-hybrid	501.90	361.50	23.288
d	107.38	69.17	3.20
Stand. Dev. Hybrid	36.57	22.78	2.860
Stand. Dev. Non-hybrid	33.71	21.66	2.671
Sx(A)	16.35	10.19	1.28
Sx(B)	15.08	9.69	1.19
Sd	22.24	14.06	1.75
t.	4.83	4.92	1.83

Table 5-19 Percentage points of t distribution*

Percentage point of t distribution		
df	alpha=0.05	alpha=0.01
1	12.71	63.66
2	4.31	9.93
3	3.19	5.85
4	2.78	4.61
5	2.58	4.04
6	2.45	3.71
7	2.37	2.45
8	2.31	3.36
9	2.27	3.25
10	2.23	3.17
11	2.21	3.11
12	2.18	3.06
13	2.16	3.02
14	2.15	2.98
15	2.14	2.95
16	2.12	2.63
100	1.99	2.61
200	1.97	2.59
infinit	1.96	2.58

* Data have been provided by (Michael S. Lewis-Beck, 1993b).
NOTE: Table value calculated by authors M.S.Beck.

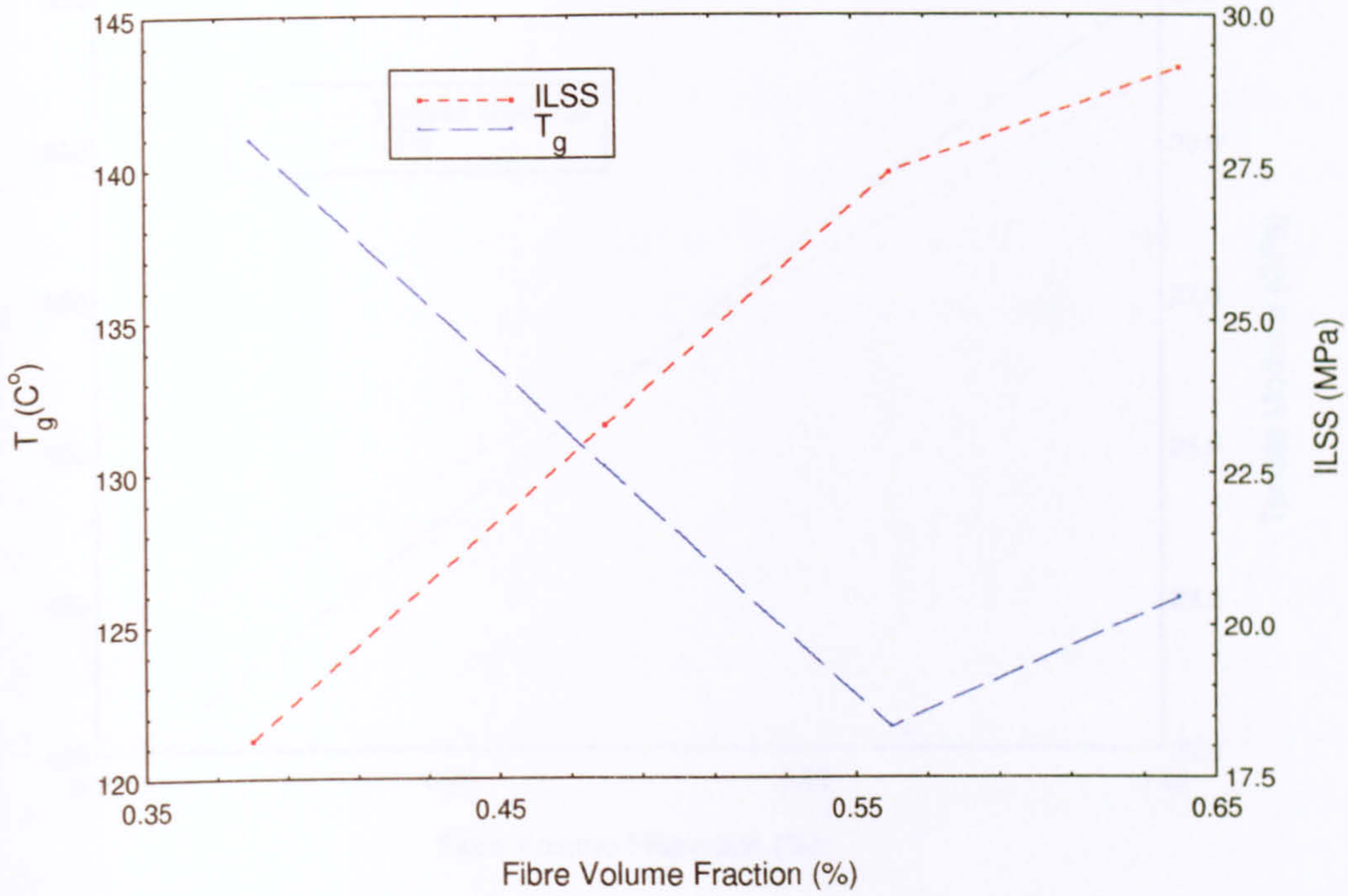

Figure (5 – 40) The relation between the glass transition temperature (T_g) and ILSS.

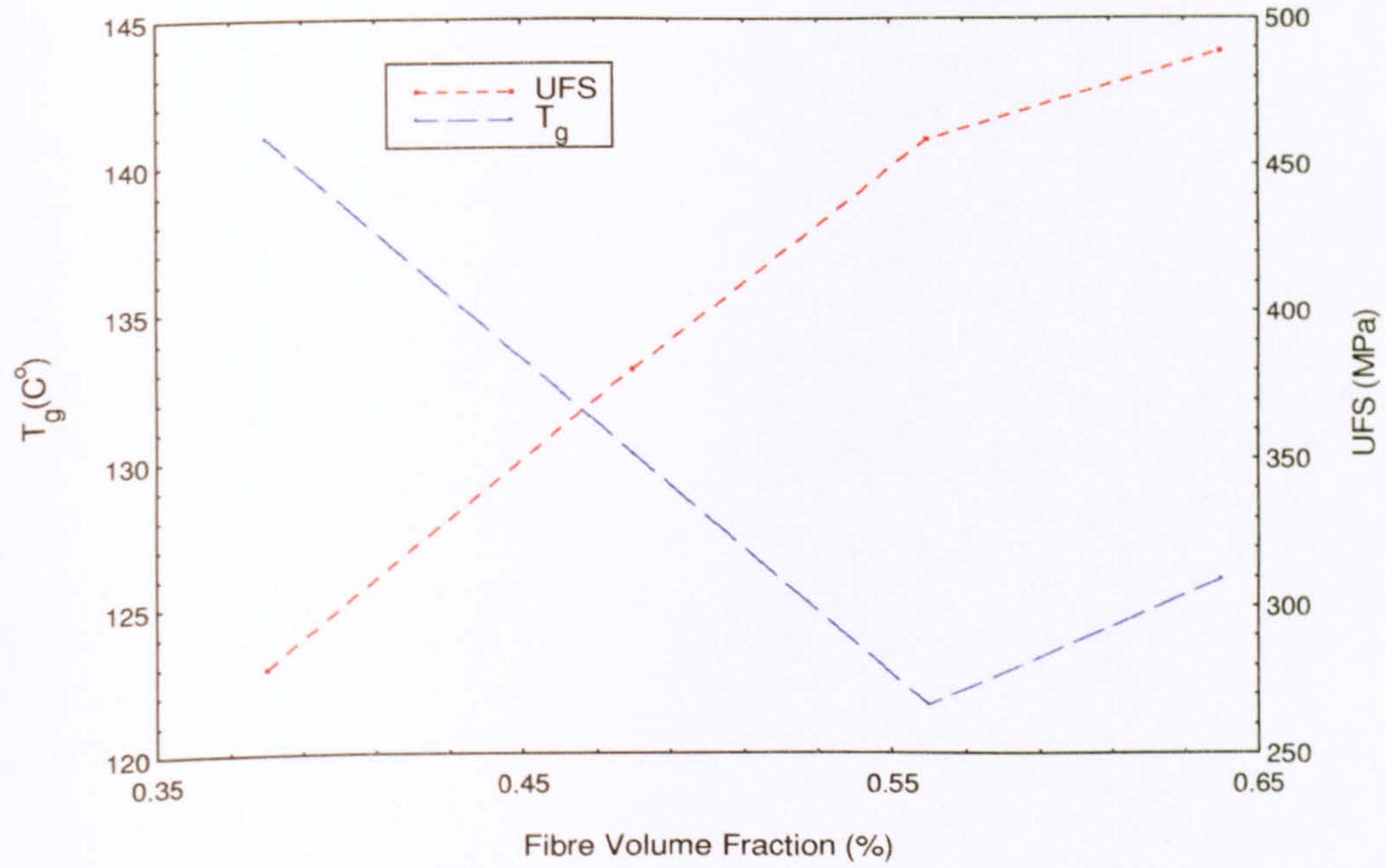

Figure (5 – 41) The relation between the glass transition temperature (T_g) and ultimate flexural strength (UFS).

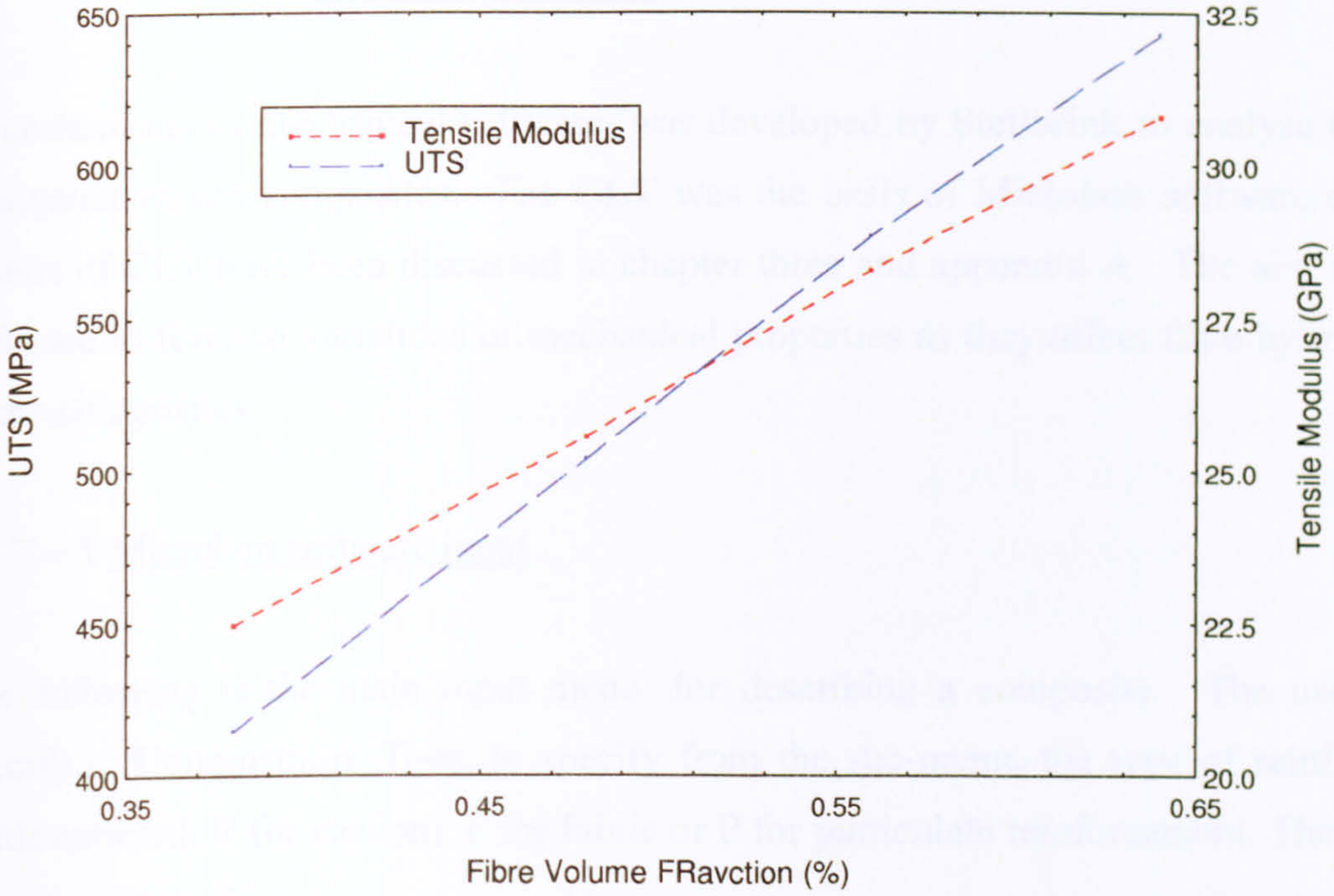

Figure (5 – 42) The Rule of mixture application on ultimate tensile strength (UTS) and tensile Modulus.

5 – 7 Section Seven Microlam software

Microlam, micro-mechanical software, was developed by Stellbrink to analyse the structures of laminated woven composites. The **CLT** was the basis of Microlam software calculations; the details of CLT have been discussed in chapter three and appendix A. The aim is to employ the software to forecast variations of mechanical properties as they affect fibre hybridisation and V_f in the composites.

5 – 7 – 1 Microlam software input

The following is the main input menu, for describing a composite. The user presses C to specify.... Composition. Then, to specify from the sub-menu, the type of reinforcement U for unidirectional, R for random, F for fabric or P for particulate reinforcement. The bold face letter specifies the topic

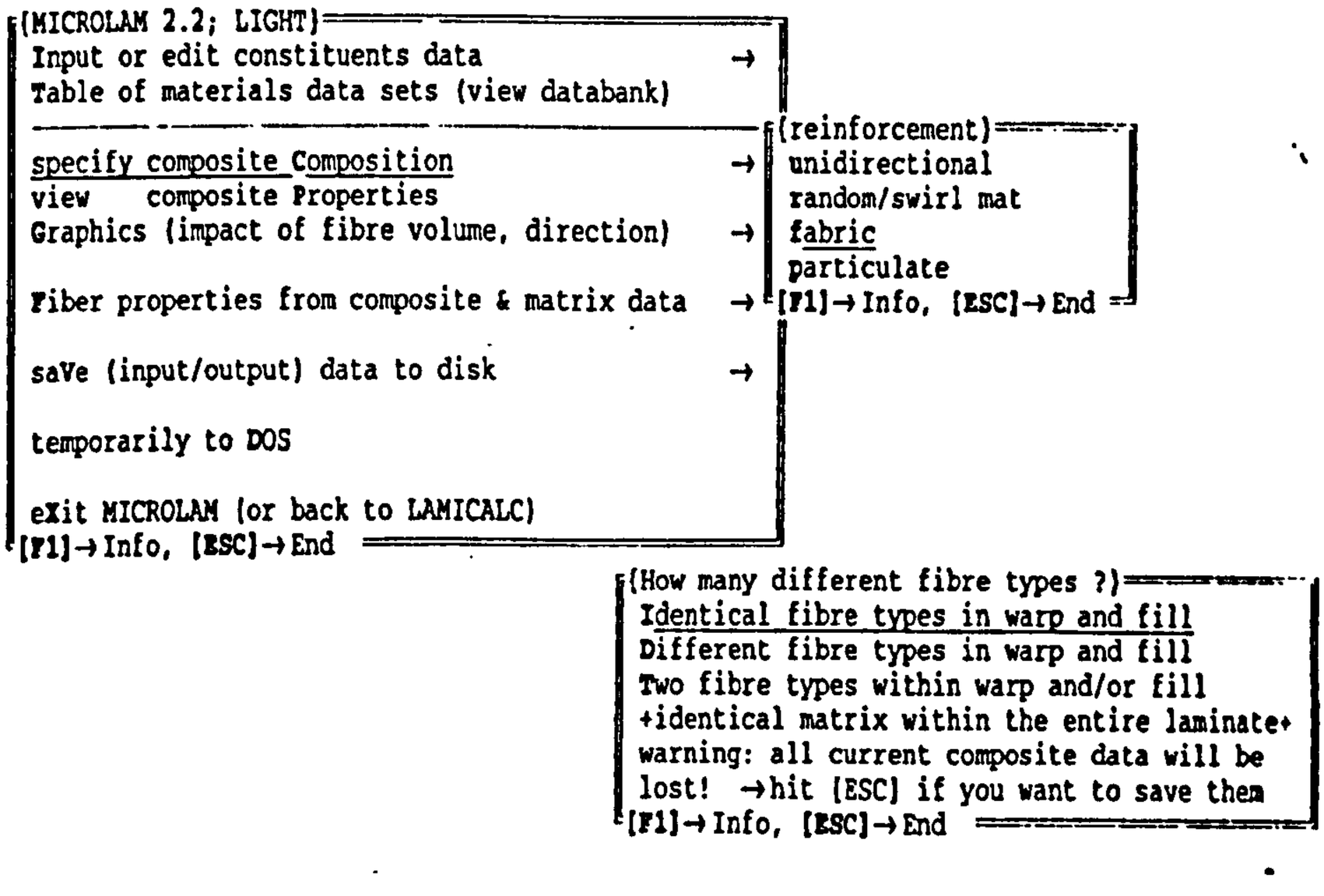

Figure S – 1: Menu sequence for fabric type specification.

F specifies fabric reinforcement from the sub-menu. The woven fabrics are often made of different fibre types, such as glass and carbon or carbon and Kevlar. There are two main principles of combinations: firstly, warp strands are made of one fibre type and fill strands are made of another fibre type or, secondly, the strands in one direction (warp or fill) alternatively consist of different materials. Microlam masters both methods and their combinations. Therefore,

the first characteristics the user must specify with fabric reinforced composites is the number of different fibre types and the way they are combined. For now, in order not to make things too complicated, Identical fibre types in the whole cloth is selected for non-hybrid and different fibre types for hybrid.

Then, the following list of chooseable matrices is displayed, marked by ranked identification letters. The user chooses the corresponding letter: A for low modulus matrix has been chosen for epoxy resin in the matrix ID submenu. The list of chooseable reinforcements is then added on screen. Again, the user has to make a choice by typing the corresponding letter: G for E-glass in the fibre ID submenu, in order to investigate the principal difference of the available fibre hybridisation methods. The non-hybrid fabric could be specified with E-glass fibre in both warp and weft directions. The hybrid fabric could be specified with E-glass fibers in warp direction and S-glass fibre (instead of R-glass fibre due to non-availability) in fill direction.

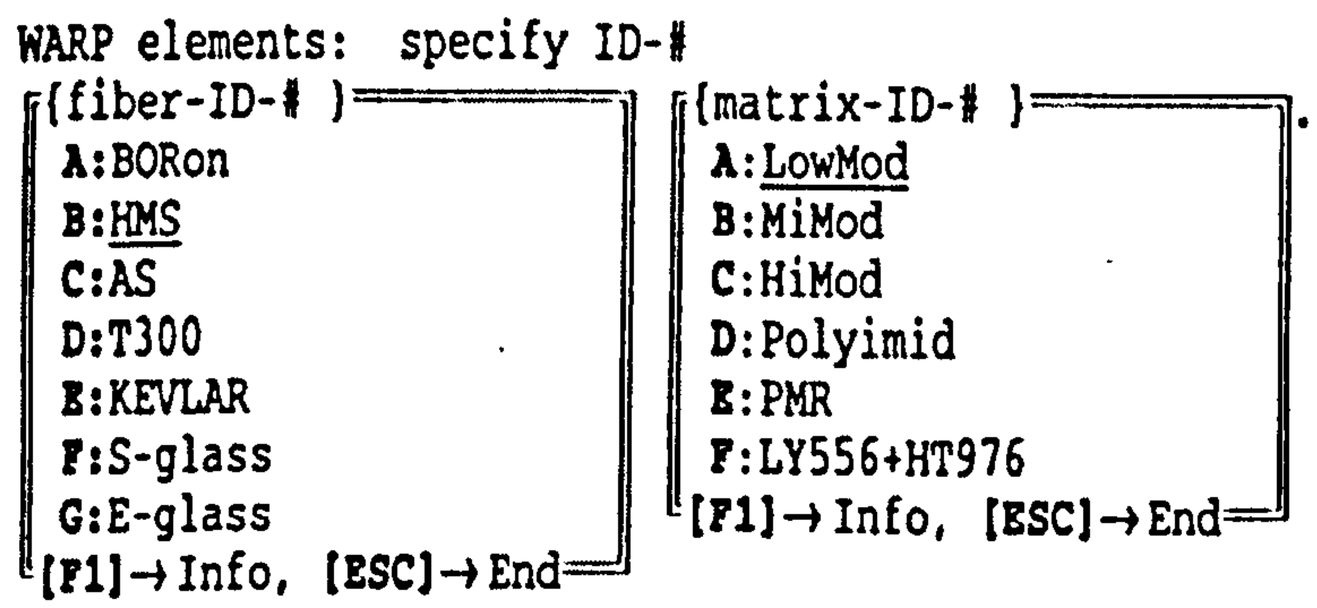

Figure S – 2: Menu sequence for fibre identification in the fabric and matrix type specification.

In order to investigate the principal difference of the available fibre volume fraction methods, the programme asks for the fibre volume fraction, a number between 20% and 90% is keyed in. With fabric composites the fibre volume fraction to be specified at that point has a special meaning. In fabric reinforced laminates, resin is distributed very unevenly. Within a strand, fibre content is high; where fill and warp strands cross, neat resin lumps exist. The global fibre content in a woven fabric reinforced laminate must be much lower than locally within a strand.
Suggestions are also made for an appropriate local fibre volume fraction within a strand. The proposed values are then confirmed or specified. Microlam then displays the data of a unidirectionally reinforced composite with the specified local V_f. This is a basic data set for

estimating properties of fabric reinforced laminates. If the fabric is composed of several fibre types, this step is repeated for each type. Due to limitation of text screen performance, subscripts are not printable so, El stands for E_1, Rlt for R_1t …etc.

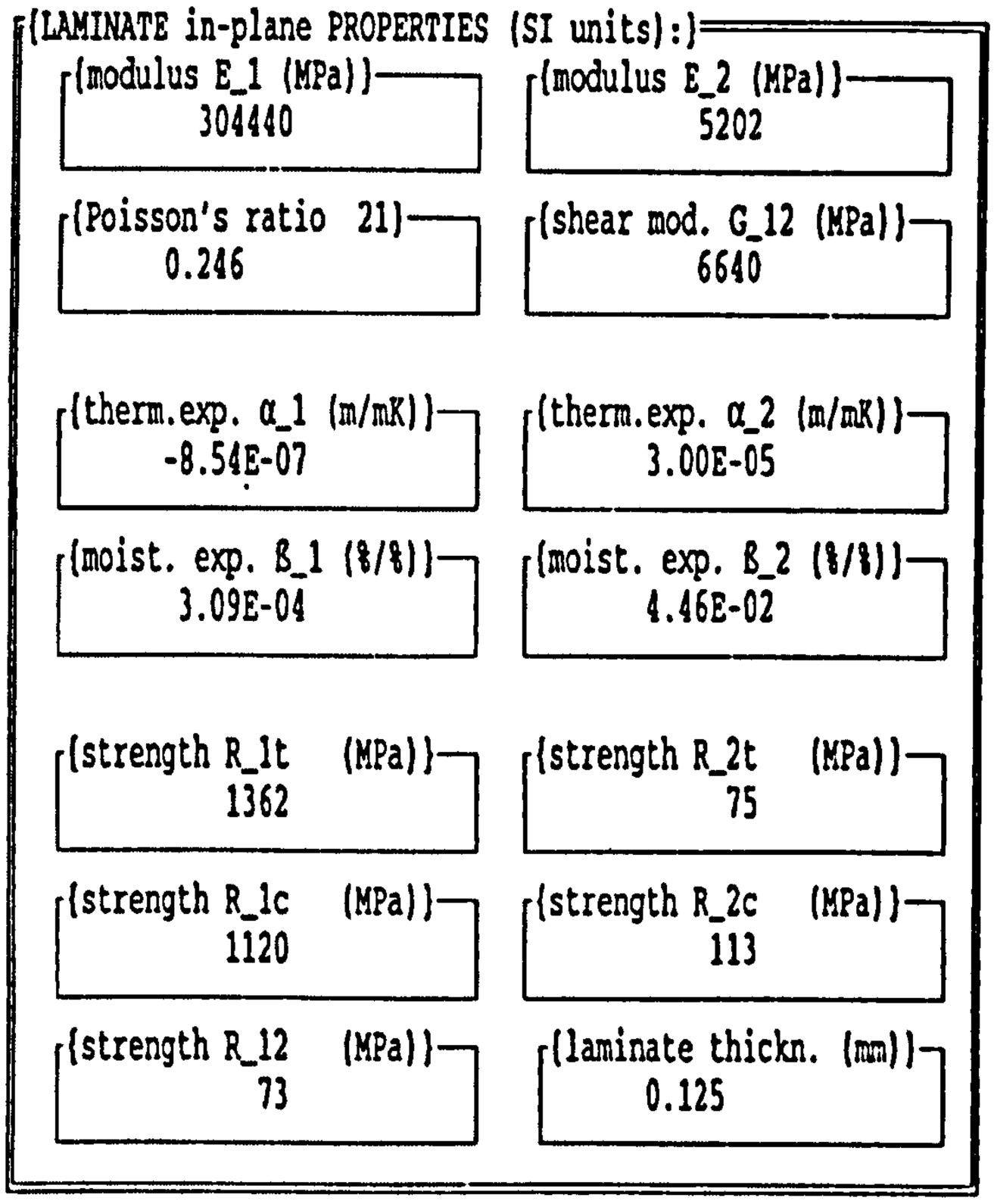

Figure S – 3 the analysed ply properties screen presentation.

The next screen shows a sketch of weave patterns, which illustrates the prompt for weave pattern specification. The user has to reply with two numbers describing the numbers of consecutively crossed transverse fibre strands. Microlam masters only symmetric weave patterns, similar in warp and fill directions.

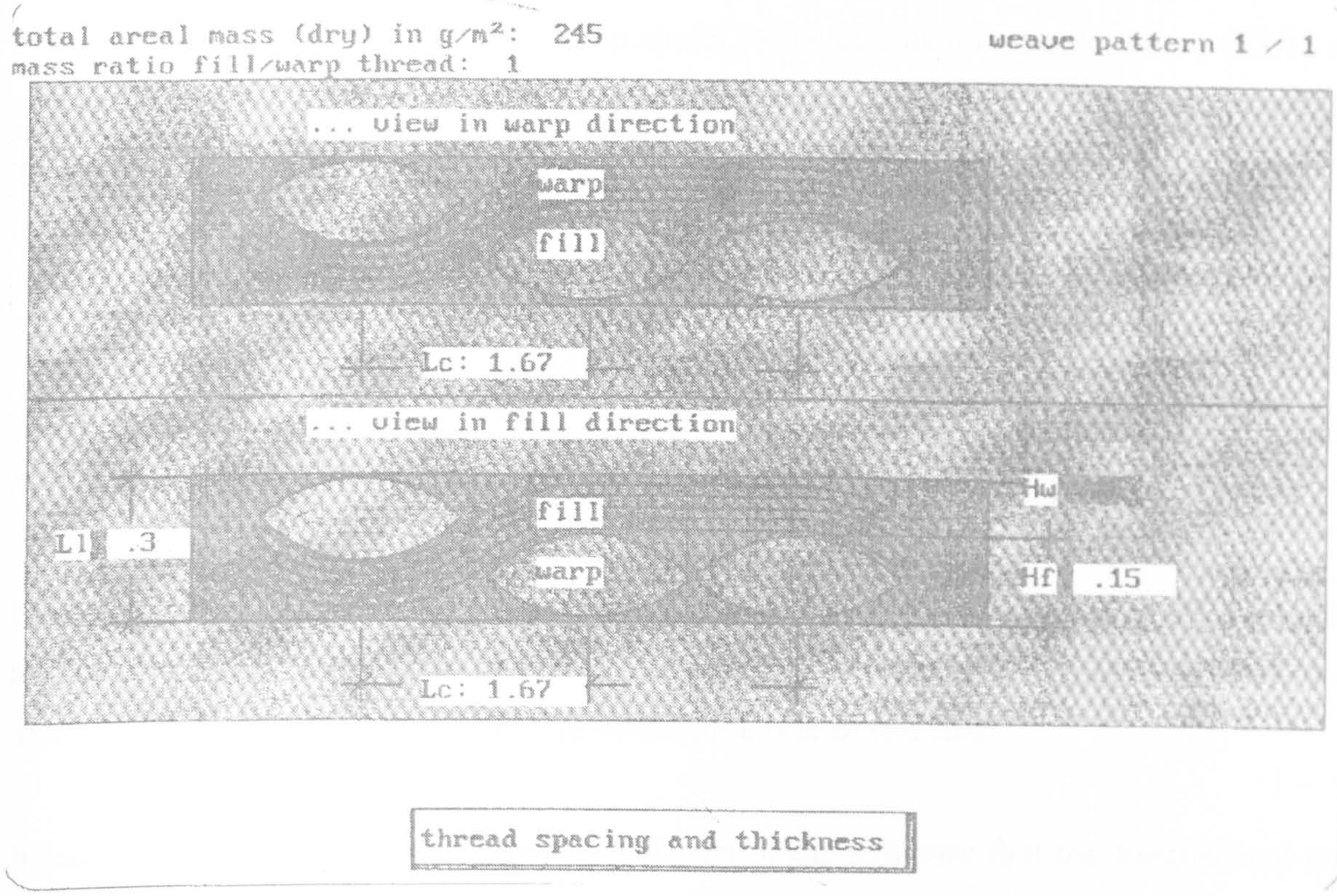

Figure S – 4 Data input screen for fabric geometry specification.

Now, it is recommended to select [1/7], which means 8-harness weave pattern in the weave pattern ID instead of the default value [1/1]. The mass area of 305-g/m^2 for the fabric used instead of the default value of 245 g/m^2, with the default mass ratio of fill/warp equal to 1. It is essential to mention that Microlam software input such L_1: the thickness of laminate, L_c: the crimp portion length of the woven cell repeat unit and Ls the straight portion length of woven fabric cell repeat unit are kept constant for each calculation. Microlam finally asks for a void volume content. Further information for specifying the fabric geometry is required. Microlam has built in default values, which describe an ordinary glass fabric. To input data the user presses [ENTER] step by step.

5 – 7 – 2 Microlam software output

Microlam then uses **classical laminate theory** to calculate the effective fabric reinforced laminate properties and displays this data on screen, see figure S – 3.

A key assumption made in the fibre crimp model is that classical laminate theory (CLT) is applicable to each infinitesimal slice of material of width dx. Then the local plate extension stiffness coefficient for the portion where the filling is composed of α material, is given by:

$$A^{\alpha\xi}{}_{ij}(x) = Q^{M}{}_{ij}(h - \frac{h_t}{2} + h_1{}^{\alpha}(x) - h^{\alpha}{}_2(x)) + Q_{ij}{}^{F\alpha}(x)\frac{h_t}{2} + Q_{IJ}{}^{W\xi}(h_2{}^{\alpha}(x) - h_1{}^{\alpha}(x))$$

where the superscripts F, W and M denotes the filling yarn region, warp yarn region, and pure matrix material, respectively; ξ stands for α or β material as presented in figures (3 – 4 and 3 – 6) and h denotes the total laminate thickness, including the pure matrix layers.

For comparison purpose, the data output of Microlam software such as stiffness and shear moduli are illustrated in table (5 – 20). In general, the user will see that stiffness is roughly determined as an arithmetic average, following the rule of mixture.

It has been observed from the output calculation of the software that the longitudinal and shear moduli increase with the increase in the overall fibre volume fraction of the glass woven composites. Similar relationships were highlighted from the experimental results. The different laminate thickness input values for the chosen V_f in the glass woven composite also hold individual values affected by the laminate thickness as illustrated in table (5 – 20). The variation between the hybrid and non-hybrid composites in the weft direction has been observed: this is consistent with the CLT, which is the basis of Microlam software calculations. It has been further observed that the hybrid longitudinal and shear moduli values are higher than the non-hybrid glass woven composites for similar V_f, primarily similar relationships were highlighted from the experimental results. Classical lamination theory is applicable for each tiny microscopic slice of the material of certain width in the case of the hybrid weave.

It is essential to mention that experimentally, the ILSS specimen with 3mm thickness contained 8 to 14 woven fabric layers. The stresses in the plane of the laminate σ_x, σ_y and τ_{xy} only are considered in CLT as discussed in chapter three and appendix A. The CLT considered the laminate to be very thin; the interaction between the plies is not taken into account according to this theory (more details in appendix A). Hence, the above reason was considered, while analysing the ILSS values. Consequently, the existence of ILSS in the experiments is deemed to relate to the thickness of the laminated test specimen. This is in agreement with the literature (Chou 1992, and Enie and Rizzo 1970).

Table 5-20 Microlam software output values & analysis

		Microlam Software Calculation											
Thickness (mm)		0.22				0.26				0.30			
Laminate	Fibre volume fraction (%)	Longit. Modulus (E1) of warp dir.(MPa)	Longit. Modulus (E1) of weft dir.(MPa)	Poisson`s Ratio	Shear Modulus (G12) Mpa	Longit. Modulus (E1) of warp dir.(MPa)	Longit. Modulus (E1) of weft dir.(MPa)	Poisson`s Ratio	Shear Modulus (G12) Mpa	Longit. Modulus (E1) of warp dir.(MPa)	Longit. Modulus (E1) of weft dir.(MPa)	Poisson`s Ratio	Shear Modulus (G12) Mpa
Non-hybrid	0.38	20949	20949	0.102	2200	18083	18083	0.109	1980	15976	15976	0.116	1818
Non-hybrid	0.48	21172	21172	0.104	2333	18271	18271	0.112	2093	16139	16139	0.119	1916
Non-hybrid	0.56	21434	21434	0.108	2507	18493	18493	0.115	2239	16331	16331	0.122	2043
Non-hybrid	0.64	21807	21807	0.112	2765	18809	18809	0.119	2458	16607	16607	0.126	2233
Hybrid	0.48	21222	24243	0.091	2344	18317	20860	0.098	2101	16081	18372	0.105	1924

CHAPTER SIX

CHAPTER SIX

6 – 1 Summary

Damage accumulation in woven fabric composites has been analysed in this study based on two reinforcement categories. The first category was to investigate the effect of V_f in the composite mechanical performance using non-hybrid woven fabric of E-glass in four different fibre volume fractions for similar specimen dimensions. The second category examines the effect of fibre **hybridisation** of the composite mechanical performance using hybrid woven fabric of E-glass in the warp and the R-glass in the weft compared with non-hybrid E-glass woven fabric composites. The comparison was for similar fibre volume fractions and specimen dimensions.

TD22 is a silane binder; which is a resin compatible option as a fibre coating for both fabrics. Epoxy resin (L20-SL) set was the sole matrix used for all laminated composite material.

The destructive tests ILSS (short-beam method), flexural (three-point bending) and uniaxial tension tests were carried out on these sets of composites. The AE technique was successfully employed on glass woven composites during mechanical testing (ILSS, flexural and tensile). The AE results were supported by specimen visual examination (SVE) and scanning electron microscopy (SEM) of fracture surfaces was performed to visualise the damage events occurring in glass woven reinforced epoxy resin laminates.

The composite properties including ILSS, flexural strength and modulus and tensile strength and modulus have been analysed in chapter five. The test results reveal higher tensile, flexural and improvement of ILSS mechanical performance for the hybrid compared with non-hybrid composites. The improvements were significant on weft (fill) direction, where R-glass fibre dominated. The hybrid composite failed to exhibit similar mechanical improvement for the warp direction, where E-glass dominated.

The results further showed a significant improvement in flexural and tensile mechanical properties and an improvement in ILSS for higher fibre volume fraction in the non-hybrid composites compared with low V_f.

In Dynamic Mechanical and Thermal Analysis (DMTA) tests (Flexural vibration – non-resonance method), the glass transition temperature (T_g) was measured for each composite by taking the maximum peak of the loss modulus. The DMTA is used to characterise the variation in the interphase properties in the glass woven composite. This is an issue of great importance since the interphase properties often dictate the gross mechanical performance and structural integrity of the composite as a whole.

The glass transition temperature of hybrid woven fabric composites was lower than the T_g of non-hybrid woven fabric composites. Thus the fibre surface treatment concentration in the hybrid composites was higher than that of the non-hybrid composites. The increase in fibre volume fraction reduced the T_g of non-hybrid E-glass woven fabric composites. In general, the increasing interaction density with the matrix caused this reduction due to the increased fibre surface treatment concentration in the composites. The T_g measurements of composites have been highlighted in this study to reveal the role of the fibre coating concentration in the composites and the relation of the fibre/matrix bond in the mechanical performance.

The correlation of DMTA results with destructive testing such as tensile, flexural and ILSS results have been established. The tensile and flexural properties and ILSS showed good correlation with DMTA results. The DMTA storage modulus as a function of load-bearing capability correlated with tensile strength. Furthermore, the DMTA storage modulus correlated to the flexural modulus at room temperature. The magnitude of tan delta was associated with the status of interfacial bonding of the composite as the outcome of V_f level or the fibre properties in the composites. The tensile modulus and strength showed a linear dependence on the fibre volume fraction, which means the rule of mixture is applicable to the results in this research.

Microlam software based on the classical laminate theory (CLT) calculation has been used to highlight the variation of elastic properties of different classes of glass woven fabric composites. The calculations gathered from Microlam software output data showed the longitudinal moduli increase with the significant increase in the overall fibre volume fraction of the glass woven composites. Microlam software output data further showed the longitudinal moduli of hybrid composite in weft direction was superior to non-hybrid composites in the weft direction. Classification of the mechanical testing results between significant and non-significant was examined using the t-test of probability.

A model has been developed in this study based on the analysis of damage event sequential process modelling. The experimental analysis relied on viscoelastic investigation of the composite using DMTA and AE techniques including AE zone classification in each zone. Specimen visual examination (SVE) and SEM of the fracture surface supported the AE results. This analysis has been applied to the bridging mathematical model introduced by Ishikawa and Chou (Chou1992), as a further development of the model. The bridging is worked effectively when increasing the fibre volume fraction in the composites. The results of tensile, flexural and ILSS tests indicate that bridging is found in the higher fibre volume fraction composites, by an increase in the number of woven cell unit repeats, but does not exist in the lower V_f composites. The hybrid glass material used over the woven cell unit repeats improved the bridging performance, which was not the case for non-hybrid glass woven fabric composites with similar V_f. The results of tensile, flexural and ILSS provided the evidence that the bridging exists in hybrid composite. The DMTA and AE parameter could be used as a quality control. The flowchart in figure (5 – 39) was designed for quality control purposes to generate satisfactory woven glass composite.

6 – 2 Conclusions and the originality of the research

1. The DMTA is used to characterise the variation of the interphase properties in the glass woven composite. This is an issue of great importance because the interphase properties often dictate the overall mechanical performance and structural integrity of the composite.

2. The mechanical properties of **hybrid** glass woven fabric composites (weft direction) improved compared to the non-hybrid glass woven fabric composites for similar fibre volume fraction and similar specimen dimensions. During the Interlaminar Shear Strength (ILSS) tests (short-beam method), the shear strength improved by approximately 6%. In flexural (three-point bending method) tests, the flexural properties (strength and modulus) of hybrid glass woven fabric composites were significantly increased by approximately 19%. In the uniaxial tensile tests, the tensile properties (strength and modulus) of hybrid glass woven fabric composites were significantly increased by approximately 18%.

3. The hybrid glass woven fabric composite failed to show a similar mechanical improvement in the warp direction. The difference between the hybrid and non-hybrid composites is that the hybrid composite is composed of **R-glass** and **E-glass** whereas the non-hybrid composite contains E-glass only. It is essential to mention that the R-glass was in the weft direction of the hybrid woven composites while E-glass was in the warp direction. Therefore there was a significant improvement of flexural and tensile properties in the weft direction, which did not occur in the warp direction. This clearly demonstrates the significant change in the properties of the woven fabric composites promoted by R-glass properties.

4. The above two points can conclude that the fabric **weave architecture** significantly influences the micro- and macro-mechanical properties of glass composites. This is promoted by fibre properties. Other weave hybridisation has been suggested to provide the designer with alternative tools for development (see the future work).

5. The flexural and tensile properties were significantly increased and an improvement achieved in the ILSS due to the increase of fibre volume fraction in the **non-hybrid** E-glass woven fabric composites for similar specimen dimensions.

6. It is essential to consider **the cost** of R-glass from the industrial point of view. For example the cost of an E-glass bobbin is £ 7 while the cost of an R-glass bobbin is £ 49 (Vetrotex, 1999). Therefore, it is fair to mention that similar micromechanical properties of hybrid composites can be achieved through the variation of V_f of non-hybrid composites within certain limits of V_f.

7. A model has been developed in this study based on the analysis of micro- and macro-mechanical damage process modelling during the tensile loading as presented in figure (5 – 37). A quantitative and qualitative relationship is established in this model so as to obtain further details of the damage event identification as presented in figure (5 – 38). **The model correlated the AE profile with quantitative values and qualitative views in order to identify the damage event and the level of failure.** The quantitative values of each mechanical test and the qualitative views of the fracture surfaces are represented by SEM and visual specimen examination (VSE). While the AE profile represented the life history of damage process during the testing.

8. The **zone classification technique** of stress-strain and its relating AE curves has been utilised in this study to extract the maximum possible information from each variation in the damage events.

9. Further development to the model is to identify the damage event process in order to classify the bridging support to maintain the coherency of the tensile specimen. Thus the catastrophic failure by the specimen splitting into two pieces can be avoided. The so-called "bridging validation" to which the analysis refers, was presented mathematically by Ishikawa and Chou (Chou 1992).

The originality of this research can be highlighted as follows:

- The results of the research programme in the absence of any other research work on R-glass are essential in the field of glass fabric composites. The material is original and has not previously been examined. The test results are considered to be an addition to previous knowledge on R-glass.

- The **zone classification technique** of stress-strain and its relating AE curves have been utilised in this study to extract the maximum possible information from each variation in the damage event. This technique does not appear previously to have been discussed in the context of woven fabric composites.

- A model has been constructed in this study based on the micro- and macro-damage event sequential process. The experimental analysis relied on viscoelastic investigation of the composite using DMTA and AE techniques including AE zone classification. The visual specimen examination and SEM of fracture surface supported the AE results. This analysis has been applied to the bridging mathematical criteria introduced by Ishikawa and Chou (Chou1992) as a further development of the model.

- The new technique of the model is to employ different tools in combination such as AE, SEM, VSE and DMTA for clearer damage events process modelling.

- The use of viscoelastic properties of fabric composites is an innovative approach facilitating the DMTA technique in the woven fabric composites. The role of the fibre properties may be studied as well as the coating concentration on the fibre surface in the composites. DMTA data has been used as an accurate parameter for the first time to correlate the results of ILSS, flexural and tensile studies.

- The test results of ILSS, flexural property and tensile property of non-hybrid glass woven fabric composites can also be improved by increasing the fibre volume fraction of non-hybrid composites. These composites compete with hybrid material. Other weave hybridisation can be predicted in order to hold higher mechanical performance as a result of this research.

6 – 3 Further Work and Development

This research work has concentrated on a single weave hybridisation. There are many other hybridisation architectures, which can be employed for design application development. These should be investigated as a separate study.

Other weave hybridisation can be suggested from the outcome of the results analysis to predict better mechanical performance.

For example alternating the R- and E-glass fibres in both warp and weft could give a 50% fibre volume fraction for each fibre and possibly balanced mechanical properties for both weft and warp directions.

Another variation might lie in varying the numbers and order of R- and E-glass yarn in both warp and weft directions to obtain different fibre volume fractions. A collection of many woven fabrics could be obtained to enable the designer to select the optimum composite for the application under development.

REFERENCES

References

Adams D.F. and Doner, D. R. Journal of Composite Material, Vol. 1, pp152-164, 1967.

Agrawal R.K. and Drzal L.T. "Adhesion mechanisms of polyurethane to glass surfaces. II-Investigation of possible physi-chemical interactions at the interphase" Journal of Adhesion - ISSN- 0021-8464 -Citation- 55, No.3-4, pp.221-43, 1996.

Ahlstrom C and Gerard JF "The adhesion of elastomer-coated glass-fibres to an epoxy matrix-the effect of the surface treatments on the tensile strength of the glass-fibres" Journal of Polymer Composites, Vol.16, No.4, pp.305-312, 1995.

Al-Moussawi H., Drown E.K. and Drzal L.T. "Silane/sizing composite interphase " Journal of Polymer Composites -ISSN- 0272-8397 -Citation- 14, No.3, pp.195-200, 1993.

Armand Soldera "Comparison between the Glass Transition Temperature of the Two PMMA Tracticities: A Molecular Dynamics Simulation Point of View" Macromolecular Symposia, and 133 p21-32, CEN Scaly, 1998.

Arrington M. "Non-destructive testing of fibre reinforced plastic composites" (editor) Summerscales J. Acoustic emission volume 1, Elsevier Applied Science Publishers, London, pp. 25-63, 1987.

Ashcroft W.R. "Curing agents for epoxy resins" Chemistry and technology of epoxy resins, In: Ellis B. (ed.) Chapman and Hall, London. Pg. 37-70, 1993.

Ashton J.E., Halpin J.C. and Petit P.H. "Primer on composite material Analysis" Technomic, Stamford, Conn., USA, 1969.

Aslanova M.S., "Glass fibres", in "Handbook of composites – strong fibres" edited by W. Watt and by. Perov. Elsevier Science Publishers, Netherlands pp.11-20, 1985.

ASM International "Composites, Engineered Material" Handbook, vol. 1, ISBN 0-87170-279-7, Metals Park, Ohio, pp779-780, 1987.

Aveston J. and Kelly A. "Tensile first cracking strain and strength of hybrid composites and laminates" Phil. Trans. Royal Soc. London A294, 519-534, 1980.

Bader M.G. and Lekakou C. "Processing for laminated structures" edited by Mallick P.K. and Marcel Decker, Inc., New York, pp.371-479, 1997.

Bader M.G., Pickering K.L., Buxton A., Rezaifard A. and Smith P.A. " Failure micromechanism in continuous carbon fibre/epoxy resin composites" Composite Science and Technology Vol. 48, pp135, 1993.

Barbero E. J. "Introduction to Composite Material Design" Taylor and Francis, pp34-35, 1998.

Blankenship G. L., Lebow L. G., Hassim A and Dutoya A., "COMPO: A System for CAD of Composite Materials." Computer Aided Design in Composite Material Technology 3. Ed. by Advani S. G., Blain W.R., Wilde W.P. de, 3. Gillespie W. and Griffin O.H. Computational Mechanics Publications Southampton pp. 331-344, 1992.

Bogy D.B. "Edge bonded dissimilar orthogonal elastic wedges under normal and shear loading" Journal of Applied Mechanics, Vol.35, pp.460-466, 1968.

Bondt S. De, Frozen L. and Delay L., "Finite element simulation of Acoustic Emission due to fibre failure in a single fibre composite" Journal of Acoustic Emissions 11, pp. 95-98, 1993.

Bray D. E. and Stanley K R. "Non-destructive Evaluation, a tool in design, manufacturing and service" CRC Press, ISBN 0-8493-2655-9, p181-189, 1996.

Broughton W R., "Correlation of Analytical Predicted and Actual Properties for Fibre Reinforced Plastic Composites, Predictive Modelling of Fibre Reinforced Polymer Composites" – Vol. 2: Laminate Theory, NFL Draft Report DMM (D) 145 Sept. 1992.

Bundles A.R. and Harris B. "Hybrid carbon and glass fibre composites" Journal of Composites - ISSN- 0010-4361 -Citation- 5, No.4, pp.157-64, July 1974.

Caldwell Donald L. "Interfacial Analysis" In: S.M. Lee (editor) Composites Encyclopaedia Vol. 2, p.366. VCH, 1992.

Cameron D. "Dynamic mechanical properties of reinforced composites" ANTEC p-1279-1281, 1992.

Carlsson L. A. and Pipes, R. B. "Experimental characterisation of advanced composite materials" Prentice-Hall, Englewood, Cliffs New Jersey 1987.

Chamis C.C. "Mechanics of load transfer at the interface" Plueddemann P. (editor) "interfaces in polymer matrix composites" Vol. 6, London, Academic Press, 49, 1974.

Chamis C.C. and Lark R.F. "Non-metallic hybrid composites: analysis, design, application and fabrication", in "Hybrids and Selected Metal-Matrix Composites: A state-of-the-art Review" W. I. Renton, ed., AIAA, New York pp. 13-51, 1978.

Chang L. E., Hwu C., Kao C. J. "Delamination fracture criteria for composite laminates" Journal of Composite Materials -ISSN- 0021-9983 -Citation- 29, No.15, pp.1962-87, 1995.

Chawla, K.K. "Composite Materials Science and Engineering" Springer-Verlag, New York 1987.

Chen F., Hilltner A. and Baer E. "Damage and failure mechanisms of continuous glass fibre reinforced polyphenylene sulfide" Journal of Composite Materials, Vol.26, No.15, pp2289-2306, 1992.

Cheng-Kuang Chan; I-Ming Chu; Wenchian Lee, Wei-Kuo Chin "Preparation and properties of organic-inorganic hybrid materials based on poly-butyl-methacrylate-co-3-methacryloxypropyl trimethoxysilane" Journal Macromolecular Chemistry & Physics -ISSN- 1022-1352 -Citation- 202, No.6, pp.911-916, 2001.

Chen B. and Chou T.W. "Local elastodynamic stresses in the unit cell of a woven fabric composite", Archive of Applied Mechanics, Vol.70, No.6, pp.423-442, 2000.

Choi N.S., Lee S.H. "Non-destructive evaluation of thermal stress-induced damage in thin composite laminates" Journal of Materials Science -ISSN- 0022-2461 -Citation- 36, No.7, pp.1685-93, 2001.

Chou T.W. "Microstructure design of fibre composites" Cambridge University press, 1992.

Chou T.W. and Kelly A. "Mechanical properties of fibre composite materials", in Annual Review of Materials Science, vol. 10, Annual Review, Inc., Palo Alto, pp. 229-259, l980a.

Chou T. W. and Ko F.K. "Textile Structural Composites" Elsevier, ISBN 0-444-42992-1, 1989.

Chou T.W. and Nomura S. "On the Thermoelastic behaviour of short fibre and hybrid composites" Proceedings of the Third International Conference on Composite Materials, Pergamon Press, New York, pp. 69-80,1980a.

Chou T.W., Nomura S. and Taya M. "A self-consistent approach to the elastic stiffness of short-fibre composites" Journal of. Composite Materials 14, 178, 1980b.

Christensen R.M. "Mechanics of Composite Materials" Wiley-Interscience, New York 1979.

Christensen R. M. "Theory of viscoelasticity" Academic Press, New York. Christensen, R. M. and Waals, F. M. 1971 "Effective stiffness of randomly oriented fibre composites", Journal of Composite Materials 6, pp518-32 1972.

Chua P.S. "Dynamic mechanical analysis studies of the interphase" Journal of Polymer Composites Vol.8, No.5, pp.308-313, 1987a.

Chua P.S. "Characterisation of the interfacial adhesion using tan delta" SAMPE Quarterly Vol.8, No.3, pp.10-15, 1987b.

Cirese P. "Introduction of a quick calculation method for the analysis of laminated composites and its experimental validation", Computer Aided Design in Composite Material Technology, Proceedings of the International Conference, Southampton, Computational Mechanics Publications pp. 89-103,1988.

Connor M., Bidhux J.E., Manson J.A.E. "Criterion for optimum adhesion applied to fibre reinforced composites" Journal of Materials Science Vol.32, no.19, pp.5059-5067, 1997.

Cousin P. and Smith P. "Dynamic mechanical properties of sulphonated polystyrene/alumina composites" Journal of Polymer Science: Polymer Physics Edition -Citation- 32, No.3, p.459-68, 1994.

Dominguez Fred S. "Engineered Material Handbook" Hurcules Aerospace company, ASM International Composites, Vol.1. 1987.

Don E. Bray and Stanley K Roderic, "Non-destructive Evaluation, a tool in design, manufacturing and service", p181-189, 1996.

Downs K.S. and Hamstad M.A. "Acoustic emission from depressurisation to detect/evaluate significance of impact damage to graphite/epoxy pressure vessels" Journal of Composite Materials, Vol.32, No.3, pp.258-307, 1998.

Drown E.K. and Drzal L.T. "Characterisation of the sizing interphase and its influence on the behaviour of glass fibre-reinforced epoxy composites" ANTEC 92 Plastics: Shaping the Future. Volume 1. Conference Proceedings - Detroit, Mi., pp.239-42. 012, 3rd-7th May 1992.

Drzal LT. "The interphase in epoxy composites" Advanced Polymer Science 75, 1-32, 1985.

Drzal LT, Drown EK and Moussawi H. "Glass fibre sizing and their role in fibre-matrix" adhesion. Journal of Adhesion Sci. & Tech. 5(10), 865-881, 1991.

Drzal LT and Larson BK "Glass fibre sizing/matrix interphase formation in liquid composite moulding: effects on fibre/matrix adhesion and mechanical properties" Journal of Composites No. 25 Vol.7, pp.711-721, 1994.

Button RE, Pagano NJ, Kim R.Y., and Parthasarathy T.A. "Modelling the ultimate tensile strength of unidirectional glass-matrix composites" Journal of American Ceramic Society vol.83, part1, 166-174, 2000.

Eckstein Y. "Role of silanes in adhesion. Part II Dynamic mechanical properties of silane-treated glass fibre/polyester composites" Journal of Adhesion Science Technology. Vol.3, No.5, pp.337-355, 1989.

Enie R.B. and Rizzo R.R. "3D laminate moduli" Journal of Composites Material Vol.4, pp.150-154, 1970.

Farouk A., Langrana N. A. and Weng G. J., "Modulus Prediction of a Cross-Ply Fibre Reinforced Fabric Composite with Voids" MD-Vol. 29 Plastics and Plastic Composites: Material Properties, Performance, and Process Simulation Part, ASME pp. 297-308, 1991.

Fowler T.J. Houlle, LS, and Strauser F.E. "Development and design of a sulphuric acid plant leak monitor system" Proceeding of the NACE, Annual Conference and Corrosion Show, paper No.239, pp.1-20, 1992.

Foye R.L., and Baker D. J. "Design analysis methods for advanced composite structures" AFML-TR-7-299, vol. 1, Wright-Patterson Air Force Base, Ohio, 1971.

Frenzel H., Bunzel U., Haessler R and Pompe G, "Influence of surface treatment of glass fibers on the dynamic mechanical properties" Journal of Adhesion Science and Technology, Vol.14, No.5, pp.651-660, 2000.

Gerard J.F., Vazquez A., Ambrustolo M., Moschiar S.M. and Reboredo M.M. "Interphase modification in unidirectional glass-fibre epoxy composites" Journal of Composites Science and Technology, 58, 549-558, 1998.

Giordano M, Calabro A., Esposito C., Damore A. and Nicolais L "An acoustic-emission characterisation of the failure modes in polymer-composite materials" Journal of Composites Science and Technology, Vol.58, No.12, pp.1923- 1928, 1998.

Griffin O.H., Kamat M.P. and Herakovich C.T. "3D inelastic FEA of laminated composites" Journal of Composites Material, Vol.15, pp.543-560, 1981.

Haessler R. and Keusch S. "Influence of surface treatment of glass fibers on the dynamic mechanical properties of epoxy resin composites" Journal of Composites: Part A 30, pp.997-1002, 1999.

Halpin J.C. "Primer on composite materials: analysis" Revised edn. Lancaster, Pa., Technomic Publishing Co. Inc., pp. vii 187. USD.25. 9ins. 627-91T, 1984.

Halpin J.C. "Evolution of design and material criteria for polymeric structural materials" Journal of Composite Structures -ISSN- 0263-8223 -Citation- 27, No.1/2, p.3-6, 1994.

Hamada H. "Evaluation of interfacial properties by various testing methods" Personal Editor Drzal L.T. and Schreiber H.P., 20th Annual Anniversary Meeting of the Adhesion Society. Conference proceedings, pp.279-281, 8(10) 1997.

Harris B., Guild F.J. and Phillips M.G. "Acoustic emission studies of damage in GRP" Journal of NDT International -Citation- 13,No.5, Oct. p.209-18, 1980.

Harris B "Engineering composite materials" Institute of Materials. London, p.44, 1986.

Harris B. and Haddell O.G., Almond D.R., Lefebvre C., Verbist J. "Study of carbon-fibre surface treatments by dynamic-mechanical analysis" Journal of Materials Science, Vol.28, No.12, pp.3353-3366, 1993.

Hashin Z. "Viscoelastic behaviour of heterogeneous media" Journal of Appl. Mech. Vol.32, No. 63, pp.1-6, 1965b.

Hashin Z. "The inelastic inclusion problem" Mt. Journal of Eng. Sci. Vol.7, pp.11-36, 1969.

Hashin Z. "Theory of Fibre Reinforced Materials" NASA CR-1974.

Hayashi T. "Analytical study of interlaminar shear stresses in a laminated composite plate" Trans. Journal of Soc. Aeronaut Space Sci., vol. 10, No. 17, pp. 43-48, 1967.

Heise M.S. and Martin G.C., Journal of Applied Polymer Science, Vol. 39, pp.721, 1990.

Herakovich CT "Mechanics of fibrous composites" Wiley & Sons, ISBN-0-47110636, 1998.

Herakovich, C. T., Post, D., Buczek, M. B., and Czamek, R. "Free edge strain concentrations in real composite laminates: Experimental-Theoretical Correlation" Journal of Applied Mechanics, vol. 52, no. 4, pp. 787-793, 1984.

Herakovich, C.T., Renieri, G.D., and Brinson, H.F. "Finite element analysis of mechanical and thermal edge effects in composite laminates" Proceeding of the army symposium on Composite materials: The Influence of Mechanics of Failure on Design, Cape Cod, MA, pp. 237-248, 1976.

Hofstee J. and Van Keulen F. "3-D Geometric modelling of a draped woven fabric" Journal of Composite Structures Vol. 54, No. 2-3, p.179-95, 2001.

Holford K.M, Carter DC "Acoustic emission source location" Key Engineering materials, Vol.167-, pp.162-171, 1999.

Hull D. and Clyne T.W. "An Introduction to Composite Materials" Cambridge University Press, ISBN 0-521-38190-8, 1996.

Interglas –Technologies "Glass fibre yarn and fabric" correspondence with Editor 1998.

Interglas –Technologies "Fabrics for plastic reinforcement" correspondence with Editor 1999.

Ishida H. and Jang J. "Adsorption behaviour and molecular structure of mixed silane with a crosslinking additive on the substrate" 44th Annual Conference & Focus '89.Conference Proceedings-Citation- Dallas, TX. Paper 9B, 012, 1989a.

Ishida H, Jang J, and Plueddemann EP "Condensation and structure of a silane with a crosslinking additive in solution" SAMPE, ISSN-0036-0821 Vol.20, No.4, p32-37, 1989b.

Ishikawa T, "Anti - Symmetric Elastic Properties of composite plates of satin weave cloth" Journal of Fibre Science and Tech Sept., Vol. 15 pp. 127-145, 1981.

Ishikawa T and Chou T. W. "Elastic behaviour of Woven Hybrid Composites" Journal of Composite Materials Vol.16, pp.2-19, 1982a.

Ishikawa T. and Chou T.W "Stiffness and strength behaviour of woven fibre composites" Journal of Materials Science Nov. Vol. 17 pp. 3211-3220, 1982b.

Ishikawa T. and Chou T.W "One Dimensional Micromechanical Analysis of Woven Fabric Composites" AIAA Journal Dec. Vol. 21 No. 12 pp.1714-1721, 1983b.

Ishikawa T. and Chou T.W "Non-linear behaviour of woven fabric." Journal of Composite Materials Sept. Vol. 17 PP. 399-413, 1983c.

Ishikawa T. and Chou T.W "Thermoelastic analysis of hybrid fabric composite" Journal of Material Science, 18, 2260-68 1983d.

Ishikawa T., Matsushima M., Hayashi Y. and Chou T.W, "Experimental confirmation of the theory of elastic moduli of fabric composites." Journal of Composite Materials Vol.19, pp. 443-458, 1985.

Ishikawa T., Matsushima M., Hayashi Y., "Geometrical and material non-linear properties of two dimensional fabric composites." AIAA Journal, Vol. 25 No.1, pp.107-113, 1987.

Ishikawa T. and Chou T.W "Analysis and modelling of two dimensional fabric composites" Composite Material series 3: Textile structural composites, Elsevier Ed. Chou and Ko pp. 209-264, 1989.

Jacques, Molinier, "Special glass fibre" 13th Reinforced Plastics Con., paper, 14, pp. 59-62, 1982.

Jang Bor Z. "Interfaces and interphase in Composites" Journal of Advanced Polymer Composites chapter 3, p. 55, ASM, 1994.

Jinen E. and NI Q.Q "Fracture behaviour and acoustic emission in bending tests on single-fibre composite" Journal of Engineering Fracture Mechanics, Vol. 56, No 6, pp.779-796 1997.

Jensen R.E, Brien E.O, Wang J., Bryant J., Ward T.C, James LT and Lewis DA, Journal of Polymer Science Part B: Polymer Physics, Vol. 36, 2781-2792, 1998.

Johnson A.F. "Engineering design properties of glass reinforced properties" A joint BPF and NPL project, The British Federation Plastic Publication, 1986.

Johnson A.F "Design analysis in polymeric materials. II. Polymer Composites" NPL-UK, High Performance Plastics -ISSN- 0264-7753 -Citation- 5,No.7, pp.1-7 1988.

Johnson A.F, Marchant A "Design and analysis of composite structures" Polymers and Polymer Composites in Construction - London, Thomas Telford, pp.33-93. 63ECi, 1990.

Johnson A.F and Costalas E. "Forming models for fabric reinforced thermoplastics" 4th International Conference on Automated Composites: Volume 2. Conference Proceedings - Nottingham, pp.341-52. 627, 6th-7th Sept.1995.

Jones F.R "Handbook of Polymer-Fibre Composites" Longman Scientific and Technical, 1994.

Jones R.M "Mechanics of composite material" Scripts, Washington, USA, 1975.

Jones R.M "Mechanics of composite material" ISBN: 1-56032-712-X, Taylor and Francis publishing, USA, pp.190-195, 1999.

Kalnin IL "Evaluation of unidirectional glass-graphite fibre/epoxy resin composites" Composite material testing and design (second conference), ASTM STP 497, American Society for Testing and Materials, Philadelphia, 1972.

Kaniej Fuji L.K, Arikawa H. and Inoue K. "Flexural properties and impact strength of denture base polymer reinforced with woven glass fibers" Journal of Dental materials, Vol.16, No.2, pp.150-158, 2000.

Kander R.G "A study of damage accumulation in unidirectional glass reinforced composites via AE monitoring" Journal of Polymer Composites, Vol.12, No.4, pp237-245, 1991.

Karger-Kocsis J. "Fracture mechanical characterisation and damage zone development in glass fibre mat-reinforced thermoplastics" Polymer Bulletin Vol.31, pp.235-241, 1993.

Kelly A. and Daves G.J "The principle of fibre reinforcement of metals" Metal. Re. Vol. 10, pp.1-78, 1965.

Kelly A. and Nicholson R.B "Strengthening methods in crystals" Elsevier Press, London, 1971.

Keusch S. and Hessler R. "Influence of surface treatment of glass fibres on the dynamic mechanical. Properties of epoxy resin composites" Journal of Composites: Part A 30, pp997-1002, 1999.

Kim Jang-Kyo, Mai Yiu-Wing "Engineered interfaces in fibre reinforced composites" Oxford, Elsevier Science Ltd., 24 xiii 627 pp.401, 1998.

Kim J.W, Park J.M and Goda K. "New method of evaluating interfacial properties of composites by means of the gradual multi-fibre fragmentation test" Composites Science & Technology - ISSN- 0266-3538 -Citation- 60, No.3, p.439-50, 2000.

Kim J.K, Sham M.L and Wu J "Nanoscale characterisation of interphase in silane treated glass fibre composites" Journal of Composites Part A: Applied Science and Manufacturing -ISSN- 1359-835X -Citation- 32A, No.5, pp.607-618, 2001.

Kline R.A. "Acoustic Emission signal characterisation" in: Matthews J.R. (ed.) "Acoustic Emission" Gordon and Breach, New York, pg. 105-138, 1983.

Kotsikos G., Evans J.T, Gibson A.G and Hale J. "Use of acoustic emission to characterise corrosion fatigue damage accumulation in glass fibre reinforced polyester laminates" Journal of Polymer Composites, Vol.20, No.5, pp.689-696, 1999.

Kumar S., Yang B., Kozey V. and Adanur S. "Bending, compression, and shear behaviour of woven glass fibre-epoxy composites" Journal of Composites Part B: Engineering -ISSN- 1359-8386 -Citation- 31B, No.8, p.715-21, 2000.

Kuzenko M. Von and Browing C.E "Dynamic Mechanical Characterisation of an Advanced Composite Epoxy Matrix Resin of Altered Composition" p694-699, 1979.

LaCourse W.C, "The strength of Glass – An Introduction to Glass Science" edited by Pye L.D., Stevens HJ and LaCourse WC, Plenum Press, New York pp. 451-465, 1972.

Larson B.K; Drzal L.T "Glass fibre sizing/matrix interphase formation in liquid composite moulding. Effects on fibre/matrix adhesion and mechanical properties" Journal of Composites - ISSN- 0010-4361 -Citation- 25, No.7, pp.711-21, Aug.1994.

Laws N. and McLaughlin R. "Self-consistent estimates for the viscoelastic creep compliance of composite materials" Proc. Royal Soc., A359, 25 1-73, 1978.

Lee H. Neville K. "Handbook of epoxy resins" McGraw Hill, New York 1967.

LeterrierY., Sutter P. and Manson J.A.E "Thermodynamic and micromechanical approaches to the adhesion between polyethylene terephthalate and silicon oxide" Journal of adhesion, Vol.69, No.1-2, pp.13-30, 1999.

Lewis T B. and Nielsen L E, "Polymer Matrix Composites" Journal of Appl. Polymer Science, Volume 14, pp1449, 1970.

Loewenstein K.L "The Manufacturing technology of continuous glass fibres" Elsevier, Amsterdam, 1983.

Loewenstein K.L and Dow J. "An investigation of the relationship between glass fibre strength, the temperature of the glass from which the fibre is drawn and fibre diameter" Glass Technology 9, pp.164-171, 1968.

Ma B.T., Schaldler L.S. and Laird C. "Acoustic Emission in single filament composites under tensile deformation", Polymer Composite Vol.11, pp. 211-216, 1990.

Madhukar M.S. and Drzal L.T. "Fibre-matrix adhesion and its effect on composite mechanical properties. I. Inplane and interlaminar shear behaviour of graphite/epoxy composites" Journal of Composite Materials -ISSN- 0021-9983 -Citation- 25,No.8 pp.932-57, 1991.

Mallick P.K. "Fibre Reinforced Composite" Marcel Dekker Inc. ISBN 0-8247-9031-6 p22-28, 40-54,121 and 136, 1998.

Manderson P.W. and Bader M.G. "The strength of hybrid glass/carbon fibre composites" Journal of Material Science Vol16, pp2233, 1979.

Mar JW and Lin KY "Characterisation of splitting process in graphite/epoxy composites" Journal of Composite Material Vol.13 pp278, 1979.

Matthews J.R. "Acoustic Emission" Gordon & Breach. NY, 1983.

Mayer C, Wang X, Neitzel M "Macro- and micro-impregnation phenomena in continuous manufacturing of fabric reinforced thermoplastic composites" Journal of Composites Part A: Applied Science and Manufacturing -ISSN- 1359-835X -Citation- 29, No.7, p.783-93, 1998.

Mehan R.L. and Mullin J.V. "Analysis of composite failure mechanisms using acoustic emission". Journal of Composite Materials, Vol. 5, pp 266-29, 1971.

Mettes DG "Handbook of Fibreglass and Advanced Plastics Composites", Ed. G. Lubin, Reinhold Book Corporation, New York, 1969.

Mezzenga R., Boogh L., Berg J.O, Manson J.A.E. and Page S.A "Surface energetic evolution during processing of epoxy resins" Journal of Colloid and Interface Science, Vol.222, No.1, pp.55-62, 2000.

Mimura K., Ito H and Fujioka H. "Improvement of thermal and mechanical properties by control of morphologies in PES--modified epoxy resins" Polymer, Vol.41, No.12, pp.4451-4459, 2000.

Mistra, JLR Computer Analysis Inc., E. Everett Mall Way, Building E, Suite 201, Everett, WA 98208, USA.

Mittleman A. and Roman T., "A new approach to the use of AE peak amplitude distribution as a tool of characterising failure mechanism in composite materials" Journal of Acoustic Emission 6, pp.73-77, 1987.

Molinier Jacques, "Special glass fibre" 13th Reinforced Plastics Conference, 8-11/paper, 14, pp. 59-62, 1982.

Naik K.N. "Woven fabric composites" Technomic Publishing co.inc. pp. 90, 1994.

Naik K.N. and Ganesh V.K. "Prediction of on-axis elastic properties of plain weave fabric composites" Journal of Composite Science and Technology Vol.45, pp.135-152, 1992.

Narisawa I. and Oba H. "An evaluation of acoustic emission from fibre-reinforced composites" Journal of Materials Science, Part1, Vol.19, pp.1777-1786, 1984.

Netravali A.N., Li Z.F and Sachse W. "Determination of fibre/matrix interfacial shear strength by an Acoustic Emission technique", Journal of Science Matters, 26 pp. 6631-6638, 1991.

Nomura, S. and Chou, T. W. "The viscoelastic behaviour of short-fibre composite materials" Journal of Mt. Eng. Sci. Vol.23, p193, 1985.

Okoli I.O., Smith G.F. "The effects of strain rate and fibre volume fraction on the failure modes of fibre reinforced composites" Journal of Material Science, Vol. 33, No.22, pp.5415-5422, 1998.

Okoroafor E.U., Priston A.M. and Hill R. "Evaluation of the interfacial tensile of composite material using AE" 3rd International Conference on Deformation Evaluation of Interfacial Tensile ST I0144466 March 518-525, 1995.

Okoroafor E.U., Priston A.M. and Hill R. "Comparison of adhesion data from the single fibre composite fragmentation method to a new multi-fibre composite method" Journal of Composite Interfaces Vol.3, No.4, pp.275-29, 1996.

Paggoit M.R. "The effect of the interface interphase on fibre composite properties" Journal of Polymer Composites" Vol.8, No.5, pp.291 –297, 1987.

Pagano, N. J. "Stress fields in composite laminates" Journal of Solids Structure, Vol. 14, pp.385-400, 1978.

Pagano, N. J. series editor Pipes R.P. "Interlaminar response of composite material" Elsevier Science Publishing Company Inc. ISBN 0-444-87285-X, 1989.

Pai R., Kamath M.S. and Rao R. MVGK "Acid resistance of glass fibre composites with different lay-up sequencing .2. Degradation studies" Journal of Reinforced Plastics and Composites, Vol.16, No.11, pp.1013-1019, 1997.

Pape P.G. and Plueddemann E.P "Methods for improving the performance of silane coupling agents" Journal of Adhesion Science and Technology -ISSN- 0169-4243 -Citation- 5,No.10, pp.831-42, 1991.

Park W.B, Park S.J., Le J.R. and Kim YK "Hybrid matrix systems to improve the properties of fibre- reinforced composites", Journal of Polymer-Korea, Vol.22, No.5, pp.824-832, 1998.

Park S.J., Kim M.H. "Effect of acidic anode treatment on carbon fibres for increasing fibre-matrix adhesion and its relationship to interlaminar shear strength of composites" Journal of Materials Science, Vol.35, No.8, pp.1901-1905, 2000.

Park S.J., Kim T.J. "Studies on surface energetic of glass fabrics in an unsaturated polyester matrix system. Effect of sizing treatment on glass fabrics" Journal of Applied Polymer Science - ISSN- 0021-8995 -Citation- 80, No.9, pp. 1439-45, 2001.

Pauchard V., Brochado S., Chateauminois A., Campion H. and Grosjean F "Measurement of sub-critical crack-growth rates in glass fibres by means of acoustic emission" Journal of Materials Science Letters -ISSN- 0022-2461 -Citation- 20, No.8, pp.777-779, 2001.

Peters S. T. "Handbook of Composites" Chapman & Hall, ISBN 0-412-54020-7, pp120, 1998.

Pipes R. B. and Pagano, N. 1. "Interlaminar stresses in composite laminates under uniform axial extension," Journal of Composite Material Vol. 4, pp. 538-548, 1970.

Pipes R. B., and Daniel, I. M. "Moire analysis of the interlaminar shear edge effect in laminated composites" Journal of Composite Materials Vol. 5, pp. 255-259, 1971.

Plueddemann E.P. "Historical background of the interface-studies and theories" in: Plueddemann, E. P. (editor) Interfaces in Polymer Matrix Composites. Vol. 6, Academic Press, 2-3, 1974a.

Plueddemann EP "Mechanism of adhesion through silane coupling agents" Interfaces in Polymer matrix composites; E. Plueddemann EP New York, London Academic Press, pp.173-216. 1974b.

Plueddemann E.P. and Stark G. "Surface modification of fillers and reinforcement in plastics" Spi, reinf. Plast-comp. Inst.32nd Annual Conference Washington, section 4-c, pp. 9. Confer. 627, 1977.

Plueddemann E.P. "Adhesion through silane coupling agents – Fundamentals of Adhesion" Citation- New York, Plenum Press, p.279-90. 9(12) 4, 1991.

Ranade S V; Xie X-Q; DiBenedetto A T - Personal Editor Drzal L.T and Schreiber H.P "Effect of interphase structure on the interfacial properties of S-glass/polycarbonate composites" 20th Annual Anniversary Meeting of the Adhesion Society. Conference proceedings Citation Hilton Head Island, S.C., pp.291-293. 8(10) 1997.

Robert M. Jones "Mechanics of composite material" Virginia, ISBN 1-56032-712x, 1999.

Rose C. A., and Herakovich, C.T. "An approximate analytical solution for Interlaminar stresses in angle-ply laminates in composites: design, manufacture, and application" (S. W. Tsai and G. S. Springer, eds.), ICCM VIII, SAMPE, Covina, CA, pp. 28-W-1—28-W-l3. 1991.

Rosen B.W. and Humphreys E.A." Properties analysis of laminates" Engineering material Handbook, Vol.1 composites, ASM international pp.218-235, 1987.

Rybicki, E. F. "Approximate three-dimensional solutions for symmetric laminates under in-plane loading" Journal of Composite Materials Vol. 5, pp. 354-360, 1971.

Scardino F. "An introduction to textile structures and their behaviour" Textile Structures Composites edited by Chou T., and Ko F.K. Vol.3, pp1-26. 1989.

Schapery, R.A. "Stress analysis of viscoelastic composite materials" Journal of Composite Materials Vol.1, pp.228-67, 1967.

Schlud B. and Lambla M. "Modification of the dynamic damping behaviour of epoxy/glass fibre composites via fibre coating with functional lattices" Journal of Polymer Composites, 6(4), 272-281, 1985.

Schwartz Mel M. "Composite Material, Properties, Non-destructive Testing and Repair" Pentice-Hall International, ISBN 013-300047-8, p109, 1997.

Sepe Michael P. "Dynamic Mechanical Analysis for Plastic engineering" Plastic Design Library pp. 6-34. 1999.

Sham Man-Lung, Kim Jang-Kyo and Hamada H "Mechanical performance of glass woven fabric laminates: effect of hybrid layers with different silane coupling agents" Journal of Polymers & Journal of Polymer Composites -ISSN- 0967-3911 -Citation- 6, No.5, pp.305-12, 1998.

Shaterzadeh M., Gauthier C. Gerard J.F., Mai C. and Perez J, "Dynamic mechanical properties of spherical inclusions in polymer composite: A self-consistent approach considering morphology" Journal of Polymer Composites Vol.19, No.6, pp.655-666, 1998.

Shindo Y. Wang, Horiguchi K. and Ueda S. "Theoretical and experimental evaluation of double-notch shear strength of G-1 OCR glass-cloth/epoxy laminates at cryogenic temperatures" Journal of Engineering Materials and Technology-Transactions of the ASME, Vol.121, No.3, pp.367-373, 1999.

Shiqiang Deng and Lin Ye "Influence of fibre-matrix adhesion on mechanical properties of graphite/epoxy composites. I. Tensile, flexure, and fatigue properties" Journal of Reinforced Plastics & Composites -ISSN- 0731 -6844 -Citation- 18, No.11, pp.1021–040, 1999.

Stellbrink Kuno K. "Micromechanics of Composite" ISBN 1-56990-206-2, 1996.

Structural Dynamics Research Corporation (SDRC), 2000 Eastman Drive, Milford, Ohio, SDRC, Milford House, Priory End, London Road, Hitching, Hertfordshire. 2000.

Sutherland L.S., Shenoi R.A and Lewis S.M. "Size and scale effects in composites: II: Woven-roving laminates" Journal of Composites Science and Technology, Vol.59, No.2, pp.235- 251, 1999.

Sutherland L.S., Shenoi R.A and Lewis S.M "Size and scale effects in composites. I-Unidirectional laminates" Journal of Composites Science & Technology -ISSN- 0266-3538 -Citation- 59, No.2, p.221-33, 1999b.

Stuart M. Lee, "Composites Encyclopaedia" ISBN-0-89573-290-4, Vol. 2, pp512 –514, 1989.

Tesero G. and Wu Y. "Silane coupling agents: the role of organofunctional group" Journal of Adhesion Science and Technology. 5(10), pp.771-784, 1991.

Theocaris P.S. "The Mesophase Concept in Composites" Springer-Verlag, ISBN 3-540-15052-8 1987.

Theocaris P.S. "Mesophase between coupling agents and main phases in particulate" Journal of Reinforced Plastics & Composites -ISSN- 0731-6844 -Citation- 7,No.4, pp.360-377, 1988.

Theocaris P.S. "Elastic modulus of the Mesophase as defined by diffusion processes" Journal of Reinforced Plastics & Composites -ISSN- 0731-6844 -Citation- 11,No.5, pp.537-551, 1992.

Theocaris P.S. "Playing with the anisotropy of the matrix and fibre for the improvement of the strength of composites" Journal of Reinforced Plastics & Composites -ISSN- 0731-6844 -Citation- 14, No.8, pp.889-907, Aug.1995.

Theocaris P.S., Stavroulakis G.E. "Effective elastic moduli of plain-weave woven fabric composites by numerical homogenisation" Journal of Reinforced Plastics & Composites -ISSN-0731-6844 -Citation- 16, No.18, pp.1675-1691, 1997.

Thomas W.F. "An investigation of the factors affecting the strength of glass fibre strand", Journal of Glass Technology, 13, pp 17-21, 1972.

Thomason J.L. "Investigation of composite interphase using dynamic mechanical analysis-artefacts and reality" Journal of Polymer Composites, Vol.11, No.2, pp.105-113, 1990.

Thomason J.L. "A note on the investigation of the composite interphase by means of thermal-analysis" Journal of Composites Science and Technology.Vol.44, No1, pp.87-90, 1992.

Thomason J.L. and Schoolenberg G.E. "An investigation of glass-fibre polypropylene interface strength and its effect on composite properties" Journal of Composites Vol. 25, No.3, pp.197-203, 1994.

Thomason J.L. "The interface region in glass fibre-reinforced epoxy resin composites: 3. Characterisation of fibre surface coatings and the interphase" Journal of Composites volume 26 number 7 1995.

Thomason J.L and Vlug MA "Influence of fibre length and concentration on the properties of glass fibre-reinforced polypropylene - Tensile and flexural modulus" Journal of Composites A, Vol.27, No.6, pp.477-484, 1996.

Thomason J.L. and Dwight D.W. "XPS analysis of the coverage and composition of coatings on glass fibres" Journal of Adhesion Science and Technology, Vol.14, No.5, pp.745-764, 2000.

Thomason J.L., Adzima L.J. "Sizing up the interphase: an insider's guide to the science of sizing" Journal of Composites Part A: Applied Science and Manufacturing -ISSN- 1359-835X -Citation-32A, Nos.3-4, p p.313-321, 2001.

Tillie M.N., Lam J., Gerard J.F. "Insertion of an interphase synthesised from a functionalist silicone into glass-fibre/epoxy composites" Journal of Composites Science and Technology, Vol.58, No.5, pp.659- 663, 1998.

Tirry L., De Willed WP and Cardon A.H., "Study of the interphase in unidirectional glass fibre/polypropylene composites" Personal Editor- Drzal L.T. and Schreiber, 20th Annual Anniversary Meeting of the Adhesion Society. Conference Proceedings 8(10) pp.45-7, 1997.

Vallittu P.K. "Flexural properties of acrylic resin polymers reinforced with unidirectional and woven glass fibers" Journal of Prosthetic Dentistry, Vol.81, No.3, pp.318-326, 1999.

Vetrotex Deutschland GmbH, "Technical report "correspondence with Editor, 1999.

Vinson J.R. and Chou T.W. "Composite materials and their use in structures" Applied Science publishers, London, 1975.

Wada A., Motogi S. and FukudaT. "Prediction of stiffness reduction in composite laminates using damage mechanics approach" Journal: Zairyo, Vol.48, and No.5, pp.454-458, 1999.

Wada A., Motogi S. and Fukuda T. "Damage mechanics formulation of the crack evolution process in composite laminates under plane stress conditions", Journal of Reinforced Plastics and Composites, Vol.19, No.3, pp.219-229, 2000.

Wan Y.Z., Wang Y.L., Luo H.L., Dong X.H., Cheng G.X. "Effects of fibre volume fraction, hot pressing parameters and alloying elements on tensile strength of carbon fibre reinforced copper matrix composite prepared by continuous three-step electrodeposition" Journal of Material Science and Engineering A288, pp.26-33, 2000.

Wang S.S. and Choi I. "Boundary layer effects in composite laminates part1- free edge stress singularities" Journal of Applied Mechanics Vol.49 pp.541-548, 1982.

Wang Youjiang and Zhao Dongming "Characterisation of interlaminar fracture behaviour of woven fabric reinforced polymeric composites" Journal of Composites 26/2, pp. 115-124, 1995.

Wevers M "Listening to the sound of materials: acoustic emission for the analysis of material behaviour" NDT&E International Vol.30, No.2, pp99-100, 1997.

Whitcomb J. D., "Three Dimensional Stress Analysis of Plain weave Composites" Journal of Composite Material – Fatigue and Fracture, Vol. 3, ASTM STPI 110, pp.417- 438, 1991.

Whitney J.M. "Influence of micromechanical parameters on the gross properties of fibre reinforced composites" Journal of Textile Research Vol. 37, pp.1008-1013, 1967.

William D. Cumming HITCO "Woven Structures Division" Engineering Material Handbook, ASM International Composites, Vol.1. 1987.

Williams R.V. "Acoustic Emission" Adam Hilger, Bristol, pp9-38, 1980.

Wooh S C; Daniel I M; Chun H J "Real-time ultrasonic and acoustic emission monitoring of damage in graphite/epoxy laminates" Journal of Composites Engineering -ISSN- 0961-9526 - Citation- 5, No.12, pp.1403-12, 1995.

Wolla J.M. and Goree J.G. " Experimental evaluation of longitudinal splitting in unidirectional composites" Journal of Composite Material, Vol. 21, pp49, 1987.

Wood W.G. and Langer E.L. "Engineering Material Handbook, Vol.1, Composites" ASM International, ISBN 0-87170-279-7, pp.299, 1987.

Zwebwen C. "A Bounding approach to the strength of composite materials" Engineering and Fracture Mechanics 4 (1), 1972.

Zeng Qlng-Dun, Wang Zhi-Li and Ling Ling "Study on the influence of interfacial damage on stress concentrations in unidirectional composites" Journal of Composites Science & Technology, Citation 57, No.1, pp.129-1351997.

Zhang Y.C. and Harding J. "Numerical micromechanical analysis of the mechanical properties of plain weave composites" Computer and Structures Vol.36 No.5 pp.839-884. 1990.

Zhang Y.P. and Cameron J. "Evaluation of fibre content in glass-fibre epoxy composites from heat-capacity data" Journal of Reinforced Plastics and Composites, vol.11, no.8, pp.939-948, 1992.

APPENDICES

Appendix (A)

Classical Laminate Theory (CLT)

The laminate is assumed to be made up of a number of perfectly bonded laminae with the bond assumed to be infinitesimally thin (Jones 1975). The laminate is thus assumed to be a single layer of material.

General assumption of classical laminate theory

The general assumption of classical laminate theory for prediction of both stiffness and strength requires that vertical stress does not vary through the thickness and that stress normal to the plate surface is negligible:

1. Stress normal to the thin ply surface and shear strain in planes perpendicular to the surface are negligible. Through thickness and interlaminar shear stresses are considered to be zero.
2. The elastic constants are invariant with strain (linear elasticity) elastic constants are invariant with temperature.
3. Measurement of the lamina in the laminate of the unidirectional composite represents the input data.
4. No stress concentration in an undamaged ply results from cracking in an adjacent damaged ply.
5. No viscoelastic relaxation and thermal expansion coefficients are constant

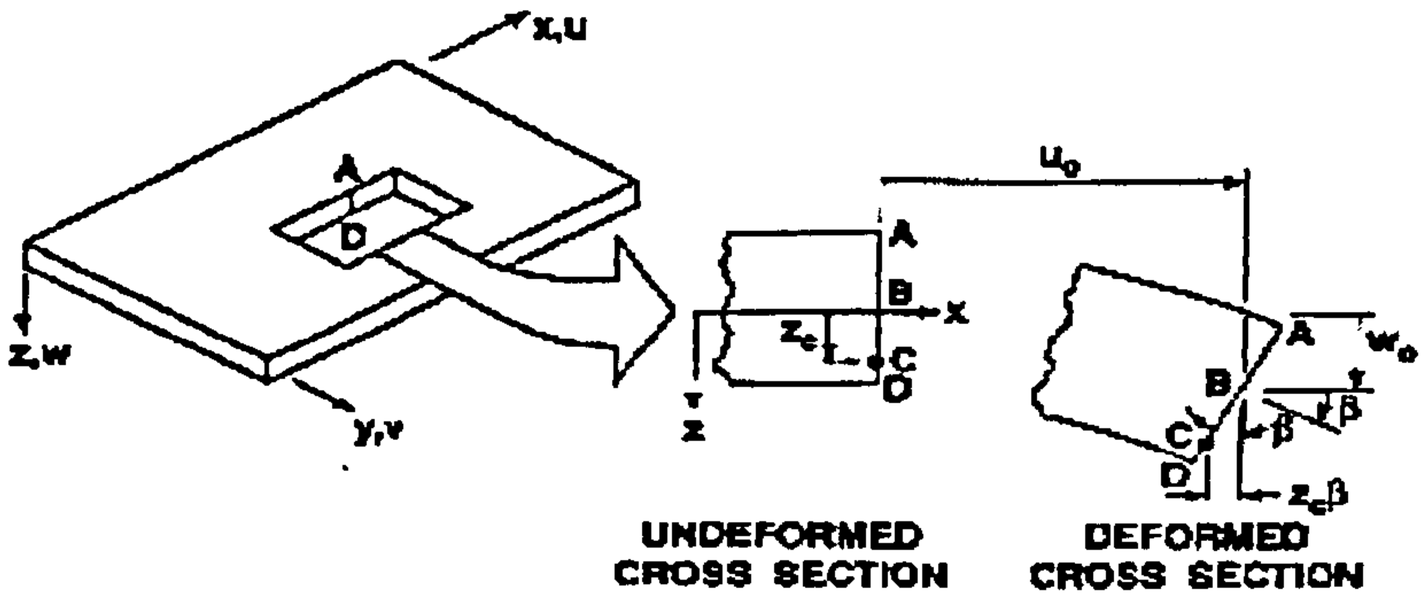

Figure A. Classical Laminate Theory view of deformation geometry in x-z plane. (after Robert M. Jones 1999).

Because line ABCD remains straight under deformation of the laminate, the displacement at point C is.

$$\beta = u_o - z_c\beta$$

But because, under deformation, line ABCD further remains perpendicular to the middle surface, β is the slope of laminate middle surface in x- direction, that is

$$\beta = \partial w_o/\partial x$$

Then, the displacement u, at any point z through the laminate thickness is

$$u = u_o - z\,\partial w_o/\partial x$$

similarly, the displacement v, in y-direction is

$$v = v_o - \partial w_o/\partial y$$

The laminate strains have been reduced to ε_x, ε_y and γ_{zz} by virtue of the Kirchhoff hypothesis.

That is $\varepsilon_z = \gamma_{xz} = \gamma_{yz} = 0$.

For small strains (linear elasticity), the remaining strains are defined in the terms of displacement as

$$\varepsilon_x = \partial u/\partial x,\ \varepsilon_y = \partial v/\partial y\ ,\ \gamma_{xy} = \partial u/\partial y + \partial v/\partial x$$

Thus, for the derived displacement u and v , the strains are:

$$\varepsilon_x = \frac{\partial u_o}{\partial x} - z\frac{\partial^2 w_o}{\partial x^2}$$

$$\varepsilon_y = \frac{\partial v_o}{\partial y} - z\frac{\partial^2 w_o}{\partial y^2}$$

$$\gamma_{xy} = \frac{\partial u_o}{\partial y} + \frac{\partial v_o}{\partial x} - 2z\frac{\partial^2 w_o}{\partial x \partial y}$$

or

$$\begin{bmatrix} \varepsilon_x \\ \varepsilon_y \\ \gamma_{xy} \end{bmatrix} = \begin{bmatrix} \varepsilon_x^o \\ \varepsilon_y^o \\ \gamma_{xy}^o \end{bmatrix} + z\begin{bmatrix} \kappa_x \\ \kappa_y \\ \kappa_{xy} \end{bmatrix}$$

where the middle-surface strains are

$$\begin{bmatrix} \varepsilon_x^o \\ \varepsilon_y^o \\ \gamma_{xy}^o \end{bmatrix} = \begin{bmatrix} \dfrac{\partial u_o}{\partial x} \\ \dfrac{\partial v_o}{\partial y} \\ \dfrac{\partial u_o}{\partial y} + \dfrac{\partial v_o}{\partial x} \end{bmatrix}$$

and the middle-surface curvatures are

$$\begin{bmatrix} \kappa_x \\ \kappa_y \\ \kappa_{xy} \end{bmatrix} = -\begin{bmatrix} \dfrac{\partial^2 w_o}{\partial x^2} \\ \dfrac{\partial^2 w_o}{\partial y^2} \\ 2\dfrac{\partial^2 w_o}{\partial x \partial y} \end{bmatrix}$$

In classical lamination theory, only the stresses in the plane of the laminate, σ_x, σ_y and τ_{xy} are considered. Thus in CLT no account was taken of stresses such as σ_z, and τ_{zx} and τ_{zy}. These stresses are called interlaminar stresses and exist on surfaces between adjacent layers although they exist within the layers but are usually largest at the layer interfaces. Accordingly, classical lamination theory does not include some of the stresses that actually cause failure of a composite laminate. High interlaminar stresses are the basis for one of the failure mechanisms uniquely characteristic of composite laminates, namely, free-edge delaminations. Classical lamination theory often implies values of σ_y and τ_{xy} where they cannot possibly exist, namely at the edge of a laminate.

This analysis can be found in the references such as (Jones 1999) (Chou 1992), (Naik and Ganesh 1992), (Chawla 1987), (Carlsson and Pipes 1987) and (Christensen 1979).

The material constants such as stiffness do not vary with strain, the strains in the deformed plate are small. Shear strains in planes perpendicular to the surface are assumed to be zero. The

theory assumes that the laminate is in a state of plane stress hence ignoring the interlaminar effects, and the out-of-plane stress components.

The extensional stiffness 'A` is given by: -

$A_{ij} = \sum Q_{ij}\, h_k$ where h_k is the thickness of each ply.

Where each ply has the same thickness h_k,

the stiffness 'Q_{ij}' is given by: -

$Q_{11} = E_{11}/(1 - \nu_{12}\nu_{21})$

$Q_{22} = E_{22}/(1 - \nu_{12}\, \nu_{21})$

$Q_{12} = \nu_{12}\, E_{22}/(1 - \nu_{12}\, \nu_{21})$

$Q_{66} = G_{12}$

The overall laminate strain system resulting from an applied mechanical stress is calculated using the laminate stiffness matrix. The overall laminate strain system, which exists equally in all the laminae, is used to calculate the individual lamina stress via each lamina stiffness matrix.

Appendix (B)

Ring Down Counting (RDC)

Emissions as received by the transducer contain information on:

(1) Rate of emissions received,

(2) Frequencies within the emitted pressure wave,

(3) Amplitudes within the emitted pressure wave arriving at the transducer.

Additionally, energy parameters can be generated from the transducer signals.

The simplest way of characterising a pulse or series of pulses produced in an acoustic emission experiment is called 'ring-down' counting. The time-amplitude trace of a pair of typical signals bursts at the transducer. Counting the number of times per second the amplitude exceeds a pre-set voltage gives a simple number characteristic for the signal. An experienced operator can use this number to make observations concerning the severity of the rate of growth of a defect under study.

It will be noted that this simple approach relies in some cases, on the measurement of an averaged signal. Sophisticated equipment, now generally preferred, adds energy to simple counting because:

(1) A ring down count is a function of signal frequency,

(2) The count is only indirectly dependent upon amplitude because a large amplitude signal, i.e. the count, is biased towards large amplitude pulses.

Energy analysis can mean any of the following:

(1) The square of the initial pulse amplitude is measured for each burst.

(2) The area under the envelope of the amplitude-time curve is measured for each burst.

(3) The area under the actual amplitude-time curve is measured for each burst. (William 1980).

Acoustic emission (AE) is the elastic energy that is spontaneously released by materials when they undergo deformation (Zwebwen 1972). The electrical signal from a transducer is subsequently amplified and as the crystals are left un-damped, the signal resulting from a single

surface displacement will be similar to that in the figure B. In an ideal situation the voltage, V, versus time (t), relationship for such a signal approximates to a decaying sinusoid:

$$V = V_p \sin 2\pi f t \exp(-t/\tau)$$

The simplest method to obtain an indication of AE activity is to count the number of amplified pulses, which exceed an arbitrary threshold voltage [Vt] (Harris et al. 1980).

The number of ring down counts (RDC) depends on the peak voltage and is given by

$$RDC = f\pi \ln (V_p/V_t)$$

where f is the resonant frequency of the transducer, τ is the decay time, t is the time and V_p is the peak voltage. The threshold voltage is usually determined after trials where the discontinuity is detected, sometimes it is set at 1V for convenience.

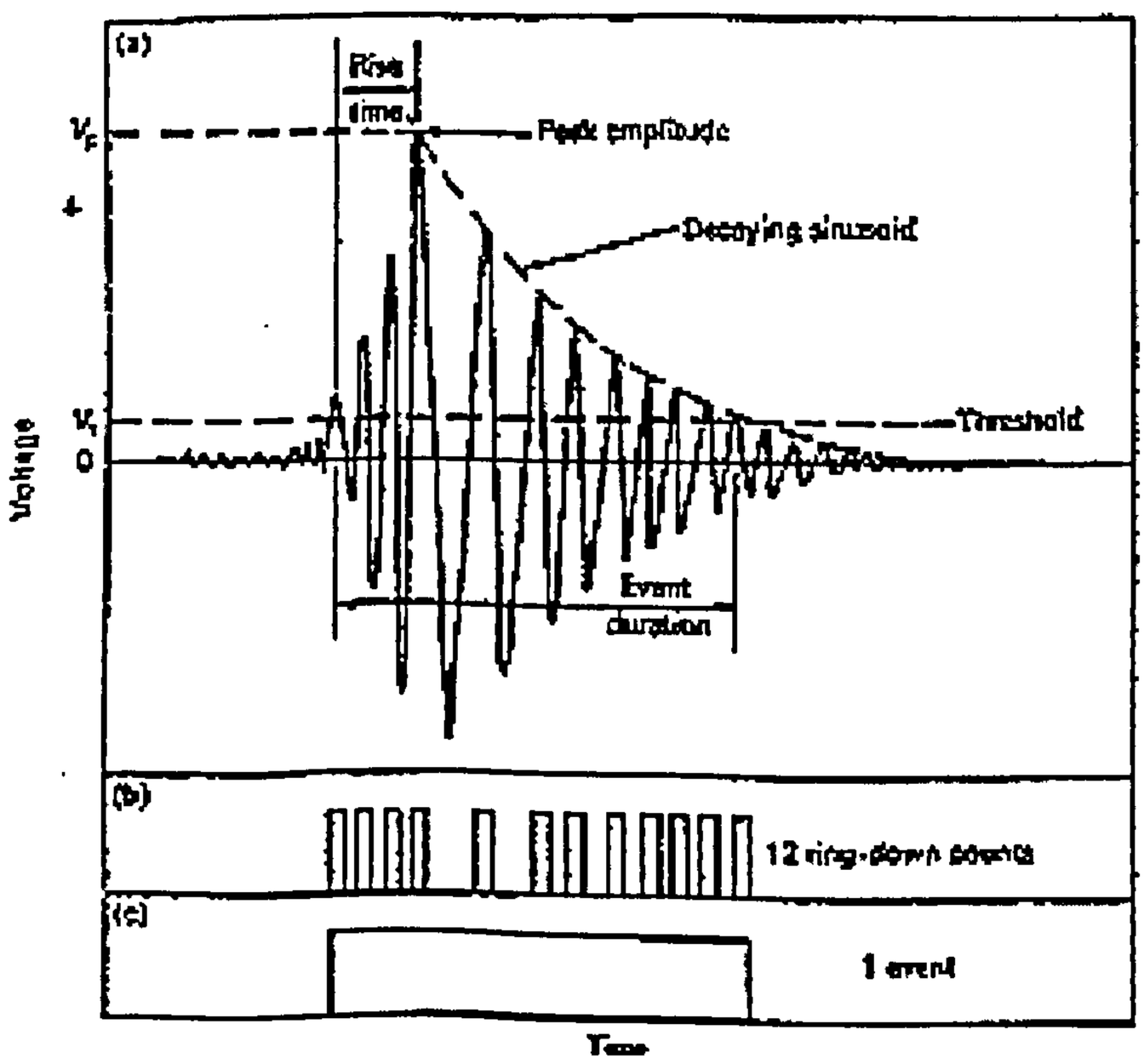

Figure B the relationship between the voltage and RDC, (after Matthews 1983).

Appendix (C)

t-Test

Very few researchers use t-tests to classify their results. Significance tests satisfy the goal of the scientist more frequently than interval estimates, by indicating whether or not a certain relationship or quantity is worth further thought whether it might repay additional research effort (Lewis-Beck 1993a).

significance test is a test of a hypothesis; H_o: $\mu A - \mu B = 0$

Where H_o is the null hypothesis, μ is the mean value. The alternative hypothesis, H_1, remains viable in the event Ho is judged untenable, then

$$H_1: \mu A - \mu B \neq 0$$

These are two competing versions of reality, and in order to determine the probability of H_o being correct, the appropriate statistical tests must be undertaken to make a choice between them, (Lewis-Beck, 1993a,b).

In choosing between H_o and H_1 it is first necessary to evaluate the dispersion of scores within each group in order to conclude with confidence that the two groups are different from one another in certain characteristics. Any difference between them must substantially exceed the differences within them with respect to that characteristic.

In order to evaluate the hypothesis that $d = \mu A - \mu B$, any dissimilarities in performance between the group H_o and H_1 need to be compared with dissimilarities within the two groups. As noted previously, the standard deviation (S) is an indicator of the average extent to which each individual score deviates from the group mean. S therefore applies to raw scores. A comparable expression applicable to the mean is the standard error of the mean:

$$S_8 = S/\sqrt{n}$$

Example

Taking two groups: A=UTS of hybrid composite (weft direction) and B=UTS of non-hybrid composite (weft direction), then:

S_8 (A) = 36.57/√(5) = 16.355

S_8 (B) = 33.71/√(5) = 15.076

With regards to the data of particular group, taking a distribution of mean values in addition to the Standard Deviation for that group gives a more reliable reading than simply taking the Standard Deviation in relation to individual scores. S_x would be a rough indicator of the average amount by which each sample mean would deviate from the population mean, which is unknown.

Because the scores in each group comprise a sample rather than the entire specimen sets, S_Y (A) and S_Y (B) both represent unexplained variability. They are expressions of the extent, on average, to which a group of specimens that have been treated identically have inexplicably failed to behave in the same way. It is therefore permissible to combine these two conceptually equivalent figures into a single measure of collective within-group variability, which is referred to as the standard error of the difference between means:

$$S_d = \sqrt{(S_x (A)^2 + S_x (B)^2)} = \sqrt{((16.355)^2 + (15.076)^2)} = 22.24$$

The ratio between average within-group difference (d =μA - μB = 107.38) and Sd = 22.24) (and group difference is referred to as a t-test,

$$t = d / Sd = 107.38/22.24 = 4.83$$

The smallest magnitude which a score must reach in order for its associated mean difference to be judged significant is given in t (table 5 – 19) for

$$df = nA + nB - 2$$

and selected alpha levels where (α) refers to probability levels considered too low to support the null hypothesis. In this example,

df = 5 + 5 - 2 = 8; at α = 0.05,

therefore, t would have to exceed (2.35).

The variability between the two specimen sets would have to be almost 2.5x greater than the standard error before the null hypothesis could be rejected and the groups could be declared to have performed in significantly different ways (Lewis-Beck, 1993a,b).